Numerical and experimental investigations of the rheological behavior of foam flow : application to the cleaning of surfaces contaminated by microorganisms in the food industries

Heni Dallagi

UNIVERSITE DE LILLE - SCIENCES ET TECHNOLOGIES
Ecole doctorale Science de la Matière, du Rayonnement et de l'Environnement

THESE DE DOCTORAT

Spécialité : Biotechnologies agroalimentaire, sciences de l'aliment, physiologie

Présentée et soutenue par

Heni DALLAGI

Pour l'obtention du grade de

DOCTEUR DE L'UNIVERSITE DE LILLE

Numerical and experimental investigations of the rheological behavior of foam flow: Application to the cleaning of surfaces contaminated by microorganisms in the food industries

Investigations numériques et expérimentales du comportement rhéologique de mousses en écoulement: Application au nettoyage des surfaces contaminées par des micro-organismes dans les industries agro-alimentaires

---

Unité Matériaux et Transformations
Équipe : Processus aux Interfaces et Hygiène des Matériaux (INRAE)

Soutenue le 28 février 2022 devant le jury composé de :

Président
M. Jack LEGRAND : *Professeur, GEPEA, Université de Nantes*

Rapporteurs
Mme Kathryn WHITEHEAD : *Professeure, Metropolitan Manchester University*
M. Arnaud SAINT-JALMES : *Directeur de recherche, CNRS - IPR / Université de Rennes*

Examinateurs
Mme Imca SAMPERS : *Professeure, Faculty of Bioscience Engineering / Université de Gand*
M. Alexis DUCHESNE : *Maître de conférences, IEMN / Université de Lille*

Invités
M. Hein TIMMERMAN : *Global Sector Specialist Food & Beverage at Diversey*
Mme Anne-Laure FAMEAU : *Chargée de recherche, INRAE - UMET / Université de Lille*

Co-Directeur de thèse
Mme Christine FAILLE : *Directrice de recherche, INRAE - UMET / Université de Lille*
M. Fethi ALOUI : *Professeur, LAMIH / Université Polytechnique des Haut-de-France*

Directeur de thèse
M. Thierry BÉNÉZECH : *Directeur de recherche, INRAE - UMET / Université de Lille*

ABSTRACT

Title: *Numerical and experimental investigations of the rheological behavior of foam flow: Application to the cleaning of surfaces contaminated by microorganisms in the food industries*

Keywords: *Foam flow; Rheological behavior; Conductimetry; Polarography; PIV; bubble size; shear stress; CFD; Cleaning-in-place; Spores; Biofilms; LCA*

Abstract: *In this research, experimental and numerical characterization of the rheological behavior of an aqueous foam flowing inside a horizontal pipe with and without singularities (presence of half-sudden expansion, and a fence) were investigated. Different conditions of foam flow were studied by varying the foam qualities (from 55% to 85%), and three Reynolds numbers (32, 65, and 97). Measurements of the pressure measurements, and at the wall the local velocity repartition and the thickness of the liquid films using respectively pressure sensors, Particle Image Velocimetry, and a conductimetry technique shown a reorganization of the foam downstream the geometry change, with a thicker liquid film at the duct bottom, larger bubble sizes at the top, as well as a larger foam void fraction increased from the bottom to the top part of the duct section. In addition, foam would present a visco-elastic character comparable to a non-Newtonian monophasic liquid. Computational Fluid Dynamics simulations were undertaken to predict this rheological behavior of the foam, the two models Herschel-Bulkley and Bingham were tested taken into account the presence of an underlying liquid film at the bottom of the channel. Comparison between experimental and numerical results showed that regardless of the foam quality, Herschel-Bulkley model could accurately describe the rheological behaviour of the aqueous foam under the different flow conditions analysed.*

The second target was to investigate the ability of a wet foam flow (quality of 50%) to clean stainless-steel surfaces contaminated by microorganisms. For this purpose, two different contamination patterns were studied, droplets containing Bacillus subtilis spores (either hydrophilic B. subtilis PY79 or hydrophobic B. subtilis PY79 spsA), and biofilms produced by three bacteria strains encountered in food industry production plants (Escherichia coli SS2, Bacillus cereus 98/4, and Pseudomonas fluorescens Pf1). Different flow conditions were performed by varying the wall shear stresses (2.2 - 13.2 Pa), and bubble sizes (0.18-0.34 mm) in a straight duct with no geometrical changes, in order to identify the mechanisms of contamination release and thus better control and optimize the foam cleaning process. Results show that compared to conventional cleaning-in-place, foam flow effectively removed B. subtilis spores as well as Bc-98/4, Ec-SS2, and Pf1 biofilms. Moreover, the combination of high shear stress at the wall and small bubble sizes (<0.2 mm) showed promise for improving the cleaning efficiency of spores. On the other hand, a clear improvement of the biofilm removal was observed when increasing the mean wall shear stress. The characterization of the foam and the interface phenomenons (using polarography, conductimetry, and bubble size analysis methods) indicated that mechanisms such as fluctuation in local wall shear stresses, or in the liquid film thickness between the bubbles and the steel wall induced by bubble passage, foam imbibition, and sweeping of the contamination within the liquid film could participate largely to the removal mechanisms. Finally, the life cycle assessment study demonstrated that foam flow cleaning could be a suitable technique to reduce water and energy consumption (7 and 8 times less, respectively) presenting less environmental impacts than CIP processes, with about 70%. Lastly, foam flow cleaning can be an alternative method, which can improve efficiency and reduce environmental impact.

Additional activities conducted during the PhD period related to hygienic design are presented highlighting the role of the contaminants (spores and biofilms), the material (other than stainless steel) and the geometry (ducts or more complex design) in hygiene monitoring.

RESUME

Titre: *Investigations numériques et expérimentales du comportement rhéologique de mousses en écoulement: Application au nettoyage des surfaces contaminées par des micro-organismes dans les industries agro-alimentaires*

Mots clés: *Mousse en écoulement; Comportement rhéologique; Conductimétrie; Polarographie; PIV; Taille des bulles; contrainte de cisaillements; CFD; Nettoyage en place; Spores; Biofilms; ACV*

Résumé: *La caractérisation expérimentale et numérique du comportement rhéologique d'une mousse aqueuse s'écoulant à l'intérieur d'un tuyau horizontal avec et sans singularités (présence d'une demi-expansion soudaine, et d'une clôture) a été étudiée. Différentes conditions d'écoulement de la mousse ont été étudiées en faisant varier les qualités de mousse (de 55% à 85%), et trois nombres de Reynolds (32, 65, et 97). Les mesures de la pression, de la répartition de la vitesse locale et de l'épaisseur des films liquides au niveau de la paroi à l'aide respectivement de capteurs de pression, de la vélocimétrie par image de particules et d'une technique de conductimétrie ont montré une réorganisation de la mousse en aval du changement de géométrie, avec un film liquide plus épais au fond du conduit, des bulles de plus grande taille au sommet, ainsi qu'une plus grande fraction de vide de la mousse augmentant de la partie inférieure à la partie supérieure de la section du conduit. En outre, la mousse présenterait un caractère visco-élastique comparable à celui d'un liquide monophasique non newtonien. Des simulations de dynamique des fluides par ordinateur ont été entreprises pour prédire ce comportement rhéologique de la mousse, les deux modèles Herschel-Bulkley et Bingham ont été testés en tenant compte de la présence d'un film liquide sous-jacent au fond du canal. La comparaison entre les résultats expérimentaux et numériques a montré que, quelle que soit la qualité de la mousse, le modèle de Herschel-Bulkley pouvait décrire avec précision le comportement rhéologique de la mousse aqueuse dans les différentes conditions d'écoulement analysées.*

Le deuxième objectif était d'étudier la capacité d'un écoulement de mousse humide (qualité de 50%) à nettoyer des surfaces en acier inoxydable contaminées par des micro-organismes. Pour cela, deux types de contamination ont été étudiés, des gouttelettes contenant des spores de Bacillus subtilis (soit hydrophiles B. subtilis PY79 ou hydrophobes B. subtilis PY79 spsA), et des biofilms produits par trois souches de bactéries rencontrées dans les usines de production de l'industrie alimentaire (Escherichia coli SS2, Bacillus cereus 98/4, et Pseudomonas fluorescens Pf1). Différentes conditions d'écoulement ont été réalisées en faisant varier les contraintes de cisaillement de la paroi (2.2 - 13.2 Pa), et la taille des bulles (0.18-0.34 mm) dans un conduit droit sans changement géométrique, afin d'identifier les mécanismes de libération de la contamination et ainsi mieux contrôler et optimiser le processus de nettoyage par mousse. Les résultats montrent que, par rapport au nettoyage en place conventionnel, le flux de mousse a éliminé efficacement les spores B. subtilis ainsi que les biofilms Bc-98/4, Ec-SS2 et Pf1. De plus, la combinaison d'une contrainte de cisaillement élevée au niveau de la paroi et de bulles de petite taille (<0,2 mm) s'est avérée prometteuse pour améliorer l'efficacité du nettoyage des spores. D'autre part, une nette amélioration de l'élimination des biofilms a été observée en augmentant la contrainte de cisaillement moyenne sur la paroi. La caractérisation de la mousse et des phénomènes d'interface (à l'aide de méthodes de polarographie, de conductimétrie et d'analyse de la taille des bulles) a indiqué que des mécanismes tels que la fluctuation des contraintes de cisaillement locales de la paroi, ou de l'épaisseur du film liquide entre les bulles et la paroi en acier induite par le passage des bulles, l'imbibition de la mousse et le balayage de la contamination dans le film liquide, pourraient participer largement aux mécanismes d'élimination. Enfin, l'étude d'analyse du cycle de vie a démontré que le nettoyage à la mousse peut être une technique appropriée pour réduire la consommation d'eau et d'énergie (7 et 8 fois moins, respectivement) présentant moins d'impacts environnementaux que les procédés CIP, avec environ 70%. Enfin, le nettoyage à la mousse peut être une méthode alternative, qui peut améliorer l'efficacité et réduire l'impact environnemental.

D'autres activités menées au cours de la période de doctorat liées à la conception hygiénique sont présentées en soulignant le rôle des contaminants (spores et biofilms), du matériau (autre que l'acier inoxydable) et de la géométrie (conduits ou conception plus complexe) dans le contrôle de l'hygiène.

REMERCIEMENTS

Je voudrais commencer par exprimer mes plus profonds remerciements à mes directeurs de thèse. Tout d'abord à Mr. Thierry BÉNÉZECH qui a toujours été présent à mes côtés pour m'orienter pendant ce voyage. Merci de m'avoir fait confiance, votre patience, votre gentillesse, et surtout vos judicieux conseils, qui ont contribué à alimenter ma réflexion et qui m'ont permis aussi de prendre confiance en moi et en mon travail. Mais également à Mme. Christine FAILLE qui m'a permis d'approfondir au maximum mes travaux afin de pouvoir être fier aujourd'hui du travail réalisé. Merci de m'avoir donné l'opportunité de participer à d'autres sujets de recherche qui m'ont permis d'élargir mes compétences et découvrir d'autres aspects. Votre soutien aussi bien scientifique que moral a été sans faille (haha). Je vous remercie de votre disponibilité et votre bienveillance inconditionnelle à mon égard. Je tiens à remercier également Mr. Fethi ALOUI de m'avoir permis d'intégrer l'INRAE pour mon stage de fin d'étude. Ce stage m'a permis de me familiariser avec le monde scientifique et m'a ouvert la voie pour y réussir. Merci pour les conseils, les discussions scientifiques et de m'avoir accordé la liberté de gérer mon travail de thèse ce qui m'a permis de développer mon autonomie et mon indépendance scientifique.

Mes sincères remerciements vont également au président du jury de thèse Mr. Jack LEGRAND et également à Mme. Kathryn WHITEHEAD et Mr. Arnaud SAINT-JALMES d'avoir accepté d'être les rapporteurs de ce travail. Je remercie également Mme. Imca SAMPERS et Mr. Alexis DUCHESNE d'avoir accepté de participer à ce jury comme examinateurs. Je voudrais aussi remercier Mr. Hein TIMMERMAN et Mme. Anne-Laure FAMEAU d'avoir accepté de participer à ce jury comme invités.

J'aimerais également remercier Mr. Guillaume DELAPLACE pour son soutien dans toutes les circonstances, ses conseils et son accueil chaleureux à l'INRAE, ce laboratoire dans lequel je me suis senti intégré et épanoui.

Mes sincères remerciements vont également à Laurent BOUVIER et Cosmin GRUESCU pour les efforts qu'ils ont inlassablement déployés pour enrichir ce travail. Merci pour m'avoir transmis avec passion vos connaissances et tous les potentiels qu'elle peuvent offrir.

Je tiens à remercier également Piyush KUMAR JHA, Maureen DELEPLACE, et Ahmad AL SAABI pour le partage de connaissances. C'était un plaisir d'avoir travaillé et publié avec vous. Je te remercie Maureen pour ton aide, ta bonne humeur et ton enthousiasme. Je te remercie Piyush pour ton amitié, tes conseils très précieux, les sortis et les discussions intéressantes. Ahmad, je te considère comme une des plus belles rencontres que j'ai faites durant ma vie. Merci de m'avoir accueilli chez toi, merci pour ton aide, et pour les inoubliables moments partagés.

J'aimerais remercier l'ensemble de l'équipe du LAMIH et en particulier Marc LIPPERT pour leur accueil, leur aide et pour les réunions d'échanges.

Je tiens à remercier également l'ensemble de l'équipe PIHM. Particulièrement, Christophe DUFOURMANTELLE et Anne PROTIN pour leur disponibilité, leur aide et la gestion administrative. Je remercie également Christelle LEMY pour son amitié, sa gentillesse, son aide, et l'énorme temps passé à faire les devis et les commandes. Merci à Pascal DEBREYNE pour son aide, ses connaissances et ses idées ingénieuses pour les mesures physiques. Un grand merci à Laurent WAUQUIER pour son travail de précision remarquable, ses précieux conseils techniques, sa patience et pour le temps passé pour la réalisation et la modification de l'installation pilote qui auront servi à cette étude. Sans toi, cette thèse n'aurait pas été aussi aboutie. Merci aussi pour les barbecues organisés. Merci à Thomas DUBOIS pour sa gentillesse, ses valeureux conseils, ses critiques constrictives et son soutien moral.

De plus, j'aimerais adresser mes reconnaissances à Anne, Amandine, Nour-Eddine, Thierry, Pascal, Oussama, Marwan, Sakhr, Weiji, Thomas, Mustapha, Raghav, Dylan, Paulo, Carolina, Luisa, Angella, Yaussra, Manon pour leur accueil, leur esprit d'ouverture, leur enthousiasme, leur soutien et les bons moments que nous avons passé ensemble, notamment lors de nos inoubliables pauses café et sorties.

Un grand merci particulier à, Samah, Audrey, Mayssane et Jina. Merci pour les beaux moments, les fous rires, et les discussions interminables. Merci Jina pour les incroyables idées de sorties qui ont apporté le sourire et la dynamique à tous les membres de l'équipe. Je ne saurais oublier ta sympathie, ta présence indispensable et irremplaçable. Merci Mayssane pour ton amitié, tes conseils et le grand soutien moral. Merci Audrey pour ta gentillesse, tes précieux conseils et les bons moments qui resteront à jamais gravés dans ma mémoire (même sans garder des photos-souvenirs). Merci Samah pour ta bonne humeur, ta générosité et le soutien moral. Tu as un grand cœur !

Je remercie aussi mes stagiaires Michael, Julien, Zoé et Manon pour l'ensemble de travail effectué.

Pour tous mes amis Amine, Mhamed, Roua, Ameni, Rihab, Khoula, Inèss et Lamia qui m'ont apporté leur soutien moral pendant ces années d'études, je les en remercie sincèrement.

De plus, je n'ai pas de mots pour exprimer mes remerciements à mon âme frère Helmi, mon frère Omar, mes sœurs Hana, Hela, Abir et Maroua, mes deux petites nièces Nourssen et Maram, et tous mes cousins, oncles et tantes. Merci pour le courage, le soutien et l'amour que vous me procurez tous les jours. Je voudrais finalement remercier du fond du cœur, ma grande mère Ajmia, ma mère Souad et mon père Fredj sans qui rien ne serait possible. Merci pour votre soutien, votre amour, pour le confort quotidien que vous m'apportez.

Toutes mes pensées se tournent vers tous mes proches qui m'ont quitté bien trop tôt mais qui avant de partir m'ont appris ce qu'était le courage et la force de tout surmonter.

SCIENTIFIC VALORISATION

Articles

Dallagi, H., Faille, C., Gruescu, C., Aloui, F., Benezech, T. (2022). Is foam flow cleaning effective and environmentally friendly in controlling the hygiene of surfaces contaminated with biofilms? (Under finalization)

Dallagi, H., Aloui, F., Bouvier, L., Wauquier, L., Benezech, T. (2022). Numerical and experimental investigations into the rheological behaviour of wet foam flowing under a fence. Food and Bioproducts Processing. https://doi.org/10.1016/j.fbp.2021.12.009

Dallagi, H., Faille, C., Bouvier, L., Deleplace, M., Dubois, T., Aloui, F., Benezech, T. (2022). Wet foam flow: A suitable method for improving surface hygiene in the food industry. Journal of Food Engineering 110976. https://doi.org/10.1016/j.jfoodeng.2022.110976

Deleplace, M., **Dallagi, H**., Dubois, T., Richard, E., Ipatova, A., Bénézech, T., Faille, C., 2022. Structure of deposits formed by drying of droplets contaminated with Bacillus spores determines their resistance to rinsing and cleaning. Journal of Food Engineering 110873. https://doi.org/10.1016/j.jfoodeng.2021.110873

Jha, P.K., **Dallagi, H**., Richard, E., Deleplace, M., Benezech, T., Faille, C., 2022. Does the vertical vs horizontal positioning of surfaces affect either biofilm formation on different materials or their resistance to detachment? Food Control 133, 108646. https://doi.org/10.1016/j.foodcont.2021.108646

Bouvier, L., Cunault, C., Faille, C., **Dallagi, H**., Wauquier, L., Bénézech, T., 2021. Influence of the design of fresh-cut food washing tanks on the growth kinetics of Pseudomonas fluorescens biofilms. iScience 24, 102506. https://doi.org/10.1016/j.isci.2021.102506

Al Saabi, A., **Dallagi, H**., Aloui, F., Faille, C., Rauwel, G., Wauquier, L., Bouvier, L., Bénézech, T., 2021. Removal of Bacillus spores from stainless steel pipes by flow foam: Effect of the foam quality and velocity. Journal of Food Engineering 289, 110273. https://doi.org/10.1016/j.jfoodeng.2020.110273

Jha, P.K., **Dallagi, H**., Richard, E., Benezech, T., Faille, C., 2020. Formation and resistance to cleaning of biofilms at air-liquid-wall interface. Influence of bacterial strain and material. Food Control 118, 107384. https://doi.org/10.1016/j.foodcont.2020.107384

Conference Paper with DOI

Dallagi, H., Al Saabi, A., Faille, C., Benezech, T., Augustin, W., Aloui, F., 2019. CFD Simulations of the Rheological Behavior of Aqueous Foam Flow Through a Half-Sudden Expansion, in: Volume 1: Fluid Mechanics. Presented at the ASME-JSME-KSME 2019 8th Joint Fluids Engineering Conference, American Society of Mechanical Engineers, San Francisco, California, USA, p. V001T01A030. https://doi.org/10.1115/AJKFluids2019-4650

Dallagi, H., Gheith, R., Al Saabi, A., Faille, C., Augustin, W., Benezech, T., Aloui, F., 2018. CFD Characterization of a Wet Foam Flow Rheological Behavior, in: Volume 3: Fluid Machinery; Erosion, Slurry, Sedimentation; Experimental, Multiscale, and Numerical Methods for Multiphase Flows; Gas-Liquid, Gas-Solid, and Liquid-Solid Flows; Performance of Multiphase Flow Systems; Micro/Nano-Fluidics. Presented at the ASME 2018 5th Joint US-European Fluids Engineering Division Summer Meeting, American Society of Mechanical Engineers, Montreal, Quebec, Canada, p. V003T20A004. https://doi.org/10.1115/FEDSM2018-83338

Dallagi, H., Benezech, T., Bouvier, L., Faille, C., Aloui, F. (2022). Experimental study of the effect of the foam flow quality and velocity on the mass transfer and bubble size distribution. 9th European Conference for Aerospace Sciences – EUCASS-3AF 2022. 27th June -1st July 2022, Lille - France (Full paper under finalization)

Oral Presentations

Dallagi, H., Richard, E., Dubois, T., Deleplace, M., Benezech, T., Faille, C., August 2021. Observation of the drying dynamics of droplets using confocal microscope, Journées de la Matière Condensée, minicolloque MMB16 "The drying dynamics in complex systems: from colloidal solutions to biological suspensions", France

Dallagi, H., Arthur, M., Al-Saabi, A., JHA, P., Bouvier, L., Wauquier, L., Deleplace, M., Aloui, F., Faille, C., Benezech, T., April 2021. Foam Flow: An Eco-Efficient Strategy for Cleaning of Contaminated Industrial Equipment, International Conference on Bacillus ACT 2021, Paris - France

Dallagi, H., JHA, P., Deleplace, M., Bouvier, L., Dubois, T., Wauquier, L., Aloui, F., Faille, C., Benezech, T., March 2021. Foam Flow Cleaning: Removal of Bacillus subtilis spores from Stainless Steel Pipes, BIOADH 2021, France

Dallagi, H., Al-Saabi, A., JHA, K., Wauquier, L., Gruescu, C., Aloui, F., Faille, C., Benezech, T., November 2019. Innovative and eco-efficient strategies for designing and cleaning industrial equipment: Applications for the vegetables and potatoes processing industry, Journée jeunes chercheurs JJC2019, Mons - Belgium

Dallagi, H., Faille, C., Aloui, F., Benezech, T., Janvier 2019. Innovative and eco-efficient strategies for designing and cleaning industrial equipment: Applications for the vegetables and potatoes processing industry, Journée des doctorants JDD2019, Lille - France

Posters

Dallagi, H., A., Bouvier, L., Faille, C., Wauquier, W., Aloui, F., Benezech, T., October 2021. Foam flow: Use of Non-Newtonian fluid for cleaning of contaminated industrial equipment, Fluids and Complexity 2, Nice - France

Dallagi, H., Al-Saabi, A., Faille, C., Wauquier, L., Gruescu, C., Augustin, W., Aloui, F., Benezech, T., June 2019. Modeling of Foam Flowing Regimes Devoted for the Detachment of Bacillus Spores from Stainless Surface, Heat Exchanger Fouling and Cleaning Conference XIII, Józefów - Poland

Dallagi, H., Al-Saabi, A., Faille, C., Aloui, F., Benezech, T., March 2019. CFD simulations of the aqueous foam flow rheological behavior through a half-sudden expansion, Journée Mardi des chercheurs 2019, Mons - Belgium

CONTENTS

Contents

FIGURES INDEX

Chapter 1

Chapter 2

Publication I

Publication II

TABLES INDEX

NOMENCLATURE

ABBREVIATIONS

Symbol	Description
CFD	Computational Fluid Dynamics
CFU	colony forming unit
CMC	Critical micelle concentration
CIP	Cleaning in place
FFC	Foam flow cleaning
PIV	Particle Imaging Velocimetry
SDS	Sodium dodecyl sulfate
WSS	Wall shear stress

ROMAN LETTERS

Symbol	Description	Units
A	Surface	m^2
b	Grid hand size	
c	Concentration	$mol.m^{-3}$
Ca	Capillary number	
CF	Friction factor	
d	Diameter	m
D	Diffusion coefficient	$m^2.s^{-1}$
e	Liquid Film Thickness	m
e_x	Unit vector in the x coordinate direction	
E	Energy	J
f	Poorly adherent fraction of the population	
f_e	Frequency	Hz
fft	fast Fourier transform	
$F_{0.05}$	Percentage of the bubbles with a diameter of less than 0.05 mm	mm
$F_{0.2}$	Percentage of the bubbles with a diameter of less than 0.2 mm	mm
$F(t)$	Normalized reducing function	
G	Shear modulus	Pa
h_1, h_2	Height of the liquid column out of the pressure outlets	m
h	Enthalpy	J
H	Total foam height	m
i	Electric current intensity	A
k	Consistency index	$Pa.s$
k_m	Mass coefficient transfer	$m.s^{-1}$
k_{max1}	Detachment rate of poorly adherent population	s^{-1}
k_{max2}	Detachment rate of highly adherent population	s^{-1}
K	Potassium	
L	Length	m
M	Momentum source	$N.s$
n	Power law index	
N_0	Quantity of population at time 0	$CFU.cm^2$

$N(t)$	Quantity of population at time t	$CFU.cm^2$
O	Oxygen	
P	Pressure	Pa
Q	Flow rate	$m^3.s^{-1}$
r	Radius of curvature of the cross section of a Plateau border	m
r_1, r_2	Radii of curvature of a Plateau border	m
R	Duct region	m
R_{32}	Sauter mean radius	m
Re	Reynolds number	
S	Wall velocity gradient	s^{-1}
Sh	Sherwood number	
S_{ij}	Strain rate tensor	s^{-1}
t	Time	s
T	Temperature	K
u	Axial velocity	$m.s^{-1}$
U	Velocity *f(x,y,z)*	$m.s^{-1}$
v	Vertical velocity	$m.s^{-1}$
V	Volume	m^3
W_{ii}	Power spectral density of the limit intensity	$A^2.s$
W_{ss}	Power spectral density of the wall velocity gradient	s^{-1}
x, y, z	Coordinates	
X, Y, Z	Characteristic length scales	

GREEK LETTERS

Symbol	Description	Units
β	Foam quality	
B	Oscillation amplitude	
$\tau 0$	Yield strain	s^{-1}
Γ	Surface tension	N/m
δ *or* e	Slip layer thickness	m
Δ	Difference	
λ	Time constant	s
μ	Dynamic viscosity	$Pa.s$
ν	Kinematic viscosity	$m^2.s^{-1}$
Π	Osmotic pressure of the foam	Pa
ρ	Density	$Kg.m^{-3}$
σ	Surface tension	N/m
τ	Shear stress	Pa
ϕ	Void fraction	
ψ	Liquid flux	$m^3.m^{-2}.s$

SUBSCRIPTS

Symbol	Description
0	Characteristic
a	Atmospheric

b	Bubble
c	Corrected
cp	Close packing
$crit$	Close packing
d	Rectangular
e	Establishment
f	Foam
g	Gas
h	Hydraulic
in	Foam generator inlet
l	Liquid
lim	Limit
loc	Local
out	Foam generator outlet
$slip$	Slip velocity
t	Total
$velocity$	Obtained through the velocity profiles
w	Foam-wall friction

SUPERSCRIPTS

Symbol	Description
$*$	Dimensionless value
$\rightarrow$	Vector
$'$	Fluctuating value
$-$	Mean
$\cdot$	Rate

GENERAL INTRODUCTION

The term "foam" comes from the old German "viem" and designates a complex system consisting of a liquid or semi-solid medium called continuous phase, intimately mixed with gas. The gas is therefore dispersed in many bubbles (Darling and Birkett, 2005). Foams show an unexpected and non-linear rheological behavior since it is influenced simultaneously by liquid and gas properties. This difficulty has not prevented foams from being a major subject of active research given their intensive use in many industrial sectors, such as food industries, cosmetics, nuclear engineering, petroleum engineering, and firefight.
In the oil industry, foams are involved in oil extraction (Abiven et al., 2009), refining, flotation of minerals (Schramm, 2000), and even in lubricating oils (Binks et al., 2010). In the textile (Lehmonen et al., 2013) and paper (Tanaka et al., 2012) industries, they are used to increase the uniformity of the fibers while decreasing their density. Foams also play a fundamental role in the fire extinguishing technology (Cantat et al., 2013). Often fire needs three conditions to spread: fuel, oxygen, and heat. Foams can address these three factors by excluding oxygen from the combustion zone, by cooling the fuel and even by trapping the fuel stream on the liquid surface (Branch and Ltd, 1989; Ratzer, 1956; Vinogradov et al., 2016). Finally, in the food industry, foams play a prominent role in manufacturing processes. Examples of food foam include chocolate foam, fruit, yogurt, whipped cream… (Brodkorb et al., 2019; Dickinson et al., 2004). Alternatively, carbonated beverages such as soda or alcoholic beverages such as beer or champagne can form a foam that contributes to the quality of the product. In addition, detergents used in the food industry are often in the form of foams, mainly for cleaning open surfaces (workshops, conveyors, floors, and walls). Compared to liquid detergents, the use of a foam cleaner has several advantages. For example, the cleaning foam is more adhesive than liquid detergents, which lengthens the application time and therefore the effectiveness of the treatments, especially for vertical surfaces. In addition, the use of foam results in the formation of fewer aerosols, which limits the recontamination of equipment surfaces and even food products. This foam often contains biocides intended to destroy the microbial flora of surfaces.

This study is part of the European Interreg programme V France-Wallonie-Vlaanderen Veg-I-Tec project and of the FEFS project (ANR-18-CE21-0010), supported by the ANR (French National Research Agency). VEG-I-TEC focuses on innovations and technological developments at an industrial scale to reduce energy and potable water consumption by improving hygiene and the organoleptic quality of processed foods. Part of the Fluid Engineering for Food Security (FEFS) project is the characterization of optimal two-phase flow patterns capable of effectively removing bacterial spores. At PIHM, we investigated whether the use of flowing foam could represent an interesting alternative to conventional cleaning-in-place procedures for the cleaning of surfaces of equipment contaminated by bacterial deposits since the hygiene of materials remains a major concern for the food and other industries. In this context, cleaning with foam was proposed as an innovative method for cleaning closed equipment that can improve the mechanical action at the equipment surface and perhaps improve the removal efficacy of the contamination. Recent works on flowing foam has shown promising results in contamination removal and inactivation (case of foam containing biocides) (Al Saabi et al., 2021; Le Toquin et al., 2020). During the first months of my thesis, I was involved in a preliminary study on the physical characterization of foams in flow. I was in charge of the set-up and development of the pilot test rig as well as in the installation of the

necessary sensors to monitor and characterize the different flow conditions of the foam. The results of the physical characterization of the foam flow have been integrated in Ahmad al-Saabi's thesis and in a recently published paper (Al Saabi et al., 2021). Further research activities were still required to investigate the foam properties that play a major role in the removal of adherent soils, as well as the efficiency of flowing foam to clean various kinds of bacterial surface contamination encountered in the food industry.

Chapter 1 devoted to the state of the art is mainly focused on foam flow and on cleaning operations (closed equipment) in the food industry leading to possible applications of foam flow cleaning. The first objective of this chapter is to deepen the understanding of the physical phenomena governing the structure, stability, hydrodynamics, and rheological behavior of foams. Thus, the analysis of the literature makes it possible to identify some key parameters to be taken into account and to define the experimental and numerical metrology required to carry out this study. The second point was to highlight the different cleaning strategies in the food industry, giving a better knowledge of surface contamination, cleaning mechanisms, parameters affecting the cleaning efficiency, and the environmental impacts of these strategies.

Chapter 2 aims to define a rheological model that can better predict the behavior of foam in flow under different flow conditions modified by the velocity and/or by the geometry of the ducts as the presence of singularities such as a half-sudden expansion or a fence. For this purpose, a detailed characterization of the foam was performed as the bubble size distribution, the static pressure evolution, velocity profiles, thickness of the liquid films at the duct walls, and the wall shear stress (mean and local values). These measurements constituted a database for the validation of the rheological models proposed by a direct comparison between experimentation and the numerical simulation (Computational Fluid Dynamics (CFD) using ANSYS-CFX® software). This CFD work would help to predict the flow behavior of the foam in complex geometrical conditions that could be related to food industry equipment. This will provide the foundation to design in the future some strategies to clean such complex systems by foam flow.

Chapter 3 reports experimental results on the efficiency of wet foam flow to remove *Bacillus* spores and biofilms of three different bacteria species as *Escherichia coli* SS2, *Bacillus cereus* 98/4, and *Pseudomonas fluorescens* Pf1 from stainless steel surfaces under different flow conditions (by velocity and structure of the foam). In parallel, a physical characterization of the chosen foam flow conditions was presented in order to understand and explain the underlying mechanisms involved. Comparison between foam flow cleaning and standard cleaning-in-place (at the same shear stress and using the same surfactant) was performed to test the potential of this novel approach to improve the cleaning efficiency.
Then using SimaPro software we attempted to evaluate the environmental impact of three cleaning processes, foam flow cleaning, CIP using SDS - no heat and CIP using NaOH at 60°C (closer conditions to what could be seen in food industries) by a Life Cycle Assessment study.

Chapter 4 presents my contribution in related topics held through again the two research projects mentioned above, VEG-I-TEC and FEFS. Presented works investigate the role of some

parameters that could affect surface contamination and the subsequent resistance to a cleaning procedure such as (i) to the equipment geometry, materials, and the bacteria species and (ii) the air-liquid-wall interfaces and (iii) the formation of deposits by evaporation of droplets and in all cases. My contribution was mainly devoted to all the cleaning aspects and to modeling activities e.g. the drying phenomenon of droplets.

Finally, we end this work by summarizing the main outcomes of this research. We also propose several avenues to improve the knowledge on the flow of aqueous foams for their use in cleaning-in-place procedures.

References

Abiven, S., Menasseri, S., Chenu, C., 2009. The effects of organic inputs over time on soil aggregate stability – A literature analysis. Soil Biology and Biochemistry 41, 1–12. https://doi.org/10.1016/j.soilbio.2008.09.015

Al Saabi, A., Dallagi, H., Aloui, F., Faille, C., Rauwel, G., Wauquier, L., Bouvier, L., Bénézech, T., 2021. Removal of Bacillus spores from stainless steel pipes by flow foam: Effect of the foam quality and velocity. Journal of Food Engineering 289, 110273. https://doi.org/10.1016/j.jfoodeng.2020.110273

Binks, T., Lye, J.C., Camakaris, J., Burke, R., 2010. Tissue-specific interplay between copper uptake and efflux in Drosophila. J Biol Inorg Chem 15, 621–628. https://doi.org/10.1007/s00775-010-0629-y

Branch, G.B.S.R. and D., Ltd, E.P.C., 1989. Survey of Fire-Fighting Foams and Associated Equipment and Tactics Relevant to the United Kingdom Fire Service: Part 3 - Large Tank Fires. Home Office Scientific Research and Development Branch.

Brodkorb, A., Egger, L., Alminger, M., Alvito, P., Assunção, R., Ballance, S., Bohn, T., Bourlieu-Lacanal, C., Boutrou, R., Carrière, F., Clemente, A., Corredig, M., Dupont, D., Dufour, C., Edwards, C., Golding, M., Karakaya, S., Kirkhus, B., Le Feunteun, S., Lesmes, U., Macierzanka, A., Mackie, A.R., Martins, C., Marze, S., McClements, D.J., Ménard, O., Minekus, M., Portmann, R., Santos, C.N., Souchon, I., Singh, R.P., Vegarud, G.E., Wickham, M.S.J., Weitschies, W., Recio, I., 2019. INFOGEST static in vitro simulation of gastrointestinal food digestion. Nat Protoc 14, 991–1014. https://doi.org/10.1038/s41596-018-0119-1

Cantat, I., Cohen-Addad, S., Elias, F., Graner, F., Höhler, R., Pitois, O., Rouyer, F., Saint-Jalmes, A., 2013. Foams: Structure and Dynamics. Oxford University Press, Oxford. https://doi.org/10.1093/acprof:oso/9780199662890.001.0001

Darling, D.F., Birkett, R.J., 2005. Food Colloids in Practice, in: Dickinson, E. (Ed.), Food Emulsions and Foams, Woodhead Publishing Series in Food Science, Technology and Nutrition. Woodhead Publishing, pp. 1–29. https://doi.org/10.1533/9781845698300.1

Dickinson, E., Ettelaie, R., Kostakis, T., Murray, B.S., 2004. Factors Controlling the Formation and Stability of Air Bubbles Stabilized by Partially Hydrophobic Silica Nanoparticles. Langmuir 20, 8517–8525. https://doi.org/10.1021/la048913k

Le Toquin, E., Faure, S., Orange, N., Gas, F., 2020. New Biocide Foam Containing Hydrogen Peroxide for the Decontamination of Vertical Surface Contaminated With Bacillus thuringiensis Spores. Frontiers in Microbiology 9. https://doi.org/10.3389/fmicb.2018.02295

Lehmonen, J., Jetsu, P., Kinnunen, K., Hjelt, T., 2013. Potential of foam-laid forming technology in paper applications. Nordic Pulp & Paper Research Journal 28, 392–398. https://doi.org/10.3183/npprj-2013-28-03-p392-398

Ratzer, A.F., 1956. History and Development of Foam as a Fire Extinguishing Medium. Ind. Eng. Chem. 48, 2013–2016. https://doi.org/10.1021/ie50563a030

Schramm, L.L. (Ed.), 2000. Surfactants: fundamentals and applications in the petroleum industry. Cambridge University Press, Cambridge, U.K. ; New York.

Tanaka, A., Hjelt, T., Sneck, A., Korpela, A., 2012. Fractionation of Nanocellulose by Foam Filter. Separation Science and Technology 47, 1771–1776. https://doi.org/10.1080/01496395.2012.661825

Toquin, E.L., 2018. Mode d'action biocide de nouveaux procédés de décontamination sur deux formes de résistances bactériennes (phdthesis). Normandie Université.

Vinogradov, A.V., Kuprin, D.S., Abduragimov, I.M., Kuprin, G.N., Serebriyakov, E., Vinogradov, V.V., 2016. Silica Foams for Fire Prevention and Firefighting. ACS Appl. Mater. Interfaces 8, 294–301. https://doi.org/10.1021/acsami.5b08653

CHAPTER 1: LITERATURE REVIEW

Contents

I. Foam structure

I.1 Foam production

The foam is generated when a large number of bubbles are formed in the continuous phase. Two distinct methods allow the creation of foam: dispersal and aggregation. In the dispersal method, the dispersed phase is directly introduced as bubbles into the solution containing surface-active agents. The gas is dispersed by agitation, insulation, or through a static contactor (porous medium, allowing the mixture of liquid and gas) (Boissonnet, 1998). Foams appear when a foaming solution, such as dishwashing liquid or shampoo, is vigorously stirred (Shafi et al., 1997). In the aggregation method, bubbles form by gathering gas molecules previously dissolved in the pressurized surfactant solution (Niranjan and Silva, 2008). When the dissolved gas becomes insoluble, due to a pressure drop for example, it condenses, and foam is created. Shaving foam, beer, and champagne foam or foam formed by a boiling liquid are part of this type of formation (Shafi et al., 1997).

I.2 Morphology of foam

Foams are fluids characterized by the dispersion of a discontinuous gas phase in a water phase whose continuity is ensured by the presence of liquid films that can be partially thick (wet foams) or thin (dry foams). The intersection of liquid films between bubbles forms a network of channels called lamella that intersect at the Plateau borders (Plateau, 1873; Princen, 1983). According to (Plateau, 1873) the formed liquid films tend to create a minimal surface area due to interfacial tension, which causes a reduction in Gibbs energy. He cited two rules that drive the morphology of foam and their conditions of balance (Figure 1):

- Three liquid films meet in an edge, making angles of 120 degrees
- The peaks are formed by the intersection of four edges, which form equal angles (θ) such as $\cos(\theta) = -\frac{1}{3} = 109\ degrees$ (Maraldi angles).

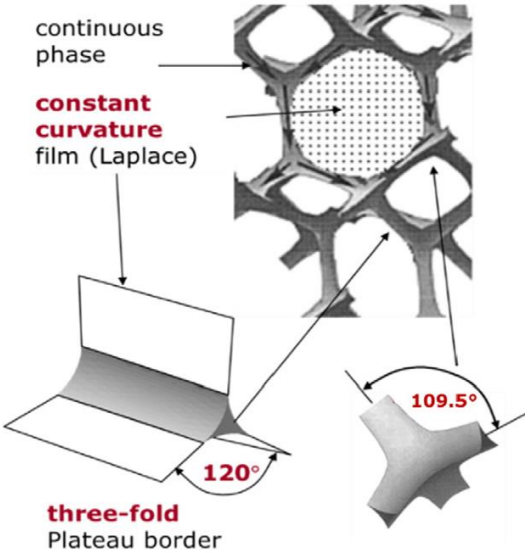

Figure 1. Plateau's law and the Young – Laplace law, govern the topology and geometry of foams in the dry limit. (The images are results of Surface Evolver simulations (Brakke, 1992)).

For the assessment of the fraction of gas in the dispersed phase, the concept of void fraction (Φ) expressed by the following relationship is used:

$$\Phi = \frac{V_G}{V_G+V_L} \quad (1)$$

Where V_G and V_L represent the volume of gas and liquid in the foam, respectively.

The quality of the foam (β) is a parameter indicating the volume of gas contained in a foam that can be expressed through the following relationship:

$$\beta = \frac{Q_G}{Q_G+Q_L} \quad (2)$$

Where Q_G and Q_L represent the flow rate in the foam of gas and liquid, respectively.

Depending on the relative amount of liquid and air in the foams, they are classified as bubbly liquid, wet foam or dry foam. When the liquid fraction is greater than 0.36, the bubbles are not in contact which each other and are perfectly spherical (Weaire and Hutzler, 1999). This condition is called bubbly liquid (Figure 2). When the liquid fraction decreases, the bubbles come into contact and are eventually only separated by a thin liquid film. Under these conditions, bubbles deform to reduce their surface energy. The foam is then said wet foam. The critical value for which foam switches from a bully liquid to a wet foam is a unique to each foam.
If the volume liquid fraction (ϕ_L) is further reduced to $\phi_L < 0.1$, the foam becomes dry. The bubbles are completely deformed because of the small amount of liquid and organize themselves geometrically into polyhedral to ensure stacking with minimal surface energy.

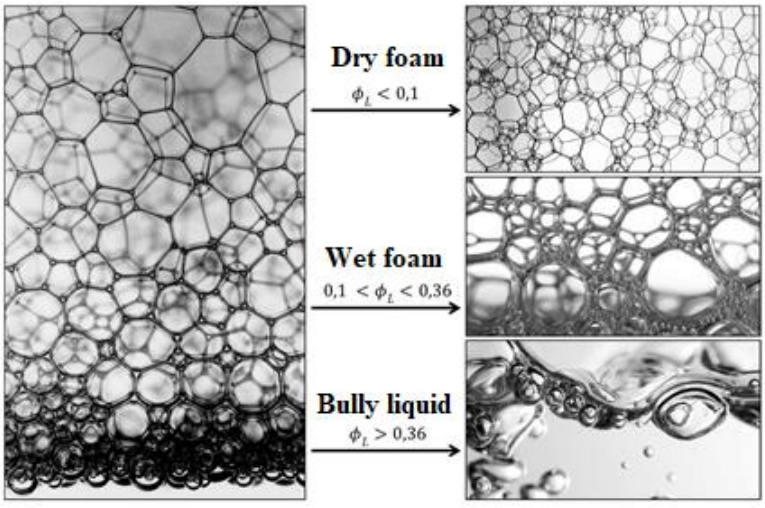

Figure 2. Illustration of foam with a fraction gradient of liquid volume (Mouquet, 2018).

For the transition from wet foam to dry foam, it is difficult based on the literature to define a universal criterion, e.g. gas fractions of 90% (Bhakta and Ruckenstein, 1995) or 95% (Hutzler et al., 1998) were proposed as a transition criterion. Other authors show that this transitional boundary would evolve due to the forces of gravity, and capillary forces, and the relative

movement of the fluids that make up it, which depend on several variables such as the size of the bubbles, temperature, pressure or the nature of fluids (Höhler and Cohen-Addad, 2005; Saint-Jalmes and Durian, 1999).

I.3 Surfactants

Surfactants are molecules composed of a hydrophilic head that can be formed by one or more ion or non-ionic polar groups (which leak water) and of a lipophilic tail made up of hydrocarbon chains (which have a strong affinity to water) (Figure 3).

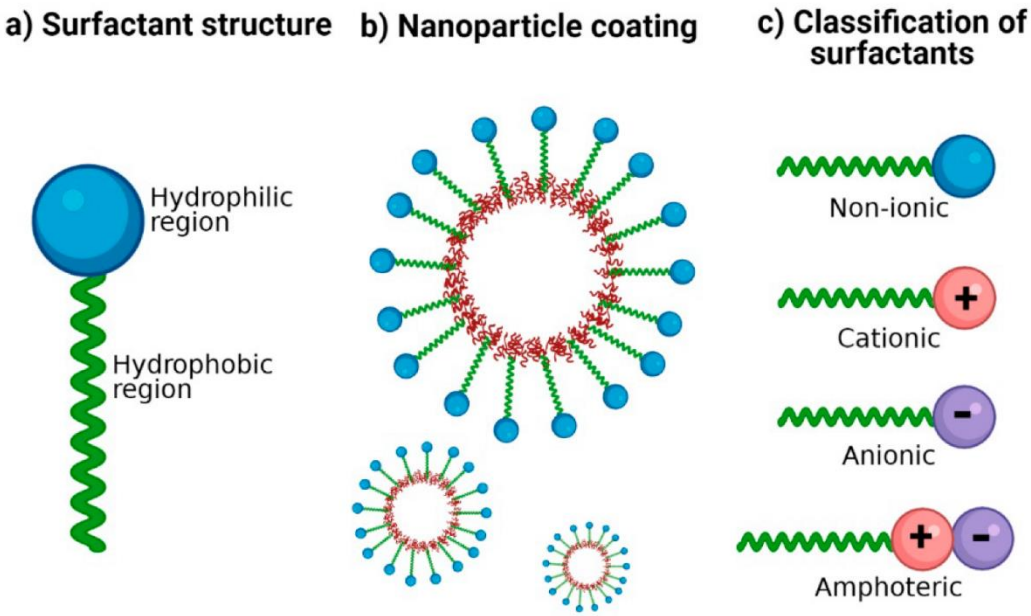

Figure 3. Diagram of the structure of surfactant molecule.

For a bubble formed from a liquid without surfactants, Van Der Waals interactions and surface tension allow the connection between the two water-to-air interfaces that will burst the bubble. It is therefore necessary to introduce a repulsive force between the two interfaces and to reduce the surface tension of the liquid to make it more deformable. This is the role of surfactant (Narchi, 2008). The reduction in surface tension can be expressed by surface pressure (Π) as follows:

$$\Pi = \gamma_0 - \gamma \qquad (3)$$

where γ_0 is the surface tension of pure water at 20°C. Surfactants have been used as foaming and stabilizing agents for decades (AlQuaimi and Rossen, 2019). In foams stabilized with a surface-active agent, gas bubbles are prevented from coalescing by adsorption of surfactant molecules at the gas-liquid interface (Bournival et al., 2014). However, they cannot maintain their stability for long due to e.g. high salinity, or variable temperatures (Singh and Mohanty, 2016). These authors have shown that hydrophilic nanoparticles have infinite potential to increase the robustness of surfactant-stabilized foams in various applications.

Since the molecules of surfactant are constituted of a hydrophilic part and a lipophilic part, they can position themselves at the interfaces, so that the hydrophilic part orients itself towards the

water and the lipophilic part towards in our case the air phase. Stretching the latter generates a gradient of surface tension responsible for a movement of water from areas that are not stretched in the stretched area. This phenomenon, called adsorption, appears at liquid-liquid, liquid-solid, and liquid-gas interfaces, and causes a decrease in surface tension between the two phases. According to Gibbs' law, surface tension decreases when the concentration of surfactants sits at the interface increases, and when this interface is saturated, the surface tension is minimal and constant (Figure 4). From this concentration, called Critical Micellar Concentration (CMC), the surplus molecules self-assemble into a solution in the form of aggregates called micelles (Nitschke and Costa, 2007).

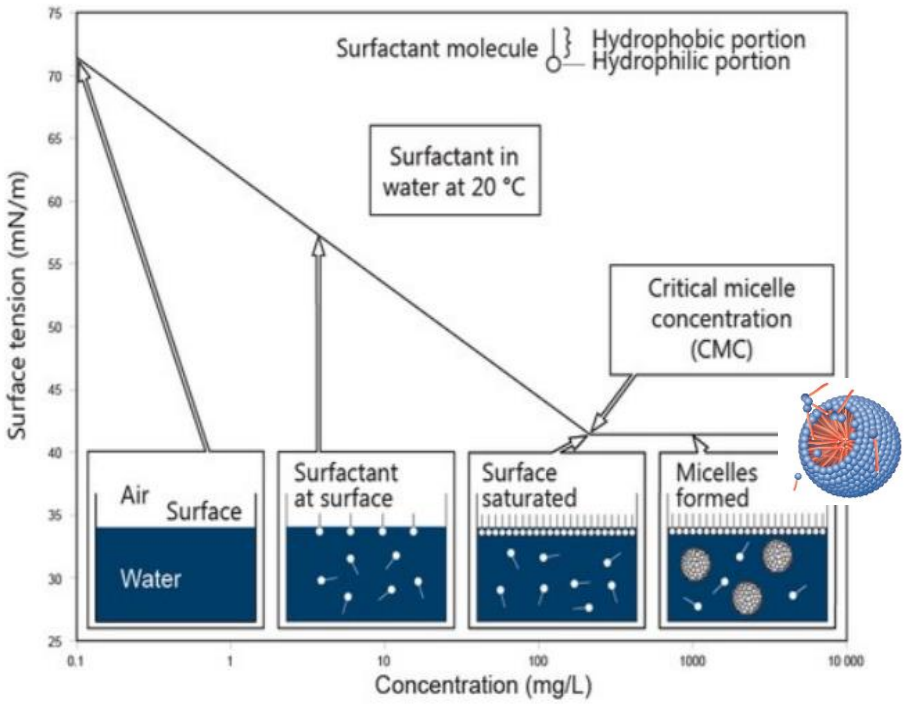

Figure 4. Evolution of surface tension based on surfactant concentration.

I.4 Size distribution of bubbles

The study of the bubble size distribution is essential to characterize the foam structure and understand its stability and flow. Several methods are used for determining the shape and size of the foam: the optical method, the sonic method, the photographic method, and the optical tomography (Hanselmann and Windhab, 1998; Sarma and Khilar, 1988).

The bubble size distribution depends on different parameters, such as the foam quality (exponential increase with this parameter (Pang et al., 2018)), surfactant type (Evgenidis et al., 2010; Gupta et al., 2007), concentration of the surfactant (Petkova et al., 2020), temperature (Thakore et al., 2021) and pressure (Rand and Kraynik, 1983). Osmotic pressure is described as the average force per unit zone needed to counter the increasing bubble-bubble repulsion, as they are squeezed together.

$$\Pi = -\left(\frac{\partial E}{\partial V}\right)_{Vg} \quad (4)$$

where E is the total surface energy as $E = \gamma S$, and V is the total foam volume.

If we have a look in works considering bubble column (Besagni and Inzoli, 2017), it could be of help in understanding the effect of the coalescence phenomena. Indeed, when the prevailing bubble size distribution shifts to larger bubbles, due to the promoted coalescence (i.e., high viscous liquid phases), the lift force pushes the larger bubbles to the center of the bubble column, and induce "coalescence-induced bubbles" and, consequently, destabilize the homogeneous flow regime. However, when the prevailing bubble size distribution shifts towards smaller bubbles, because of the reduced coalescence (i.e., organic and inorganic active compounds, and low viscous liquid phases), the lift force pushes the small bubbles to the wall, inducing cluster of bubbles and, therefore, stabilizing the homogeneous flow regime.
However, there are very few results on foam behavior under high static pressure. The stability of a static foam under high pressure has been studied by (Rand and Kraynik, 1983). They measured the drainage velocity of an aqueous foam formed under pressure (1 to 20 bar) in an autoclave. Their results showed that drainage time did increase a lot with pressure; the explication for this enhanced stability is a diminution of the bubble size, measured with microphotography (Figure 5).

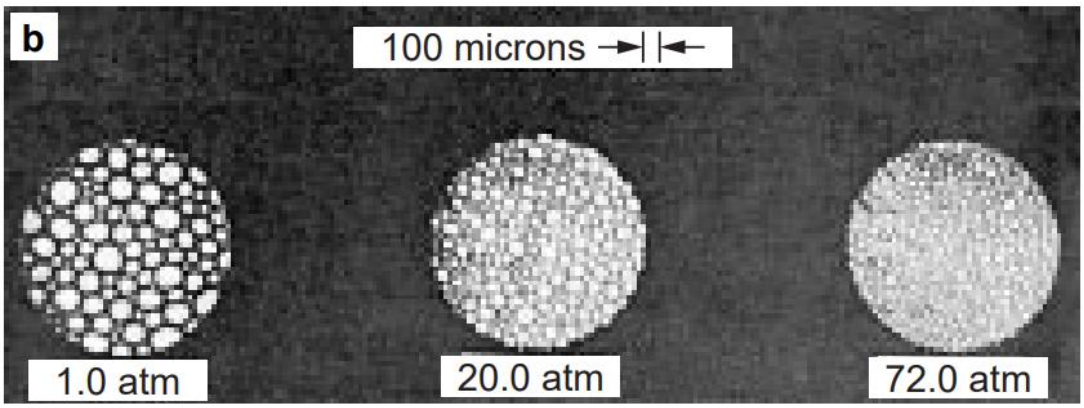

Figure 5. Effect of pressure on drainage time and bubbles size (from (Rand and Kraynik, 1983)).

The concentration of surfactants plays a significant role in the stability and foaming ability of the system (Petkova et al., 2020). The higher the concentration, the more stable is the foam (Egea, 2014; Xu et al., 2020). With the increase in the concentration of surfactants the bubbles are more uniform with a higher degree of contact with each other without obvious coalescence (Argillier et al., 2009; Eftekhari and Farajzadeh, 2017). In the same time, the average diameter of the bubbles decreases, and the maximum frequency of distribution of the bubbles is constant (Figure 6).

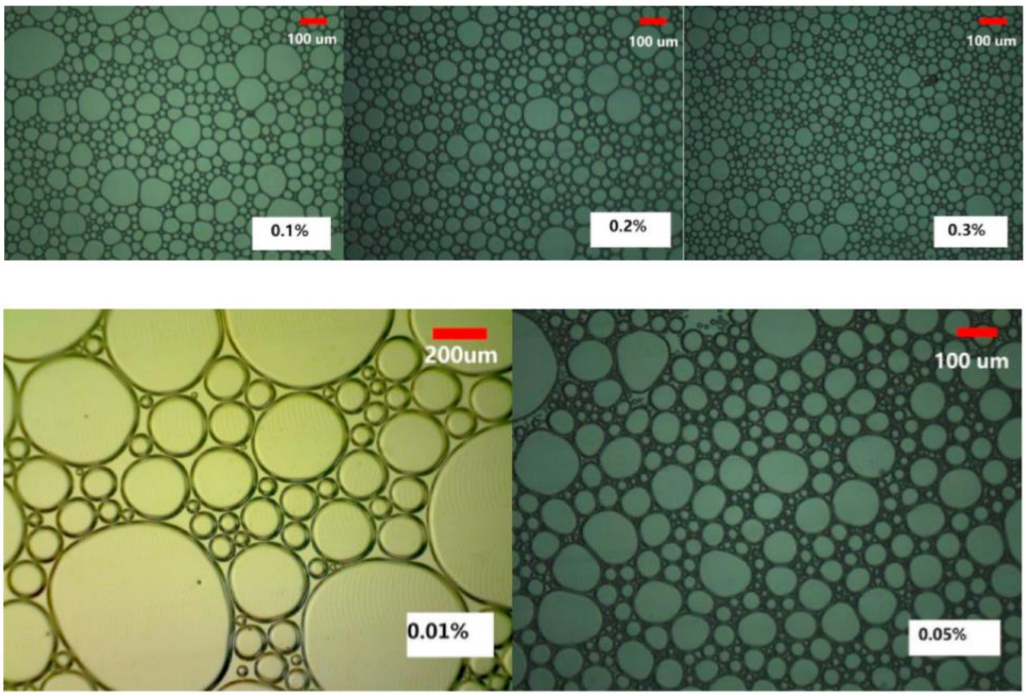

Figure 6. Role of surfactants concentration (from (Li et al., 2019)).

A high viscosity of a surfactant may also influence its stability by slowing down liquid drainage of the Plateau's borders and, therefore, causing a strong resistance while thinning or thickening of the liquid films. The slats and Plateau boundaries created by this combination of surfactants were supposed to be thicker than other surfactants with lower viscosity (Osei-Bonsu et al., 2015).

I.5 Stability of foam

Foam can be easily established and disappear in a few moments. It is well known that it is intrinsically unstable because it constitutes a mixture of two non-miscible phases whose density masses and viscosities are very different and which are thermodynamically unstable (Dickinson, 1992).

For example, the elements defining its structure may increase over time, such as the thickness of the liquid film accentuating the drainage and leading to a rupture, causing the bubbles to coalescence (Bhakta and Ruckenstein, 1997). Gravity may promote fluid drainage (Carrier and Colin, 2003) and even the gas can also diffuse from smaller to larger bubbles thanks to the ripening of Ostwald (Louvet et al., 2009) (Figure 7). Controlling the stability of foams at an industrial level is therefore a crucial point (Kapetas et al., 2016; Pal, 1996).

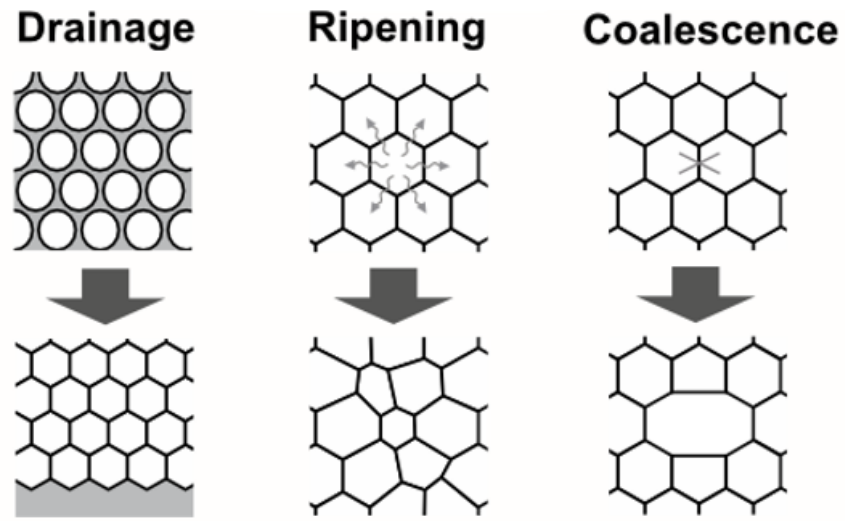

Figure 7. Schema of the three foam destabilization mechanisms (Bikerman, 1973).

To be more precise, drainage is the flow under the effect of capillarity and the gravity of the liquid present in the films, it tends to dry the foams upwards by decreasing the volume fraction of the liquid as one rise considering a foam column (Figure 8). Foams made up of the larger bubbles drain more, they have larger cross-sectional areas at the Plateau borders (for the same humidity of the foam); therefore, under gravity, it empties more quickly (Bikerman, 1973; Guillerme et al., 1993). The amount of liquid draining through the channel is influenced by the cross-distribution of the velocity of foam bubbles (Zdankus et al., 2018).
In order to limit the foam drainage, it is possible to:

- increase the viscosity of the solution by using liquids such as glycerin or by significantly lowering the temperature of the solution,
- create as thin foam as possible to reduce the size of the edges of the Plateau borders where the flow takes place,
- limit or cancel gravity. This can be done by applying a force opposite to gravity, such as a magnetic field directed upwards to the foaming solution.

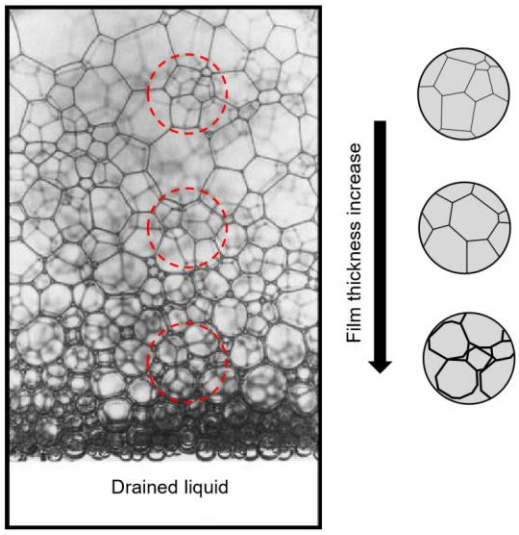

Figure 8. Foam drainage is caused by gravity and capillary forces, which results in a polyhedral shape of the bubbles (dry foam (Saint-Jalmes and Durian, 1999)).

I.6 Foam flow and wall sliding

Experimental measurements by Particle Image Velocimetry as numerical simulation (CFD) highlighted the behavior of foam flowing in a horizontal linear pipe of square section (Blondin and Doubliez, 2002; Tisné et al., 2003). They revealed that depending on the Reynolds number or the foam velocity (for a pipe section of 21 mm^2), the foam could flow in three different regimes (Figure 9):

- A one-dimensional regime corresponding to an average velocity (U_{mean} = 2 cm s^{-1}), whose velocity vectors have only one uniform axial component in the flow direction:

$$\vec{u} = u\,\overrightarrow{e_z} = cte\ \ \overrightarrow{e_z} \quad (5)$$

- A two-dimensional regime corresponding to an intermediate velocity (U_{mean} = 4 cm s^{-1}), whose velocity vector has an axial component that depends only on the vertical coordinate (y):

$$\vec{u} = u\,(y)\,\overrightarrow{e_z} \quad (6)$$

- A three-dimensional regime corresponding to an average velocity (U_{mean} = 6 cm s^{-1}), whose axial component depends on the horizontal (x), and vertical coordinates (y):

$$\vec{u} = u\,(x,y)\,\overrightarrow{e_z} \quad (7)$$

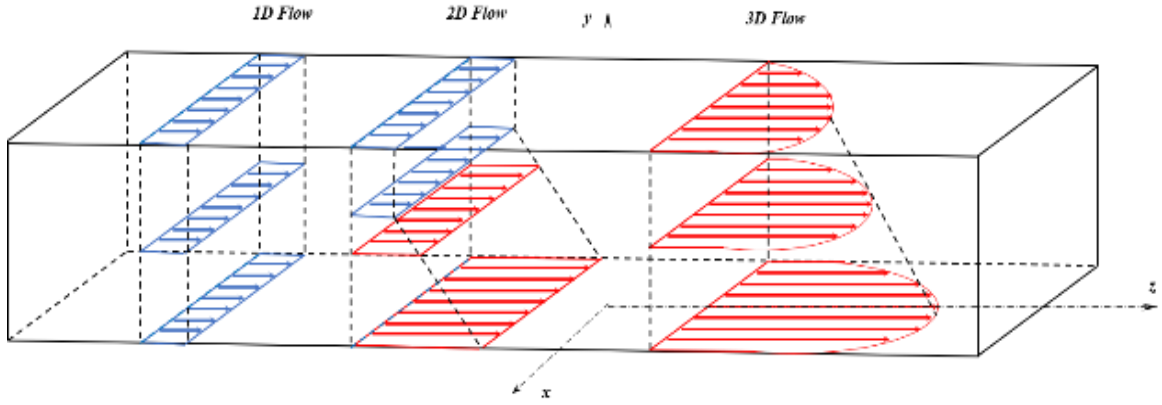

Figure 9. Foam flow regimes.

In 1922, Bingham found that when a suspension flows over a smooth surface, there is "a lack of adhesion between the material and the shearing surface. This causes a layer of liquid to develop between the shear surface and the main body of the suspension" (Bingham, 1924). The rheological studies of foams are based on the existence of a sliding layer near the wall. Indeed, near a smooth solid wall, the migration of bubbles generates a layer rich in liquid, which gives the effect of a slip between the foam and the wall (Figure 10). The rheological studies of foams are based on the existence of a sliding layer near the wall. Indeed, near a smooth solid wall, the migration of bubbles generates a liquid layer, which enables the sliding of the foam and the wall (Figure 10). This layer performs the role of a lubricating layer of pure liquid separating the foam and the surface. It is therefore called the slip layer: it is a few micrometers in thickness at the top side and up to millimeters at the bottom side of the duct. This wall sliding is a surface phenomenon and is therefore sensitive to the roughness, the pipe diameter, the surfactant concentration, the concentration of the dispersed phase, the bubble size distribution, and the viscosity of the liquid phase (Marchand et al., 2020).

This slip layer was first observed in foam flow by (Miller and Wenzel, 1985) using a rotary rheometer. The authors considered the flow of foam as a combination of two phenomena: the shear in the middle of the foam and the slip of the foam on a liquid film flowing at the wall. For the most commonly used forms, different methods have been developed to determine the average flow velocity (Enzendorfer et al., 1995; Jastrzebski, 1967). The latter showed that the slip velocity not only depends on the wall shear stress but also on the pipe diameter. According to these authors, the slip velocity can be described as:

$$U_{slip} = \frac{b_c}{D_h}\,\tau_w \tag{8}$$

where D_h is the equivalent or hydraulic diameter of the pipe and b_c is the modified slip coefficient. The slip velocity can be directly related to the layer thickness δ. As the layer thickness increases, so does the velocity.

$$\delta = 3.7 \cdot 10^{-4}\, {U_{slip}}^{1-\beta} \tag{9}$$

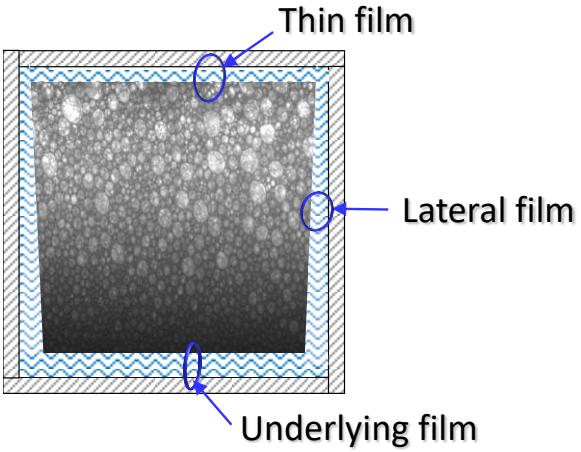

Figure 10. Liquid films.

II. Foam rheology

Foams exhibit unpredicted and non-linear rheological behavior as it is influenced by both liquid and gas properties. The complexity of the interactions and processes that are involved have positioned foam as a major subject of current research (Singh and Mohanty, 2016; Tanaka et al., 2012). Rheology is the science that focuses on the deformations of matter and looks for links between the stresses imposed and the deformations induced (Oswald et al., 2005). The most common techniques used in the experimental study of foam rheology are based on the use of rotary rheometers. They allow highlighting parameters such as the yield stress and the viscosity of the foam.

II.1 Dynamic behavior

The rheological properties of foams, such as elasticity, plasticity, and viscosity, have a major impact on the production, transport, and applications of foam. They are complex, not only

because the elastic and viscous responses are nonlinear functions with the applied stress, but also because of the variation in the local shear stress generated during a deformation.
Eventually, foam can be viscous, elastic, or plastic, depending on the perturbation that is being imposed on it. Certainly, from one foam to another, the specific properties change. One type of foam is rigid, another tolerates greater deformation, and another foam will break if we try to deform it too quickly. These differences come from the proportion of liquid, or the distribution of bubble sizes. Fundamentally, its behavior is related to its structure, more precisely to its nature as a cellular material (Cheddadi et al., 2015).
It has been shown (Princen, 1985) that the continuous shearing of a two dimensional (2D) foam leads to its flow according to a local process of rearrangement of neighboring bubbles that is called T1. The bubbles deform appropriately, overlap to change places, and then fall into a new configuration where some bubbles are moving apart while others are moving together. This is illustrated by the following figure (Figure 11):

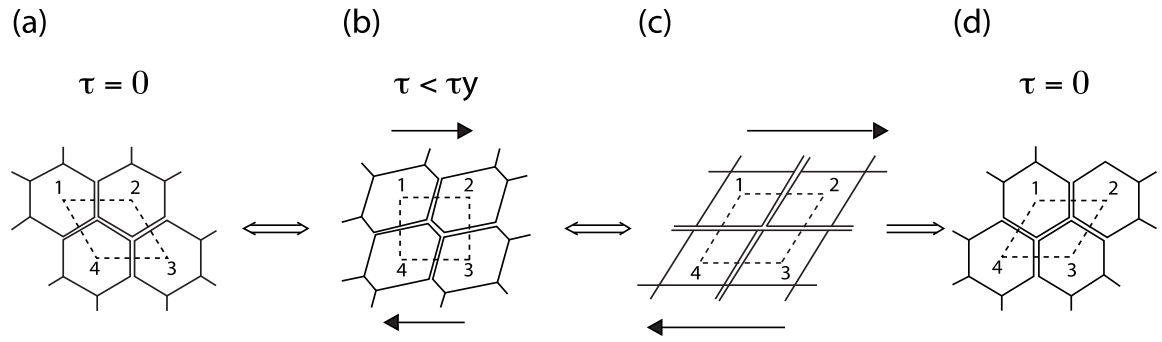

Figure 11. Topological rearrangement T1: Foam yielding and plastic deformation, under applied shear stress, increasing from (a) to (c). This structure can relax either elastically, by returning to structure (a), or by a bubble rearrangement, leading to structure (d) (inspired from (Princen, 1985)).

These images illustrate a change of neighboring bubbles. The two bubbles 2 and 4, which were in contact, move apart, while the two other bubbles 1 and 3 get closer and become neighbors. This change of neighbors is called topological rearrangement T1, passing through an intermediate step (in the center) where the four bubbles share a common vertex. These images were obtained with a 2D foam, located between two glass plates separated by 2 mm (Princen, 1985).

A foam can deform only when it is subjected to stress. However, before flowing, several structural changes can be observed:

- At low strains, the interfaces are slightly stressed, the deformation are reversible, and the stress required to deform the interfaces is proportional to the deformation applied. The foam is then characterized by the response of a solid. In this regime, foams behave like shear-thinning fluids, with their effective viscosity decreasing as a function of shear rate (Weaire, 2008).

- When the deformation increases, without generalizing to the whole foam, T1 reorganizations start to occur. The energy in the interfaces is partially relaxed and dissipated, this is the irreversible plastic deformation. The macroscopic stress necessary for the deformation of the foam continues to increase.
- When the foam deformation is large enough to separate neighboring bubbles, and reaches the yield stress τy, a steady shear flow occurs, and the bubbles slide along each other. The T1 process generalizes throughout the foam leading to a local shear flow of liquid within the foam films, resulting in energy dissipation. The foam flows like a non-Newtonian viscous fluid (Höhler and Cohen-Addad, 2005).

The stress reaches its maximum at the start of macroscopic flow and then it eventually decreases before becoming constant (Figure 11). This maximum stress is called the yield stress τ_y (Kröger and Vermant, 2000). Indeed, for a given shear rate, the stress required to get the material to flow is greater than this yield stress value. Simulations on 2D aqueous foams have put forward two hypotheses to explain this phenomenon: the initial orientation of the films in a direction other than that of the flow (Raufaste et al., 2010), which is not sufficient to explain the importance of overshoots (peak of the stress), and the effects of interfacial dissipation which can retard the beginning of T1 rearrangements (Rouyer et al., 2003).

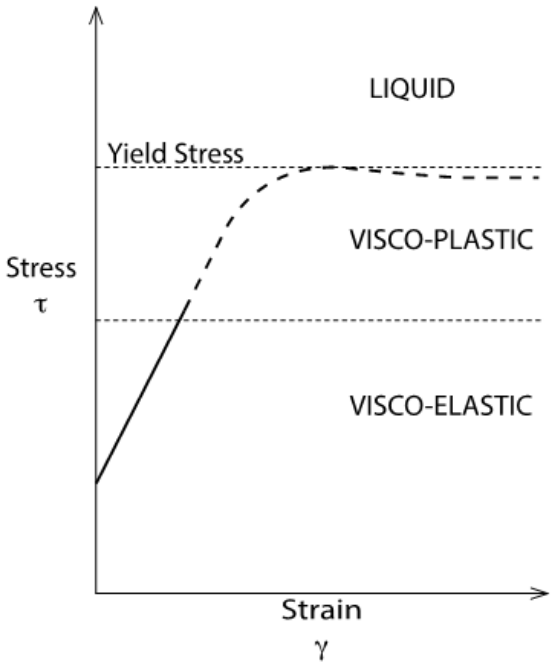

Figure 12. Schematic representation of the relationship between the shear and the strain for aqueous foam.

Thanks to experiments on emulsions, whose rheological properties are the same as for foams, the following semi-empirical equation of the threshold stress has been proposed (Mason et al., 1996):

$$\tau_y = \beta \frac{\gamma}{R} (\Phi - \Phi_c)^2 \quad (10)$$

Where β is the foam quality, γ is the surface tension, Φ is the volume fraction and R is the average bubble radius. This correlation attests to the importance of the interfaces, by their proportionality with γ/R and its dependence on the volume fraction Φ as illustrated in Figure 13 below. This yield stress is maximal for dry foams and zeroes at the blocking transition for the volume fraction of gas Φ_c (=0.64).

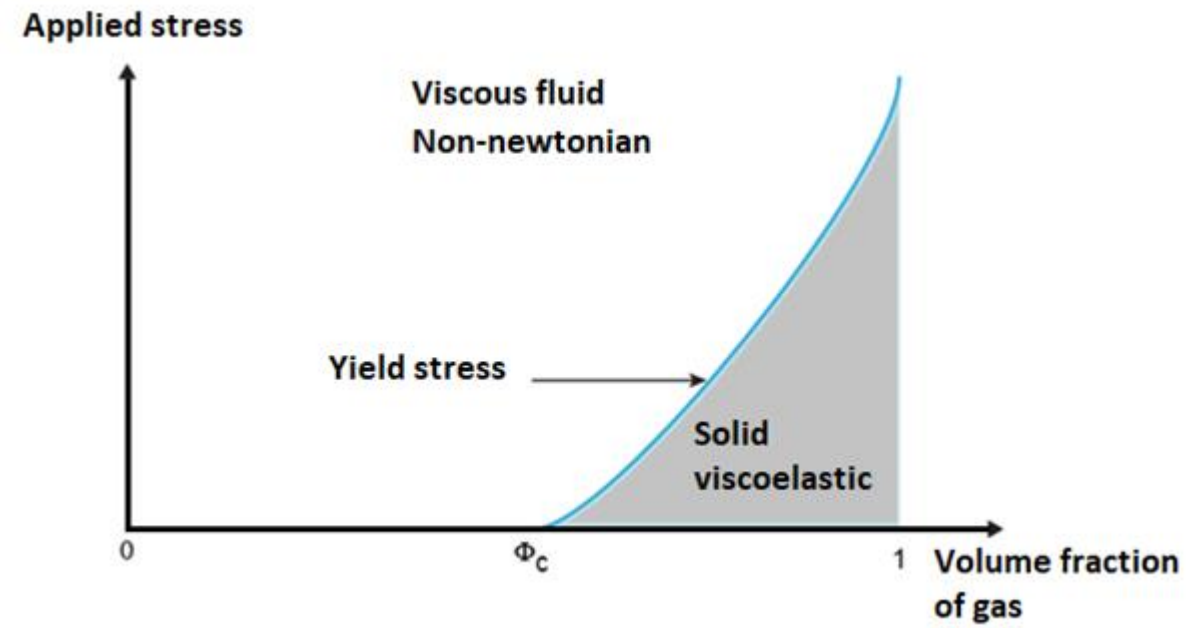

Figure 13. Schematic representation of the liquid and solid mechanical behavior of foam (Höhler and Cohen-Addad, 2005).

II.2 Linear Viscoelasticity

Foam is considered as a viscoelastic fluid with an intrinsic elasticity and viscosity. Its response to deformation is not entirely elastic but involves a dissipation phenomenon of multiple origins. The energy dissipation can be due to the viscosity of the interstitial fluid or to the properties of the surfactants (viscosity and diffusivity) (Buzza et al., 1995; Cantat, 2011). Moreover, it has been shown that dissipation during foam sliding probably has three different origins (Huerre et al., 2014) : the viscosity of the interstitial fluid in liquid foams, friction at the liquid-air interface, and the friction of the Plateau borders in the case of dry foams. The aqueous foam, therefore, exhibits many relaxation times specific to the dissipation mechanisms, which can be observed by changing the degree of deformation applied. Viscosity influences the strength of the foam structure at the Plateau edges and inter-bubble films. Also, a high viscosity limits the thinning of the liquid films allowing them to be stabilized in the long term. Moreover, it plays a role in the drainage speed which decreases when the viscosity increases (Briceño et al., 2001).

II.3 Linear Elasticity

Linear elasticity is a change in stress proportional to the strain applied to the foam. In the linear regime, the bubbles are deformed, but the applied strain is too small to change their collapsing topologies. The specific surface of the foam increases with the applied stress, as does the volume density of the surface energy of the bubbles. The elastic response of the foams comes

from the elasticity of the liquid films and the elasticity of the interfaces with bubbles. Indeed, the liquid films in the foam are characterized by their ability to withstand mechanical stresses lower than the twice value of their surface tensions. Consequently, for low shear stresses (below the yield stress) the films at the Plateau borders remain in static mechanical equilibrium, and the bubbles become trapped in their initial structures which retards the beginning of T1 rearrangement. The Gibbs elasticity E_{Gibbs} of the interface of the bubbles corresponds to the response of the interfacial tension γ to a relative increase of a surface A (Guignot, 2008; Langevin, 2014).

$$E_{Gibbs} = \frac{d\gamma}{dLnA} \tag{11}$$

The Gibbs elasticity is measurable for deformations far below the yield stress τ_y. The elastic modulus depends on the number of interfaces stressed during deformation and thus depends on ϕ and γR (Princen, 1983). Kraynik simulations proposed an expression for the elastic modulus when $\Phi \rightarrow 1$: $G = 0.5\ \gamma R$; an expression that is confirmed by extrapolations of experimental data by (Princen, 1983)) and (Mason et al., 1996), on aqueous foams and emulsions, respectively. The proposed semi-empirical expression for the elastic modulus is :

$$G = \alpha\ \frac{\gamma}{R}\ \Phi(\Phi - \Phi_c) \tag{12}$$

With α = 1.4 when the foams are monodispersed and α = 1.6 when the foams are polydisperse.

II.4 Foam rheology models

Newtonian fluid is defined as a fluid whose viscosity depends neither on its shear rate nor on the time during which the liquid is sheared. The characteristic relationship that depends on the properties and nature of the material:

$$\boldsymbol{\tau_{ij} = f(\dot{\gamma}_{ij})} \tag{13}$$

where $\boldsymbol{\dot{\gamma}_{ij}}$ is the strain rate tensor.

However, For the non-Newtonian fluids, the viscosity is not constant but depends on the shear rate. It can define as:

$$\boldsymbol{\tau_{ij} = \mu_{app}\ \dot{\gamma}_{ij}} \tag{14}$$

The foam flow can behave like a non-Newtonian fluid. It can be characterized by a viscoelastic behavior law (Ostwald type fluid) or by the possible existence of a yield stress (Herschel-Bulkley or Bingham type fluid). These models consider the foam as a continuous fluid by assuming a shear in the middle of the fluid. They are expressed by the following relations:

<u>Ostwald de Weale: Power-law model</u>

$$\boldsymbol{\tau = k\dot{\gamma}^n} \tag{15}$$

$$\boldsymbol{\mu = k(\lambda\dot{\gamma})^{n-1}} \tag{16}$$

Bingham

$$\begin{cases} \boldsymbol{\tau} \leq \boldsymbol{\tau_y} \; ; \; \mu \rightarrow \infty \\ \boldsymbol{\tau} \geq \boldsymbol{\tau_y} \; ; \; \boldsymbol{\tau} = \boldsymbol{\tau_y} + \boldsymbol{k}.\dot{\boldsymbol{\gamma}} \end{cases} \quad (17)$$

Herschel-Bulkley

$$\frac{\partial \boldsymbol{\tau}}{\partial \dot{\boldsymbol{\gamma}}} = \boldsymbol{n}.\boldsymbol{k}.\dot{\boldsymbol{\gamma}}^{\boldsymbol{n-1}} \quad (18)$$

$$\mu = \frac{\boldsymbol{\tau_0}}{\boldsymbol{\lambda}\dot{\boldsymbol{\gamma}}} + \boldsymbol{k}(\boldsymbol{\lambda}\dot{\boldsymbol{\gamma}})^{\boldsymbol{n-1}} \quad (19)$$

Model of Bird Carreau

$$\boldsymbol{\mu} = \boldsymbol{\mu}_{\infty} + \frac{\boldsymbol{\mu_0} - \boldsymbol{\mu}_{\infty}}{(\mathbf{1}+(\boldsymbol{\lambda}\dot{\boldsymbol{\gamma}})^{\mathbf{2}})^{\frac{\mathbf{1}-\boldsymbol{n}}{\mathbf{2}}}} \quad (20)$$

With

-μ_0 is the viscosity for a zero-shear rate

-μ_∞ is the asymptotic viscosity for a very high shear rate

Model parameters for a Newtonian fluid are $\mu = \mu_0$, n = 1, or $\lambda = 0$.
Three variables are involved in these models, the yield stress τ_y, the consistency index k, and the fluid behavior index n.

II.5 Yield stress τy

It was found that the complex structure of the foam gives it a higher shear strength than that of a homogeneous fluid, which is interpretable by the existence of a yield stress $\boldsymbol{\tau_y}$, beyond which the flow starts (Camp, 1998) Indeed, when foam is subjected to an increasing shear deformation, it presents a transition between a solid type behavior and a fluid type behavior, called "yielding" which is characterized by the threshold stress (Kröger and Vermant, 2000). Therefore, the foams require a minimum amount of energy to be able to flow. This energy is represented by a threshold stress $\boldsymbol{\tau_y}$ which depends mainly on the mean diameter, void fraction Φ, and surface tension γ. The value of the threshold stress becomes zero for a critical void fraction Φ_c and is further affected by the viscosity of the liquid. In contrast, dry foams are characterized by $\phi > 0.64$, and in this case, the values of the yield stress and the elastic modulus are in the same range (Höhler and Cohen-Addad, 2005) showed that dry foams are characterized by $\phi > 0.64$, and in this case, the values of the yield stress and the elastic modulus are in the same range. Other authors have studied the influence of this void fraction on the texture and morphology of flowing foams in pipes. They have shown that the yield stress increases with the volume fraction of the dispersed phase (Princen, 1983). For this reason, some laws appear necessary to relate the rheological parameters to the volume fraction of injected gas (Reidenbach et al., 1986).

$$\tau_y = 7 \cdot 10^{-2}\phi \qquad if\ \phi \leq 0.6 \quad (21)$$

$$\tau_y = 2 \cdot 10^{-4} exp(9\phi) \qquad if\ \phi > 0.6 \quad (22)$$

$$k = 2 \cdot 10^{-4} exp(3.6\phi + 0.75\phi) \quad (23)$$

Other studies have related this parameter to the bubble diameter. Using a rotary rheometer, it has been shown that the yield stress increases as the bubble diameter decreases. The relationship established is due to the following (Miller and Wenzel, 1985):

$$\tau_C = 5.2\overline{d_b}^{-0.648} \quad (24)$$

II.6 Fluid behavior index n

This index represents the viscous non-perfection of the fluid compared to a Newtonian fluid (Latifi et al., 1989). Generally, depending on the value of n, three main cases can occur (Figure. 14):

- if n = 1, μapp = μ and the fluid behaves like a Newtonian fluid.
- if n > 1, the apparent viscosity increases as the velocity gradient increases. The fluid is dilatant or shear-thickening.
- if n < 1, the fluid has a pseudo-plastic behavior, the apparent (effective) viscosity decreases when the velocity gradient (the stress) increases. The fluid is said to be shear-thinning.

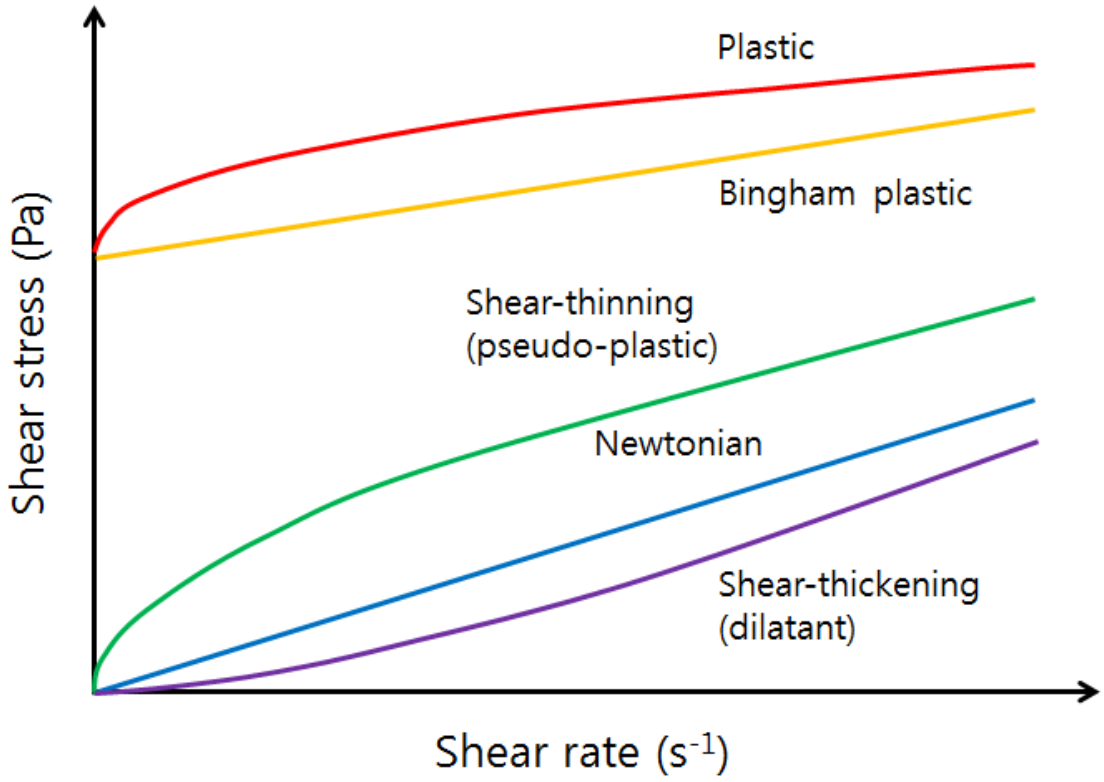

Figure 14. Shear in non-Newtonian fluids.

Aqueous foams could be considered as shear-thinning fluids since the index n is lower than 1. The origin of this behavior of foam is attributed to the viscous dissipation in the films. The liquid is sheared into the films with a local shear rate. As the macroscopic shear rate increases, the thickness of the films increases (Denkov et al., 2005), which leads to a reduction in the dissipative phenomena with the shear rate. Experiments using sheared foams have shown that

the viscous friction within the foam also depends strongly on the surface mobility of the bubbles. The rheology behavior of dry foam (air volume fraction of 0.90) was very well described by the Herschel-Bulkley model with power-law index n ranged from 0.24 to 0.02 and from 0.42 to 0.02 for tangentially immobile and tangentially mobile bubble surfaces, respectively (Princen, 1985, 1983; Princen and Kiss, 1989). The reasons behind the different values of the index n are not clear at this time, and further experimental and numerical studies are needed to better understand the viscous friction within these systems and define a rheological model that predicts the behavior of foams.

II.7 Viscous dissipation in regularly sheared foams

Experimental studies and theoretical modeling of foams or emulsions considering two main mechanisms describing the viscous energy dissipation in sheared foams can be performed: (i) in the foam films, formed between two neighboring bubbles, and (ii) in the adsorption of the surfactant layer on the surfaces of the bubbles (Denkov et al., 2008; Tcholakova et al., 2008).

II.7.1 Predominant viscous friction in foam films

The theoretical modeling (Tcholakova et al., 2008) demonstrated that the movement of liquid within sheared foam films could be decomposed into two coexisting fundamental processes:

- The sliding movement of the opposite surfaces of the film, resulting from the relative movement of the neighboring bubbles in the sheared foam (Figure 15a).
- Thinning of the foam film, which is due to the high dynamic pressure within the film (imposed by the capillary pressure of the bubbles), as compared to the pressure in the surrounding channels of the Plateau borders (Figure 15b).

By applying a hydrodynamic approach with reasonable assumptions, the energy dissipation rate within the liquid film was calculated and used to derive an approximate equation for the viscous stress in the sheared foams (Denkov et al., 2008; Tcholakova et al., 2008).

$$\tau_{VF} \simeq 1.16\, Ca^{0.47} \Phi^{5/6} \frac{(\Phi - 0.74)^{0.1}}{(1-\Phi)^{0.5}} \qquad (25)$$

Where Ca is the capillary number $Ca = \frac{\mu_l v}{\sigma}$. μ_l and v is the dynamic viscosity of the liquid solution and the foam velocity, respectively.

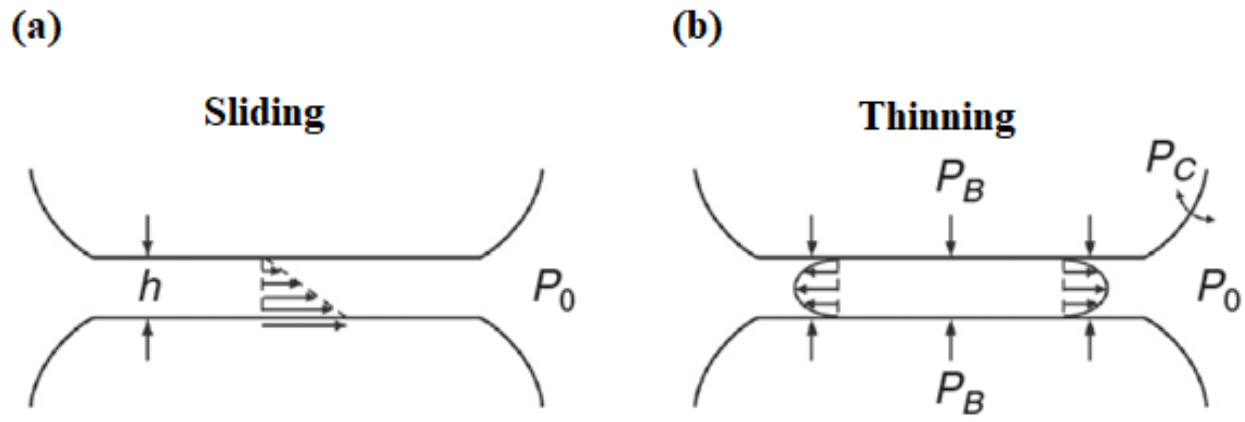

Figure 15. (a): Schematic presentation of the sliding process: the opposing surfaces of the film move at velocities which are driven by the relative motion of the neighboring bubbles in the flowing foam. The film thickness h determines the local shear rate of the liquid in the film. (b): Schematic presentation of the thinning of the film. This process is driven by the excess pressure P_B in the bubbles compared to the pressure P_0 in the liquid outside the film.

II.7.2 Predominant viscous friction in the surfactant adsorption layer

Theoretical studies show that bubble collisions in sheared foams lead to bubble surface oscillations. This fluctuation leads to viscous energy dissipation in the surfactant adsorption layer, due to the surface expansion viscosity. The following expression was derived theoretically for this contribution (noted as τ_{VS} to the total viscous stress (Tcholakova et al., 2008):

$$\tau_{VS} \simeq 9.8\,\Phi\left(\frac{E_{LD}}{\gamma}\right)\Phi\,{a_0}^{0.1} \quad (26)$$

E_{LD} is the viscous surface modulus and a_0 is the relative amplitude of bubble oscillations. In general, the viscous stress in sheared foams includes the contributions of energy dissipation in both the foam films and adsorption layers:

$$\tau_V = \tau_{VS} + \tau_{VF} \quad (27)$$

and

$$\tau = \tau_c + \tau_V \quad (28)$$

Several experimental works have studied flowing foam in a horizontal square pipe (Blondin and Doubliez, 2002; Tisné et al., 2003). It was shown that that the flow arrangement, depending on the Reynolds number and foam quality, can vary from a plug-flow up to a complex regime affecting the liquid films along the surfaces and the foam itself, both in terms of velocity and of structure (bubble arrangement). These observations were confirmed by other studies with the same experimental device (Aloui and Madani, 2008).

The most common flow models proposed for foam were mainly those of Power-law, Bingham, and Herschel-Bulkley (Akhtar et al., 2018). Under low-stress conditions, foam behaved like a soft solid and can show some sort of elasticity. Over a threshold value of the shear stress (yield

stress), foam behaved as a viscoelastic fluid exhibiting a Newtonian-like behaviour with constant viscosity, as in the case of the Bingham law (n = 1), or a shear rate-dependent viscosity as in the case of Herschel-Bulkley law. Additionally, many authors have proposed correlations between the viscosity and the foam structure (Du et al., 2018; Khan and Armstrong, 1987; Wu et al., 1984). In regards to the complexity of the rheological behaviour of foam, Computational Fluid Dynamics (CFD) could be proposed to quite accurately describe the flow behaviour of such a complex system at least macroscopically, some experimental data being of need to validate the CFD calculations. However, quite a few numerical studies have been performed. Some authors proposed a simulation of a bubble's movement in a capillary tube prior to relating these results to a foam system (Chen et al., 2009; Dalmon et al., 2018), or being more elaborate using the Lattice Boltzman (LB) approach which solves the flow at the microscopic scale as well as the interface scale (case of CFD simulation of bubble columns) (Bhole et al., 2008; Mühlbauer et al., 2019). Others have attempted to simulate the liquid film between the bubbles (Plateau border) by highlighting the drainage phenomenon in foams (Koehler et al., 2004; Wang and Narsimhan, 2006). (Chovet et al., 2014) simulated the horizontal foam flow inside the duct using the non-Newtonian Bingham model. The comparison of the pressure drop and the velocity profiles obtained experimentally with those obtained numerically showed a good description of the foam flow for low Reynolds numbers (plug flow) however it was found to be challenging to expand toward other flow regimes. In this study, a robust rheological model will be defined able to predict the rheological behaviours of the foam for different qualities, different flow regimes (Reynolds Numbers), and in the case of a simple linear pipe as well as in the presence of singularities that are complex geometries found in the industrial plants.

III. Cleaning in food industries

III.1 Food surfaces contamination

Food hygiene procedures are implemented to ensure the safety and quality of food products from the production phase to the consumption phase (Raposo et al., 2021). Indeed, due to the complex nature of the food supply chain, contamination of food can occur at any stage from primary production to use by the final consumer (Schlegelová et al., 2010), that is, during harvesting, processing, storage, distribution, transportation, and preparation. The contamination of food with pathogenic microorganisms, leading to foodborne diseases, is a major security threat for the food production and processing industry. Foodborne illnesses have been associated with improper storage and reheating (50%), inadequately odd storage (45%), and cross-contamination (39%) (Bean and Griffin, 1990). In 2018, 1,630 foodborne illnesses outbreaks (FIO) were reported in France, affecting 14,742 people, of which 5% were hospitalized and 2 died. Compared to 2017, the number of notified FIO is increasing (+24%). The most commonly suspected pathogens were *Staphylococcus aureus*, *Clostridium perfringens*, and *Bacillus cereus* corresponding to 70% of the FIO (Fournet et al., 2019).

Contact surfaces found in the food industry play a significant role in affecting the safety of foods. For example, according to Bennett (2013), the most common errors causing cross-contamination would be inadequate cleaning of processing equipment or utensils (67%) and storage in a contaminated environment (39%). In France, equipment surfaces contaminated

with microorganisms are thought to have contributed to more than half of all foodborne illnesses reported between 2006 and 2008 (Delmas et al., 2010). Bacteria responsible for large-scale outbreaks from contaminated equipment surfaces include *Staphylococcus aureus* (Asao et al., 2003), *Vibrio parahaemolyticus* (Chen et al., 2017), *Listeria monocytogenes* (Gaulin et al., 2012; Schmitz-Esser et al., 2015), and *Salmonella tiphymurium* (Finn et al., 2013). Non-pathogenic bacteria are also often isolated from surfaces in food environments. *Pseudomonas fluorescens* is among the more dominant species on food contact surfaces that are highly resistant to cleaning and disinfection operations (Fagerlund et al., 2017; Maes et al., 2019). It has a marked occurrence in food processing plants since it is able to form biofilms in different environmental conditions (Jara et al., 2021; Meliani and Bensoltane, 2015; Stellato et al., 2017). Even if these bacteria are not responsible for food poisoning, they might behave as a "helper" for further pathogenic bacteria to persist in food facilities, mainly using its matrix as cover and/or as an anchoring surface (Puga et al., 2018).

When equipment surfaces are contaminated, the surface properties of the materials may affect either the interaction strength between microorganisms and surfaces or shear stress release efficiency thus affecting the effectiveness of cleaning procedures (Faille et al., 2018; Puga et al., 2018; Whitehead et al., 2015). Among the different materials encountered in the food processing industry, stainless steel is by far the most used, for example in the fabrication of pipes, tanks, conveyor belts, worktops, or complex pieces of equipment such as valves or pumps.

Bacterial contamination is usually observed in the form of biofilm (Bénézech and Faille, 2018; Gibson et al., 1999; Jha et al., 2020; Weber et al., 2019), one of the most widely distributed modes of life on Earth (Stoodley et al., 2002). A biofilm (Figure 16) consists of consortia of microorganisms in which cells are frequently embedded in a self-produced matrix of extracellular polymeric substances (EPS) that are adherent to each other and/or a surface (Flemming et al., 2016). One of the specificities of these biofilms is that the way of life of cells within biofilms is clearly distinct from that of free bacterial cells, which gives them properties that are sometimes distant from those of their free-living counterpart. This is particularly the case for their resistance to environmental conditions, and in the case of undesirable biofilms in the food industry, their resistance to conditions implemented to limit their establishment or their expansion (for example: low temperatures, disinfection procedures...). Furthermore, the EPS, mainly composed of polysaccharides, proteins, nucleic acids, and lipids, acts as a protective layer preventing cell dehydration, providing resistance to UV light radiation as well as to disinfectants (Crouzet et al., 2014). Another reason for the remarkable persistence of these biofilms in the processing lines is their very high resistance to detachment, both during rinsing and cleaning procedures as previously shown (Al Saabi et al., 2021; Al Saabi, 2020; Bénézech and Faille, 2018; Bouvier et al., 2021; Jha et al., 2020).

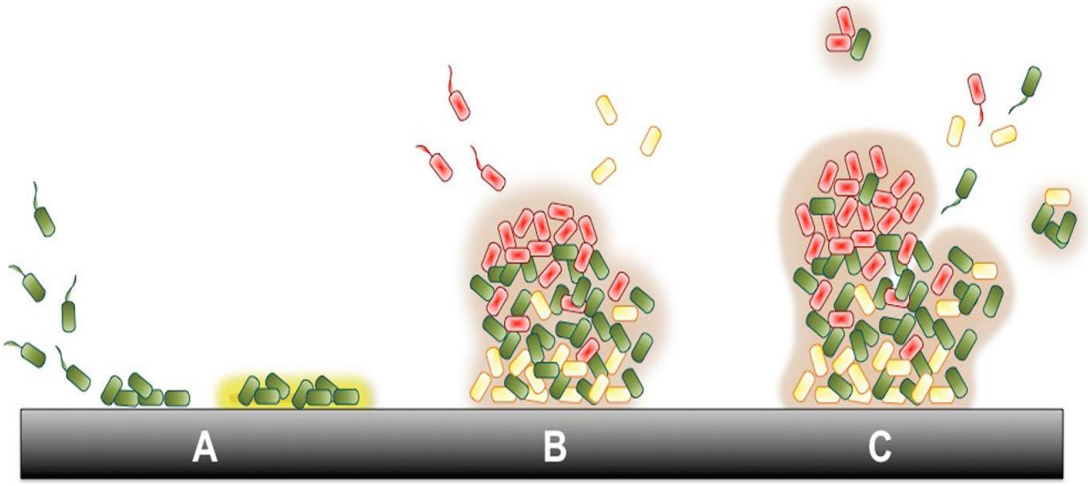

Figure 16. Different steps of biofilm formation, inspired by (Cappitelli et al., 2014). A dynamic process involves attachment A, maturation B, and dispersal C.

III.2 Cleaning of contamination / Cleaning In Place

Cleaning is the action of removing all the residues and the soiling from surfaces, making them clean and able to be disinfected efficiently (Avila-Sierra et al., 2019; Goode et al., 2010; Wilson, 2005). It allows the elimination of both organic dirt (grease, blood, sugar, starch, proteins) and inorganic dirt (mineral salts, rust, carbonization residues). It also allows the removal of foreign objects (Héry et al., 2003).

Nowadays, Cleaning-In-Place (CIP) is a common method in the food and pharmaceutical industries. It is an automated process that consists of the cleaning of equipment, without having to remove or disassemble pipes and equipment, by circulating a turbulent fluid flow or by high-pressure spray impingement. This saves time between productions and can therefore increase revenues (Avila-Sierra et al., 2019; Bremer et al., 2006). The method usually involves stages such as pre-washing, caustic solution cleaning usually between 1-3% of NaOH, immediate rinse, acid solution descaling, and the final rinse.

CIP is operated according to the different TACT principles according to the Sinner's circle (Figure 17) (Basso, 2017):

- Temperature: The setting defines an optimum temperature of the liquids (water or detergents). A minimum / maximum temperature level is expected depending on various factors such as the equipment materials or the type of soil.

- Action: The mechanical action of the washing depends on the flow, characterized by the flow rate inducing ranges of wall shear stress directly in relation to pressure variations along the lines. The internal parts of the tanks are usually cleaned using spray balls to enhance the effectiveness of mechanical cleaning by impacting the surfaces with liquid jets.

- Chemistry: The use of cleaning agents such as alkaline (NaOH) or acidic (HNO_3) products is necessary to remove organic matter or dissolve mineral matter.

- Time: The minimum expected duration for the previous criteria is quantified in advance according to the washing phase. This is an important parameter in determining the necessary

level of efficiency to be achieved and to avoid excessive cleaning resulting in over-consumption of chemicals, water, and energy.

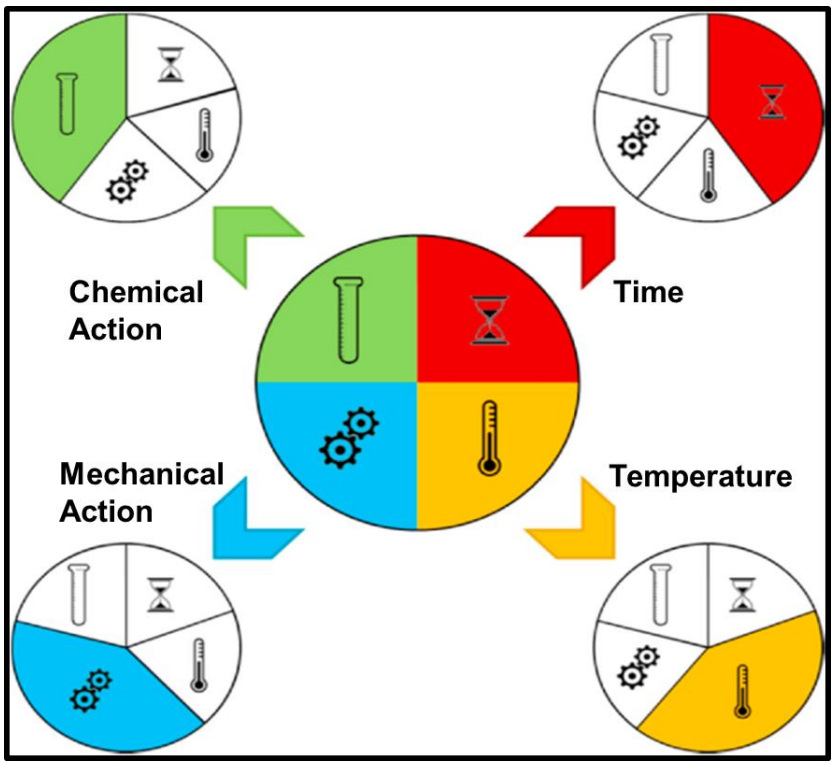

Figure 17. Representation of Sinner's circle (Basso et al., 2017).

The accurate combination of the influencing factors of time, temperature, chemistry, and mechanical action generated by the fluid flow tends to make cleaning a reliable and optimized process to save time, water, and energy consumption (Grandillo and Tatianchenko, 2020). To optimize the overall CIP systems process, several works were performed to study the effect of the hydrodynamics of the cleaning fluid on CIP efficiency. In particular, the importance of the flow parameters such as the generated shear stress at the wall of equipment (Blel et al., 2007), fluid velocity (Bénézech and Faille, 2018), flow regimes (Brugnoni et al., 2012), and the formation of recirculation areas and local turbulence (Blel et al., 2007).

In the literature, many studies have focused on the removal of biocontamination (bacterial biofilms or spores). One of the aims of this research was to identify the mechanisms by which these micro-organisms detach from surfaces by varying the shear forces applied to the wall. For some studies, the wall shear forces allow detachment or at least disruption of the contaminations. Others have defined yield stress, below which the detachment of a biofilm can be achieved. However, exceeding this stress value, a compression of biofilms could occur.

On the other hand, turbulence has a significant effect on the cleaning process. Indeed, the increase in the presence of turbulent structures generated at the walls improves the cleaning efficiency. (Blel et al., 2009a) shows a relationship between the size distribution of the turbulent structures at the walls and the deposition of spore contamination in the circulating flow, a trend as an increase in flow rate (turbulence) reduces the cleaning time required to remove the spore's contamination. The use of non-stationary flows, such as pulsed flows and jet flows, would increase CIP efficiency (Absi and Azouani, 2018; Blel et al., 2013, 2007; Silva et al., 2021).

These flows affect both the mean and fluctuating components of the wall shear stress and consequently reduce the residual contamination. Indeed, pulsed flows demonstrated the beneficial effect of increasing the wall shear stress and its fluctuations on the enhancement of bacterial removal from stainless steel surfaces. As an example, pulsed flow in turbulent regime allows an increase of mean and fluctuating shear rates and a consequent enhancement of *Bacillus cereus* spores removal rates from surfaces (Blel et al., 2009a, 2009b), which corresponds to twice that obtained for the steady condition at high Reynolds number (Re of 35000). The increase in turbulent level and thus in velocity of the fluid (a velocity of 3 $m.s^{-1}$) has also shown a relevant role to remove a backed tomato deposit (Absi and Azouani, 2018). In both cases, the authors explained that this increase in the local velocity gradient at the surface plays a relevant role in convective mass and heat transfer inducing a weakening and breaking of the bonds between the contaminations and the solid surface. It should be noted that such a velocity of 3 $m.s^{-1}$ is far to be realistic in CIP of processing lines.

Gas-liquid two-phase flows, which are also non-stationary flows, are likely to be of similar interest to pulsed flows. It can be as foam flow or just an air bubbles flow (Al Saabi et al., 2021; Le Toquin et al., 2020; Thobie, 2018). In (Thobie, 2018), different bubbles sequences (where the size, shape, and frequency of bubble passage were varied) were used to try to limit the biofilm development or elimination once formed. They studied the elimination of biofilms of *Chlorella Vulgaris* fouled on the surfaces of a photobioreactor. Their results show that the surface layers of the biofilm considered as the least adhered are periodically detached, but the first layers of the biofilm do not detach and provide a bonding medium for new cells. Fluctuation of the shear stress was the mean response for the increase of the detachments rates which depend mainly on the bullet sizes. Indeed, flow with an injection of big bubbles seems to be less effective at removing the superficial layers of the biofilm. Additionally, CIP with microbubbles can be a new method to increase cleaning efficiency (Lee et al., 2016). It was found that CIP with microbubbles can control irreversible fouling more successfully than conventional CIP. Moreover, the cleaning mechanism of microbubbles has improved the cleaning efficiency of adhering foulants from 32.6% to 81.9%.

It was shown that the best option of cleaning was concluded when both chemical and mechanical actions were studied. Indeed, several works have examined the role of chemicals and hydrodynamics to control biocontamination. A conclusion as a synergy of both effects improves the efficiency of the cleaning process. Recently, (Gomes et al., 2021) investigated the effect and the efficiency of combined treatment of chemical and mechanical on *B. cereus* and *P. fluorescence* biofilms formed on high-density polythene HDPE. Results showed that a combination of the surfactant solution of BDMDAC (benzyl dimethyl dodecyl ammonium chloride, 300 µg/Ml) with the increase of the shear stress enhanced the removal of *B. cereus* and dual-species biofilms from 25% and 40% to 17% and 19% respectively. These results were in line with (Pechaud et al., 2012). In fact, different scenarios of treatment were performed: hydrodynamic (shear stress applied from 0.01 to 2.5 Pa using white water), chemical (NaClO, 150mg/L), enzymatic (Savinas, 6UP/mL), and combination treatments of chemical or enzymatic treatment with hydrodynamic treatments. As shown in Figure 18, compared to the single effect of hydrodynamic (65% of biomass removal), chemical (35% of biomass removal), and enzymatic (less than 5% of biomass removal) the combination of treatments improved the biofilm removal up to 90%. Another example concern the evaluation of the effects of

mechanical vs. chemical action (using NaOH 0.5% at 60°C) on the removal of *Bacillus* spores (Faille et al., 2013) and *Pseudomonas fluorescens* (Bénézech and Faille, 2018) from stainless steel surfaces. For the model of spores, the rinsing step with water at 500 Pa removed between 53% and 89% of the *Bacillus* spores. However, when a solution of NaOH was used at 4 Pa the cleaning efficiency was improved up to 80% and 99% for *Bacillus cereus* and *Bacillus subtilis* respectively. The improvement in spore detachment is related to the surface properties of the spores and the strength of the interaction between them and the solid, which weakens over time in the presence of these chemicals and then becomes susceptible to easy removal by shear stress. In the same way, after 30 min of cleaning with NaOH in static condition removed about 4 log, while cleaning with water at 0.14 Pa removed less than 3 log. Combination of both aspects, CIP using NaOH at 0.14 Pa improves the cleaning efficiency with about 5 log reduction. When the detachment kinetics of biofilms were studied, the synergistic action of chemical and mechanical treatment (CIP using NaOH at 0.14 Pa) mostly affected the first detachment phase (less than 1 minute of cleaning). In addition, the chemical agents weakened the cohesive forces of the biofilm, causing the destabilization of its structure, as hypothesized by the authors.

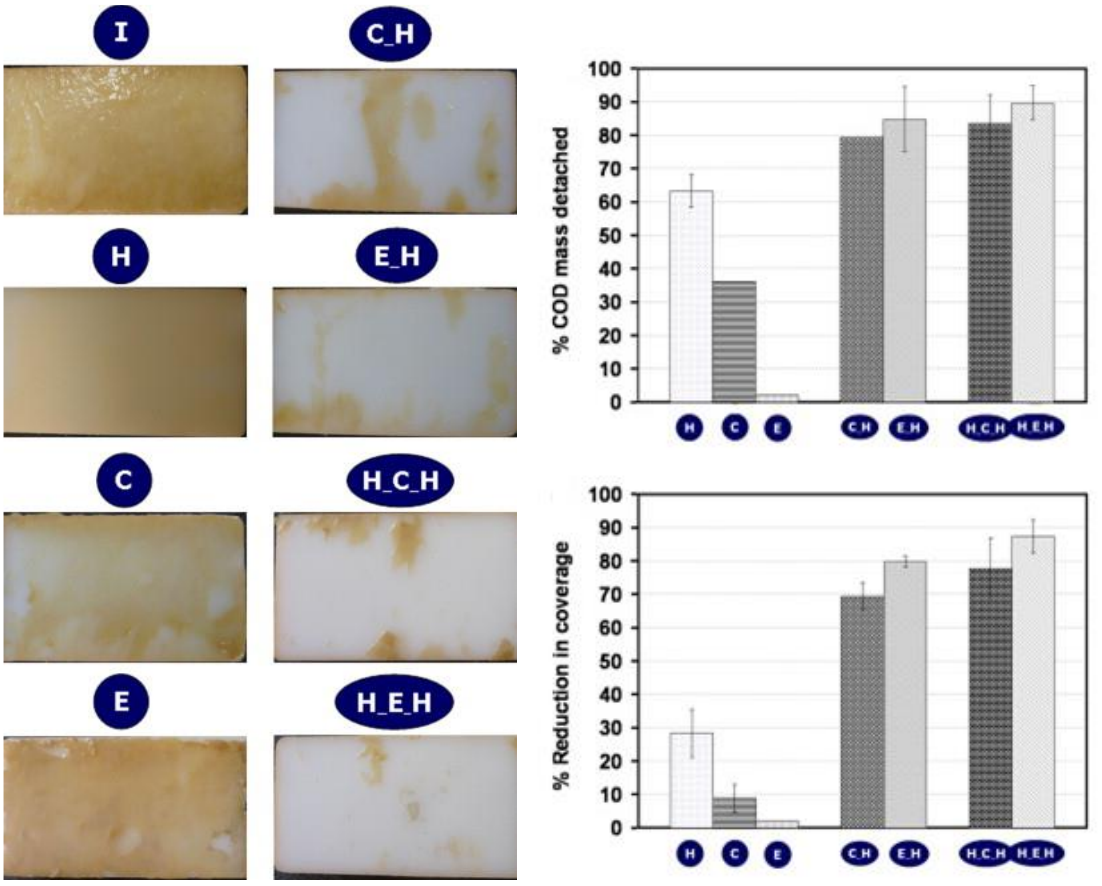

(*I*): after 40 day of growth and before any treatment
(H): after hydrodynamic treatment (0.01 Pa→2.5 Pa; 1 h)
(C): after chemical treatment (NaClO 100 mM, 2 h)
(E): after enzymatic treatment (Savinase 6 UP, 20 h)
(C_H): after chemical treatment followed by hydrodynamic treatment
(E_H): after enzymatic treatment followed by hydrodynamic treatment
(H_C_H): after hydrodynamic treatment followed by chemical treatment, itself followed by another hydrodynamic treatment
(H_E_H): after hydrodynamic treatment followed by enzymatic treatment, itself followed by another hydrodynamic treatment

Figure 18. Effect of single and combined treatment on the percentage of the biofilm detachment (Pechaud et al., 2012).

The cleaning performance and treatment parameters are directly dependent on the hygienic design. The design of the installation must limit the presence of singularities, cavities, gaps, corners, and more generally dead zones, as these structures are particularly delicate to clean or disinfect because fluids do not circulate, or very little, in these places. It is essential to study the cleaning of pipes in order to optimize cleaning operations and improve the reuse of cleaning solutions and rinsing water. (Yang et al., 2019) compared the cleaning efficiency of several piping geometries using CFD tools. This type of comparison helps to understand the determinants of the cleaning efficiency of an installation. For example, dead zones occur primarily in areas where flow recirculation is very high. They found that the size of dead zones can be reduced by using a smooth connection or a high flow velocity. However, the dead zones do not disappear completely. The modeled pressure drops are consistent with the analytical results obtained in the literature. CFD can provide sufficient information to calculate the equivalent lengths of various geometries. Many researchers apply the CFD code to improve the hygienic design. CFD simulation has been used to study good cleaning practices for a spherical shaped valve (Jensen and Friis, 2004) and to predict the local shear stress distribution at the pipe walls (Jensen et al., 2005). The cleaning of membranes fouled by proteins (Delaunay et al., 2008), and the cleaning of stainless-steel surfaces of a CIP plant and its accessories (case of a pump) contaminated by *P. fluorescens* biofilms and spores (Bénézech et al., 2002), were estimated by CFD simulations and approved using fluid dynamics mechanisms.

Other works have included surface modifications in CIP facilities, intending to understand the effects of surface topography (micro and nano), hydrophobicity, and wettability on biofouling formation and removal (Evans et al., 2021; Saubade et al., 2021; Whitehead et al., 2015; Whitehead and Verran, 2007). This could potentially help in the development of innovative food processing and cleaning technologies targeted at industrial applications to minimize energy and product waste (Avila-Sierra et al., 2019; Jha et al., 2022, 2020; Richard et al., 2020). When the impact of surface properties on CIP cleaning efficiencies in the food industry was studied, researchers showed that surface properties play a significant role in the interaction strength of the contamination and therefore the ease of cleaning (Evans et al., 2021; Saubade et al., 2021; Schnöing et al., 2020; Wilson-Nieuwenhuis et al., 2017). Several studies tried to define a correlation between the surface hydrophobicity, electron donor/acceptor properties, and bacterial attachment with a trend as the highest interaction strength for materials with relatively lower γ^+ and γ^- values (Hamadi et al., 2014; Silva et al., 2008). As an example, *Listeria monocytogenes* and *Staphylococcus aureus* strains were found to prefer hydrophilic material like stainless steel and glass for biofilm formation rather than hydrophobic one (polystyrene) (Di Bonaventura et al., 2008; Lee et al., 2015) while hydrophobic materials were difficult to clean following adhesion of *Bacillus cereus* and *Bacillus subtilis* spores onto the surface (Faille et al., 2002). Concerning the surface topography, the roughness parameters such as the arithmetical mean deviation of the profile (R_a) and the point height of irregularities (R_z) were found to significantly affect the soling of hydrophobic *B. cereus* spores, while no impact of these parameters was observed for *E. coli* cells adhesion. On the other hand, R_{vk} (reduced valley depth within the evaluation length) affected strongly the adhesion of both *B. cereus, B. subtilis* spores and *E. coli* cells, however, this parameter could not be related to the strength of adhesion. By testing different types of stainless still surfaces (R_a ranged between 0.03 and 0.89 µm), (Akhidime et al., 2020) have demonstrated that bacterial adhesion on stainless steel surface

decreases with R_a until a threshold. The minimal attachment was found at a R_a of 0.16 µm. The fact that smoother and rougher surfaces resulted in greater adhesion could be explained by the orientation of the cells adhering to the surface and the nature of the scratches in the materials. (Faille et al., 2018) have hypothesized that surfaces with microbial size characteristics can hold the bacteria in greater numbers than the rougher or smoother surfaces by increasing the exchange surface with the attached bacteria providing them better protection against shear stress. One of the widely used technologies to modify the energy of surfaces is coating. As an example, compared to titanium, stainless steel, or silver surfaces coated stainless steel surfaces with Ag-PTFE were found to reduce the attachment of *Escherichia coli* biofilms by 94% to 98% (Verran et al., 2010; Whitehead and Verran, 2007; Zhao et al., 2005a). Other composite coatings based on phosphorus, nickel, copper, or PTFE have also been used to provide surfaces with specific free energies that can reduce biofouling (Gu et al., 2021; Li et al., 2021; Zhao et al., 2005b; Zhao and Liu, 2006). Furthermore, silver nanoparticle technology as an antimicrobial material is an interesting research topic. Indeed, these nanoparticles have been shown to prevent the development and attachment of biofilms (Palanisamy et al., 2014). This would in principle be an effective prevention strategy against the proliferation of unwanted microorganisms.

III.3 Water/Energy consumption

The CIP hygiene procedure requires many resources such as water, chemical agents, energy, and time (Peng et al., 2002; Speranza and Corbo, 2017; Wilson, 2005). In addition, cleaning-in-place causes huge quantities of wastewater with an additional economic burden for the industry and environmental burden for the general public (Lyndgaard et al., 2014). Not only does it use a high amount of water, but recent studies have also shown that standard Cleaning in Place practices does always ensure a safe cleaning practice and this resulted in residual microorganisms left in the CIP parts or the production sector in the industries (Schlegelová et al., 2010).

The highest water consumption in the food industry concerns the cleaning of processing equipment and food products. This can be as much as 70% of total water consumption. Procedures such as dry cleaning, cleaning in place, and pipe pigging can contribute to reducing this high consumption (Bhagwat, 2019). However, cleaning optimization and effluent concentration control can easily reduce this level without investing in new and complex strategies (Mancosu et al., 2015). For example, the dairy industry consumes significant amounts of water in food processing (Figure 19). Depending on the final products, water consumption ranges from 0.6 to 6 L per liter of raw milk processed. As estimated by (Li et al., 2019), the dairy industry consumes about 28% of the total water in hygiene procedures. In addition, from an energy perspective, this operation requires up to 13.5-14% of the total energy consumption of the process (Khan et al., 2010; Piepiórka-Stepuk et al., 2017).

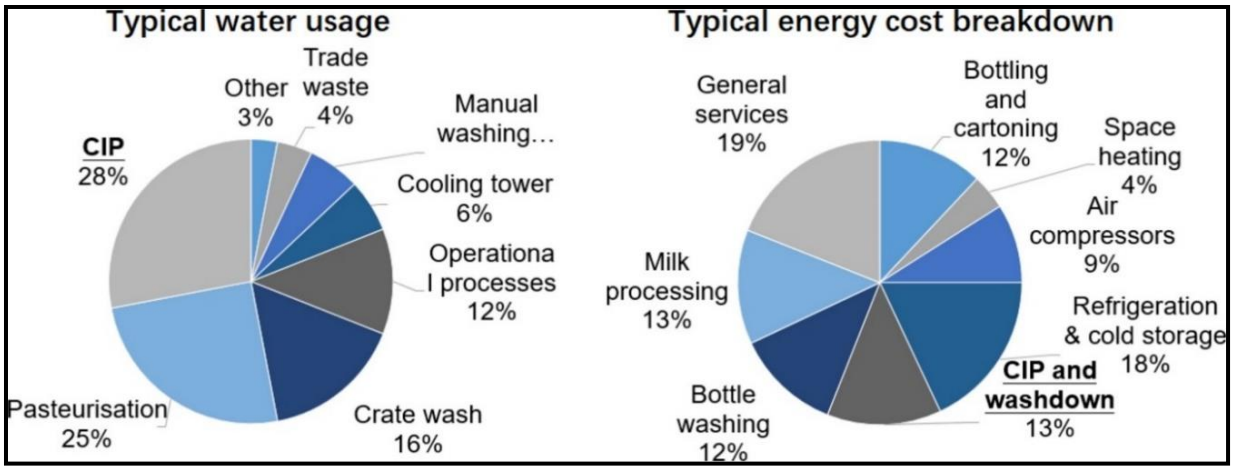

Figure 19. Percentages of water consumption and energy cost in dairy manufacturing (Dairy Australia and Dairy Manufacturers Sustainability Council (Australia), 2006).

Energy is the main component of all cleaning processes. It is usually a combination of several factors. The interaction of these factors determines the efficiency of the method. The objective is to achieve a consistent balance between cost, efficiency, and food safety. Optimization of CIP processes, maintenance, and redesign lead to a potential reduction in water/energy consumption and improved product quality. The modification of the CIP system with detergent and rinse aid recovery systems has reduced the chemicals used by up to 15%, water consumption in the CIP process by 35%, and energy consumption by 15%. At the same time, effluent discharges were significantly reduced (Pinguli et al., 2017)

Some industries are equipped with technology to re-use or recycle their wastewater. This does not only give a second life to water but also makes this cleaning method sustainable. However, most industries are not capable of recycling used water. This poses a big problem for the continuation of the usage of this method of cleaning (Blel et al., 2015; Dif et al., 2013). Recent proposals could be however mentioned (Garnier et al., 2020) by a significant reduction of wastewater using membrane technology.

III.4 Foam cleaning

The importance of foam in the food and pharmaceutics industries can be summed up in the cleaning of equipment's surfaces fouled with food and/or microorganisms. This technique is mainly used to clean open surfaces, such as workshops, walls, floors, doors, and external parts of equipment and machines (Holah and Saunders, 2019; HP Concept, 2020; Mierzejewska et al., 2015; Mierzejewska and Piepiórka-Stepuk, 2016). It is often used due to many advantages such as the ease of use and the flexibility of the processing system (foam generated by pushing water, detergent, and air through a nozzle) (BOONS FIS, 2017), the generation of significant drag forces at walls (up to 1000 times higher than single-phase flow) (Blondin and Doubliez, 2002; Tisné et al., 2003), and the chemical properties of the surfactant as cleaned agents (Naim et al., 2012; Sar et al., 2019). Static foam often contains cleaning agents intended to destroy the liaison of impurities to surfaces. The foam is deposited on the surfaces and after a variable contact time depending on the detergents and the temperature of the factory, then the surfaces are rinsed with potable water. In this way, using a foaming product generates fewer aerosols and reduces the risk of spreading pathogens and spoilage organisms leading to positive hygienic

results. Good examples of the use of this method to clean processing lines and membrane-new filters were described in (Gahleitner et al., 2014, 2013). In fact, the foam was distributed into the filter module for 2 min and then kept in contact with the inner surfaces for some time (from 5 min to 3 h). Compared to standard CIP procedures, foam cleaning has proven to be of high potential. Better efficiency was demonstrated by reducing the reaction time from 2 h to 30 min, reducing the amount of cleaning agents required per filling volume up to 4-10 times, and a full recovering of the performance of the membrane after multiple filtration and cleaning experiments. Recently, foamed surfactant solution was successfully tested to clean glass surfaces contaminated with florescent oil, showing a better efficiency than a non-foamed solution due to the presence of air-liquid interface, foam drainage, and imbibition (Schad et al., 2021). Indeed, the air-liquid interface was founded to play a significant role in cleaning silicon wafers, as demonstrated in (Jones et al., 2016). It was found that the air/liquid interface has the highest concentration of surfactant, and thus locations where impurities were more easily embedded in micelles. Authors suggest also that the contact line (air-liquid interface and impurities) can be distorted by the wettability (solid or liquid) and can help in removing dust, oil, and bacteria (Andreev et al., 2010; Kriegel and Ducker, 2019; Mierzejewska et al., 2014). This parameter is favored at low liquid fractions. Imbibition effect was known as the absorption of the impurities into the foam Plateau borders by capillary forces. This effect is stronger for foams with smaller bubble sizes and low liquid fractions.

Nerveless, very little works have been carried out on the elimination of bacterial contamination using foam. Foam in a dynamic state has been used for the removal of suspended substances and bacteria from coastal seawater (Brambilla et al., 2008; Suzuki et al., 2008). Indeed, the foam fractionation process was efficient to remove heterotrophic bacteria from a recirculating seabass system. However, this efficiency depends on operation times. The removal was ranged between 54, and 88% for 5'on/5'off and 30'on/30'off respectively (Brambilla et al., 2008). When viable bacteria, enterococci, *Salmonella-like*, and *Vibrio* bacteria were analyzed using a foam separator, the removal efficiency exceeds 80%, highlighting the absorption effect of the bacteria onto the bubble surface (Suzuki et al., 2008).

Current researches have investigated for the first time the removal kinetics of *Bacillus* spores and *Pseudomonas* biofilms under different conditions of foam flowing (containing Sodium dodecyl sulfate surfactant: SDS) in a horizontal pipe (Al Saabi et al., 2021; Al Saabi, 2020). The efficiency of foam cleaning to remove *Bacillus amylolichefaciens* from stainless steel surfaces was dependent on foam quality, foam velocity, and cleaning time. The wet foam was found to be more efficient than a dry one. As an example, the detachment after 1 min of wet foam cleaning (quality of 50%) was 1.8 log reduction, while it was 0.5 log reduction for the case of foam at a quality of 70%. However, after 20 min of cleaning the spore detachment achieved 2, and 1 log reduction for the 50% and 70% foam respectively. When the authors have compared the best option of foam (50% at the lower velocity) to the standard cleaning in place at a shear stress of 5 Pa, the removal of spores using foam was 0.3 and 0.5 log higher than that using CIP. The effect of foam flow cleaning was then tested with hydrophobic spores (*Bacillus cereus*). Results showed a similar trend of kinetics' removal with about 1 log less than the case of hydrophilic spores. The authors hypothesized that the efficiency of foam cleaning is related to the bubbles' sizes, capillary forces, and the variation of the wall liquid film at the walls (Al Saabi et al., 2021). It should be noted that the flow rate of water used in the case of CIP was

650 L/h, whereas only 4.5 L/h was used with the foam cleaning process which shows the potential role of foam to reduce the consumption of water and energy (Al Saabi, 2020). Surfactants also can affect foam cleaning efficiency. As an example, after 20 min of cleaning with foam was the removal of *B. amylolichefaciens* was decreased from 2 log reduction (using SDS surfactant) to 1 log and 0.4 log reduction when the foam was produced from Ammonyx® LO and Capstone® FS respectively. These two surfactants differ by their chemical proprieties, thus producing different foam structures in terms of bubble size, thickness of liquid film, and stability. The unstable foam was less efficient than the stable foam. In addition, foam flow through singularities harms the removal efficiency of bacteria since after singularities the flow is subject to mechanical perturbations, leading to changes in the foam structure which becomes less stable (reorganization of the bubble and drainage) (Dallagi et al., 2019). Cleaning of *B. amylolichefaciens* spores with foam flow in a straight pipe was better (0.8 log reduction more, after 20 min) than that with foam after sudden expansion/gradual reduction and 90° bending (Al Saabi, 2020). Therefore, foam flows would constitute an alternative method in surface hygiene permitting a promising efficient cleaning and can easily be combined with decontamination (e.g. the use of wet foam containing hydrogen peroxide to clean *Bacillus thurengiensis* spores (Le Toquin et al., 2020).

This PhD work provides a detailed study of the experimental characterization of the foam which will give a better understanding of the flow behavior of the foam and in particular its stability while submitted to differing hydrodynamic conditions and its rheology. Through this experimental characterization, we will investigate the ability of the foam to clean surfaces contaminated by microorganisms (case of spores and biofilm) and explain the underlying mechanisms that allow the best optimization of the cleaning efficiency. At the same time, the numerical modeling of this complex fluid in different flow situations, especially in the presence of singularities, was studied. An LCA analysis was carried out to compare the environmental impacts of foam cleaning with other common cleaning conditions such as CIP.

References

Absi, R., Azouani, R., 2018. Toward automatic cleaning of industrial equipment: pulsed flow-induced wall shear stress. Procedia CIRP 78, 359–363. https://doi.org/10.1016/j.procir.2018.10.001

Akhidime, I.D., Slate, A.J., Hulme, A., Whitehead, K.A., 2020. The Influence of Surface Topography and Wettability on Escherichia coli Removal from Polymeric Materials in the Presence of a Blood Conditioning Film. IJERPH 17, 7368. https://doi.org/10.3390/ijerph17207368

Al Saabi, A., Dallagi, H., Aloui, F., Faille, C., Rauwel, G., Wauquier, L., Bouvier, L., Bénézech, T., 2021. Removal of Bacillus spores from stainless steel pipes by flow foam: Effect of the foam quality and velocity. Journal of Food Engineering 289, 110273. https://doi.org/10.1016/j.jfoodeng.2020.110273

Al Saabi, A.-A., 2020. Mousses en écoulement pour le nettoyage d'équipements fermés contaminés par des spores de Bacillus cereus ou des biofilms de Pseudomonas fluorescens (These de doctorat). Lille.

Aloui, F., Madani, S., 2008. Experimental investigation of a wet foam flow through a horizontal sudden expansion. Experimental Thermal and Fluid Science 32, 905–926. https://doi.org/10.1016/j.expthermflusci.2007.11.013

AlQuaimi, B.I., Rossen, W.R., 2019. Characterizing foam flow in fractures for enhanced oil recovery. Journal of Petroleum Science and Engineering 175, 1160–1168. https://doi.org/10.1016/j.petrol.2018.06.020

Andreev, V.A., Prausnitz, J.M., Radke, C.J., 2010. Meniscus-Shear Particle Detachment in Foam-Based Cleaning of Silicon Wafers with an Immersion/Withdrawal Cell. Ind. Eng. Chem. Res. 49, 12461–12470. https://doi.org/10.1021/ie1012954

Argillier, J.F., Zeilinger, S., Roche, P., 2009. Enhancement of Aqueous Emulsion and Foam Stability with Oppositely Charged Surfactant/Polyelectrolyte Mixed Systems. Oil & Gas Science and Technology - Rev. IFP 64, 597–605. https://doi.org/10.2516/ogst/2009043

Asao, T., Kumeda, Y., Kawai, T., Shibata, T., Oda, H., Haruki, K., Nakazawa, H., Kozaki, S., 2003. An extensive outbreak of staphylococcal food poisoning due to low-fat milk in Japan: estimation of enterotoxin A in the incriminated milk and powdered skim milk. Epidemiol. Infect. 130, 33–40. https://doi.org/10.1017/S0950268802007951

Avila-Sierra, A., Zhang, Z.J., Fryer, P.J., 2019. Effect of surface characteristics on cleaning performance for CIP system in food processing. Energy Procedia 161, 115–122. https://doi.org/10.1016/j.egypro.2019.02.067

Basso, 2017. Study of chemical environments for washing and descaling of food processing appliances: An insight in commercial cleaning products - ScienceDirect [WWW Document]. URL https://www.sciencedirect.com/science/article/pii/S1226086X17301582 (accessed 10.23.19).

Basso, M., Simonato, M., Furlanetto, R., De Nardo, L., 2017. Study of chemical environments for washing and descaling of food processing appliances: An insight in commercial cleaning products. Journal of Industrial and Engineering Chemistry 53, 23–36. https://doi.org/10.1016/j.jiec.2017.03.041

Bean, N.H., Griffin, P.M., 1990. Foodborne Disease Outbreaks in the United States, 1973–1987: Pathogens, Vehicles, and Trends. Journal of Food Protection 53, 804–817. https://doi.org/10.4315/0362-028X-53.9.804

Bénézech, T., Faille, C., 2018. Two-phase kinetics of biofilm removal during CIP. Respective roles of mechanical and chemical effects on the detachment of single cells vs cell clusters from a Pseudomonas fluorescens biofilm. Journal of Food Engineering 219, 121–128. https://doi.org/10.1016/j.jfoodeng.2017.09.013

Bénézech, T., Lelièvre, C., Membré, J.M., Viet, A.-F., Faille, C., 2002. A new test method for in-place cleanability of food processing equipment. Journal of Food Engineering 54, 7–15. https://doi.org/10.1016/S0260-8774(01)00171-6

Besagni, G., Inzoli, F., 2017. The effect of liquid phase properties on bubble column fluid dynamics: Gas holdup, flow regime transition, bubble size distributions and shapes, interfacial areas and foaming phenomena. Chemical Engineering Science 170, 270–296. https://doi.org/10.1016/j.ces.2017.03.043

Bhakta, A., Ruckenstein, E., 1997. Drainage and Coalescence in Standing Foams. Journal of Colloid and Interface Science 191, 184–201. https://doi.org/10.1006/jcis.1997.4953

Bhakta, A., Ruckenstein, E., 1995. Foams and Concentrated Emulsions: Dynamics and "Phase" Behavior. Langmuir 11, 4642–4652. https://doi.org/10.1021/la00012a012

Bhole, M.R., Joshi, J.B., Ramkrishna, D., 2008. CFD simulation of bubble columns incorporating population balance modeling. Chemical Engineering Science 63, 2267–2282. https://doi.org/10.1016/j.ces.2008.01.013

Bikerman, J.J., 1973. Foams. Springer-Verlag.

Bingham, E.C., 1924. Plasticity and elasticity. Journal of the Franklin Institute 197, 99–115. https://doi.org/10.1016/S0016-0032(24)90500-X

Blel, W., Bénézech, T., Legentilhomme, P., Legrand, J., Le Gentil-Lelièvre, C., 2007. Effect of flow arrangement on the removal of Bacillus spores from stainless steel equipment surfaces during a Cleaning In Place procedure. Chemical Engineering Science 62, 3798–3808. https://doi.org/10.1016/j.ces.2007.04.011

Blel, W., Dif, M., Sire, O., 2015. Effect of a new regeneration process by adsorption-coagulation and flocculation on the physicochemical properties and the detergent efficiency of regenerated cleaning solutions. Journal of Environmental Management Complete, 1–10. https://doi.org/10.1016/j.jenvman.2015.03.011

Blel, W., Le Gentil-Lelièvre, C., Bénézech, T., Legrand, J., Legentilhomme, P., 2009a. Application of turbulent pulsating flows to the bacterial removal during a cleaning in place procedure. Part 1: Experimental analysis of wall shear stress in a cylindrical pipe. Journal of Food Engineering 90, 422–432. https://doi.org/10.1016/j.jfoodeng.2008.07.008

Blel, W., Legentilhomme, P., Bénézech, T., Fayolle, F., 2013. Cleanabilty study of a Scraped Surface Heat Exchanger. Food and Bioproducts Processing 91, 95–102. https://doi.org/10.1016/j.fbp.2012.10.002

Blel, W., Legentilhomme, P., Bénézech, T., Legrand, J., Le Gentil-Lelièvre, C., 2009b. Application of turbulent pulsating flows to the bacterial removal during a cleaning in place procedure. Part 2: Effects on cleaning efficiency. Journal of Food Engineering 90, 433–440. https://doi.org/10.1016/j.jfoodeng.2008.07.019

Blondin, E., Doubliez, L., 2002. Particle imaging velocimetry of a wet aqueous foam with an underlying liquid film. Experiments in Fluids 32, 294–301. https://doi.org/10.1007/s003480100318

Boissonnet, G., 1998. Etude de l'écoulement d'une mousse aqueuse de décontamination. Mécanismes de drainage et comportement hydrodynamique (These de doctorat). Montpellier 2.

BOONS FIS, 2017. The advantages of cleaning and disinfecting with foam [WWW Document]. URL https://www.boonsfis.com/en/blog/the-advantages-of-cleaning-and-disinfecting-with-foam/24

Bournival, G., Du, Z., Ata, S., Jameson, G.J., 2014. Foaming and gas dispersion properties of non-ionic surfactants in the presence of an inorganic electrolyte. Chemical Engineering Science 116, 536–546. https://doi.org/10.1016/j.ces.2014.05.011

Bouvier, L., Cunault, C., Faille, C., Dallagi, H., Wauquier, L., Bénézech, T., 2021. Influence of the design of fresh-cut food washing tanks on the growth kinetics of Pseudomonas fluorescens biofilms. iScience 24, 102506. https://doi.org/10.1016/j.isci.2021.102506

Brakke, K.A., 1992. The Surface Evolver. Experimental Mathematics 1, 141–165. https://doi.org/10.1080/10586458.1992.10504253

Brambilla, F., Antonini, M., Ceccuzzi, P., Terova, G., Saroglia, M., 2008. Foam fractionation efficiency in particulate matter and heterotrophic bacteria removal from a recirculating seabass (Dicentrarchus labrax) system. Aquacultural Engineering 39, 37–42. https://doi.org/10.1016/j.aquaeng.2008.05.004

Bremer, P.J., Fillery, S., McQuillan, A.J., 2006. Laboratory scale Clean-In-Place (CIP) studies on the effectiveness of different caustic and acid wash steps on the removal of dairy biofilms. Int J Food Microbiol 106, 254–262. https://doi.org/10.1016/j.ijfoodmicro.2005.07.004

Briceño, M., Salager, J.L., Bertrand, J., 2001. Influence of Dispersed Phase Content and Viscosity on the Mixing of Concentrated Oil-in-Water Emulsions in the Transition Flow Regime. Chemical Engineering Research and Design 79, 943–948. https://doi.org/10.1205/02638760152721794

Brugnoni, L.I., Cubitto, M.A., Lozano, J.E., 2012. Candida krusei development on turbulent flow regimes: Biofilm formation and efficiency of cleaning and disinfection program. Journal of Food Engineering 111, 546–552. https://doi.org/10.1016/j.jfoodeng.2012.03.023

Buzza, D.M.A., D. Lu, C.-Y., Cates, M.E., 1995. Linear Shear Rheology of Incompressible Foams. J. Phys. II France 5, 37–52. https://doi.org/10.1051/jp2:1995112

Camp, C.R., 1998. SUBSURFACE DRIP IRRIGATION: A REVIEW. Transactions of the ASAE 41, 1353–1367. https://doi.org/10.13031/2013.17309

Cantat, I., 2011. Gibbs elasticity effect in foam shear flows: a non quasi-static 2D numerical simulation. Soft Matter 7, 448–455. https://doi.org/10.1039/C0SM00657B

Cappitelli, F., Polo, A., Villa, F., 2014. Biofilm Formation in Food Processing Environments is Still Poorly Understood and Controlled. Food Eng Rev 6, 29–42. https://doi.org/10.1007/s12393-014-9077-8

Carrier, V., Colin, A., 2003. Coalescence in Draining Foams. Langmuir 19, 4535–4538. https://doi.org/10.1021/la026995b

Cheddadi, I., Saramito, P., Graner, F., 2015. Pourquoi la mousse liquide est-elle si solide ? [WWW Document]. URL https://membres-ljk.imag.fr/Pierre.Saramito/image-des-maths/toto.html (accessed 1.6.22).

Chen, A.J., Hasan, N.A., Haley, B.J., Taviani, E., Tarnowski, M., Brohawn, K., Johnson, C.N., Colwell, R.R., Huq, A., 2017. Characterization of Pathogenic Vibrio parahaemolyticus from the Chesapeake Bay, Maryland. Front. Microbiol. 8, 2460. https://doi.org/10.3389/fmicb.2017.02460

Chen, Y., Kulenovic, R., Mertz, R., 2009. Numerical study on the formation of Taylor bubbles in capillary tubes. International Journal of Thermal Sciences 48, 234–242. https://doi.org/10.1016/j.ijthermalsci.2008.01.004

Chovet, R., Aloui, F., Keirsbulck, L., 2014. Gas-Liquid Foam Through Straight Ducts and Singularities: CFD Simulations and Experiments. Presented at the ASME 2014 4th Joint US-European Fluids Engineering Division Summer Meeting collocated with the ASME 2014 12th International Conference on Nanochannels, Microchannels, and Minichannels, American Society of Mechanical Engineers Digital Collection. https://doi.org/10.1115/FEDSM2014-21190

Crouzet, M., Le Senechal, C., Brözel, V.S., Costaglioli, P., Barthe, C., Bonneu, M., Garbay, B., Vilain, S., 2014. Exploring early steps in biofilm formation: set-up of an

experimental system for molecular studies. BMC Microbiology 14, 253. https://doi.org/10.1186/s12866-014-0253-z

Dairy Australia, Dairy Manufacturers Sustainability Council (Australia) (Eds.), 2006. Australian dairy manufacturing industry state of the environment report. Dairy Australia, Southbank, Vic.

Dallagi, H., Al Saabi, A., Faille, C., Benezech, T., Augustin, W., Aloui, F., 2019. CFD Simulations of the Rheological Behavior of Aqueous Foam Flow Through a Half-Sudden Expansion. Presented at the ASME-JSME-KSME 2019 8th Joint Fluids Engineering Conference, American Society of Mechanical Engineers Digital Collection. https://doi.org/10.1115/AJKFluids2019-4650

Dalmon, A., Lepilliez, M., Tanguy, S., Pedrono, A., Busset, B., Bavestrello, H., Mignot, J., 2018. Direct numerical simulation of a bubble motion in a spherical tank under external forces and microgravity conditions. J. Fluid Mech. 849, 467–497. https://doi.org/10.1017/jfm.2018.389

Delaunay, D., Rabiller-Baudry, M., Gozálvez-Zafrilla, J.M., Balannec, B., Frappart, M., Paugam, L., 2008. Mapping of protein fouling by FTIR-ATR as experimental tool to study membrane fouling and fluid velocity profile in various geometries and validation by CFD simulation. Chemical Engineering and Processing: Process Intensification 47, 1106–1117. https://doi.org/10.1016/j.cep.2007.12.008

Delmas, G., Jourdan Da Silva, N., Pihier, N., Weill, F.-X., Vaillant, V., De Valk, H.C., 2010. Les toxi-infections alimentaires collectives en France entre 2006 et 2008. Bulletin Epidémiologique Hebdomadaire - BEH 31–32, 344–348.

Denkov, N.D., Subramanian, V., Gurovich, D., Lips, A., 2005. Wall slip and viscous dissipation in sheared foams: Effect of surface mobility. Colloids and Surfaces A: Physicochemical and Engineering Aspects 263, 129–145. https://doi.org/10.1016/j.colsurfa.2005.02.038

Denkov, N.D., Tcholakova, S., Golemanov, K., Ananthapadmanabhan, K.P., Lips, A., 2008. Viscous Friction in Foams and Concentrated Emulsions under Steady Shear. Physical Review Letters 100. https://doi.org/10.1103/PhysRevLett.100.138301

Di Bonaventura, G., Piccolomini, R., Paludi, D., D'Orio, V., Vergara, A., Conter, M., Ianieri, A., 2008. Influence of temperature on biofilm formation by Listeria monocytogenes on various food-contact surfaces: relationship with motility and cell surface hydrophobicity. J Appl Microbiol 104, 1552–1561. https://doi.org/10.1111/j.1365-2672.2007.03688.x

Dickinson, E., 1992. An introduction to food colloids. Oxford University Press, Oxford ; New York.

Dif, M., Blel, W., Tastayre, G., Lendormi, T., Sire, O., 2013. Identification of transfer mechanisms involved in soiled CIP solutions regeneration at extreme pH and high temperature. Journal of Food Engineering 114, 477–485. https://doi.org/10.1016/j.jfoodeng.2012.08.036

Du, D., Li, Y., Chao, K., Wang, C., Wang, D., 2018. Laboratory study of the Non-Newtonian behavior of supercritical CO2 foam flow in a straight tube. Journal of Petroleum Science and Engineering 164, 390–399. https://doi.org/10.1016/j.petrol.2018.01.069

Eftekhari, A.A., Farajzadeh, R., 2017. Effect of Foam on Liquid Phase Mobility in Porous Media. Sci Rep 7, 43870. https://doi.org/10.1038/srep43870

Egea, C.B., 2014. Formation, stabilité et cassage des mousses non aqueuses : Contribution à l'étude des mousses pétrolières (phdthesis). Université Pierre et Marie Curie - Paris VI.

Enzendorfer, C., Harris, R.A., Valkó, P., Economides, M.J., Fokker, P.A., Davies, D.D., 1995. Pipe viscometry of foams. Journal of Rheology 39, 345–358. https://doi.org/10.1122/1.550701

Evans, A., Slate, A.J., Akhidime, I.D., Verran, J., Kelly, P.J., Whitehead, K.A., 2021. The Removal of Meat Exudate and Escherichia coli from Stainless Steel and Titanium Surfaces with Irregular and Regular Linear Topographies. IJERPH 18, 3198. https://doi.org/10.3390/ijerph18063198

Evgenidis, S.P., Kazakis, N.A., Karapantsios, T.D., 2010. Bubbly flow characteristics during decompression sickness: Effect of surfactant and electrolyte on bubble size distribution. Colloids and Surfaces A: Physicochemical and Engineering Aspects 365, 46–51. https://doi.org/10.1016/j.colsurfa.2010.02.032

Fagerlund, A., Møretrø, T., Heir, E., Briandet, R., Langsrud, S., 2017. Cleaning and Disinfection of Biofilms Composed of Listeria monocytogenes and Background Microbiota from Meat Processing Surfaces. Appl Environ Microbiol 83, e01046-17, e01046-17. https://doi.org/10.1128/AEM.01046-17

Faille, C., Bénézech, T., Blel, W., Ronse, A., Ronse, G., Clarisse, M., Slomianny, C., 2013. Role of mechanical vs. chemical action in the removal of adherent Bacillus spores during CIP procedures. Food Microbiol 33, 149–157. https://doi.org/10.1016/j.fm.2012.09.010

Faille, C., Cunault, C., Dubois, T., Bénézech, T., 2018. Hygienic design of food processing lines to mitigate the risk of bacterial food contamination with respect to environmental concerns. Innovative Food Science & Emerging Technologies, Food Science and Technology in France: INRA's contribution to this area 46, 65–73. https://doi.org/10.1016/j.ifset.2017.10.002

Faille, C., Jullien, C., Fontaine, F., Bellon-Fontaine, M.-N., Slomianny, C., Benezech, T., 2002. Adhesion of Bacillus spores and Escherichia coli cells to inert surfaces: role of surface hydrophobicity. Can J Microbiol 48, 728–738. https://doi.org/10.1139/w02-063

Finn, S., Condell, O., McClure, P., Amézquita, A., Fanning, S., 2013. Mechanisms of survival, responses and sources of Salmonella in low-moisture environments. Front. Microbiol. 4. https://doi.org/10.3389/fmicb.2013.00331

Firoze Akhtar, T., Ahmed, R., Elgaddafi, R., Shah, S., Amani, M., 2018. Rheological behavior of aqueous foams at high pressure. Journal of Petroleum Science and Engineering 162, 214–224. https://doi.org/10.1016/j.petrol.2017.12.050

Flemming, H.-C., Neu, T.R., Wingender, J., 2016. The Perfect Slime: Microbial Extracellular Polymeric Substances (EPS). Water Intelligence Online 15, 9781780407425–9781780407425. https://doi.org/10.2166/9781780407425

Fournet, N., Edith, L., Jones, G., Jourdan Da Silva, N., Tourdjman, M., Chereau, F., Nisavanh, A., De Valk, H., 2019. Santé publique France / Le point épidémio / Surveillance des toxi-infections alimentaires collectives. Données de la déclaration obligatoire, 2018 [WWW Document]. URL https://www.santepubliquefrance.fr/maladies-et-traumatismes/maladies-infectieuses-d-origine-alimentaire/toxi-infections-alimentaires-collectives/documents/bulletin-

national/surveillance-des-toxi-infections-alimentaires-collectives.-donnees-de-la-declaration-obligatoire-2018

Gahleitner, B., Loderer, C., Fuchs, W., 2013. Chemical foam cleaning as an alternative for flux recovery in dynamic filtration processes. Journal of Membrane Science 431, 19–27. https://doi.org/10.1016/j.memsci.2012.12.047

Gahleitner, B., Loderer, C., Saracino, C., Pum, D., Fuchs, W., 2014. Chemical foam cleaning as an efficient alternative for flux recovery in ultrafiltration processes. Journal of Membrane Science 450, 433–439. https://doi.org/10.1016/j.memsci.2013.09.046

Garnier, C., Guiga, W., Lameloise, M.-L., Degrand, L., Fargues, C., 2020. Toward the reduction of water consumption in the vegetable-processing industry through membrane technology: case study of a carrot-processing plant. Environ Sci Pollut Res 27, 42685–42703. https://doi.org/10.1007/s11356-020-10160-0

Gaulin, C., Ramsay, D., Bekal, S., 2012. Widespread Listeriosis Outbreak Attributable to Pasteurized Cheese, Which Led to Extensive Cross-Contamination Affecting Cheese Retailers, Quebec, Canada, 2008. Journal of Food Protection 75, 71–78. https://doi.org/10.4315/0362-028X.JFP-11-236

Gibson, H., Taylor, J.H., Hall, K.E., Holah, J.T., 1999. Effectiveness of cleaning techniques used in the food industry in terms of the removal of bacterial biofilms. J Appl Microbiol 87, 41–48. https://doi.org/10.1046/j.1365-2672.1999.00790.x

Gomes, I.B., Lemos, M., Fernandes, S., Borges, A., Simões, L.C., Simões, M., 2021. The Effects of Chemical and Mechanical Stresses on Bacillus cereus and Pseudomonas fluorescens Single- and Dual-Species Biofilm Removal. Microorganisms 9, 1174. https://doi.org/10.3390/microorganisms9061174

Goode, K.R., Asteriadou, K., Fryer, P.J., Picksley, M., Robbins, P.T., 2010. Characterising the cleaning mechanisms of yeast and the implications for Cleaning In Place (CIP). Food and Bioproducts Processing 88, 365–374. https://doi.org/10.1016/j.fbp.2010.08.005

Grandillo, A., Tatianchenko, S., 2020. Optimization of Clean-In-Place Sanitation Systems for McCain Supply Chain [WWW Document]. URL http://id.loc.gov/vocabulary/iso639-2/eng

Gu, T., Meesrisom, A., Luo, Y., Dinh, Q.N., Lin, S., Yang, M., Sharma, A., Tang, R., Zhang, J., Jia, Z., Millner, P.D., Pearlstein, A.J., Zhang, B., 2021. Listeria monocytogenes biofilm formation as affected by stainless steel surface topography and coating composition. Food Control 130, 108275. https://doi.org/10.1016/j.foodcont.2021.108275

Guignot, S., 2008. Rôle de particules colloïdales sur la stabilité de mousses de décontamination (These de doctorat). Paris Est.

Guillerme, C., Loisel, W., Bertrand, D., Popineau, Y., 1993. STUDY OF FOAM STABILITY BY VIDEO IMAGE ANALYSIS: RELATIONSHIP WITH THE QUANTITY OF LIQUID IN THE FOAMS. J Texture Studies 24, 287–302. https://doi.org/10.1111/j.1745-4603.1993.tb01285.x

Gupta, A.K., Banerjee, P.K., Mishra, A., Satish, P., Pradip, 2007. Effect of alcohol and polyglycol ether frothers on foam stability, bubble size and coal flotation. International Journal of Mineral Processing 82, 126–137. https://doi.org/10.1016/j.minpro.2006.09.002

Hamadi, F., Asserne, F., Elabed, S., Bensouda, S., Mabrouki, M., Latrache, H., 2014. Adhesion of Staphylococcus aureus on stainless steel treated with three types of milk. Food Control Complete, 104–108. https://doi.org/10.1016/j.foodcont.2013.10.006

Hanselmann, W., Windhab, E., 1998. Flow characteristics and modelling of foam generation in a continuous rotor/stator mixer. Journal of Food Engineering 38, 393–405. https://doi.org/10.1016/S0260-8774(98)00129-0

Héry, Binet, Gagnaire, Gérardin, 2003. Nettoyage et désinfection dans l'industrie agroalimentaire : évaluation des expositions aux polluants chimiques. undefined.

Höhler, R., Cohen-Addad, S., 2005. Rheology of liquid foam. J. Phys.: Condens. Matter 17, R1041–R1069. https://doi.org/10.1088/0953-8984/17/41/R01

Holah, J., Saunders, D., 2019. Open Plant Cleaning Methods & Equipment, in: Reference Module in Food Science. Elsevier, p. B9780081005965212000. https://doi.org/10.1016/B978-0-08-100596-5.21205-5

HP Concept, 2020. Solutions de nettoyage agroalimentaire et batiment agricole. HP Concept. URL https://hp-concept.fr/solutions-nettoyage-agroalimentaire-batiment-agricole/ (accessed 1.6.22).

Huerre, A., Miralles, V., Jullien, M.-C., 2014. Bubbles and foams in microfluidics. Soft Matter 10, 6888–6902. https://doi.org/10.1039/C4SM00595C

Hutzler, S., Weaire, D., Crawford, R., 1998. Convective instability in foam drainage. Europhys. Lett. 41, 461–466. https://doi.org/10.1209/epl/i1998-00174-3

Jara, J., Alarcón, F., Monnappa, A.K., Santos, J.I., Bianco, V., Nie, P., Ciamarra, M.P., Canales, Á., Dinis, L., López-Montero, I., Valeriani, C., Orgaz, B., 2021. Self-Adaptation of Pseudomonas fluorescens Biofilms to Hydrodynamic Stress. Front. Microbiol. 11, 588884. https://doi.org/10.3389/fmicb.2020.588884

Jastrzebski, Z.D., 1967. Entrance Effects and Wall Effects in an Extrusion Rheometer during Flow of Concentrated Suspensions. Ind. Eng. Chem. Fund. 6, 445–454. https://doi.org/10.1021/i160023a019

Jensen, B.B.B., Friis, A., 2004. PREDICTION of FLOW IN MIX-PROOF VALVE BY USE of CFD - VALIDATION BY LDA. J Food Process Engineering 27, 65–85. https://doi.org/10.1111/j.1745-4530.2004.tb00623.x

Jensen, B.B.B., Friis, A., Bénézech, Th., Legentilhomme, P., Lelièvre, C., 2005. Local Wall Shear Stress Variations Predicted by Computational Fluid Dynamics for Hygienic Design. Food and Bioproducts Processing 83, 53–60. https://doi.org/10.1205/fbp.04021

Jha, P.K., Dallagi, H., Richard, E., Benezech, T., Faille, C., 2020. Formation and resistance to cleaning of biofilms at air-liquid-wall interface. Influence of bacterial strain and material. Food Control 118, 107384. https://doi.org/10.1016/j.foodcont.2020.107384

Jha, P.K., Dallagi, H., Richard, E., Deleplace, M., Benezech, T., Faille, C., 2022. Does the vertical vs horizontal positioning of surfaces affect either biofilm formation on different materials or their resistance to detachment? Food Control 133, 108646. https://doi.org/10.1016/j.foodcont.2021.108646

Jones, S., Rio, E., Cazeneuve, C., Nicolas-Morgantini, L., Restagno, F., Luengo, G.S., 2016. Tribological influence of a liquid meniscus in human sebum cleaning. Colloids and Surfaces A: Physicochemical and Engineering Aspects 498, 268–275. https://doi.org/10.1016/j.colsurfa.2016.03.047

Kapetas, L., Vincent Bonnieu, S., Danelis, S., Rossen, W.R., Farajzadeh, R., Eftekhari, A.A., Mohd Shafian, S.R., Kamarul Bahrim, R.Z., 2016. Effect of temperature on foam flow in porous media. Journal of Industrial and Engineering Chemistry 36, 229–237. https://doi.org/10.1016/j.jiec.2016.02.001

Khan, S., Abbas, A., Rana, T., Carroll, J., 2010. Dairy water use in Australian dairy farms: past trends and future prospects. https://doi.org/10.4225/08/58615CA753885

Khan, S.A., Armstrong, R.C., 1987. Rheology of foams: II. Effects of polydispersity and liquid viscosity for foams having gas fraction approaching unity. Journal of Non-Newtonian Fluid Mechanics 25, 61–92. https://doi.org/10.1016/0377-0257(87)85013-9

Koehler, S.A., Hilgenfeldt, S., Stone, H.A., 2004. Foam drainage on the microscale. Journal of Colloid and Interface Science 276, 420–438. https://doi.org/10.1016/j.jcis.2003.12.061

Kriegel, A.T., Ducker, W.A., 2019. Removal of Bacteria from Solids by Bubbles: Effect of Solid Wettability, Interaction Geometry, and Liquid–Vapor Interface Velocity. Langmuir 35, 12817–12830. https://doi.org/10.1021/acs.langmuir.9b01941

Kröger, M., Vermant, J., 2000. The Structure and Rheology of Complex Fluids. Applied Rheology 10, 110–111. https://doi.org/10.1515/arh-2000-0024

Langevin, D., 2014. Surface shear rheology of monolayers at the surface of water. Advances in Colloid and Interface Science 207, 121–130. https://doi.org/10.1016/j.cis.2013.10.030

Latifi, M.A., Midoux, N., Storck, A., Gence, J.N., 1989. The use of micro-electrodes in the study of the flow regimes in a packed bed reactor with single phase liquid flow. Chemical Engineering Science 44, 2501–2508. https://doi.org/10.1016/0009-2509(89)85194-2

Le Toquin, E., Faure, S., Orange, N., Gas, F., 2020. New Biocide Foam Containing Hydrogen Peroxide for the Decontamination of Vertical Surface Contaminated With Bacillus thuringiensis Spores. Frontiers in Microbiology 9. https://doi.org/10.3389/fmicb.2018.02295

Lee, E.-J., Kim, Y.-H., Lee, C.-H., Kim, Hyung-Soo, Kim, Hyung-Sook, 2016. Effect of different physical conditions on fouling control in in-situ chemical cleaning in place (CIP) for flat sheet membranes fouled by secondary effluents. Chemical Engineering Journal 302, 128–136. https://doi.org/10.1016/j.cej.2016.05.039

Lee, J.-S., Bae, Y.-M., Lee, Sook-Young, Lee, Sun-Young, 2015. Biofilm Formation of Staphylococcus aureus on Various Surfaces and Their Resistance to Chlorine Sanitizer. J Food Sci 80, M2279-2286. https://doi.org/10.1111/1750-3841.13017

Li, B., Li, H., Cao, A., Wang, F., 2019. Effect of surfactant concentration on foam texture and flow characteristics in porous media. Colloids and Surfaces A: Physicochemical and Engineering Aspects 560, 189–197. https://doi.org/10.1016/j.colsurfa.2018.10.027

Li, G., Tang, L., Zhang, X., Dong, J., 2019. A review of factors affecting the efficiency of clean-in-place procedures in closed processing systems. Energy 178, 57–71. https://doi.org/10.1016/j.energy.2019.04.123

Li, H., Huang, D., Ren, K., Ji, J., 2021. Inorganic-polymer composite coatings for biomedical devices. Smart Materials in Medicine 2, 1–14. https://doi.org/10.1016/j.smaim.2020.10.002

Louvet, N., Rouyer, F., Pitois, O., 2009. Ripening of a draining foam bubble. Journal of Colloid and Interface Science 334, 82–86. https://doi.org/10.1016/j.jcis.2009.02.042

Lyndgaard, C.B., Rasmussen, M.A., Engelsen, S.B., Thaysen, D., van den Berg, F., 2014. Moving from recipe-driven to measurement-based cleaning procedures: Monitoring the Cleaning-In-Place process of whey filtration units by ultraviolet spectroscopy and chemometrics. Journal of food engineering.

Maes, S., Heyndrickx, M., Vackier, T., Steenackers, H., Verplaetse, A., Reu, K.D., 2019. Identification and Spoilage Potential of the Remaining Dominant Microbiota on Food Contact Surfaces after Cleaning and Disinfection in Different Food Industries. Journal of Food Protection 82, 262–275. https://doi.org/10.4315/0362-028X.JFP-18-226

Marchand, M., Restagno, F., Rio, E., Boulogne, F., 2020. Roughness-Induced Friction on Liquid Foams. Phys. Rev. Lett. 124, 118003. https://doi.org/10.1103/PhysRevLett.124.118003

Mason, T.G., Bibette, J., Weitz, D.A., 1996. Yielding and Flow of Monodisperse Emulsions. Journal of Colloid and Interface Science 179, 439–448. https://doi.org/10.1006/jcis.1996.0235

Meliani, A., Bensoltane, A., 2015. Review of Pseudomonas Attachment and Biofilm Formation in Food Industry. Poult Fish Wildl Sci 03. https://doi.org/10.4172/2375-446X.1000126

Mierzejewska, S., Mas, S., owska, Piepiórka-Stepuk, J., 2015. Evaluation of efficiency of removing protein deposits from various surfaces by foam cleaning [WWW Document]. URL https://www.semanticscholar.org/paper/EVALUATION-OF-EFFICIENCY-OF-REMOVING-PROTEIN-FROM-Mierzejewska-Mas/5d345ceb91bfae9fa4cde9fd6243b74aebdc64dc (accessed 1.6.22).

Mierzejewska, S., Masłowska, S., Piepiórka-Stepuk, J., 2014. Evaluation of the efficiency of removing protein deposits from various surfaces by foam cleaning. Agricultural Engineering 131–137. https://doi.org/10.14654/ir.2014.149.014

Mierzejewska, S., Piepiórka-Stepuk, J., 2016. Concentration and time of aeration selected cleaning solutions influence on stability of foam 3.

Miller, B.A., Wenzel, H.G., 1985. Analysis and Simulation of Low Flow Hydraulics. Journal of Hydraulic Engineering 111, 1429–1446. https://doi.org/10.1061/(ASCE)0733-9429(1985)111:12(1429)

Mouquet, A., 2018. Structure et élasticité des films moussés : Effets de la distribution des tailles des bulles (These de doctorat). Paris Est.

Mühlbauer, A., Hlawitschka, M.W., Bart, H., 2019. Models for the Numerical Simulation of Bubble Columns: A Review. Chemie Ingenieur Technik 91, 1747–1765. https://doi.org/10.1002/cite.201900109

Naim, R., Levitsky, I., Gitis, V., 2012. Surfactant cleaning of UF membranes fouled by proteins. Separation and Purification Technology 94, 39–43. https://doi.org/10.1016/j.seppur.2012.03.031

Narchi, I., 2008. Etude du procédé de foisonnement en continu des milieux modèles : interaction formulation-procédé sur les propriétés du produit fini (phdthesis). Université Blaise Pascal - Clermont-Ferrand II.

Niranjan, K., Silva, S.F.J., 2008. Bubbles in Foods: Creating Structure out of Thin Air!, in: Gutiérrez-López, G.F., Barbosa-Cánovas, G.V., Welti-Chanes, J., Parada-Arias, E. (Eds.), Food Engineering: Integrated Approaches, Food Engineering Series. Springer New York, New York, NY, pp. 183–192. https://doi.org/10.1007/978-0-387-75430-7_10

Nitschke, M., Costa, S.G.V.A.O., 2007. Biosurfactants in food industry. Trends in Food Science & Technology 18, 252–259. https://doi.org/10.1016/j.tifs.2007.01.002

Osei-Bonsu, K., Shokri, N., Grassia, P., 2015. Foam stability in the presence and absence of hydrocarbons: From bubble- to bulk-scale. Colloids and Surfaces A: Physicochemical and Engineering Aspects 481, 514–526. https://doi.org/10.1016/j.colsurfa.2015.06.023

Oswald, J., Mullen, R., Steinetz, B., Dunlap, P., 2005. Modeling of Canted Coil Springs and Knitted Spring Tubes as High Temperature Seal Preload Devices, in: 41st AIAA/ASME/SAE/ASEE Joint Propulsion Conference & Exhibit. American Institute of Aeronautics and Astronautics. https://doi.org/10.2514/6.2005-4156

Pal, R., 1996. Rheological properties of mixed polysaccharides and polysaccharide-thickened emulsions. AIChE J. 42, 1824–1832. https://doi.org/10.1002/aic.690420704

Palanisamy, N., Ferina, N., Amirulhusni, A., Mohd-Zain, Z., Hussaini, J., Ping, L., Durairaj, R., 2014. Antibiofilm properties of chemically synthesized silver nanoparticles found against Pseudomonas aeruginosa. J Nanobiotechnol 12, 2. https://doi.org/10.1186/1477-3155-12-2

Pang, X., Singh, J., Cuello Jimenez, W., 2018. Characterizing gas bubble size distribution of laboratory foamed cement using X-ray micro-CT. Construction and Building Materials 167, 243–252. https://doi.org/10.1016/j.conbuildmat.2018.02.030

Pechaud, Y., Marcato-Romain, C.E., Girbal-Neuhauser, E., Queinnec, I., Bessiere, Y., Paul, E., 2012. Combining hydrodynamic and enzymatic treatments to improve multi-species thick biofilm removal. Chemical Engineering Science 80, 109–118. https://doi.org/10.1016/j.ces.2012.06.014

Peng, J.-S., Tsai, W.-C., Chou, C.-C., 2002. Inactivation and removal of Bacillus cereus by sanitizer and detergent. Int J Food Microbiol 77, 11–18. https://doi.org/10.1016/s0168-1605(02)00060-0

Petkova, B., Tcholakova, S., Chenkova, M., Golemanov, K., Denkov, N., Thorley, D., Stoyanov, S., 2020. Foamability of aqueous solutions: Role of surfactant type and concentration. Advances in Colloid and Interface Science 276, 102084. https://doi.org/10.1016/j.cis.2019.102084

Piepiórka-Stepuk, J., Diakun, J., Jakubowski, M., 2017. The Parameters of Cleaning a CIP System Affected Energy Consumption and Cleaning Efficiency of the Plate Heat Exchanger. Chemical and Process Engineering 38, 111–120. https://doi.org/10.1515/cpe-2017-0009

Pinguli, L., Malollari, I., Lici, L., 2017. Optimization of cleaning process in breweries an important tool in efficient use of water and minimization of discharges. European Journal of Engineering and Technology 5, 7.

Plateau, J., 1873. Statique expérimentale et théorique des liquides soumis aux seules forces moléculaires. Gauthier-Villars.

Princen, H.M., 1985. Rheology of foams and highly concentrated emulsions. II. experimental study of the yield stress and wall effects for concentrated oil-in-water emulsions. Journal of Colloid and Interface Science 105, 150–171. https://doi.org/10.1016/0021-9797(85)90358-3

Princen, H.M., 1983. Rheology of foams and highly concentrated emulsions: I. Elastic properties and yield stress of a cylindrical model system. Journal of Colloid and Interface Science 91, 160–175. https://doi.org/10.1016/0021-9797(83)90323-5

Princen, H.M., Kiss, A.D., 1989. Rheology of foams and highly concentrated emulsions: IV. An experimental study of the shear viscosity and yield stress of concentrated emulsions. Journal of Colloid and Interface Science 128, 176–187. https://doi.org/10.1016/0021-9797(89)90396-2

Puga, C.H., Dahdouh, E., SanJose, C., Orgaz, B., 2018. Listeria monocytogenes Colonizes Pseudomonas fluorescens Biofilms and Induces Matrix Over-Production. Front. Microbiol. 9, 1706. https://doi.org/10.3389/fmicb.2018.01706

Rand, P.B., Kraynik, A.M., 1983. Drainage of Aqueous Foams: Generation-Pressure and Cell-Size Effects. Society of Petroleum Engineers Journal 23, 152–154. https://doi.org/10.2118/10533-PA

Raposo, A., Ramos, F., Raheem, D., Saraiva, A., Carrascosa, C., 2021. Food Safety, Security, Sustainability and Nutrition as Priority Objectives of the Food Sector. IJERPH 18, 8073. https://doi.org/10.3390/ijerph18158073

Raufaste, C., Cox, S.J., Marmottant, P., Graner, F., 2010. Discrete rearranging disordered patterns: Prediction of elastic and plastic behavior, and application to two-dimensional foams. Phys. Rev. E 81, 031404. https://doi.org/10.1103/PhysRevE.81.031404

Reidenbach, V.G., Harris, P.C., Lee, Y.N., Lord, D.L., 1986. Rheological Study of Foam Fracturing Fluids Using Nitrogen and Carbon Dioxide. SPE Production Engineering 1, 31–41. https://doi.org/10.2118/12026-PA

Richard, E., Dubois, T., Allion-Maurer, A., Jha, P.K., Faille, C., 2020. Hydrophobicity of abiotic surfaces governs droplets deposition and evaporation patterns. Food Microbiology 91, 103538. https://doi.org/10.1016/j.fm.2020.103538

Rouyer, F., Cohen-Addad, S., Vignes-Adler, M., Höhler, R., 2003. Dynamics of yielding observed in a three-dimensional aqueous dry foam. Phys. Rev. E 67, 021405. https://doi.org/10.1103/PhysRevE.67.021405

Saint-Jalmes, A., Durian, D.J., 1999. Vanishing elasticity for wet foams: Equivalence with emulsions and role of polydispersity. Journal of Rheology 43, 1411–1422. https://doi.org/10.1122/1.551052

Sar, P., Ghosh, A., Scarso, A., Saha, B., 2019. Surfactant for better tomorrow: applied aspect of surfactant aggregates from laboratory to industry. Res Chem Intermed 45, 6021–6041. https://doi.org/10.1007/s11164-019-04017-6

Sarma, D.S.H.S.R., Khilar, K.C., 1988. Effects of initial gas volume fraction on stability of aqueous air foams. Ind. Eng. Chem. Res. 27, 892–894. https://doi.org/10.1021/ie00077a029

Saubade, F., Pilkington, L.I., Liauw, C.M., Gomes, L.C., McClements, J., Peeters, M., El Mohtadi, M., Mergulhão, F.J., Whitehead, K.A., 2021. Principal Component Analysis to Determine the Surface Properties That Influence the Self-Cleaning Action of Hydrophobic Plant Leaves. Langmuir 37, 8177–8189. https://doi.org/10.1021/acs.langmuir.1c00853

Schad, T., Preisig, N., Blunk, D., Piening, H., Drenckhan, W., Stubenrauch, C., 2021. Less is more: Unstable foams clean better than stable foams. Journal of Colloid and Interface Science 590, 311–320. https://doi.org/10.1016/j.jcis.2021.01.048

Schlegelová, J., Babák, V., Holasová, M., Konstantinová, L., Necidová, L., Šišák, F., Vlková, H., Roubal, P., Jaglic, Z., 2010. Microbial contamination after sanitation of food contact surfaces in dairy and meat processing plants. Czech Journal of Food Sciences 28, 450–461. https://doi.org/10.17221/65/2009-CJFS

Schmitz-Esser, S., Müller, A., Stessl, B., Wagner, M., 2015. Genomes of sequence type 121 Listeria monocytogenes strains harbor highly conserved plasmids and prophages. Front. Microbiol. 6. https://doi.org/10.3389/fmicb.2015.00380

Schnöing, L., Augustin, W., Scholl, S., 2020. Fouling mitigation in food processes by modification of heat transfer surfaces: A review. Food and Bioproducts Processing 121, 1–19. https://doi.org/10.1016/j.fbp.2020.01.013

Shafi, M.A., Joshi, K., Flumerfelt, R.W., 1997. Bubble size distributions in freely expanded polymer foams. Chemical Engineering Science 52, 635–644. https://doi.org/10.1016/S0009-2509(96)00433-2

Silva, L.D., Filho, U.C., Naves, E.A.A., Gedraite, R., 2021. Pulsed flow in clean-in-place sanitization to improve hygiene and energy savings in dairy industry. J Food Process Eng 44. https://doi.org/10.1111/jfpe.13590

Silva, S., Teixeira, P., Oliveira, R., Azeredo, J., 2008. Adhesion to and viability of Listeria monocytogenes on food contact surfaces. J Food Prot 71, 1379–1385. https://doi.org/10.4315/0362-028x-71.7.1379

Singh, R., Mohanty, K.K., 2016. Foams With Wettability-Altering Capabilities for Oil-Wet Carbonates: A Synergistic Approach. SPE Journal 21, 1126–1139. https://doi.org/10.2118/175027-PA

Speranza, B., Corbo, M.R., 2017. Chapter 11 - The Impact of Biofilms on Food Spoilage, in: Bevilacqua, A., Corbo, M.R., Sinigaglia, M. (Eds.), The Microbiological Quality of Food, Woodhead Publishing Series in Food Science, Technology and Nutrition. Woodhead Publishing, pp. 259–282. https://doi.org/10.1016/B978-0-08-100502-6.00014-5

Stellato, G., Utter, D.R., Voorhis, A., De Angelis, M., Eren, A.M., Ercolini, D., 2017. A Few Pseudomonas Oligotypes Dominate in the Meat and Dairy Processing Environment. Front. Microbiol. 8. https://doi.org/10.3389/fmicb.2017.00264

Stoodley, P., Sauer, K., Davies, D.G., Costerton, J.W., 2002. Biofilms as Complex Differentiated Communities. Annu. Rev. Microbiol. 56, 187–209. https://doi.org/10.1146/annurev.micro.56.012302.160705

Suzuki, Y., Hanagasaki, N., Furukawa, T., Yoshida, T., 2008. Removal of bacteria from coastal seawater by foam separation using dispersed bubbles and surface-active substances. Journal of Bioscience and Bioengineering 105, 383–388. https://doi.org/10.1263/jbb.105.383

Tanaka, A., Hjelt, T., Sneck, A., Korpela, A., 2012. Fractionation of Nanocellulose by Foam Filter. Separation Science and Technology 47, 1771–1776. https://doi.org/10.1080/01496395.2012.661825

Tcholakova, S., Denkov, N.D., Golemanov, K., Ananthapadmanabhan, K.P., Lips, A., 2008. Theoretical model of viscous friction inside steadily sheared foams and concentrated emulsions. Physical Review E 78. https://doi.org/10.1103/PhysRevE.78.011405

Thakore, V., Ren, F., Voytek, J., Wang, H., Wang, J.-A.J., Polsky, Y., 2021. High Temperature Stability of Aqueous Foams for Potential Application in Enhanced Geothermal System (EGS). Oak Ridge National Lab. (ORNL), Oak Ridge, TN (United States).

Thobie, C., 2018. Caractérisation de l'hydrodynamique et des transferts gaz-liquide dans un photobioréacteur intensifié : étude de l'effet du bullage sur le développement de biofilm micro-algal (These de doctorat). Nantes.

Tisné, P., Aloui, F., Doubliez, L., 2003. Analysis of wall shear stress in wet foam flows using the electrochemical method. International Journal of Multiphase Flow 29, 841–854. https://doi.org/10.1016/S0301-9322(03)00038-7

Verran, J., Packer, A., Kelly, P., Whitehead, K.A., 2010. Titanium-coating of stainless steel as an aid to improved cleanability. International Journal of Food Microbiology 141, S134–S139. https://doi.org/10.1016/j.ijfoodmicro.2010.04.027

Wang, Z., Narsimhan, G., 2006. Model for Plateau border drainage of power-law fluid with mobile interface and its application to foam drainage. Journal of Colloid and Interface Science 300, 327–337. https://doi.org/10.1016/j.jcis.2006.03.023

Weaire, D., 2008. The rheology of foam. Current Opinion in Colloid & Interface Science 13, 171–176. https://doi.org/10.1016/j.cocis.2007.11.004

Weaire, D., Hutzler, S., 1999. The Physics of Foams, Clarendon Press. ed. Oxford.

Weber, M., Liedtke, J., Plattes, S., Lipski, A., 2019. Bacterial community composition of biofilms in milking machines of two dairy farms assessed by a combination of culture-dependent and –independent methods. PLoS ONE 14, e0222238. https://doi.org/10.1371/journal.pone.0222238

Whitehead, K.A., Olivier, S., Benson, P.S., Arneborg, N., Verran, J., Kelly, P., 2015. The effect of surface properties of polycrystalline, single phase metal coatings on bacterial retention. International Journal of Food Microbiology 197, 92–97. https://doi.org/10.1016/j.ijfoodmicro.2014.12.030

Whitehead, K.A., Verran, J., 2007. The effect of surface properties and application method on the retention of Pseudomonas aeruginosa on uncoated and titanium-coated stainless steel. International Biodeterioration & Biodegradation 60, 74–80. https://doi.org/10.1016/j.ibiod.2006.11.009

Wilson, D.I., 2005. Challenges in Cleaning: Recent Developments and Future Prospects. Heat Transfer Engineering 26, 51–59. https://doi.org/10.1080/01457630590890175

Wilson-Nieuwenhuis, J.S.T., Dempsey-Hibbert, N., Liauw, C.M., Whitehead, K.A., 2017. Surface modification of platelet concentrate bags to reduce biofilm formation and transfusion sepsis. Colloids and Surfaces B: Biointerfaces 160, 126–135. https://doi.org/10.1016/j.colsurfb.2017.09.019

Wu, M.-S., Sullivan, M.E., Yee, D.J., 1984. The viscosity of a foam (air in water emulsion). Colloids and Surfaces 12, 375–380. https://doi.org/10.1016/0166-6622(84)80112-2

Xu, C., Wang, H., Wang, D., Zhu, X., Zhu, Y., Bai, X., Yang, Q., 2020. Improvement of Foaming Ability of Surfactant Solutions by Water-Soluble Polymers: Experiment and Molecular Dynamics Simulation. Polymers 12, 571. https://doi.org/10.3390/polym12030571

Yang, J., Kjellberg, K., Jensen, B.B.B., Nordkvist, M., Gernaey, K.V., Krühne, U., 2019. Investigation of the cleaning of egg yolk deposits from tank surfaces using continuous and pulsed flows. Food and Bioproducts Processing 113, 154–167. https://doi.org/10.1016/j.fbp.2018.10.007

Zdankus, T., Gylys, M., Paukstaitis, L., Jonynas, R., 2018. Experimental investigation of heat transfer from a horizontal flat surface to aqueous foam flow. International Journal of Heat and Mass Transfer 123, 489–499. https://doi.org/10.1016/j.ijheatmasstransfer.2018.02.116

Zhao, Q., Liu, Y., 2006. Modification of stainless steel surfaces by electroless Ni-P and small amount of PTFE to minimize bacterial adhesion. Journal of Food Engineering 72, 266–272. https://doi.org/10.1016/j.jfoodeng.2004.12.006

Zhao, Q., Liu, Y., Wang, C., 2005a. Development and evaluation of electroless Ag-PTFE composite coatings with anti-microbial and anti-corrosion properties. Applied Surface Science 252, 1620–1627. https://doi.org/10.1016/j.apsusc.2005.02.098

Zhao, Q., Liu, Y., Wang, C., Wang, S., Müller-Steinhagen, H., 2005b. Effect of surface free energy on the adhesion of biofouling and crystalline fouling. Chemical Engineering Science 60, 4858–4865. https://doi.org/10.1016/j.ces.2005.04.006

CHAPTER 2: FOAM RHEOLOGY

Contents

Objectives, main approaches, and progress

The rheological properties of foams are very complex and they play a significant role in defining the foam behavior and its related industrial applications. Accessing this complexity becomes a major challenge. Computational fluid dynamics is an appropriate approach to obtain an adequate estimation of the flow behavior of fluids in various conditions where experimental approaches are too challenging. This chapter presents experimental and numerical results on foam flow behavior for different foam qualities under various Reynolds numbers. A flow in a straight pipe then a flow with perturbation features (half expansion and fence) which could mimic what could be observed in complex food equipment were studied. In this chapter, three sections will be presented in the form of three publications. The first and second parts are two conference papers that consisted of a brief comparison of numerical simulation and existing experimental results in the literature, whereas the third part is a research paper presenting an improvement of the previous simulations with detailed experimental data in case of the foam flow under a fence.

The first publication is part of research on the rheological behavior of liquid foams that studies foam flow in a horizontal straight square channel. It is devoted particularly to defining a robust model for describing this fluid by an inversed approach of a numerical simulation using the Herschel- Bulkley model: foam could be considered as a non-Newtonian fluids. This inversed method is based on the idea of starting from experimental results (already existing in the literature) such as pressure losses, velocity fields, velocity profiles, and wall shear stress variations in case of flow foam and identify the different parameters of this model allowing the best fit with the experimental data. Different parameters were studied such as the foam quality (varies from 55 to 85%) and the velocity (2 and 6 cm/s), affecting the nature of the flow, the rheological behavior, and the foam flow regime evolution along the channels' length. Whatever the foam quality, the velocity profiles for the condition of foam flow at 2 cm/s were constant and exhibited a plug flow behavior (moving like a block). However, at 6 cm/s a three-dimensional regime appeared with a stretch of the foam at the pipe's bottom presenting there a pic value of the velocity. The liquid film thickness evolution being thin at the top part of the channel while it is thick at the bottom due to the drainage phenomenon was assumed theoretically from the velocity and the pressure loss. Comparison between numerical results and experimental work deduced from Particle Imaging Velocimetry (PIV) technique shown a good agreement. Finally, this numerical study shown that the Herschel-Bulkley rheological

model can correctly suit the experimental behavior of such a complex fluid and for different foam qualities.

The second publication aimed to expand the previous research work to verify the ability of the Herschel-Bulkley model to describe a foam flowing in a half-sudden expansion (under various regimes, and for differing foam qualities) and to predict the modifications brought by such a diameter change. The numerical results of the CFD simulation obtained were compared with an experimental database available in the literature. The CFD results highlighted the fact that the sudden expansion of the pipe cross-section resulted in energy degradation with a reduction in total pressure loss in the immediate vicinity of the singularity accompanied by a larger pressure gradient in the expansion than downstream. Regardless of the foam quality, the Herschel-Bulkley model modeled well the behavior of foam through the sudden half-expansion in a one-dimensional regime (plug-type flow) which is consistent with the experimental results. While in the case of higher velocity, a slight difference could be clearly related to the intrinsic rheological properties of the foam apparently not completely taken into account.

In the third paper, experimental and numerical investigations were carried out to identify the flow of a wet foam (quality of 65%: 35/100 water-SDS surfactant volume) through a fence placed in the middle of the pipe. The aim was to characterize the foam flow behavior in a more complex situation relevant again to geometries encountered in industrial systems. The fence effects on the foam structure, foam reorganization, and foam flow dynamics were characterized for three different flow rate conditions involving three flow regimes: 1D plug flow, 2D sheared flow and 3D sheared flow. Measurements using pressure sensors, Particle Image Velocimetry (PIV) and a conductimetry technique allowed the entire reorganization of the foam flow to be described, both in terms of pressure distribution and dynamics upstream and downstream of the fence. Results show a reorganization of the foam downstream, with a thicker liquid film at the bottom, larger bubble sizes at the top, and a larger void fraction increasing from the bottom up to the top of the cross-section.

These results confirmed the importance of foam properties in its rheology and physics, demonstrating how sensitive and complex foams are. This information will facilitate our simulation, which aims to predict the viscoelastic character of foam, as for a non-Newtonian fluid, when passing through the fence. For this purpose and based on the previous publication, Herschel-Bulkley and/or Bingham laws relating to the presence of an underlying liquid film at the bottom of the channel were selected. In these rheological models, the parameters such as

yield stress, foam consistency, and flow index were adjusted from the experimental data obtained. Thus, these models were applied to simulate the foam flow dynamics using CFD simulations. The results obtained showed a close agreement with experiments for all flow regimes using the Herschel-Bulkley model but presenting more deviation at higher velocity.
Despite the complexity of the properties involved in the physics of foams (border stability plateau, effect of surface tension, drainage of liquid, bubble movements, coarsening, ripening, coalescence, etc.), the non-Newtonian fluid model with a yield stress gives an approximation of the foam's flow behavior and its deformation on encountering singularities. In the current state of research, experimental efforts must focus primarily on the adjustment of the rheological parameters, which depend on the geometry and the flow conditions dependant on the foam quality, on the dynamics of the surfactant used and on the Reynolds number / flow regime, foam being prone to internal movements (turbulences). Knowing all these aspects will help us to understand the mechanisms when foam flow will be used to clean contaminated surfaces related to the food industry. CFD simulation is a relevant helpful tool to improve the cleaning efficiency when modeling and designing industrial equipment and installing its accessories, thereby ensuring high foam stability and fast recovery of the flow regime due to a better flow organization.

Highlights

CFD was used to describe the flow of wet foam by comparing the results obtained from experimental studies for both a simple pipe and more complex geometrical situations such as sudden expansion or the presence of obstacles within the pipe

Reorganization and structural changes of the foam are clearly observed downstream of the singularities

There is a significant effect of the liquid films at the wall on the pressure drop and on the parietal stress organization

A simple non-Newtonian 3-parameters' model allows for accurate rheological behavior of foam flow for both simple and complex pipe geometries

Publication I: CFD characterization of a wet foam flow rheological behavior

https://doi.org/10.1115/FEDSM2018-83338

Proceedings of the 5th Joint US-European Fluids Engineering Summer Conference
FEDSM18
Jul 15 - 20, 2018, Le Centre Sheraton, Montreal, Quebec Canada
FEDSM2018-83338

CFD CHARACTERIZATION OF A WET FOAM FLOW RHEOLOGICAL BEHAVIOR

Heni DALLAGI [1]
Dallagi.heni@gmail.com
UMET UMR 8207, National Institute for Agricultural Research, 369, Rue Jules Guesde, BP 39 F-59651 Villeneuve d'Ascq Cedex France

Ramla GHEITH
ramla2gheith@yahoo.fr
University of Monastir, National High Eng. School of Monastir, Laboratory LESTE, Avenue Ibn El Jazzar 5019 Monastir Tunisia

Ahmad AL SAABI [2]
ahmad.al-saabi@inra.fr
UMET UMR 8207, National Institute for Agricultural Research, 369, Rue Jules Guesde, BP 39 F-59651 Villeneuve d'Ascq Cedex France

Christine FAILLE [3]
Christine.faille@inra.fr
UMET UMR 8207, National Institute for Agricultural Research, 369, Rue Jules Guesde, B.P.39, F-59651 Villeneuve d'Ascq Cedex France

Wolfgang AUGUSTIN
w.augustin@tu-braunschweig.de Technische Universität Braunschweig, Institute for Chemical and Thermal Process Engineering, Langer Kamp 7, 38106 Braunschweig - Germany

Thierry BENEZECH [4]
Thierry.Benezech@inra.fr
UMET UMR 8207, National Institute for Agricultural Research, 369, Rue Jules Guesde, B.P.39 F-59651 Villeneuve d'Ascq Cedex France

*** Fethi ALOUI**
** Corresponding author: fethi.aloui@univ-valenciennes.fr*
LAMIH UMR CNRS 8201, University of Valenciennes (UVHC), Department of Mechanical Engineering, Campus Mont Houy, F-59313 Valenciennes Cedex 9 - France

ABSTRACT
In some industrial processes, aqueous foams flow presents an important phase of the process, whereas, they cause pressure drop when designing and dimensioning systems. Identifying the different rheological parameters of foam flow is an interesting key to understanding the interfacial phenomena. Actually, the difficulty to model the rheological parameters of foam flow is a major challenge.
In this study, we present a robust model to describe the foam fluid inside horizontal channels by the reverse approach of a numerical simulation (Computational Fluid Dynamics: CFD), based on the behavior laws of the Herschel-Bulkley type, for the non-Newtonian fluids. This reverse method starts from experimental (deduced from Particle Image Velocimetry (PIV) technique) results of the previous experimental work of Chovet (2015). The pressure losses measurements near-wall velocity fields, velocity profiles, and the wall shear stress evolution including the void fraction from 55% to 85%, are considered in order to identify the different parameters of the developed model to determine the nature of the flow, the foams rheological behavior and the foam flow regime along the length of the channel.
The numerical study (CFD) is applied for two conditions: the first one for a wet foam flow with a void fraction of 70% and a foam flow velocity of 2cm/s (one-dimensional regime) and the second one, for a foam quality of 55% and a flow rate of 6cm/s. The numerical evolutions are identical to experimental ones for these same conditions. Therefore, we can conclude that the Herschel-Bulkley rheological model can correctly describe the aqueous foam flow behavior.

KEYWORDS
Aqueous foam flow, Rheology, Herschel-Bulkley model, Particle Image Velocimetry (PIV), Wall shear stress, Pressure losses, CFD simulations, Liquid-slipping layer, Void fraction.

[1,2,3,4] INRA (National Institute for Agricultural Research)

I. INTRODUCTION

Foams admit unforeseen and nonlinear rheological behavior since it is influenced by the properties of both liquids and gases. This difficulty did not prevent foam to be a major subject of active research, due to its intensive presence in the industry field. The presence of foams is essential in cosmetics, nuclear engineering, petroleum engineering, fire extinguishers, and in the food industry. In contact with the pipe walls, foam presents an important friction coefficient, which explains its use for cleaning hydraulic circuits in various industrial fields [1-2].

Rheology is the science treating the deformation and the material flow that seeks links between the imposed stresses and the strains produced [3]. The foam is considered as an elasto-visco-plastic fluid. It can be elastic, viscous, or plastic, according to the disruption that we apply [4-5-6-7]. Certainly, from one foam to another, special properties will change. Foam can be more rigid, can tolerate larger deformations, or can break if we try to distort it quickly. These differences come from the liquid proportion, or from the distribution of the bubbles' sizes. But basically, its behavior is related to its structure, more exactly to the nature of cellular materials [8].

It appears that the foam complex structure gives it a higher shear resistance, which is interpretable according to Camp (1988) by the existence of yield stress. Indeed, foams require a minimum amount of energy to be in flow, when foam flows, the stress is greater or equal to the yield stress, to which is added a viscous contribution, which depends on applied shear rate whose rheological behavior, can be described as a non-Newtonian. In a general approach, the most common models are those that consider a shear at the middle of the foam [9-10-11]. The continuum non-Newtonian models are:

Bingham: $\tau = \tau_0 + k.\dot{\gamma}$ (1)

Ostwald de Weale: $\tau = k.\dot{\gamma}^n$ (2)

Herschel-Bulkley: $\tau = \tau_0 + k.\dot{\gamma}^n$ (3)

However, some previous studies show that a Bingham fluid can predict the behavior of a foam flow, only for low velocity and most of its results present a deviation of 25% and 50%. Then, we consider a power law of Herschel-Bulkley model and test its efficiency to describe such flow situations [9-12].

In addition, the experimental measurements of axial velocity profiles at the lateral wall of the foam flowing inside horizontal channels, made by Blondin (1999), Tisné (2003) and Aloui and Madani (2008) helped to highlight three flow regimes whose scope depends on both the velocity

of gas and liquid, on the average velocity inside the pipe's measurement and its geometry [13-14-15-16].

These three flow regimes are:

- One-dimensional regime, the velocity vector has only one uniform axial component in the flow direction.
- Two-dimensional regime corresponding to a vertically sheared flow.
- Three-dimensional regime corresponding to a completely sheared foam flow.

II. NUMERICAL PARAMETERS

In order to simulate the foams flow inside horizontal straight channels, the Computational Fluid Dynamics (CFD) geometry dimensions, must be the same as the experimental facility. Therefore, was 3D geometry formed of a tube of a square cross-section of 21x21mm^2 and a length L of 3.2m, is considered (Figure 20). From experimental results (Aloui and Madani, 2008), we consider velocity values, static pressure, and velocity gradients corresponding to each flow regime along the channel's length. Several profiles are matched and those, which are validated, will be pulled.

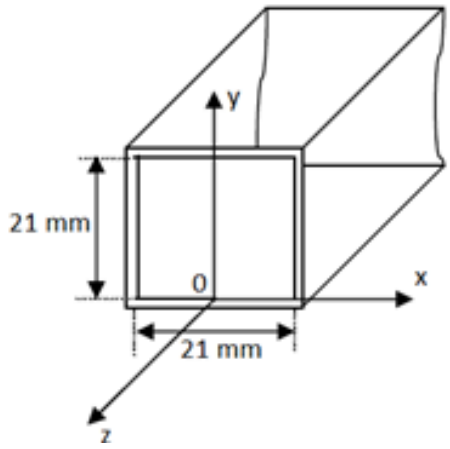

Figure 20. 3D geometry of test-section.

For constraints greater than the yield stress, and in order to simplify the study, we assumed:

- the foam behaves as a pseudo-fluid (an air-water mixture that proportions are fixed by foam quality β),
- non-Newtonian rheo-fluidifying behavior (Power Law index values lower than 1)
- flow with a nonlinear behavior's law which is modeled by an equation of Herschel-Bulkley that related the shear stress, with the shear strain rate, such as:

$$\frac{\partial \tau}{\partial \dot{\gamma}} = n.k.\dot{\gamma}^{n-1} \tag{4}$$

$$\mu = \frac{\tau_0}{\lambda.\dot{\gamma}} + k\,(\lambda.\dot{\gamma})^{n-1} \tag{5}$$

where n is known as the flow index, k the consistency index, and $\dot{\gamma}$ the shear rate. In this case, the stress does not surpass the yield stress, $\dot{\gamma}=0$.
The consistency index k is given by the following relationship:

$$k = 2.10 - 4.e^{4.35\Phi_G} \quad (6)$$

The constant flow index n, was set equal to 0.8, after calibrating the model with the experimental data.
Concerning the yield stress, the foam density, the molar mass, the specific heat capacity, and the quality, they are respectively defined as follow:

Yield stress: $\tau_0 = 3.1\,Pa$

Density: $\rho_M = (1-\beta).\rho_L + \beta.\rho_G \quad (7)$

Molar mass: $M_M = (1-\beta).M_L + \beta.M_G \quad (8)$

$M_M = (1-\beta).M_L + \beta.M_G \quad (9)$

$C_{PM} = (1-\beta).C_{PL} + \beta.C_{PG} \quad (10)$

$$\beta = \frac{Q_G}{Q_L + Q_G} \quad (11)$$

The setting of these parameters was not done randomly, but it was chosen after several simulations. Indeed, the power-law index n was varied from 0 to 1 and the yield stress τ_0 changed for each value.
Also, it is necessary to specify in the creation of the involved complex fluid model, the reference pressure, the reference temperatures, and the flow nature for this problem:

- Isotherm complex fluid flow,
- Considering the effect of gravity that can improve the drainage of liquids,
- Permanent regime: the characteristics of the fluid do not change with time,
- Laminar pseudo-complex fluid flow.

The following Table 1 illustrates all properties of liquid and air for each foam quality β

Table 1. Properties of the used fluids for foam

Foam quality β [%]	Yield Stress τ_0 [Pa]	Consistency k [Pa.s]	Flow Index n	Density ρ [kg.m^{-3}]	Molar mass M_M [kg.kmol^{-1}]	Specific heat capacity Cp_M [J. kg^{-1}. K^{-1}]
55	3.10	0.0013	0.80	449.30	24.04	2434.18
60	3.10	0.0014	0.80	399.51	24.58	2275.32
65	3.10	0.0015	0.80	349.72	25.13	2116.45
70	3.10	0.0016	0.80	299.93	25.68	1952.59
75	3.10	0.0017	0.80	250.14	26.22	1798.72
80	3.10	0.0018	0.80	222.56	26.77	1639.86
85	3.10	0.0019	0.80	150.56	27.32	1430.67
Air	//////	//////	//////	1.18	28.96	1004.40
Water	//////	//////	//////	997	18.02	4181.70

III. RESULTS AND DISCUSSIONS

The results obtained from the CFD simulations are presented in terms of pressure gradients, pressure losses, and velocity profiles of a foam flowing with an averaged velocity of 2cm/s and 6cm/s. These results will be compared to the experimental ones obtained by PIV method (Aloui and Madani, 2008) of an aqueous foam flow under the same conditions.

III.1 Case of One-dimensional regime (V=2cm/s)

III.1.1 Pressure losses and pressure gradient

Pressure losses are considered to be the most interesting of these complex fluid characteristics. Indeed, Aloui and Madani [9] have studied the effect of the singularity on the behavior of the foam by the determination of frictional pressure losses, upstream and downstream of the singularities. Thus, they noticed that the thickness of the film has reduced regularly under the dead zone to reach a minimum value at the entrance (below the singularity). Exceeding this section, the flow of foam comes out gradualy This relaxation is accompanied by a gradual increase in the thickness of the liquid film to reach a limit value that remains stable after establishing the regime away from the recirculation zone. The increase in this thickness of the film is at the origin of gravitational drainage, which becomes more important with the acceleration of the flow going from the passage section.

Therefore, it is important to check if the calculation of the pressure distribution generated by foam flow along a horizontal channel confirms the experimental result [9]. Figure 21 shows the static pressure losses ($P-P_0$) inside the channel.

It is clear that the variation of static pressure for all foam qualities β, generated by foam flowing throughout the channel, is linear (Figure 21). A slight difference of pressure loss between the different foam qualities of a few Pascal are observed. From this measure, we can see the longitudinal pressure gradient curve based on the foam quality.

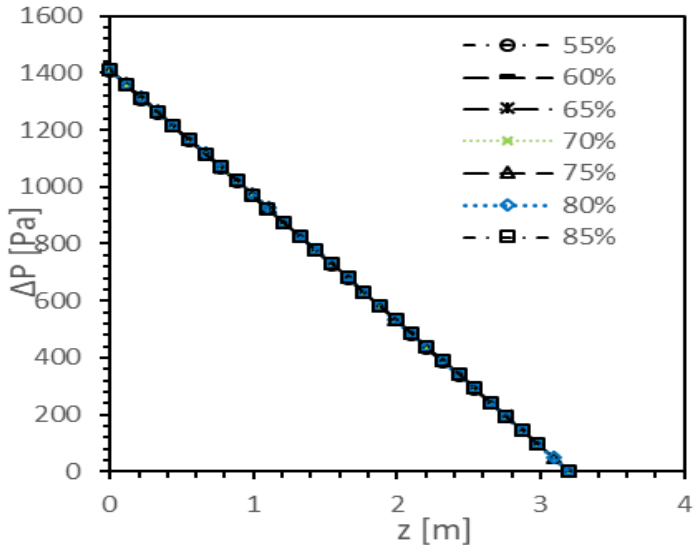

Figure 21. Evolution of the static pressure losses of the foam flowing along the square channel for different foam quality.

We note that regardless of the change in the foam quality, the longitudinal pressure gradient is also linear and it remains almost constant in the range of 440 $Pa.m^{-1}$ (Figure 22), which is in good agreement with the static pressure gradient obtained experimentally by Aloui and Madani (2008).

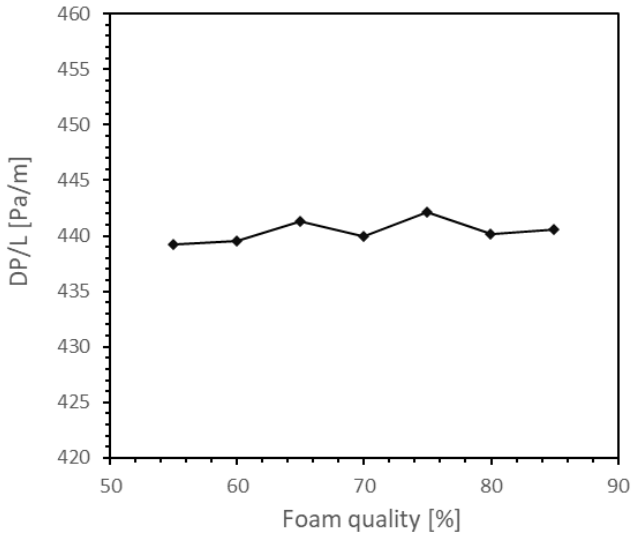

Figure 22. Static pressure gradient for a foam flow inside a straight channel for different foam qualities.

III.1.2 Velocity profiles

For all the foam qualities, the axial velocity profiles are presented as average velocity values in Figure 23. For different foam qualities β, the obtained velocity profiles, present an agglomerated foam flow that behaves like a block where the regime is one-dimensional of a piston's type, defined by Blondin [1] in 1997. Indeed, foam's velocity is constant on the whole channel's section in agreement with the experimentation with a single generator (2cm/s).
However, there is a deviation of the averaged velocity profiles as a function of the fixed quality β. It presents a maximum for the dry foam (β=85%) where the foam averaged velocity value is V=2.9cm/s. In the case of a wet foam (β=55%) it is about 1.65cm/s. This is due to the fact that the foam's displacement is fast when the imposed gas flow rate is higher.
It is important to note that the thin liquid film between the foam and walls gives rise to a wall slip layer. This film's friction on the wall explains the slight foam's velocity reduction in contact with the film, addressed to y range, which is between 1.8mm and 20.5mm (the total height of the cross-section is 21mm).

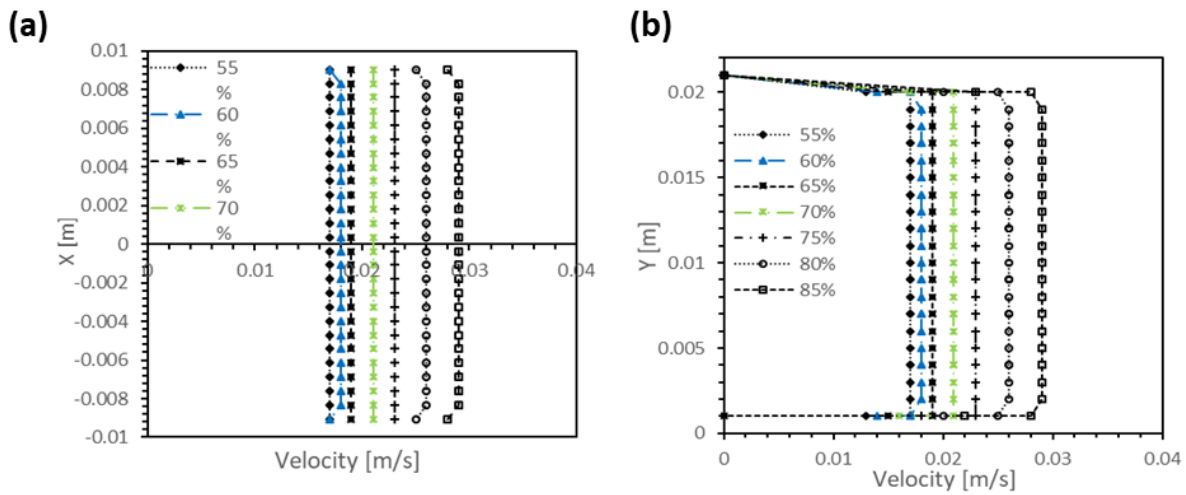

Figure 23. Averaged axial velocity profiles' component of the foam flowing through a straight channel with different qualities.

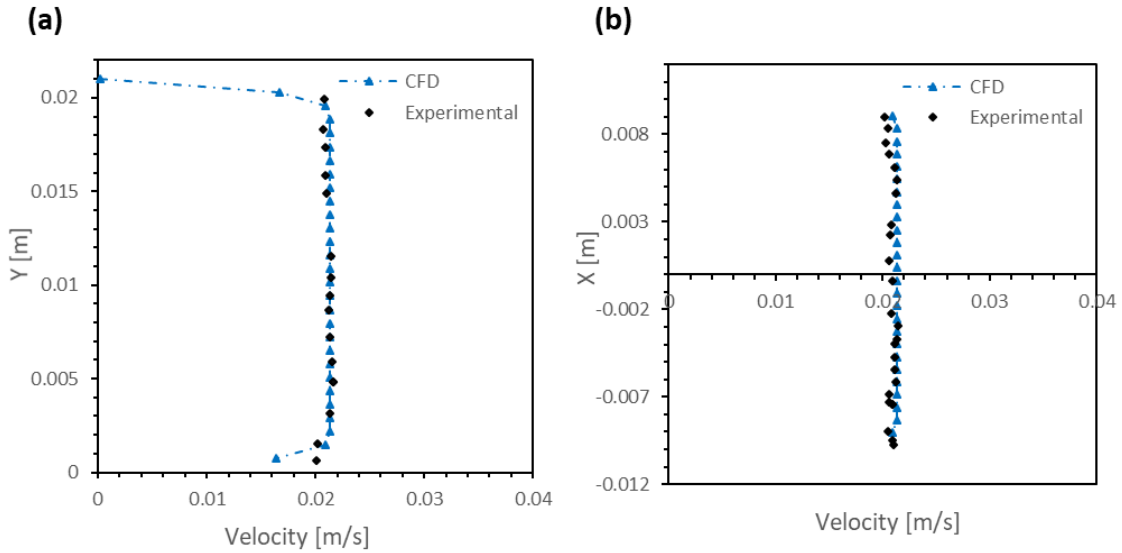

Figure 24. Averaged axial velocity profiles for an aqueous foam with a quality of 70% and a velocity of 2 cm/s.

Figures 24 above Show the axial velocity profiles evolution for a wet foam flowing with a foam quality of 70% and mean foam flow velocity of 2cm/s for their respectively Herschel-Bulkley behavior.

There, the CFD simulations match the experimental data found in the literature. They are almost similar. These results allow validation, on the one hand, the chosen boundary conditions adopted (different input and output pressure). Parameters used in this simulation, validate the chosen model, which can accurately predict and represent the one-directional regime, for foams flow behavior for a quality of 70%.

III.1.3 Liquid film thickness

Based on the model of Thondavadi and Lemlich [17], we estimated the wall liquid film thickness evolution in rheology rating on the lateral wall, to determine the influence of drainage (the passage of fluid through the bubbles' contours) for all imposed qualities (β) [18-19].

$$\delta = \frac{\mu_L . U_M}{\tau_p} = \frac{16.\mu_L . L_P . Q_M}{\pi D^3 \Delta P} \tag{11}$$

According to Figure 25 at the right column, we note a rising thickening of liquid film approaching to the liquid/foam interface (wall's bottom of the pipe).

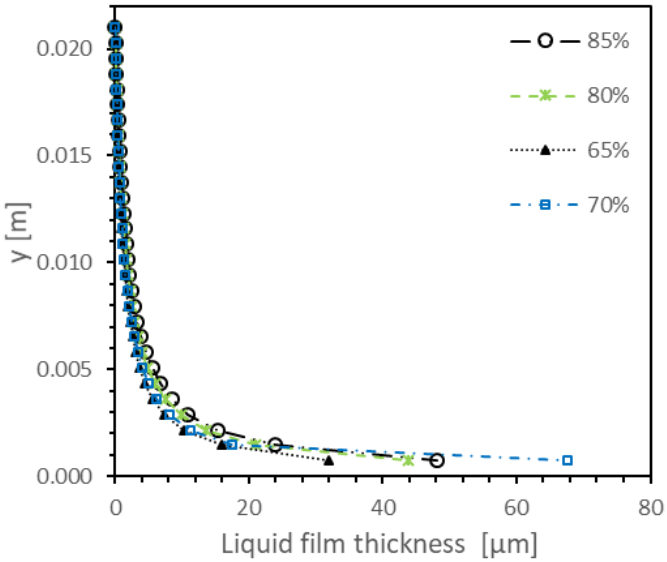

Figure 25. Estimation of the liquid film thickness the evolution on the lateral wall for all studied foam qualities β.

Also, it should be noted that it varies significantly with the foam's quality: less than 50 µm for the β of 85% and 80%, and in the order of 70 µm for the β of 65% and 70%. Therefore, for the wettest foams, the wall slip layer is thicker than for dry layers. This is due especially to the fact that wet foams drain more liquid than dry foams.

Indeed, due to the complexity of aqueous foam flow (mixture of water and air), under the effect of gravitational force, the liquid inside the foam tends toward the pipe bottom and the gas bubbles are moved to the top of the channel. The liquid film becomes thicker in this region and gives rise to a change in the structure according to the height of the foam.

III.2 Case of three-dimensional regime (mean foam velocity flow is V=6 cm/s)

In this case, is of interest in the foam's velocity profile. So, the profiles calculated out of the channel and near the lateral wall are presented in Figure 26.

It is so clear that velocity profiles are not more uniform and a new flow regime appears with a completely sheared foam flow at the bottom of the channel, where the axial velocity will be

also moved on the x-direction. It is the three-dimensional regime defined in the previous works by analyzing the results obtained from PIV technique by Aloui and Madani (2008).
Due to thinner plateau borders, and weaker internal forces, dryer foams tend to shear more easily than wet foams. However, when an elevation of mean foam flow velocity 2cm/s to 6 cm/s, averaged axial velocity profiles of the foam flowing through a straight channel with different qualities increases and particularly the slip layer thickness at the bottom of the channel increases.
Therefore, for this case, the foam is characterized by the higher velocity at the bottom of the duct where the shear occurs and foam deforms more easily. As the average velocity is high, more the influence of the liquid film is important and the foam is subject to the stretching effect of a liquid film flowing down with a high velocity.

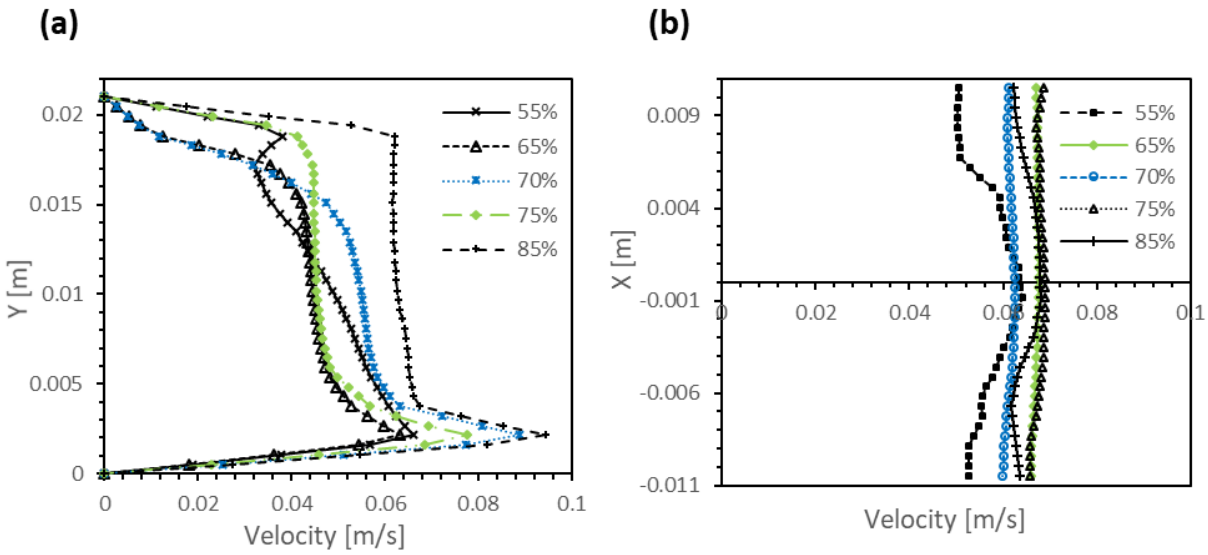

Figure 26. Averaged axial velocity profiles' component of the foam flowing through a straight channel with different qualities β.

This approach seems to give values that are relevant to the experimental reality with a stretch of foam at the bottom of the duct in contact with a liquid film.
In this case (Figure 27), the agreement between the CFD numerical simulations and experimental results is still so remarkable. Comparison between both results shows good similarity with a slight deviation. In addition, these results demonstrate the ability of the Herschel-Bulkley model to represent the three-dimensional behavior for a foam quality of 55% and a velocity of 6cm/s.

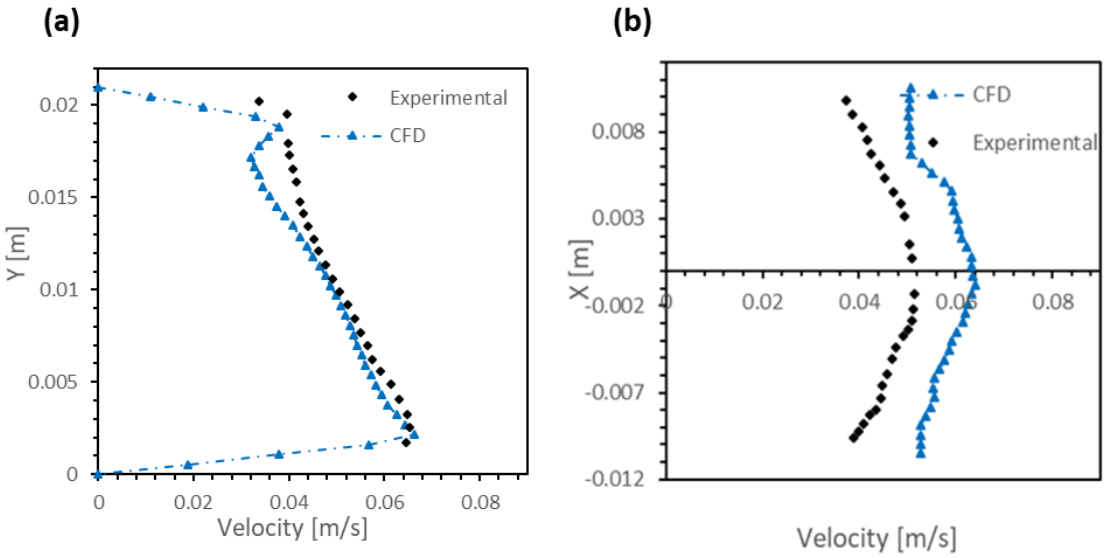

Figure 27. Averaged axial velocity profiles for an aqueous foam with a quality of 55% and a mean foam velocity of 6cm/s.

IV. CONCLUSIONS

The presented work summarized a numerical study of aqueous non-Newtonian foam flow in a horizontal channel of a square cross-section. Its goal was to extend the previous work of Chovet [9-12] in an interesting numerical model of the rheological behavior of foam flow.

The first case presents a linear static pressure gradient and a one-dimensional regime that foam at the top of the channel behaves as a piston. However, for the case of three foam generators, the foam flow becomes three-dimensional that velocity profile is a function of the x-coordinate, presenting a pic at the bottom of the channel where the liquid film is thicker.

The CFD results for this numerical study of Herschel-Bulkey behavior obtained either for a foam flow regime as piston type (characteristic velocity profiles), whether for three-dimensional regime (particular deviation of velocity profiles in channel's output) are very close to the actual behavior and in relevance to the previous experimental work for these same conditions. Therefore, the Power Law rheological model can accurately describe foam behaviors and their different flow regimes.

Future trials should be conducted in order to track the foam behavior in the channel's middle and check if the Herschel-Bulkley model can be used properly to see its evolution throughout the duct. Finally, studies in regular geometry may be extended to different singularities cases to be able to model the foam flow in complex situations in relevance with the geometries encountered in industrial equipment.

NOMENCLATURE

C_{PM}: Specific heat capacity ($J.kg^{-1}.K^{-1}$)
D: Hydraulic diameter (m)
K: Consistency index (Pa.s)
L: Length (m)
M_M: Molar mass (kg/kmol)
N: Power Law index

Q: Volumetric flowrate (m^3/s)
P_0: Static pressure at the exit of the duct (Pa)
P: Static pressure (Pa)
x, y, z: Cartesian coordinates (m)
β: Foam quality (%)
λ: Time constant (s)
μ: Dynamic viscosity (Pa.s)
ρ: Density (kg/m^3)
τ: Stress (Pa)
τ_0: Yield stress (Pa)
$\dot{\gamma}$: Shear rate (1/s)
δ: Slip layer thickness (m)
ϕ_G: Gas fraction (m^3/s)

ACKNOWLEDGMENTS
This work was supported by the laboratory LAMIH CNRS UMR 8201 (University of Valenciennes, France), the National Institute for Agricultural Research INRA (Villeneuve d'Ascq, France, laboratory UMET UMR 8207) and the laboratory LESTE (ENIM, University of Monastir, Tunisia). These supports are gratefully acknowledged.

References

[1] E. Blondin, L. Doubliez, Particle imaging velocimetry of a wet aqueous foam with an underlying liquid film, *Exp. Fluids* 32 (2002) 294-301.
[2] P. Saramito. A new constitutive equation for elasto-visco-plastic fluid flows. *J. Non-Newt. Fluid Mech.*, 145(1) (2007) 1–14.
[3] P. Oswald. Rhéophysique. Belin, Paris, 2005.
[4] S. Hutzler, D. Weaire. The mechanics of liquid foams: History and new developments. *Colloids Surf. A*, 382 (2011) 3-7.
[5] R.G. Larson. The Structure and Rheology of Complex Fluids. Oxford University Press, Oxford, 1999.
[6] A. M. Kraynik. Foam flows. *Ann. Rev. Fluid Mech.,* 20 (1988) 325–357.
[7] R. Höhler, S. Cohen-Addad. Rheology of liquid foam. *J. Phys. Condens. Matter*, 17 (2005) R1041-R1069.
[8] I. Cheddadi, P. Saramito, B. Dollet, C. Raufaste, F. Graner. Understanding and predicting viscous, elastic, plastic flows. *Eur. Phys. J. E. Soft matter*, 34(1) (2011)11001.
[9] F. Aloui, S. Madani, Wet foam flow under a fence located in the middle of a horizontal duct of square section. Colloids and Surfaces A: Physicochem. Eng. Aspects 309 (2007) 71–86
[9] R. Chovet, Experimental and Numerical Characterization of the Rheological Behavior of a Complex Fluid: Application to a Wet Foam Flow Through a Horizontal Straight Duct with and without Flow Disruption Devices (FDD), PhD Thesis, University of Valenciennes, France.
[10] S.A. Khan, R.C., Amstrong, Rheology of foams: II. Effects of polydispersity and liquid viscosity for foams having gas fraction approching unity", *J. Non-Newtonian Fluid Mech*., 25 (1988) 61-92.

[11] R.G. Larson, The Structure and Rheology of Complex Fluids. New York: Oxford University Press, 1999.
[12] R. Chovet, F.Aloui, Gas-Liquid Foam through straight ducts and singularities: CFD simulations and experiments. , ASME 2014 4th Joint US-European Fluids Engineering Division Summer Meeting collocated with the ASME 2014 12th International Conference on Nanochannels, Microchannels, and Minichannels, Volume 1B, Paper No. FEDSM2014-21190, pp.V01BT14A003, 8 pages,Chicago, Illinois, USA, August 3–7, 2014, ISBN: 978-0-7918-4622-3, doi:10.1115/FEDSM2014-21190.
[13] P. Tisne, F. Aloui, L. Doubliez (2003). Analysis of wall shear stress in wet foam flows using the electrochemical method, International Journal of Multiphase Flow, Vol. 29 (5), 841-854
P. Tisné, L. Doubliez, F. Aloui (2004).
[14] P. Tisne, L. Doubliez, F. Aloui, Determination of the slip layer thickness for a wet foam flow, Colloids Surf. A: *Physicochem. Eng. Aspects* 246 (2004) 21–29.
[16] F. Aloui, S. Madani, Experimental investigation of a wet foam flow through a horizontal sudden expansion. *Experimental Thermal and Fluid Science* 32 (2008) 905-926
[17] N. Thondavadi, R. Lemlich, A capitance sensor for two-phase liquid film thickness measurements in a square duct, *Journal of Fluids Engineering* 119 (1985) 164-169.
[18] A. Saint-Jalmes, D.J. Durian, Vanishing elasticity for wet foams: Equivalence with emulsions and role of polydispersity, *J. Rheol*. 43 (1999) 1411-1422.
[19] A. Marzec, E. Jakubczyk, Rheological properties of foams prepared for drying. *Acta Agrophysica*, 13 (2009) 185-194.

Publication II: CFD simulations of the rheological behavior of aqueous foam flow through a half-sudden expansion

https://doi.org/10.1115/AJKFluids2019-4650

Proceedings of the ASME-JSME-KSME 2019 Joint Fluids Engineering Conference
AJKFLUIDS2019
July 28-August 1, 2019, San Francisco, CA, USA
AJKFLUIDS2019-4650

CFD SIMULATIONS OF THE RHEOLOGICAL BEHAVIOR OF AQUEOUS FOAM FLOW THROUGH A HALF-SUDDEN EXPANSION

Heni Dallagi, Ahmad Al Saabi, Christine Faille, Thierry Benezech

UMET UMR 8207, National Institute for Agricultural Research - Villeneuve d'Ascq, France

Wolfgang Augustin

Technische Universität Braunschweig, Institute for Chemical and Thermal Process Engineering Braunschweig, Germany

Fethi ALOUI [2] [a, b]

[a] Univ. Valenciennes, UMR 8201 - LAMIH - Laboratoire d'Automatique de Mécanique et d'Informatique Industrielles et Humaines, F-59313 Valenciennes, France
[b] CNRS, UMR 8201, F-59313 Valenciennes, France

ABSTRACT

Aqueous foam is a non-Newtonian complex fluid. Its flow through the singularities presents many fundamental aspects. The rheological character of the foams flowing in this kind of geometry can create an important disturbance on its behavior, according to the flow rate set and therefore a modification in its texture and in the nature of its established regime. During this study, numerical simulation for the case of a half-sudden expansion was developed using the Herschel-Bulkley rheological model. The model is used to describe the response of foams under flowing conditions through this type of singularity. Obtained CFD results are focused on the pressure losses, velocity fields of the foam flow in various positions of the channel using different qualities (variation of void fraction) for lower velocities' case (one-dimensional regime) and for the three-dimensional regime. Firstly, we validated the use of this type of non-Newtonian foam flow fluid to describe the flow reorganization through a half-sudden. In a second step, we used an experimental database to validate our CFD pressure losses and velocity fields. The comparison of these results with those obtained experimentally by Chovet shows a good agreement for lower speed foam flow, but with some uncertainty for higher foam flow velocities.

KEYWORDS:
Foam flow, Non-Newtonian fluid, Half-sudden expansion, Herschel-Bulkley model, CFD, PIV.

[2] Contact author: fethi.aloui@uphf.fr

I. INTRODUCTION

Foam admits an unexpected and non-linear rheological behavior since it has original mechanical properties giving rise to many industrial applications (agriculture, cosmetics, nuclear engineering, petroleum engineering, etc.) [1,2]. One of our renovating projects is to study certain procedures for cleaning solid surfaces (metallic materials and polymers) contaminated by microorganisms, using foam flows. These can be proven only by a better knowledge of the foam structure, the understanding of its behavior in contact with a wall, and the modeling of the phenomena induced by its intrinsic rheological properties when it is flowing. Consequently, our later numerical work [3] was spread out to the case of different singularities in order to be able to model the flow of foam in complex situations relevant to the geometries encountered in industrial equipment.
The behavior of foam flowing differs completely according to diverse parameters such as the ratio of the gas flow rate and the liquid flow rate injected, the initiate velocity, the relative importance of the viscous strengths, and the inertia force as well as pressure losses involvements [4,5]. All these parameters can influence directly the nature and the regime of established foam flow, in fact its flow results from the combination of two phenomena:

- A sliding of the foam on an underlying liquid film and the flow of this liquid film.
- A cutting at the center of the foam.

In the literature, the works of Tisne [6,7], Madani [8] and Chovet [9], concern the experimental determination of the liquid film thickness, some parietal shear stress, and the regimes of foam flowing in a horizontal linear pipe of square section. Where their measurements by Particle Image Velocimetry (PIV) revealed that the foam can flow in three different regimes:

- A one-dimensional regime corresponding to an average velocity (U_{mean} = 2 cm/s), whose velocity vectors have only one uniform axial component in the flow direction:

$$\vec{u} = u\,\overrightarrow{e_z} = cte\ \ \overrightarrow{e_z} \quad (1)$$

- A two-dimensional regime corresponding to an intermediate velocity (U_{mean} = 4 cm/s), whose velocity vector has an axial component that depends only on the vertical coordinate (y):

$$\vec{u} = u\,(y)\overrightarrow{e_z} \quad (2)$$

- A three-dimensional regime corresponding to an average velocity (U_{mean} = 6 cm/s), whose velocity vector has an axial component that depends on the horizontal (x) and vertical coordinates (y):

$$\vec{u} = u\,(x,y)\overrightarrow{e_z} \quad (3)$$

Also, they conclude that the transition velocity of the regime depends at the same time on the structure of the foam, the function of the flow rate of the gas and the liquid in the foam generator, and the alteration of the rheological properties of foam with the geometry given that the foam behaves as a non-Newtonian fluid.

Previous CFD numerical work concerns essentially the definition of a rheological model which allows describing exactly the complex behavior of foam flowing along a horizontal square channel. In a study using a non-Newtonian model with a yield shear stress, Chovet [9] proposed the Bingham model to model the foam flow in low speed in a straight channel with and without singularities. However, this proposed model limits itself with the low velocity, then we suggested in a former subject using the Herschel-Bulkley model which gave us a good concordance between the numerical forecasts and the available experimental results in the description of the foam flow in various velocities [3].

The flow in a half-sudden expansion causes important variations in the foam flow. Their influences on the flow, can lead, for example, to the shear stress, or still to the increase of local transfer of mass quantities and even still on the nature of the established regime [10–12]. In this setting, the aim of this present study is to expand our previous research work to verify the ability of the Herschel-Bulkley model to describe a foam flowing in the half-sudden expansion with various regimes, various foam qualities and to predict the modifications brought by this kind of singularity. The numerical results of the CFD simulation obtained are compared with an experimental database available in the literature [9], which are the results coming from the Particale Image Velocimetry technique.

II. Numerical Parameters

This numerical work examines the modifications in the flow structure of foams through a plane sudden expansion by using a geometry that has been studied experimentally. Accordingly, our physical domain is a horizontal channel (Figure 28) of length 3.87m, undergoing a sudden widening at x = 0m with a positive variation of section (dS > 0) and a ratio of section h/H =0.5 where the left half has the section of 21x 21 mm^2 and the right half has the section of 21x 42 mm^2.

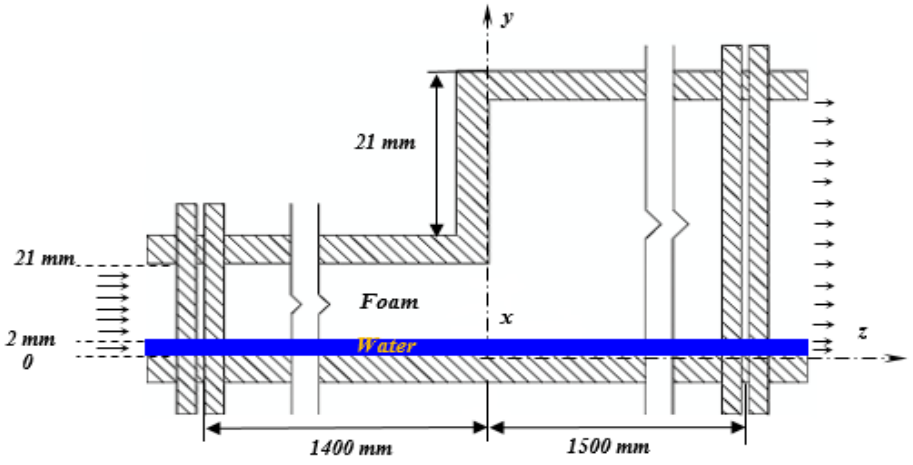

Figure 28. Lateral view of the of the half-sudden expansion.

The ANSYS CFX calculation code has been dedicated to carrying out this study. The Solver uses finite-volume modeling, which means that the equations governing the fluid are integrated into a control volume defined by the spatial discretization of the field of study. The set of equations solved by this code is the unsteady Navier-Stokes equations in their conservation form. The following instantaneous equation of momentum and mass conservation are presented as:

Balance mass:

$$\frac{\partial \rho}{\partial t} + \vec{\nabla}(\rho\, \vec{U}) \quad (4)$$

Balance momentum:

$$\rho \frac{\partial \vec{U}}{\partial t} = -\vec{\nabla} p + \vec{\nabla}(\bar{\bar{\tau}}) + \rho\, \vec{g} \quad (5)$$

where:

$$\bar{\bar{\tau}} = \bar{\bar{\tau_0}} + k(\dot{\gamma})^n \quad (6)$$

We defined the foam as being a non-Newtonian pseudo-fluid with the yield shear stress described by the law of Herschel-Bulkley as:

$$\begin{cases} \tau \leq \tau_0 \;\; ; \;\; \tau = \tau_0 \quad because\; k \to \infty \\ \tau \geq \tau_0 \;\; ; \;\; \tau = \tau_0 + k\dot{\gamma}^n \end{cases} \quad (7)$$

Furthermore:

$$\mu = \frac{\tau_0}{\lambda\dot{\gamma}} + k(\lambda\dot{\gamma})^{n-1} \quad (8)$$

where:

$$\rho_M = (1-\beta).\rho_L + \beta.\rho_G \quad (9)$$

$$\beta = \frac{Q_G}{Q_L + Q_G} \quad (10)$$

Therefore, the flow is assumed laminar incompressible and unsteady. Table 2 shows the rheological parameters that describe the used fluids:

Table 2. Properties of the used fluids.

β [%]	τ_0 [Pa]	k [Pa.s]	n	ρ [Kg.m^{-3}]
65	3.10	0.0015	0.80	349.72
85	3.10	0.002	0.80	150.56
Water	//////	//////	//////	997

These values were obtained by fixing the known velocities from the experimental results and varying the rheological parameters until we get good concordance results.

For the grid construction, a 3D mesh of high quality is adopted in the geometry where it is twice as refined at the level of the singularity, then tetrahedral elements are generated (6878385 elements).

The boundary conditions are defined according to the flow regime. In the case of a one-dimensional regime (low-velocity), a uniform average velocity was imposed at the inlet (velocity of 2 cm/s), an atmospheric pressure field at the outlet of the pipe, and a non-slip condition imposed on the lateral solid walls.

As for the case of high velocities (three-dimensional regime), we considered that the foam is subjected to the stretching effect of the liquid film flowing at the bottom of the pipe at a higher

speed, which is essentially a way of considering two fluids, the foam (a shear-thinning non-Newtonian fluid at a velocity of 6 cm/s) and the liquid film (a Newtonian fluid: water at a velocity of 10 cm/s) in the lower part of the pipe (to a thickness of 2 mm). At the outlet and the atmospheric pressure is defined with a zero velocity for walls.
In order to rediscover numerically the changes due to abrupt enlargement as an obstacle in the flow on one hand, and its effect on the nature of the flow regime established, on the other hand, the profiles of the pressure losses were plotted throughout the channel, as a result of the pressure gradient upstream and downstream of the half-sudden for different qualities of foams.

III. Results and Discussions

The results obtained from this numerical work are presented in terms of pressure gradients, head losses and velocity profiles of a foam flowing with two averaged velocities (2cm/s and 6cm/s) through a half-sudden expansion. These results will be compared to the literature results [9] based on PIV method of an aqueous foam flow under the same conditions.

III.1 Case of Foam Flowing with Velocity of 2cm/s

III.1.1 Pressure losses and pressure gradient

In order to estimate the accuracy of our numerical CFD simulations, the boundary conditions should represent the real physics of the problem. To validate these boundary conditions, the similarity of pressure gradients was verified. Figures 29-30 represent the static pressure losses and pressure gradients for different foams qualities to illustrate the effect of the expansion on the flow.

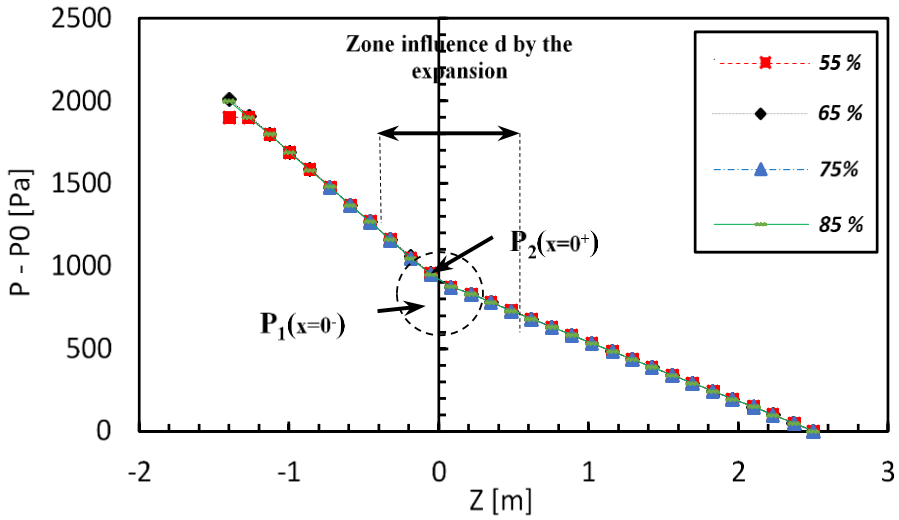

Figure 29. Evolution of the static pressure losses of the foam flowing along the test channel.

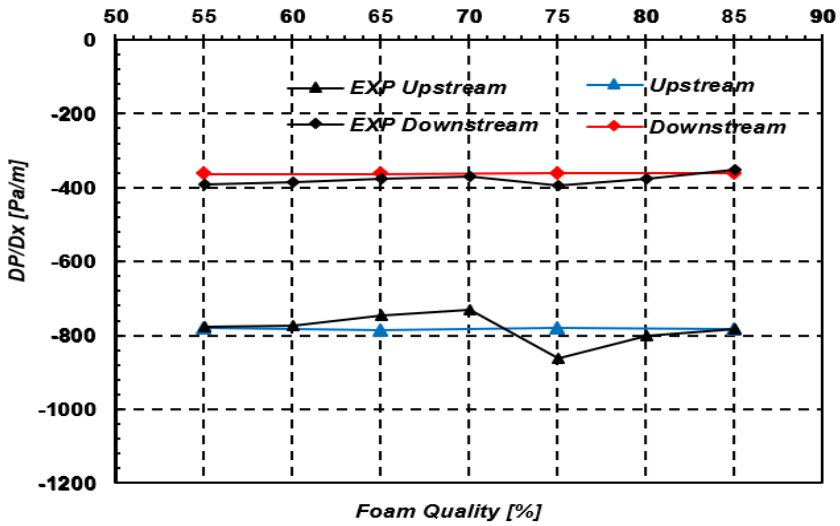

Figure 30. Static pressure gradient for a foam flow inside the singularity for the different qualities.

Figure 29 shows that the static pressure falls linearly upstream and downstream of the expansion, presenting a crossing point at the fed level where the slope of the curve is two-currency (at z = 0m) and causes a disturbance by giving rise to a new linear pressure evolution that allows setting a second regime recovery length. This disturbance in the pressure losses is due to the sudden change of the section of the geometry. It can be more remarkable by visualizing the profiles of the gradients of pressure. Both the CFD's numerical results and experimental pressure gradient (Figure 30) show the same behavior along the channel. These results allow validation of the chosen boundary conditions adopted, the rheology model used and its parameters fixed in this simulation. As a result, they accurately describe the transition from one side to the other when the foam is approaching the obstacle and enters its surrounding. Even they describe the degradation of the energy obtained at the half-sudden expansion, the surface ratio of the channel lowers the value of the pressure gradient up to half. The rate of this degradation coincides with the ratio (1/2) of two sections of the pipe (upstream and downstream). It is mainly due to the reduction of the total head loss (major and minor head losses) influenced by the increase in the diameter of the duct. There is no significant difference between the different qualities of the foams where they all behave in the same way to the HSE.

III.1.2 Local averaged velocity fields

With the aim of having a better description of foam flow on the lateral section of the pipe, we analyzed the axial and vertical velocities of two studied fluids (the Herschel – Bulkley fluid for numerical simulation and the aqueous foam for experimentation)

Figure 31 below represents the average axial and vertical velocity fields for the numerical simulations compared to the experimental results of Chovet [9].

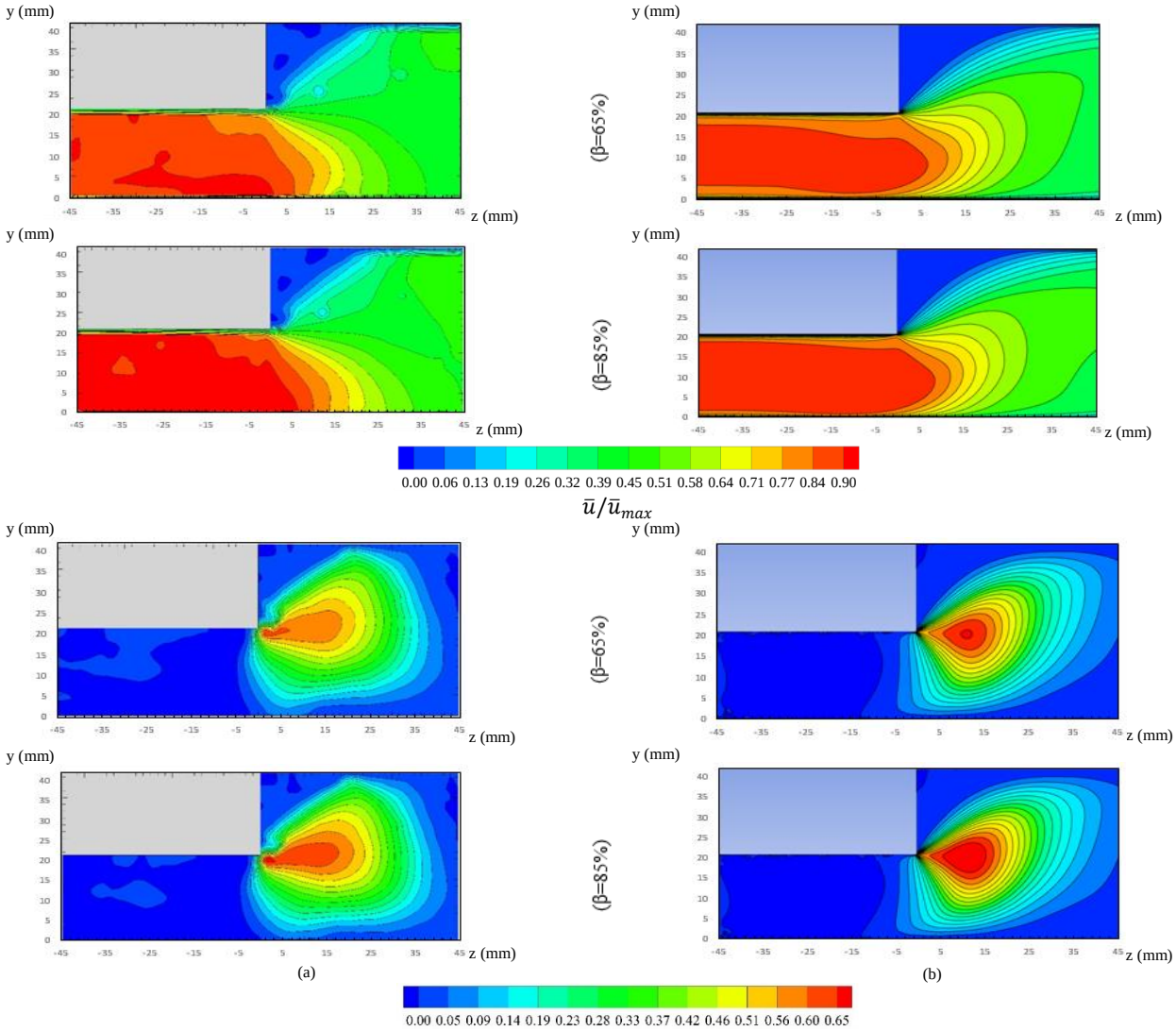

Figure 31. Averaged axial and vertical velocity field of an (a) experimental foam and the CFD Herschel–Bulkley fluid (b) flowing through a half-sudden expansion.

These results (Figure 31) show a higher velocity upstream of the expansion than in downstream. Indeed, these images highlight the existence of three different zones of flow, first an upstream characterized by a plug flow where the velocity vectors have the same average value of 2 cm/s over the whole section of the pipe. The second downstream is characterized by a slow plug regime establishment with half flow rates (velocity of 1 cm/s) in which the axial velocity field is no longer zero and is placed at the middle of the pipe. While this section changes, the disturbance generates a third zone called stagnation void zones (on the pipe top at z = 0m).
It should be noted also that there was some similarity between the experimental results and the CFD, of which in these two cases the foam is constant throughout the pipe but with an attenuated velocity after the singularity. The creation of the dead zones coincides with a remarkable increase of the vertical velocities after the regime recovery returns to its values 0. The wet foam appears faster than the driest under the density effect. The velocity profiles allow a better comparison between the foam flow and the numerical simulations. The curves below (Figure 32) show overall similarities and, differences. The profiles below allow their quantification.

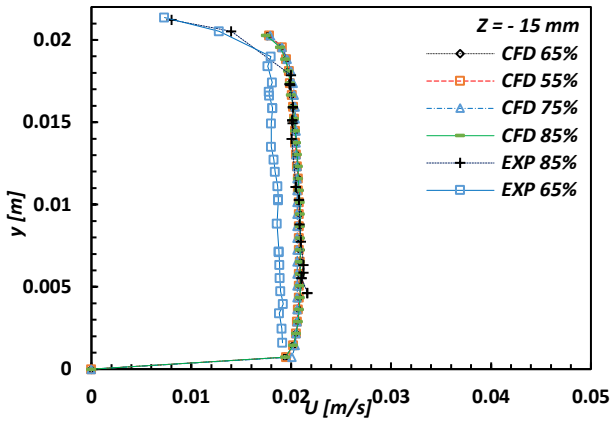
Z = - 15 mm
CFD 65%
CFD 55%
CFD 75%
CFD 85%
EXP 85%
EXP 65%
y [m]
U [m/s]

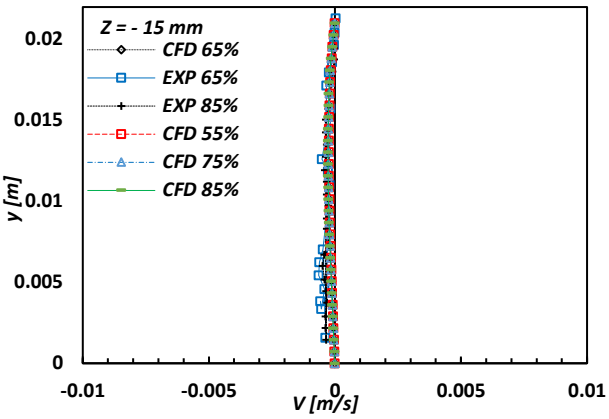
Z = - 15 mm
CFD 65%
EXP 65%
EXP 85%
CFD 55%
CFD 75%
CFD 85%
y [m]
V [m/s]

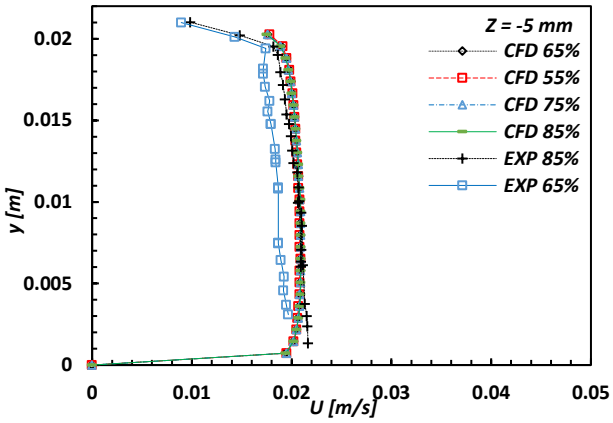
Z = -5 mm
CFD 65%
CFD 55%
CFD 75%
CFD 85%
EXP 85%
EXP 65%
y [m]
U [m/s]

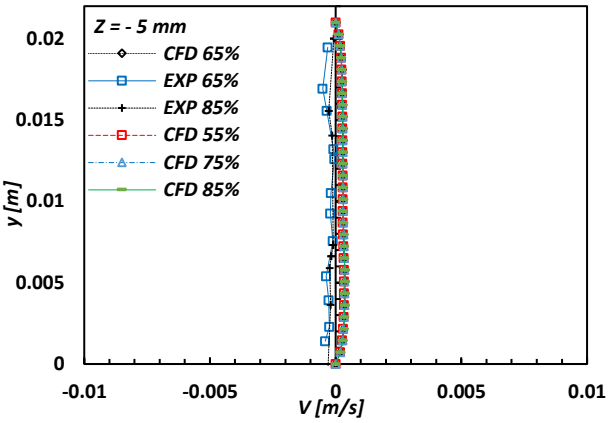
Z = - 5 mm
CFD 65%
EXP 65%
EXP 85%
CFD 55%
CFD 75%
CFD 85%
y [m]
V [m/s]

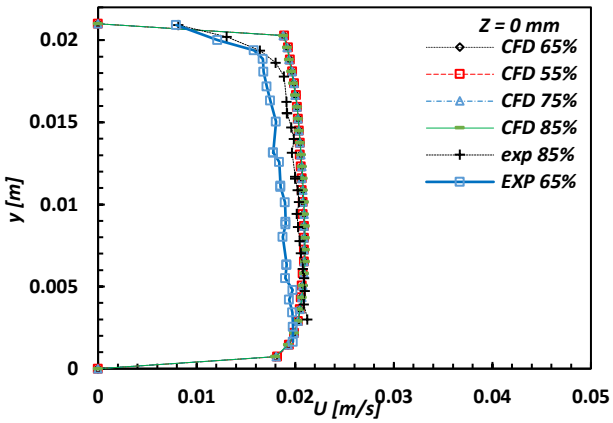
Z = 0 mm
CFD 65%
CFD 55%
CFD 75%
CFD 85%
exp 85%
EXP 65%
y [m]
U [m/s]

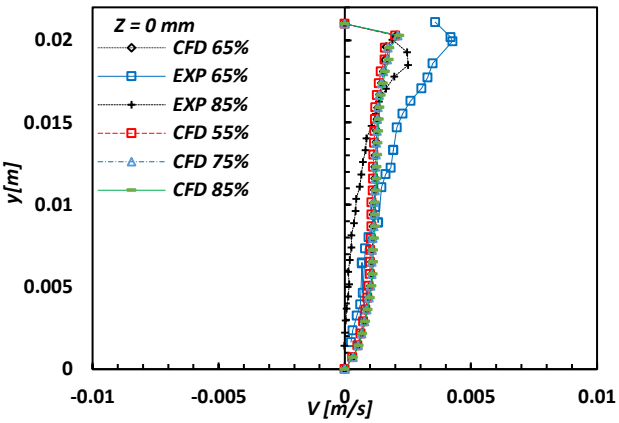
Z = 0 mm
CFD 65%
EXP 65%
EXP 85%
CFD 55%
CFD 75%
CFD 85%
y[m]
V [m/s]

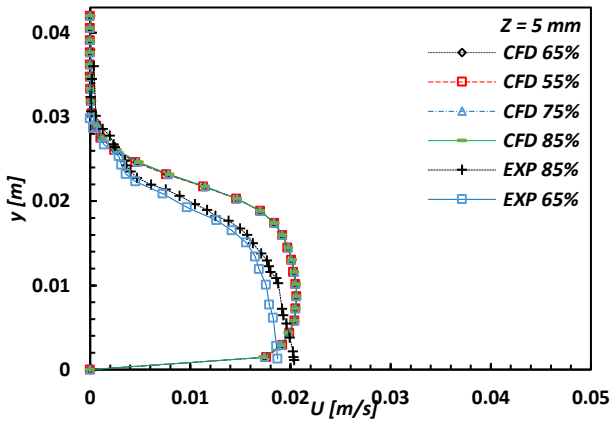
Z = 5 mm
CFD 65%
CFD 55%
CFD 75%
CFD 85%
EXP 85%
EXP 65%
y [m]
U [m/s]

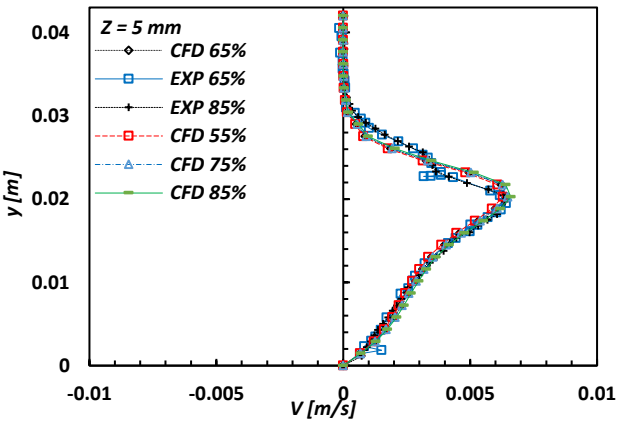
Z = 5 mm
CFD 65%
EXP 65%
EXP 85%
CFD 55%
CFD 75%
CFD 85%
y [m]
V [m/s]

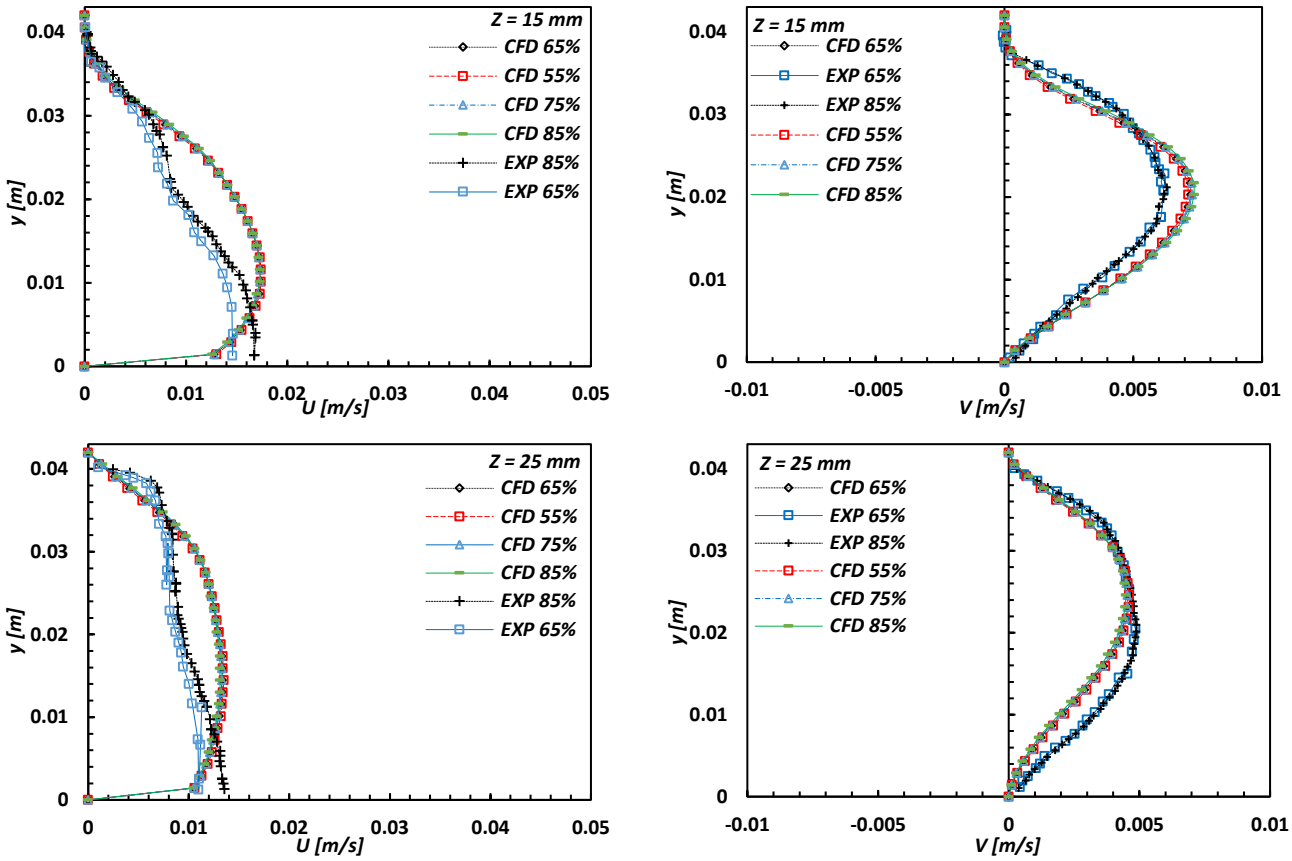

Figure 32. Lateral averaged axial and vertical mean velocity profiles for different qualities and distances over the singularity.

It is noted that the one-dimensional flow regime of the foam maintains its plug character throughout the section until the singularity (-15 mm < z < 0 mm), in which it has been undergoing an immediate perturbation: a pre-slowing of the change of the section with the creations of a dead zone at the top of channel, where the average velocity is zero. Once the flow regime is established, the foam reaches the dynamic equilibrium and resumes its stability. By recharging the entire height of the pipe section, it becomes homogeneous again and flows once in a plug-type (15 mm < z), it is the recovery of the initial state but with a velocity attenuation. This modification proves that the enlargement disturbs the texture of the foam, so it modifies its properties.

Vertical velocity profiles (Figure 32) show an important value in the immediate proximity of the half-sudden expansion (at x = 0 mm). This is related to the upward circulation of foams that is given to fill out the other pipe areas. Regarding the upstream of the half-sudden, zero vertical velocities are obtained where the flow of foam is under the effect of its axial motion. While, downstream of the expansion, the foam stream reaches the equilibrium at a well determined distance (we can call this distance as a second length of regime establishments), the axial movement settles, and the vertical velocity component will return to its initial zero value (25 mm < z).

The foams in flow (either dry or wet), have the same response character in relation to the half-sudden singularity whose behaviors are identical for the different qualities chosen, but with a certain difference in their speed values. This difference is related to the specificity of the

gravitational forces and the internal forces of each vacuum rate of the foam behavior. The analysis of all these results shows a similarity between CFD and the experimental results with a slight deviation from the proximity of the singularity. This small difference can be explained by the influence of the viscous-plastic reaction of the latter, in other words, the ability of the Herschel–Bulkley model to describe the intrinsic rheological properties of the foam.
Despite the reliability of the photographic method (PIV) to record the velocity profiles of the aqueous foam, it is not able to characterize its foam flow only to the side walls of the pipe. Therefore, it is important to visualize the axial velocity profiles and the response of the foam on the transverse wall in several planes (Figure 33) : the liquid-foam interface (channel bottom, y = 3mm) and at the top (y = 20mm for upstream case and y = 41mm for downstream).

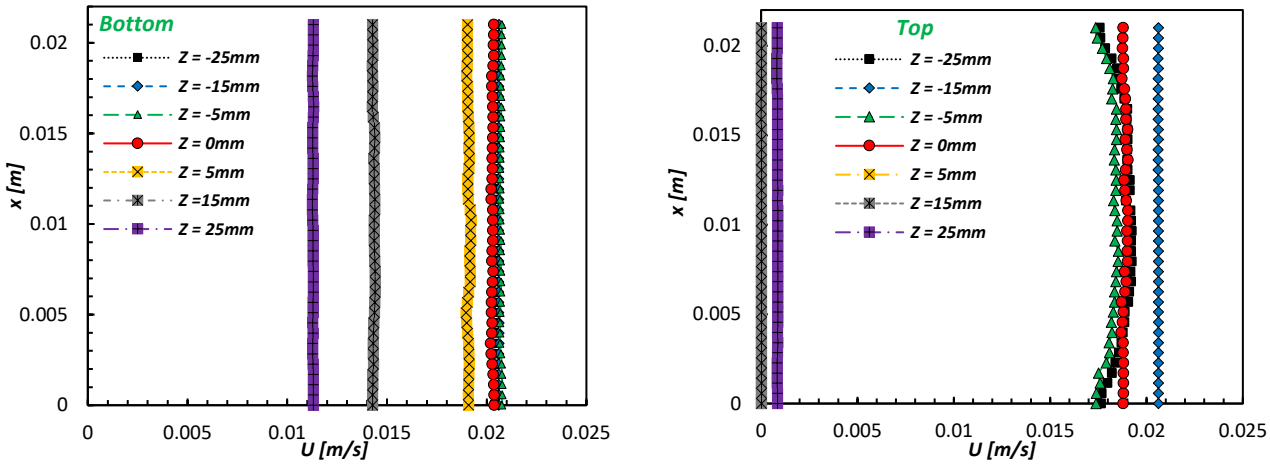

Figure 33. Span wise (top side) averaged axial velocity profiles for different distances over the singularity.

Before the singularity (-15 mm < z < 0 mm) and at the bottom of the channel, figure 11 shows a plug flow regime which was recorded on the cross section at the same velocity (2 cm/s). However, at the top of the channel the foam flows less quickly (1.8 cm/s) and the flow is almost like a block. This is due to the fact of taking a non-slip condition (zero-wall velocity) during the numerical calculation.
In the immediate proximity of the abrupt enlargement (z = 0 mm), the velocity at the top becomes zero and the foam becomes faster at the bottom under the effect of the creation of the stagnation zones. To a recovery languor (z = 25 mm) the velocity at the bottom of the channel is no longer zero and gradually increases until the total recovery of the flow regime.

III.2 Case of Foam Flowing with Velocity of 6cm/s

It is important to check if the rheological model of Herschel–Bulkley can also describe the foam flow into the three-dimensional regime for a half-sudden expansion. For this purpose, we present below the profiles of the velocities of the foam flowing at a high flow rate (Figure 34) in order to visualize the behavior adopted by the foam near the singularity.

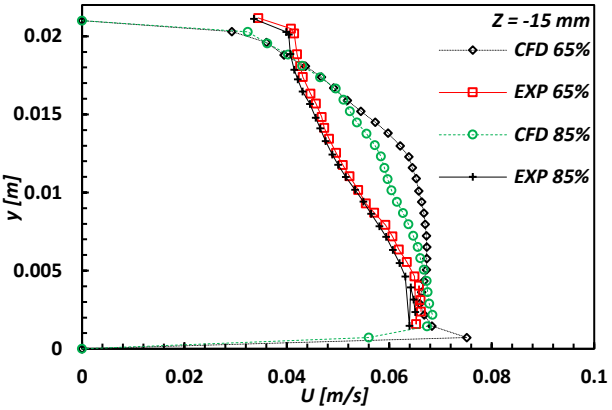
Z = -15 mm
CFD 65%
EXP 65%
CFD 85%
EXP 85%
y [m]
U [m/s]

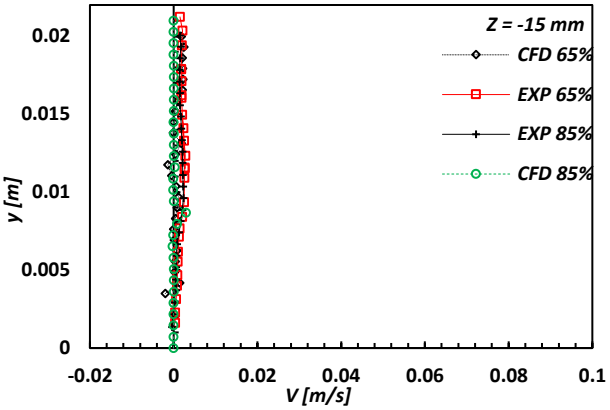
Z = -15 mm
CFD 65%
EXP 65%
EXP 85%
CFD 85%
y [m]
V [m/s]

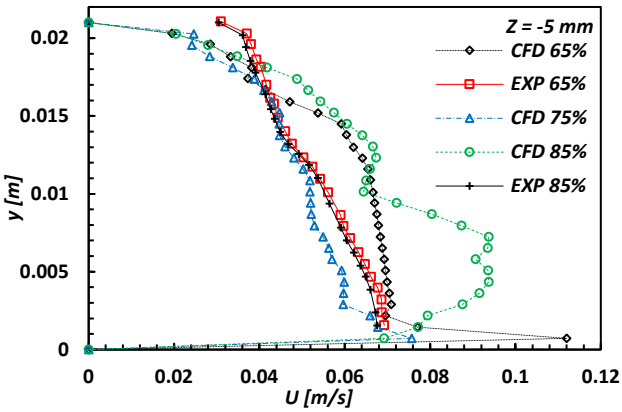
Z = -5 mm
CFD 65%
EXP 65%
CFD 75%
CFD 85%
EXP 85%
y [m]
U [m/s]

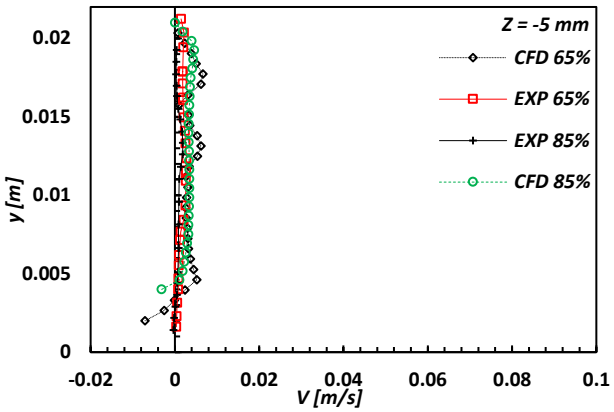
Z = -5 mm
CFD 65%
EXP 65%
EXP 85%
CFD 85%
y [m]
V [m/s]

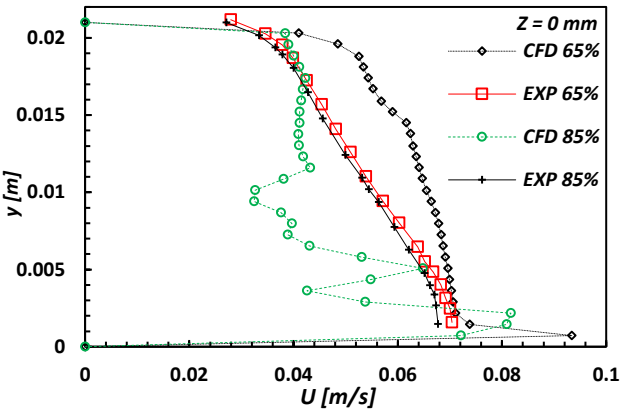
Z = 0 mm
CFD 65%
EXP 65%
CFD 85%
EXP 85%
y [m]
U [m/s]

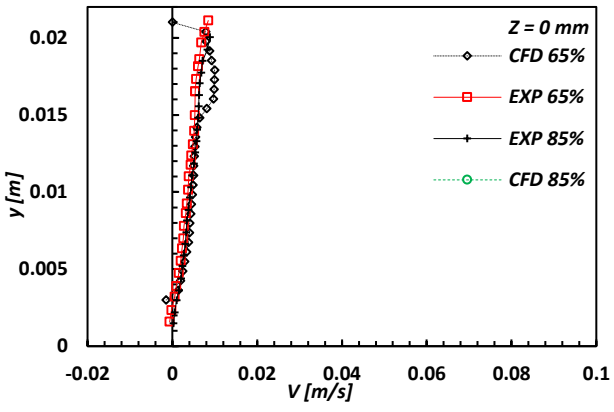
Z = 0 mm
CFD 65%
EXP 65%
EXP 85%
CFD 85%
y [m]
V [m/s]

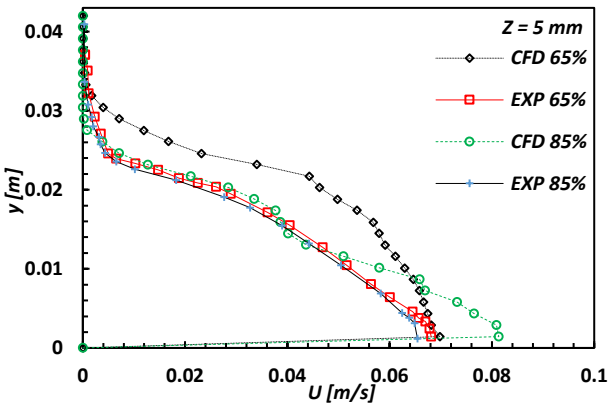
Z = 5 mm
CFD 65%
EXP 65%
CFD 85%
EXP 85%
y [m]
U [m/s]

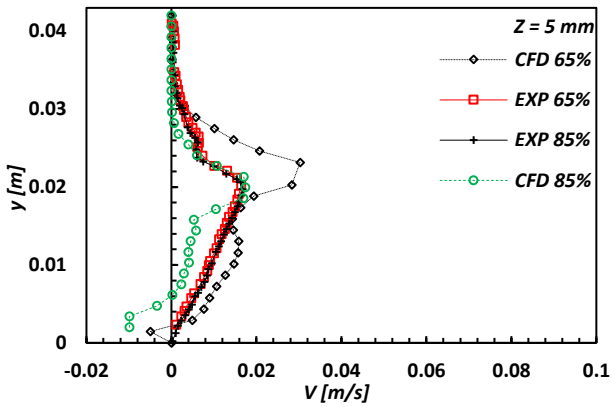
Z = 5 mm
CFD 65%
EXP 65%
EXP 85%
CFD 85%
y [m]
V [m/s]

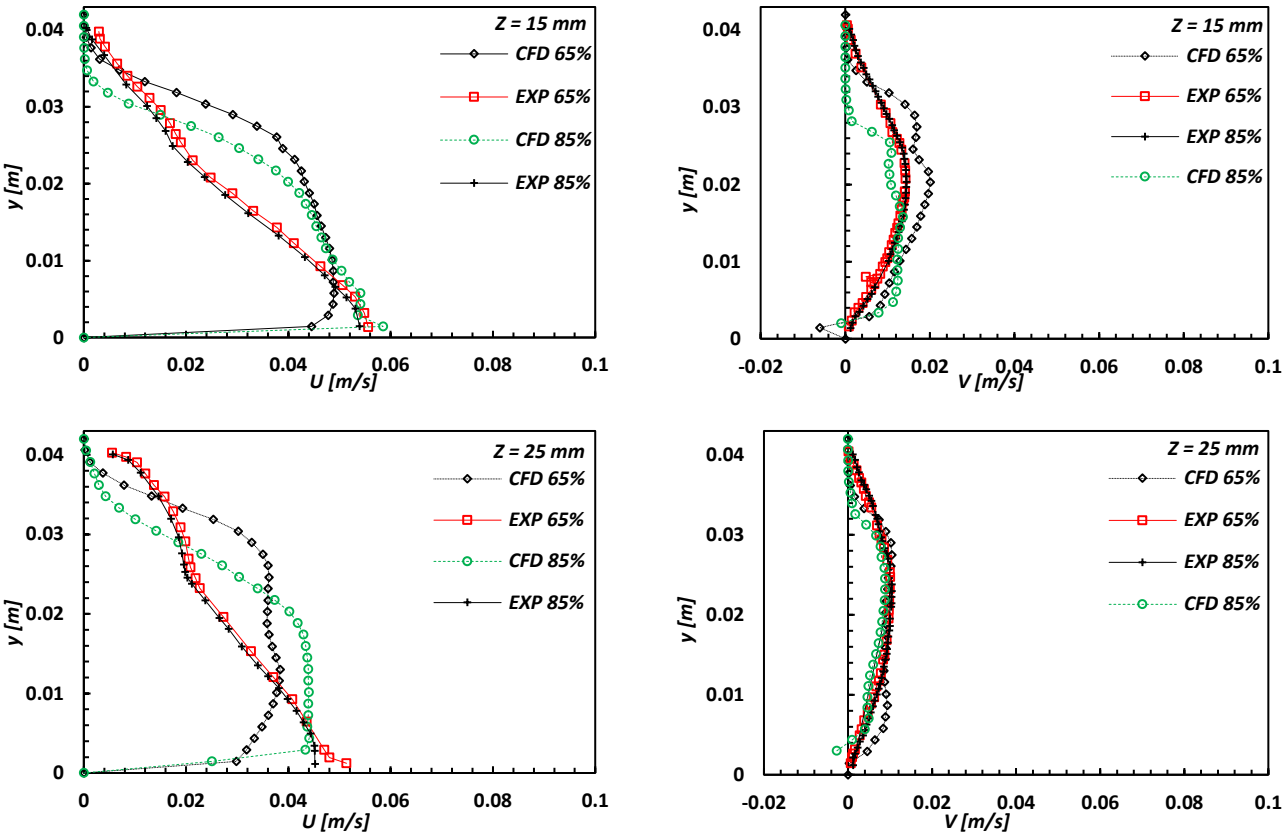

Figure 34. Lateral averaged axial (a) and vertical (b) mean velocity profiles' component of the foam flowing for different qualities and different distances over the singularity.

Lateral averaged axial (a) and vertical (b) mean velocity profiles' component of the foam flowing for different qualities and different distances over the singularity.

At all the z position, a clear appearance of the three-dimensional regime is when the foam has a deformation at its velocity profiles. The foam flow is completely sheared throughout the section, while at the bottom of the channel the foam is faster where it is under the effect of stretching of the formed liquid film whose slip layer is more important. This approach seems to give values close to the experimental reality.

The influence of the section changes results in the modification of the induced foam behavior. First, the foam keeps its behavior until the expansion where it reaches an important axial velocity presented by a peak at the top of the channel in the enlargement plan (z = 0 mm). At the same time a creation of a dead zone characterized by mean zeroes velocities below it, the foam flow gradually comes out with a steady acceleration near the lower slip layer located at the bottom of the pipe. When the flow regime is established and achieves an equilibrium (25 mm < z), the stagnation zone disappears, the axial velocity profiles are no longer null and no longer uniform and they reach its maximums in the middle of the right section.

In contrast to the case of one-dimensional flow the CFD shows a difference between the selected qualities of foam in the average velocity values, but with the same behavior, in addition the rheological model of Herschel–Bulkley defined in this study shows a presence of a secondary flow opposite to the main flow accompanied of vortices, near and downstream of this singularity. However, this turbulence is indicated by the presence of a negative axial velocities, it is not presented in previous experimental work.

Although the numerical results obtained show an agreement with the experimental results [9], but they mostly show some deviations. This difference essentially derives from the choice of a pseudo-fluid, and the limitation of this rheological model to describe certain phenomena such as the reorganization of the bubbles and its sliding conditions between them, as well as the resistances mechanically induced in the bubble-bubble and bubble-liquid film interfaces of the half-sudden singularity. So, it's hard for Herschel Buckley's CFD to give good compliance with experimental reality.

The Figure 35 show the axial velocity profiles on the transverse wall at the bottom of the canal (y = 3mm), and at the top (y = 20mm for upstream case and y = 41mm for downstream). These profiles are the results of the CFD, the absence of the experimental results is because of the inability of the PIV to visualize the flow inside the pipe.

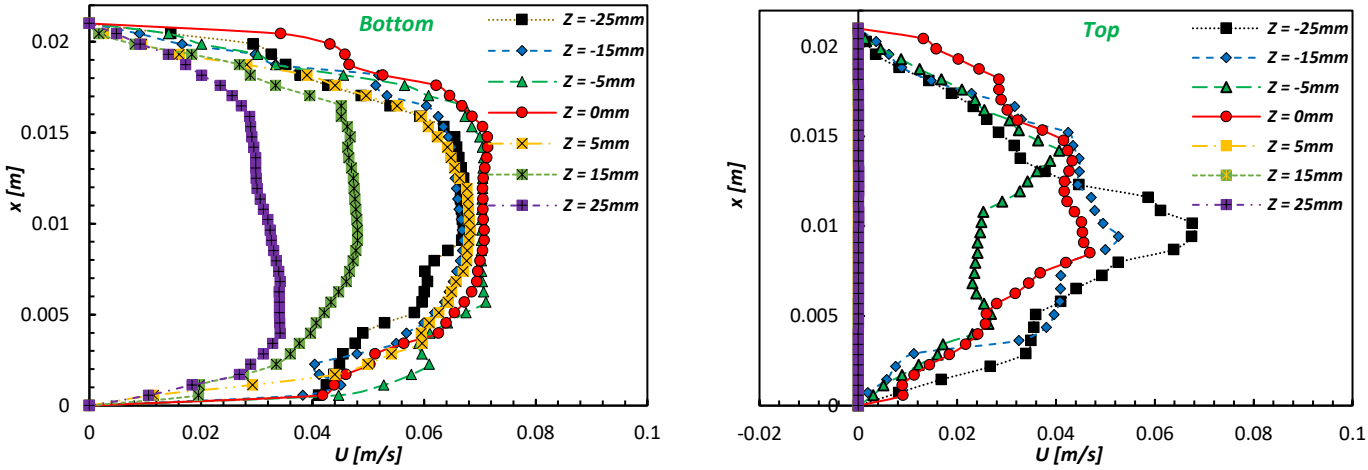

Figure 35. Span wise (top side) axial mean velocity profiles for different qualities and distances over the singularity.

These profiles in figure 8 shows a deformation in the flow regime that is three-dimensional where the foam flows faster in the middle than at the extremities. On the other hand, the slower flow is always recorded at the top of the channel.

Unlike the one-dimensional regime, at z = 25 mm upstream of the singularity the speed at the top remains zero. Therefore, the empty areas persist at this distance and therefore for a three-dimensional system the foam requires a longer recovery distance (also a longer recovery time) than a one-dimensional regime.

IV. CONCLUSIONS

In this work the effect of the half-sudden expansion on the characteristics of the flowing foams as well as on the different phenomena appearing has been studied, considering two different flow rates (velocity of 2 cm /s and 6 cm/s) and in different chosen foam qualities.

The CFD results highlight the fact that the sudden widening of the pipe section leads to a degradation of energy, and a reduction of the total head loss in the immediate vicinity of the singularity, accompanied by a more important pressure gradient in the expansion than in the downstream. The rheological model of Herschel-Bulkley models well the behavior of foam through the half-sudden in a one-dimensional regime (plug-type flow) while it is consistent

with the experimental results. Whereas in the case of higher speed, some slight difference is neatly related to the intrinsic rheological properties of the foam, the sliding bubbles between them and to the phenomena present at the bubble-bubble and bubble-liquid film interface.
Despite the ability of the Herschel–Bulkley model to model the rheological parameters of this kind of complex fluid and to predict its flow behavior in different complicated situations, there remain uncertainties fundamentally due to the phenomena of which it is difficult for this rheological law to take them into account. Finally, this numerical study may be extended to different singularity cases which can be used to study the foam rheology and behavior, like a fence, circle, half-sudden narrowing etc. Also, the thin film liquid (water) adjacent to the top wall of the channel may be considered in future works.

ACKNOWLEDGEMENTS
This work was supported by the laboratories LAMIH CNRS UMR 8201 (University of Valenciennes, France), the National Institute for Agricultural Research INRA (Villeneuve d'Ascq, France, laboratory UMET UMR 8207) and the Technical University of Braunschweig (Institute for Chemical and Thermal Process Engineering, Germany). These supports are gratefully acknowledged.

References

[1] E. Blondin et L. Doubliez, « Particle imaging velocimetry of a wet aqueous foam with an underlying liquid film », *Exp. Fluids*, vol. 32, nº 3, p. 294-301, mars 2002.

[2] E. Blondin, « Etude expérimentale d'une mousse humide en écoulement en conduite horizontale de section rectangulaire », *PhD Thesis, Université de Nantes, Nantes, France*, 1999.

[3] H. Dallagi *et al.*, « CFD Characterization of a Wet Foam Flow Rheological Behavior », in *Volume 3: Fluid Machinery; Experimental, Multiscale, and Numerical Methods for Multiphase Flows; Gas-Liquid, Gas-Solid, and Liquid-Solid Flows; Performance of Multiphase Flow Systems; Micro/Nano-Fluidics*, Montreal, Quebec, Canada, 2018, p. V003T20A004.

[4] I. Cantat, « Liquid meniscus friction on a wet plate: Bubbles, lamellae, and foams », *Phys. Fluids*, vol. 25, nº 3, p. 031303, mars 2013.

[5] A. Saugey, W. Drenckhan, et D. Weaire, « Wall slip of bubbles in foams », *Phys. Fluids*, vol. 18, nº 5, p. 053101, mai 2006.

[6] P. Tisné, F. Aloui, et L. Doubliez, « Analysis of wall shear stress in wet foam flows using the electrochemical method », *Int. J. Multiph. Flow*, vol. 29, nº 5, p. 841-854, mai 2003.

[7] P. Tisné, L. Doubliez, et F. Aloui, « Determination of the slip layer thickness for a wet foam flow », *Colloids Surf. Physicochem. Eng. Asp.*, vol. 246, nº 1-3, p. 21-29, oct. 2004.

[8] F. Aloui et S. Madani, « Wet foam flow under a fence located in the middle of a horizontal duct of square section », *Colloids Surf. Physicochem. Eng. Asp.*, vol. 309, nº 1-3, p. 71-86, nov. 2007.

[9] R. Chovet, F. Aloui, et L. Keirsbulck, « Experimental and Numerical Characterization of the Rheological Behavior of a Complex Fluid: Application to a Wet Foam

Flow Through a Horizontal Straight Duct with and without Flow Disruption Devices (FDD) », *PhD Thesis, University of Valenciennes, France*, 2015.

[10] R. Chovet, F. Aloui, et L. Keirsbulck, « Gas-Liquid Foam Through Straight Ducts and Singularities: CFD Simulations and Experiments », in *Volume 1B, Symposia: Fluid Machinery; Fluid-Structure Interaction and Flow-Induced Noise in Industrial Applications; Flow Applications in Aerospace; Flow Manipulation and Active Control: Theory, Experiments and Implementation; Multiscale Methods for Multiphase Flow; Noninvasive Measurements in Single and Multiphase Flows*, Chicago, Illinois, USA, 2014, p. V01BT14A003.

[11] F. Aloui et S. Madani, « Experimental investigation of a wet foam flow through a horizontal sudden expansion », *Exp. Therm. Fluid Sci.*, vol. 32, n° 4, p. 905-926, févr. 2008.

[12] J. R. Calvert, « Pressure drop for foam flow through pipes », vol. 11, n° 3, p. 6, 1990.

Publication III: Numerical and experimental investigations into the rheological behaviour of wet foam flowing under a fence

https://doi.org/10.1016/j.fbp.2021.12.009

Numerical and experimental investigations into the rheological behaviour of wet foam flowing under a fence

Heni Dallagi[1,2], Fethi Aloui[2], Laurent Bouvier[1], Laurent Wauquier[1], Marc Lippert[2], Thierry Benezech[1*]

[1]Univ. Lille, CNRS, INRAE, Centrale Lille, UMR 8207 - UMET - Unité Matériaux et Transformations, F-59000 Lille, France
[2]Polytechnic University Hauts-de-France, LAMIH CNRS UMR 8201, Campus Mont-Houy, F-59313 Valenciennes Cedex 9, France

Highlights

- Flow behaviour of a wet foam flow under a fence is described numerically.
- Downstream of the fence, foam undergoes reorganization and structural changes.
- Significant role of the liquid films surrounding the foam on the wall shear stress.
- Herschel-Bulkley model accurately described the rheological behaviour of the wet foam flow.

Abstract

In this study, experimental and numerical investigations were carried out to describe the flow of a wet foam under a fence placed in the middle of a horizontal duct with a square cross-section. The aim was to characterize the foam's flow behaviour and model it using CFD in complex geometrical situations such as those encountered in industrial systems as for the cleaning of food equipment. As fences affect foam structure, organization and flow dynamics, these were characterized for three different flow rate conditions. Measurements using pressure sensors, PIV and a conductimetry technique show a reorganization of the foam downstream, with a thicker liquid film at the bottom, larger bubble sizes at the top, as well as a larger void fraction increasing from the bottom to the top. The foam revealed a viscoelastic character as would be the case for a non-Newtonian fluid when passing through the fence. Herschel-Bulkley and/or Bingham laws relating to the presence of an underlying liquid film at the bottom of the channel were selected as being appropriate for this description. After adjusting these parameters from experimental data, CFD simulations were carried out. Results shown a close agreement with experiments using the Herschel-Bulkley model for two very different flow regimes.

Keywords

Wet foam flow, fence, rheology, Bingham, Herschel-Bulkley, CFD.

I. Introduction

Foam is a two-phase gas-liquid fluid. It consists of gas dispersion in a continuous liquid phase containing surfactants. It presents, when considered from a physical process aspect relating to the mechanical evolution of its behaviour (Chen et al., 2020, 2019), various organizational scales (liquid-gas interfaces, wall liquid films, bubbles, plateau borders, capillarity phenomenon, etc.). However, the behaviour of this material varies far more than the fluids that compose it. It possesses both the mechanical properties of a solid and those of a liquid (AlQuaimi and Rossen, 2019; Blondin and Doubliez, 2002). The mechanical properties of foam (low density, high specific surface, disjoining pressure, foam-wall viscous friction) are sought in many industrial applications, from cosmetics to oil extraction, firefighting, mineral flotation and the cleaning of industrial equipment especially in agro-food industries (Al Saabi et al., 2021; Cappello et al., 2015; Schramm, 2000).

Static foam cleaning is widely used for open surfaces in food industries due to its interesting mechanical properties e.g. its generation of significant drag forces and the chemical properties of the surfactant as a cleaning agent (Mierzejewska et al., 2014). Recently it has been tested in closed system cleaning. When compared to the cleaning-in-place procedure in a linear pipe, foam flow cleaning showed higher efficiency for the removal of *Bacillus* spores from stainless steel surfaces (Al Saabi et al., 2021). However, preliminary data on the use of foam flow cleaning in complex situations such as cleaning over long distances or in the presence of singularities showed a decrease in the removal effectiveness (Al Saabi et al., 2020). The latter suggest that the change in foam proprieties after singularities was responsible for reducing the contamination removal efficiency. These can only be proven by a better knowledge of the foam structure, the understanding of its behavior in contact with a wall and also the modeling of the phenomena induced by its intrinsic rheological properties when flowing.

Most theoretical studies concerning foam properties are restricted to microscopic system analysis, such as the temporal evolution of its texture (bubble sizes and shapes) (Cantat, 2013; Farahmandfar et al., 2019) and its macroscopic properties, including its mechanical behaviour and its structure (bubbles trapped by different slipping films) (Panckow et al., 2021; Parikh et al., 2019). Foam under strong mechanical stresses behaves as a viscous liquid, while under low stresses it behaves like an elastic solid whose structure is deformed and returns to its initial state when constraint ceases. The common description of foam rheology suggests that for shear stresses lower than a yield stress of τ_0, the foam behaves as a solid, whereas for stresses exceeding the yield stress, the foam flows. Foam rheology has been studied to date between these two physical characters (the linear elasticity as a solid and fluid behaviour) (Benzenine et

al., 2010; Marchand et al., 2020). Given this complexity, several rheological studies have proposed a rheological model using a Power law (Firoze Akhtar et al., 2018), a Bingham model (Calvert and Nezhati, 1986), or a Hershel-Bulkley law (Marchand et al., 2020).

Flow around objects is a phenomenon that occurs frequently in practical life. Indeed, most transport systems in industrial facilities have various peculiarities, which cause major changes in the flow behaviour (Calvert, 1988; Deshpande and Barigou, 2001). Besides, flow under a fence has been studied in the contexts of loading on civil structures (Fang et al., 1999), solar collectors, the cooling of industrial machines and electronic components (Benzenine et al., 2010), particle transport (Dong et al., 2010), windbreak aerodynamics (Çoşkun et al., 2017), the design of nuclear reactors (Endres and Möller, 2001) and in that of heat exchangers (Cukurel et al., 2015; Tandiroglu, 2006). The optimization of industrial processes is closely related to the control of the systems' hydrodynamics. It should be noted that most studies carried out on the flow of a yield-stress fluid around obstacles propose experimental results interpreted on the basis of empirical or semi-empirical models (Badve and Barigou, 2020).

Foam flow through singularities has yet to be studied in depth, particularly in the case of fences. There is not enough information on the reorganization of a foam flow downstream of these singularities to fully understand the degradation of energy (Farahmandfar et al., 2019; Stevenson, 2012). A non-Newtonian rheological model had been proposed to model foam flow. As one might expect, the intensity of the effects induced by the presence of a fence, depends on the behaviour of the foam flow, the Reynolds number and the consequent flow regime conditions, the stress field and the flow morphology (Chovet et al., 2014; Dallagi et al., 2019, 2018).

Several experimental works have studied flowing foam in a horizontal square pipe with a built-in cross-section (Blondin and Doubliez, 2002; Tisné et al., 2003). These have shown that the flow arrangement, depending on the Reynolds number and foam quality, can vary from a plug-flow up to a complex regime affecting the liquid films along the surfaces and the foam itself, both in terms of velocity and of structure (bubble arrangement). This identification was confirmed by other studies (Aloui and Madani, 2008).

Given our current knowledge of foam flow behaviour, it would appear relevant to use CFD tools to describe this type of flow. Consequently, in a 2D simulation, using a non-Newtonian model with a yield shear stress τ_0, the Bingham law was used to model the plug foam flow at low velocities in a straight channel with and without singularities (Chovet et al., 2014). However, this model only seemed to be adapted to plug flow regimes. However, in our previous

numerical studies (Dallagi et al., 2019, 2018), CFD was successfully carried out using the Herschel-Bulkley law to describe the flow in a straight pipe or through half-sudden expansion. This research investigates the flow characteristics of aqueous wet foam in a horizontal channel containing a fence, a relatively simple geometrical situation compared to the complexity encountered in agro-industrial equipment. The experimental part concerns the measurements of the pressure distribution, liquid film thicknesses, as well as the foam flow dynamics using PIV. The objective was to identify and model the foam structures and reorganization consequences both upstream and downstream of a fence, by selecting an adequate rheological model. Based on these models, 3D CFD numerical simulations were performed using the ANSYS CFX commercial code.

II. Materials and methods

II.1 Experimental device

Figure 36 (a) shows the experimental setup of the foam flow used in this study. This setup was designed to study horizontal foam flows in varying flow conditions both with and without a fence. The test pipe was 3.41 m long, with a 21 mm square cross-section. The fence was located 1.43 m downstream of the pipe inlet and was 10.5 mm high, and 5 mm wide, with a 45° angle evacuation. The coordinate system (Cartesian *x, y, z)* was located at the fence site at the channel bottom. The foam flow followed the x-axis as shown in Figure 36 (b). The flat surfaces of the duct allowed the easy implementation of the different measurement techniques for pressure outlets, particle image velocimetry (PIV), and conductometry.

The foams were generated by the injection of pressurized air through a permeable media (DURAN, pores size: 1 - 1.6 µm) into the generator container's water-surfactant solution. The role of the surfactant was to reduce the interfacial tension between gas and liquid in order to allow the formation of bubbles. The surfactant used in this experiment was sodium dodecyl sulfate (SDS) dissolved in osmosis water for 0.15% (w/w). The surface tension and the viscosity of this aqueous solution were respectively, 26.2 $mN.m^{-1}$ and 0.94 mPa.s.

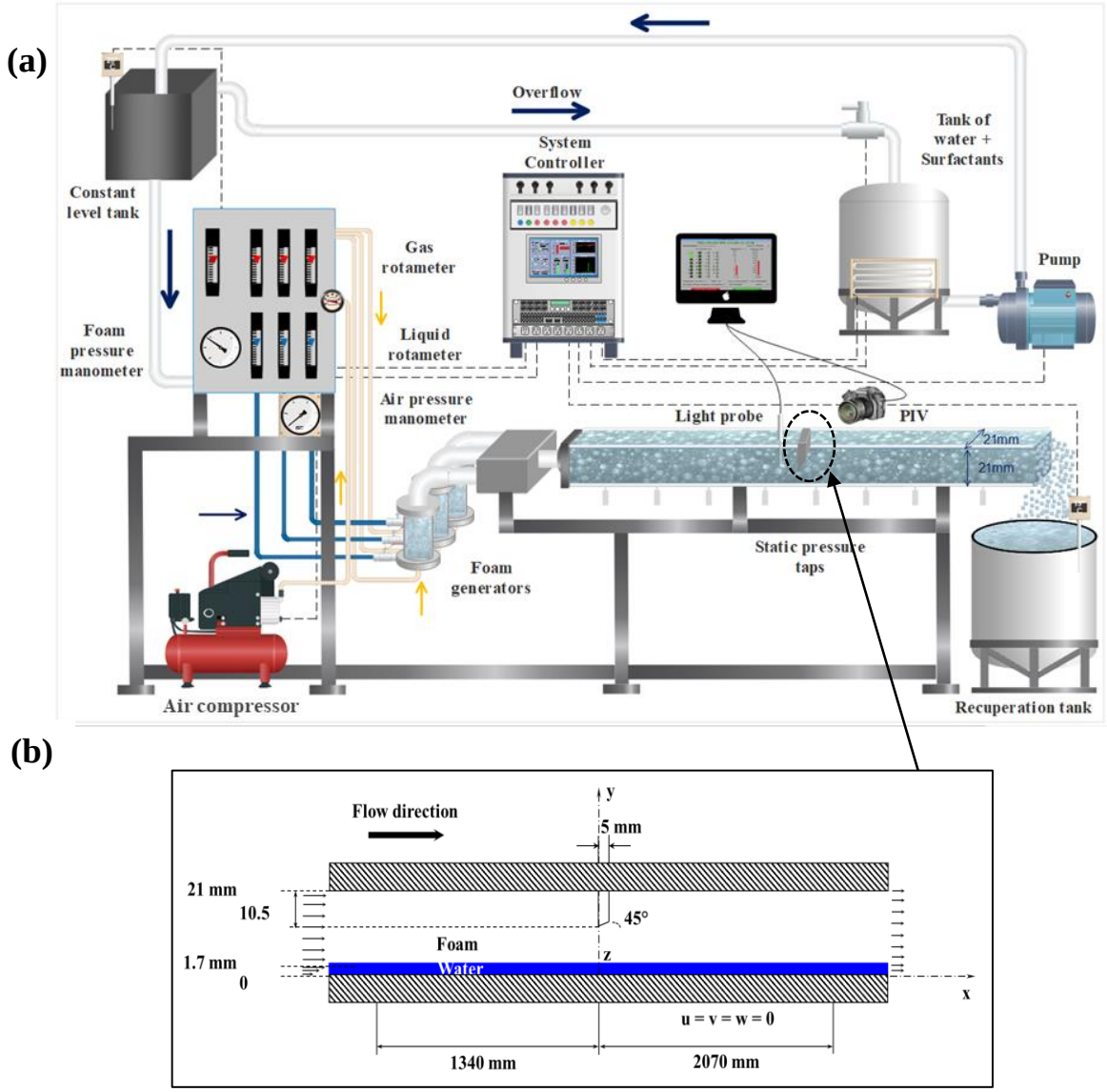

Figure 36. Experimental set-up. (a): Design of the device. (b): Dimension of the pipe zone studied.

Three different foam flow cases were generated (Case 1: foam at average velocity of 2 cm.s^{-1}, Case 2: foam at average velocity of 4 cm.s^{-1}, and Case 3: foam at average velocity of 6 cm.s^{-1}). These three flow regimes were obtained based on recommendations in previous works (Blondin and Doubliez, 2002; Tisné et al., 2003). At *Re* of 32 (average velocity $\bar{u}$ of 2 cm.s^{-1}), the foam behaved as a plug flow, called a one-dimensional regime. In this regime, the velocity vectors ($\vec{U}$) have a single uniform axial component in the flow direction ($\vec{U} = constant\ \overrightarrow{e_x}$). At *Re* of 65 (mean velocity of 4 cm.s^{-1}), the foam flow becomes faster at the bottom of the duct than at the top. The velocity vectors, in this case, have an axial component that depends solely on the vertical (y) coordinate ($\vec{U} = U\ (y)\ \overrightarrow{e_x}$). The third, a three-dimensional regime (*Re* = 97; $\bar{u}$ = 6 cm.s^{-1}) was a completely sheared foam flow, where the velocity vector has an axial component

depending on both horizontal (z) and vertical (y) coordinates ($\vec{U} = U\,(y,z)\,\vec{e_x}$). These three conditions are summarized in Table 3.

A foam quality $\beta = \frac{Q_G}{Q_L+Q_G} = 65\%$ was chosen as corresponding to an aqueous wet foam, where Q_L and Q_G are designated as the volumetric flow rates (L.s^{-1}) of water and gas, respectively.

The Reynolds number of foam flow was calculated as:

$$Re = \frac{\rho_f.\bar{u}.d_h}{\mu_f} \quad (1)$$

where $\bar{u}$ is the average velocity, d_h is the hydraulic diameter (21 mm in this geometry cross-section). ρ_f is the foam density, based on the foam quality β (65%), liquid density ρ_L, and gas density ρ_G as:

$$\rho_f = (1-\beta).\rho_L + \beta.\rho_G \quad (2)$$

μ_f is the apparent viscosity of foam. This is determined from the viscosity of the liquid phase μ_L and the foam quality (Hatsehek, 1907). It should be noted that this calculated viscosity was used only to estimate the Reynolds number and does not imply a shear independent viscosity.

$$\mu_f = \frac{\mu_L}{1-\beta^{1/3}} \quad (3)$$

Table 3. Foam flow conditions at temperature of 20°C.

Flow Regime	Density (kg.m^{-3})	Viscosity (mPa.s)	Mean velocity (cm.s^{-1})	Reynolds number
Case 1: 1D	349.7	4.6	2	32
Case 2: 2D			4	65
Case 3: 3D			6	97

II.2 Measurement techniques

To measure the static pressure along the channel, different pressure taps were used along the bottom wall and in the vertical symmetry plane of the channel. 23 pressure outlets were installed near the fence, eight of them being located upstream of the flow restriction mechanism and the

other 15 downstream of it. The underlying liquid film located at the bottom of the channel ensured no bubbles flowed through the pressure measuring lines.

The velocity was measured using the Particle Image Velocimetry (PIV) technique and the method adopted for the foam flow was that described previously (Chovet et al., 2015). The PIV method is a non-intrusive optical technique, capable of measuring the displacement of particles in a laser light sheet. In foam flow, the gas/liquid interphase is darker than the rest of the flow (Chovet et al., 2015) and the contour of the bubble describes the whole flow movement (not the movement of each bubble), which obviates the use of particles in tracking the flow. The flow is illuminated by a double-pulsed laser ND-YAG with 15 Hz of the "NEW WAVE" type, marketed by DANTEC. A synchronized CCD KODAK camera was installed with FLOWMAN software for the acquisition and processing. There is a 5% maximum error for the velocity measurements.

To determine the thickness of the liquid films at the pipe wall, the conductimetry method was used. This is an experimental technique based on the measurement of the impedance Z of the volume of liquid between the liquid-foam interface and two outcropping electrodes (powered by a generator that provides an alternative sinusoidal voltage) on the pipe wall as described previously (Tisné et al., 2004). In a square cross-section duct, the thickness of the liquid film between the foam and the walls increased from the top wall (few microns) to 2 mm at the bottom wall. The estimated error for the film thickness was of 8%.

II.3 Rheological model and numerical parameters

Simulations with the Eulerian-Eulerian multiphase models were made using ANSYS-CFX® software. To simplify physical problems such as the interactions between bubbles and their slides over liquid films at the walls, the foam was defined as a pseudo-fluid, where its properties depend on those of the air and the water in laminar and isothermal conditions, as shown in the equations below. The underlying liquid film at the bottom of the channel was considered separately.

The ability of the proposed model to predict a wet foam behaviour in different cases of Reynolds numbers was ascertained by comparing the CFD results to the experimental data. Only the two extreme regimes observed in Case 1 and Case 3 were considered in this work.

Since the velocity conditions were quite low, the foam flow in this study can be considered as an instant laminar flux in isothermal conditions.

The following instantaneous equation of mass and momentum balances are presented as:

Mass balance:

$$\frac{\partial \rho}{\partial t} + \vec{\nabla}\left(\rho\, \vec{U}\right) = 0 \quad (4)$$

where $\vec{U}$ is the velocity vector, ρ is the density and t is the time.

Momentum balance:

$$\rho \frac{\partial \vec{U}}{\partial t} = -\vec{\nabla} p + \vec{\nabla}(\bar{\bar{\tau}}) + \rho\, \vec{g} \quad (5)$$

with p is the total static pressure, $\bar{\bar{\tau}}$ the stress tensor and $\rho\, \vec{g}$ the source term (volume forces).

where:

$$\bar{\bar{\tau}} = \bar{\bar{\tau_0}} + k(\dot{\gamma})^n \quad (6)$$

The foam is considered as a non-Newtonian pseudo-fluid with the yield shear stress (τ_0) described by the Herschel-Bulkley law as:

$$\begin{cases} \tau \leq \tau_0 \;\; ; \;\; \tau = \tau_0 \quad because\ \mu(\dot{\gamma}) \rightarrow \infty \\ \tau \geq \tau_0 \;\; ; \;\; \tau = \tau_0 + k\dot{\gamma}^n \end{cases} \quad (7)$$

Where $\dot{\gamma}$ is the shear rate, τ_0 is the yield stress, k, the consistency parameter, and n is the index of flow which depends on the specific mechanism of viscous dissipation through the flow. When n = 1, the Bingham law was applied. These parameters were identified experimentally and were adjusted numerically after validation by comparison of the results.

A consideration of the compressibility of the foam would not improve the precision of our numerical calculation. Indeed, according to Wood's law (equation 8, where the sound constant $k_s = 10$) (Pierre and Leroy, 2016), the sound velocity (v_s) in an aqueous foam is equal to 21 m.s^{-1}. Therefore, the Mach number (*Ma*) for all foam flow conditions is less than 0.3 (*Ma*=0.026, 0.055, and 0.058 for cases 1, 2, and 3 respectively).

$$v_s = \frac{k_s}{\sqrt{(\beta(1-\beta)}} \quad (8)$$

Unlike our previous simulations (Chovet et al., 2014; Dallagi et al., 2019, 2018), we considered the presence of the underlying liquid film developed at the bottom of the pipe for the two cases chosen. The thickness of this liquid film was around δ_{Bottom}=1.7 mm (Figure 36 (b)) (Aloui and Madani, 2007). Hence, two average foam velocity conditions were chosen: 2 and 6 cm.s^{-1} respectively inducing experimental 1D and 3D flow regimes. The other initial parameters relating to the water velocity U_{film} (Newtonian fluid) depend on the underlying film thickness, which can be defined as resembling a falling film with maximum velocity U_{max}. For the 1D flow regime U_{film} = 2 cm.s^{-1}. As for the case of high-velocity U_{max}=10 cm.s^{-1}, the foam was

subjected to the stretching effect of the liquid film flowing at the bottom of the pipe at a higher velocity (Blondin and Doubliez, 2002; Tisné et al., 2004). The non-slipping conditions imposed zero velocities at the internal walls. The atmospheric pressure was defined as the output condition.

III. Results and discussions

III.1 Description of the foam flow

The evolution of the static pressure and the velocity profiles are the most important parameters when describing the rheological behaviour of the foam flow under the fence.

Figure 37 shows the longitudinal pressure gradient that was obtained from the static measurements of a series of pressure outlets along the channel (over 80 and 150 cm of length upstream and downstream of the fence respectively).

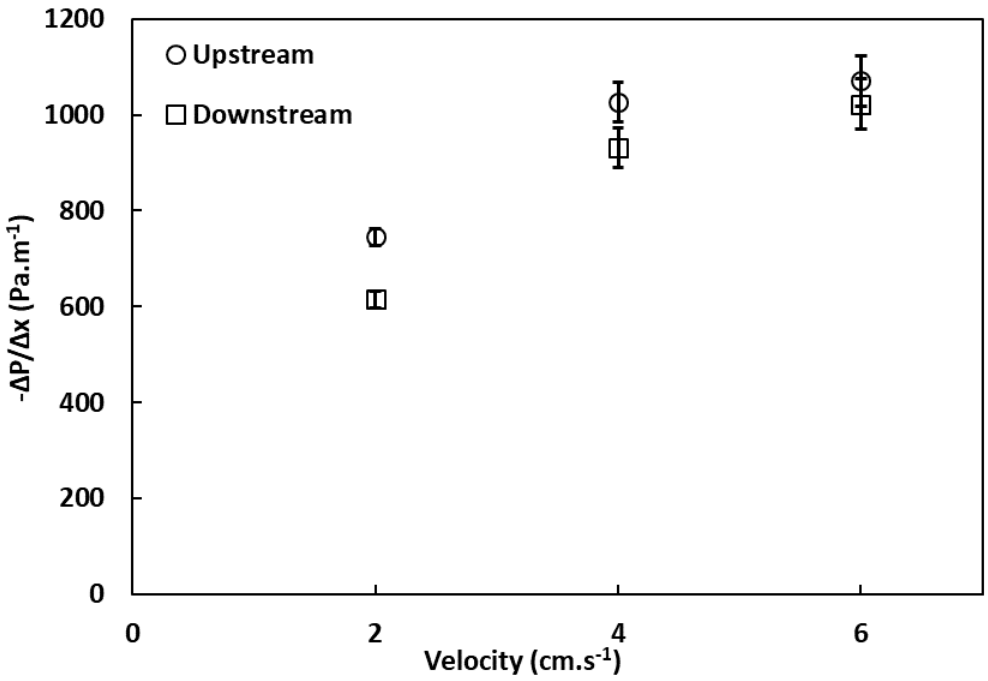

Figure 37. Longitudinal pressure gradient upstream and downstream the fence.

For both sides of the fence, both the pressure gradient and the velocity increased, so that the viscous dissipation close to the wall was greater in Case 3 than in Cases 1 and 2. Moreover, this gradient was higher upstream than downstream of the fence for the slowest foam (Cases 1 and 2). This could be directly related to the change in the foam's texture and structure, as a product of the bubble's reorganization and phase separation (forced gravitational drainage and coalescence). The same behaviour has been observed in other studies of foam flow under half-sudden expansion (Dallagi et al., 2019).

To better understand these observations, a study was carried of the velocity field over the lateral wall using the PIV system (Figure 38).

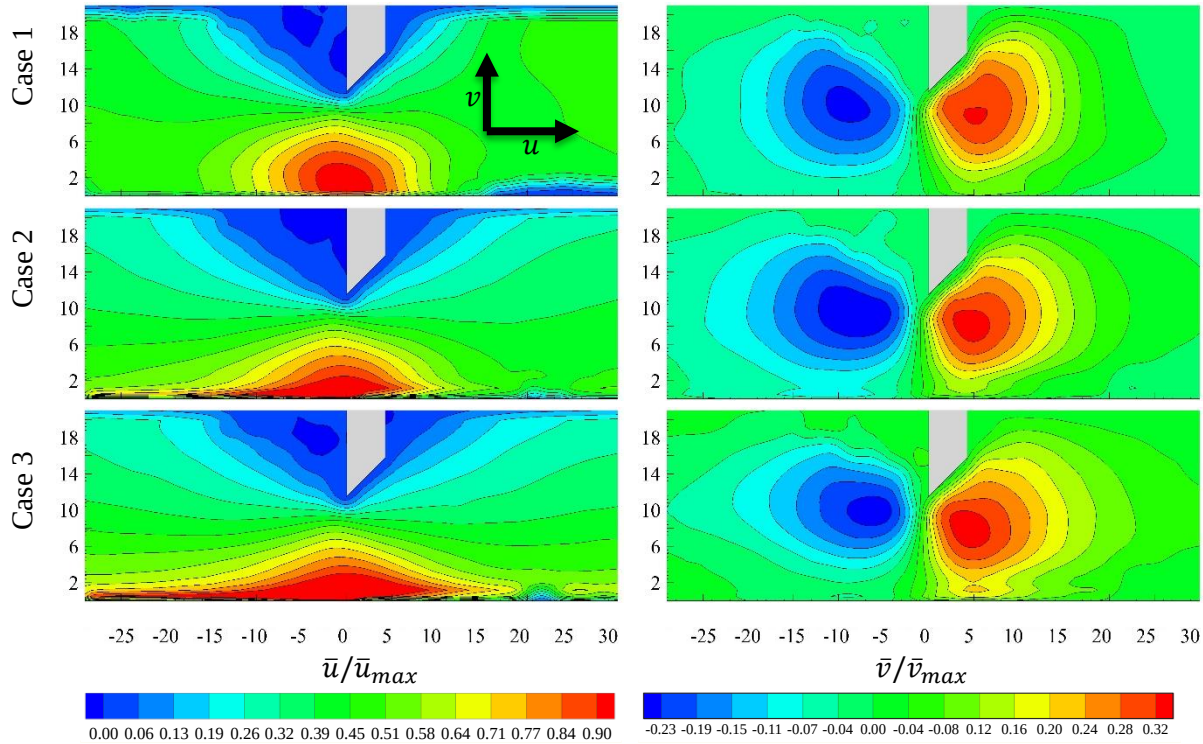

Figure 38. Averaged axial (u), and vertical (v) mean velocity components' fields for all cases under the fence. Velocity measurements were obtained using the PIV technique. u_{max} was 4.3, 9, and 14 cm.s^{-1} and v_{max} was 1.3, 2.2, and 2.4 cm.s^{-1} for cases 1,2 respectively.

Plug flow was observed for Case 1. As the bubbles' velocities increased for Cases 2 and 3, the influence of the underlying liquid film was noted, as it seemed to pull the foam and deform it along the lateral and spanwise sides. Therefore, when approaching the fence, the foam flow became highly disturbed. First, under the contraction of the section, created by the fence, the static pressure increased, the foam slowed down and formed an aggregate of reduced-sized bubbles. Simultaneously, the fence created the first obstacle for bubbles, thereby generating a "stagnant" cover, altering the velocity of other bubbles passing through the fence. Then, when passing under the fence (x = 0 mm), the foam opposed the compression of the bubbles and accelerated brusquely and reached its maximum axial velocity (4.3, 9, and 14 cm.s^{-1} for Cases 1, 2, and 3 respectively). Downstream, when the foam came out of this acceleration forced by the obstacle, a second smaller stagnant area was generated at the top of the duct near the obstacle.

In addition, an asymmetry was observed between the vertical velocity fields upstream and downstream of the fence (maximum 47, 38, and 29% for Cases 1, 2, and 3 respectively). At

greater distances from the fence, whether upstream or downstream (for x > -25 mm and x > 25 mm), the vertical velocities fell to zero and the foam flow only reacted axially. Therefore, three transition states of behaviour were observed; deceleration, acceleration, and stabilization. At a distance of x > -25 mm, the foam began to resist the section reduction. The deceleration was greatest at x = -5 mm (-0.8, -1.8, -3.6 cm.s^{-1} for Cases 1,2 and 3 respectively). However, the foam passing under the fence (at $0 < x \leq 5$ mm) and therefore subjected to compression shown just after the fence a clear acceleration. The vertical velocity profile became parabolic and attained its highest speed (1.5, 2.6, and 3.8 cm.s^{-1} for Cases 1, 2, and 3 respectively). Then, at x = 25 mm the foam flow developed fully and gradually slowed down to return to its initial state for the rest of the channel.

The flow behaviour of the foam is thus clearly described here. When passing through a fence, an increase in stress occurs, where the foam yield passes the threshold and flows as a viscoelastic fluid. Visibly, even though the velocity field seems to be identical to that upstream side when distant from the fence, a reorganization of the foam ensues whereby the foam texture and granulometry change to present a coalescence phenomenon (shown in the Supplementary Data 1, for Case 1- Figure 39).

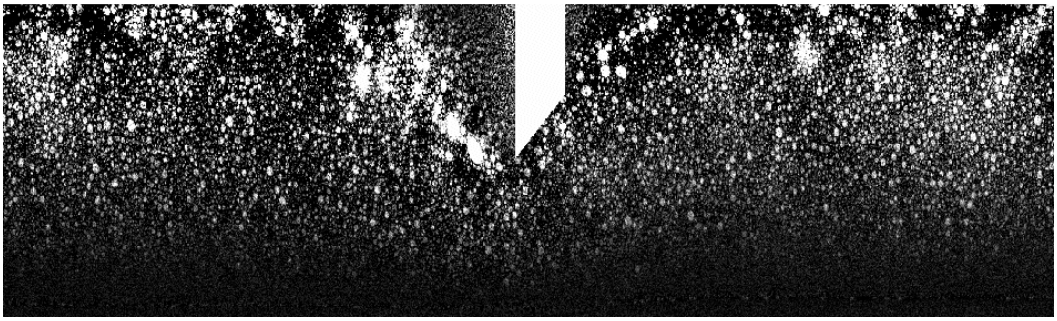

Supplementary data- Figure 39. Example of a PIV image obtained on the lateral wall for the case A.

The change of the pipe section leads to a change in the foam structure and texture. Indeed, under the decrease of the pressure induced by the section reduction, foam bubbles are distorted, and the inter-bubble liquid film varies. This deformation induces an increase in the surface energy of the bubbles that consequently store elastic energy in proportion to the surface tension (Dollet and Raufaste, 2014; Höhler and Cohen-Addad, 2005). The foam reveals its elastic character (Gorlier et al., 2017) as the low density and the high active surface push the bubbles up into the channel to fill the entire height of the duct's cross-section, to return to its initial equilibrium. The elastic modulus $G = 0.5\ \frac{\gamma}{R}$ for the three cases is 13, 29, and 29.5 Pa for the 1D, 2D, and

3D regimes respectively. γ and *R* are the surface tension and the bubble radius, respectively (Gorlier et al., 2017).

In this case, the foam became wetter at the bottom of the duct due to gravitational drainage followed by an increase in the size of the bubbles in the upper part, ensuing from various phenomena such as the coalescence and expansion of the bubbles. The consequence of this phenomenon is the non-uniformity of both heat and mass transfers along the duct and of the wall shear stress.

The analysis of the bubble size shows a change in the foam structure after the fence. Figure 40 (a) presents an example of the bubble size distribution for a section of 2 cm^2 just upstream and downstream of the fence for Case 1, fitted by a lognormal model. PIV images were taken and treated with Piximètre 1.5 software. These results confirmed the change in the foam texture after the fence previously observed (Aloui and Madani, 2007). As seen in cumulative probability, the bubbles downstream of the fence were 20% larger than upstream, as a consequence of the various factors associated with the fence and the coalescence of the bubbles. The evolution of the global and local void fraction can be deduced, with the global fraction remaining almost unchanged the same and the local void increasing as it approaches the top of the duct, where the largest bubbles are located after the fence. Such phenomena would be related both to the variation of the pressure, gas density and the temperature, the two later which in turn are governed by the heat exchange between the gas and the liquid phases.

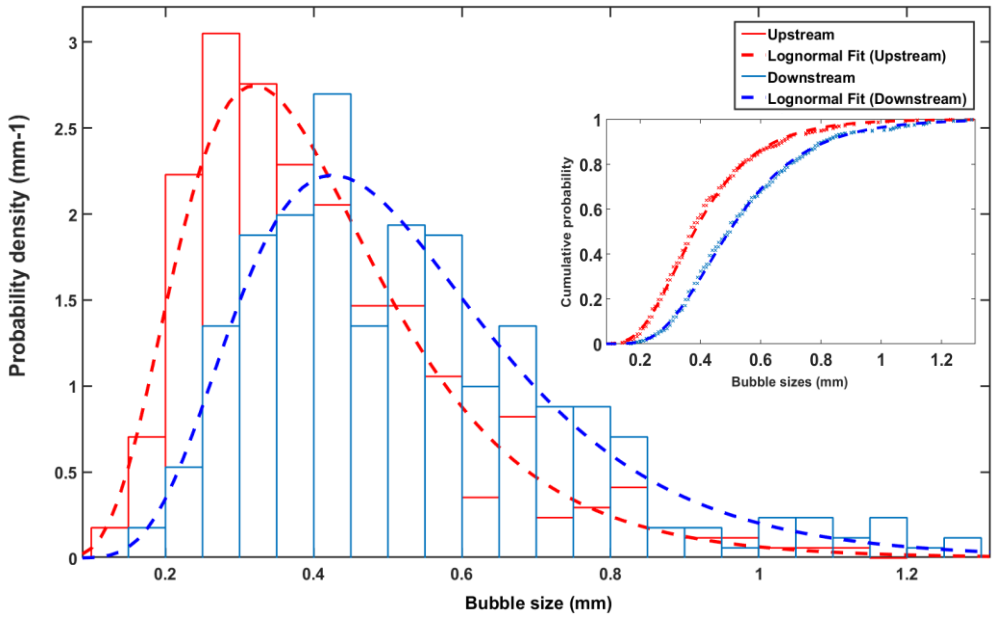

Figure 40. Experimental example of the bubble size distribution for the case of foam at Re = 32. Density and cumulative probability of the bubble size upstream and downstream of the fence.

III.2 Rheological model

Foam flow presents complex properties that make it difficult to define the wall shear rate and the velocity gradient (opacity, reflections, small scales, etc.). One way to obtain this is to assume that the velocity gradient is equal to the bubble's velocity over the wall of the channel, in relation to the thickness of the liquid slip layer (*e*) at the top side of the duct (Blondin and Doubliez, 2002):

$$\dot{\gamma}_w = \frac{\partial u}{\partial y} \quad (9)$$

The average slip layer thickness was measured by the conductometry method at the top of the channel (30, 26, and 33 µm for Cases 1, 2, and 3 respectively). Supplementary Data 2- Figure 41 (conductometry signal over the top wall for Cases 1, 2, and 3) represents a typical signal delivered at the top of the wall for the three cases).

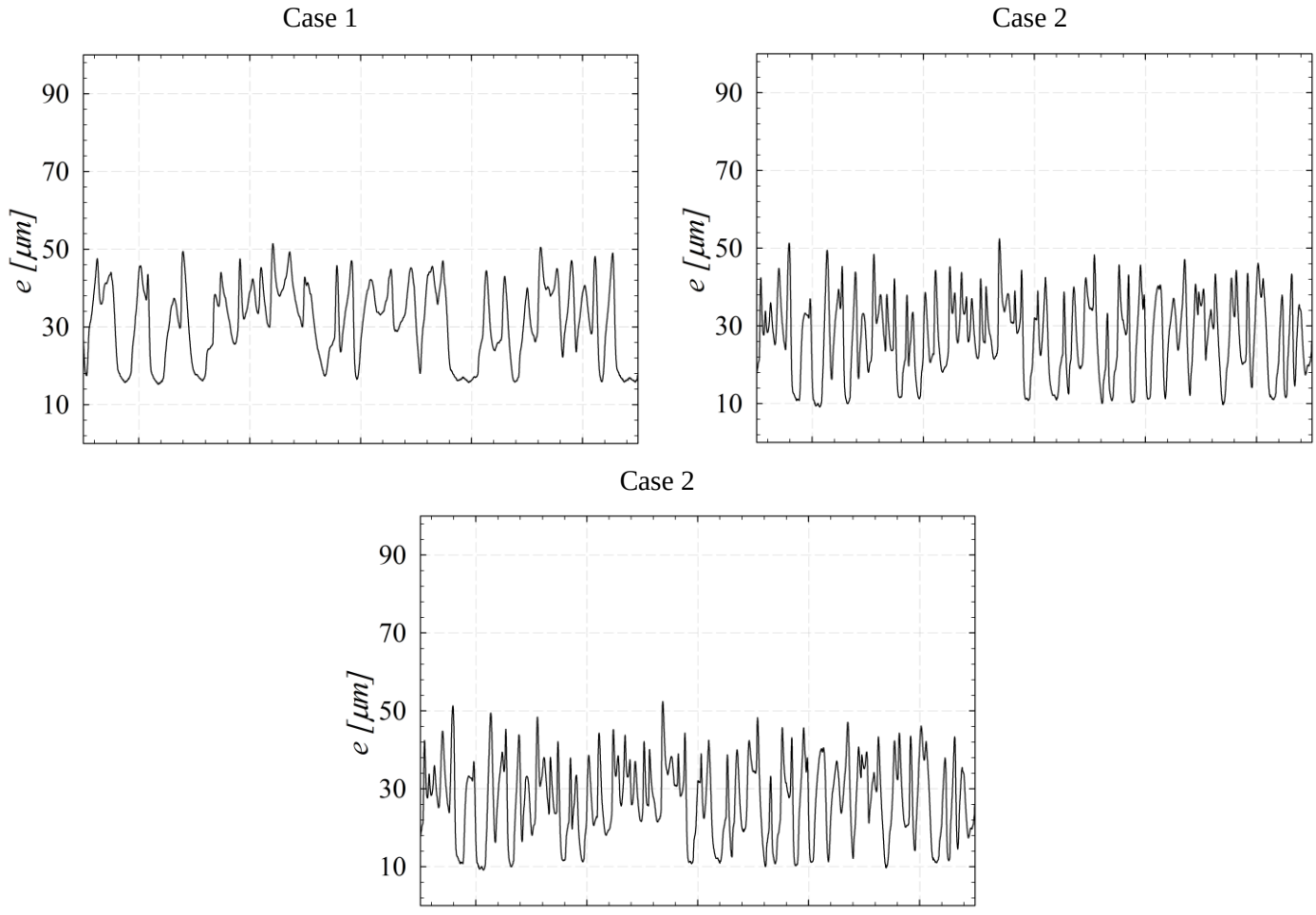

Supplementary data- Figure 41. Conductimetry signal over the top wall for Cases 1, 2 and 3.

The mean wall shear stress can be computed as:

$$\bar{\tau}_w = \frac{\Delta P}{\Delta x}\frac{d_h}{4} \quad (10)$$

where $\frac{\Delta P}{\Delta x}$ is the pressure gradient and $d_h(= 21mm)$ is the hydraulic diameter.

Several methods exist for measuring the yield stress developed for non-Newtonian fluids such as stress relaxation, stress ramping, frequency sweeping and viscometry. These techniques are applied for static foam conditions and present a great uncertainty due to foam instability issues, such as degradation, expansion, and the absence of wall slip (Khan and Armstrong, 1987; Sullivan and Yee, 1984).

Determining the flow curve of the foam can be the most appropriate way to identify the rheological behaviour of this fluid complex under dynamic conditions (Sherif et al., 2015). Figure 42 describes the change in the shear stress as a function of the shear rate for the three cases studied.

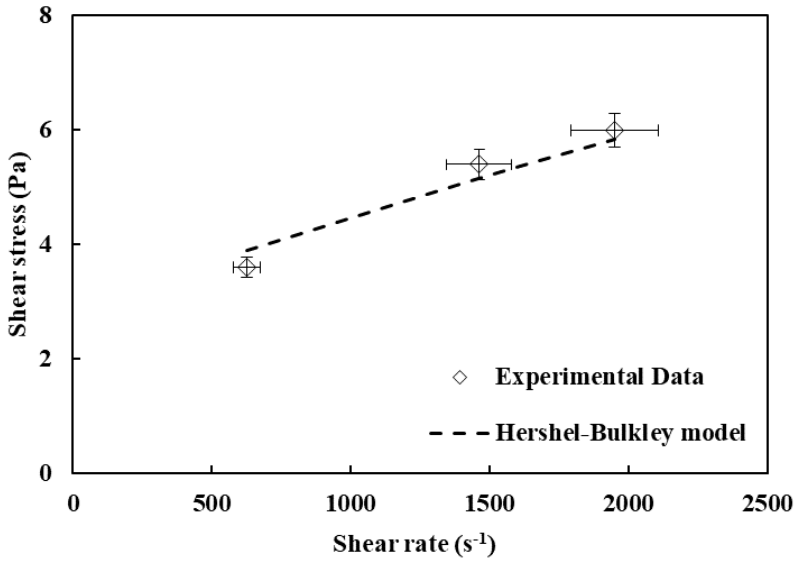

Figure 42. Experimental flow curve of the wet foam studied.

The flow curve of the foam obtained exhibits a strong non-Newtonian fluid behaviour, with a threshold stress ($\tau(\dot{\gamma} = 0) \neq 0$), whose apparent viscosity is highly sensitive to the shear rate change. This can be attributed to the development of the foam structure discussed above. This behaviour best matches the Herschel-Bulkley rheological model.

The flow behaviour index *n* can be determined from the slope of Log $(\tau_w - \tau_{\dot{\gamma}_w \to 0})$ versus Log $(\dot{\gamma}_w)$ plot (Equation 11). For our case, the foam presented as a shear-thinning fluid.

$$n = \frac{d\left(ln\left(\tau_w - \tau_{\dot{\gamma}_w \to 0}\right)\right)}{d\,(ln\,(\dot{\gamma}_w))} \qquad (11)$$

The method used is based on the Rabinowitsch-Mooney equation, which provides the wall shear rate for non-Newtonian flow (Firoze Akhtar et al., 2018). This is presented elsewhere (Khan and Armstrong, 1987).

Modeling foam flows experimentally is a challenge, given the complexity of the foam structure, the experimental artefacts, and the possibility of error presented by the different measurement methods used.

A numerical simulation can be a solution to adjust the parameters of the rheological model identified experimentally.

Table 4 shows the rheological parameters identified that describe the Hershel-Bulkley model and the Bingham model proposed in previous work (Chovet et al., 2014). The density of air and water fluids are respectively taken as being 1.21 and 1003 $kg.m^{-3}$.

However, this rheological model also has its limits, as it is sensitive to the choice of parameters which change with the geometry and the foam quality (Dallagi et al., 2018; Marchand et al., 2020). The numerical identification of these parameters was chosen after the experimental identification discussed before. It then was adjusted based on the inverse simulation: starting with known experimental results, setting the parameters, and checking the velocity and pressure profiles obtained, then comparing these to the experimental ones. Validations of these results are always mandatory to ensure their relevance to experiments (results will be discussed below and display close agreement). The second instrument for adjusting this parameter is the CFD convergence, which minimizes the residue calculation. Indeed, this model presents a severe discontinuity in its rheological behaviour due to the threshold yield stress and the index number. It also induces some numerical difficulties in the convergence if the parameters imposed are not coherent with the boundary conditions (Messelmi, 2019). This problem has been the subject of other studies aiming to regularize the discontinuity of the exact visco-plastic behaviour, in order to allow its implementation in standard numerical solvers (Liu et al., 2002; Moreno et al., 2016).

Accepting these limits of experimental uncertainty, a lack of wall slip and numerical convergence, the Herschel-Bulkley model seems to fit the experimental observations more closely at low shear stress, with a slight deviation under higher conditions. In contrast, the Bingham model proposed previously by (Chovet et al., 2014) fails to support the experimental data shown in Table 4. The numerical results for the two rheological models (Bingham and Hershel-Bulkley) presented in Table 4, will be compared below with experimental ones for Cases 1 and 3.

Table 4. Parameters of the two rheological models used. The parameters of the Herschel-Bulkley (CFD) model derived from the experimental flow curve (experimental, 20°C) were thus refined to obtain the best match between the CFD results and the experimental data.

Model	Yield Stress τ_0 (Pa)	Consistency k (Pa.s)	index n	Density ρ (kg.m^{-3})
Hershel-Bulkley (experimental; 20°C)	2.7	0.005	0.85	350
Bingham (CFD)	6.4	0.001	1	350
Hershel-Bulkley (CFD)	3.9	0.0015	0.80	350

III.3 Case of Foam Flow (plug flow) at low velocity (Re=32)

III.3.1 Longitudinal pressure distribution

To validate the CFD numerical calculations, it is necessary to examine whether the pressure distribution generated by the Herschel-Bulkley model confirms the experimental results. Figure 43 shows the longitudinal static pressure losses ΔP inside each cross-section of the horizontal duct including the fence at its centre.

As illustrated in Figure 43 (a), when distant from the fence, whether upstream or downstream, we respectively have an establishment and a re-establishment of the foam flow regime. Results show a linear decrease in the static pressure upstream and downstream of the fence. The transition through the fence is followed by a slight disturbance in the pressure drop with the same energy degradation on both sides of the fence. This similarity can result in a similar pressure gradient value upstream and downstream of the fence, where both curves have almost the same slope (-615 Pa.m^{-1} for the upstream and -745 Pa.m^{-1} for the downstream). The presence of the fence in the pipe represents a disruption for the foam flow. Its influence extends upstream as well as downstream of the fence. Indeed, according to the magnification in Figure 43, the change in the flow starts approximately from the x = -260 mm ($\simeq$-12.4d_h) until x = 220 mm ($\simeq$10.5d_h).

CFD simulations and experimental measurements present the same evolution with a maximum deviation close to 5% near the fence. This comparison allows a validation of the chosen boundary conditions adopted i.e. the rheology model used, and the parameters fixed for the simulation.

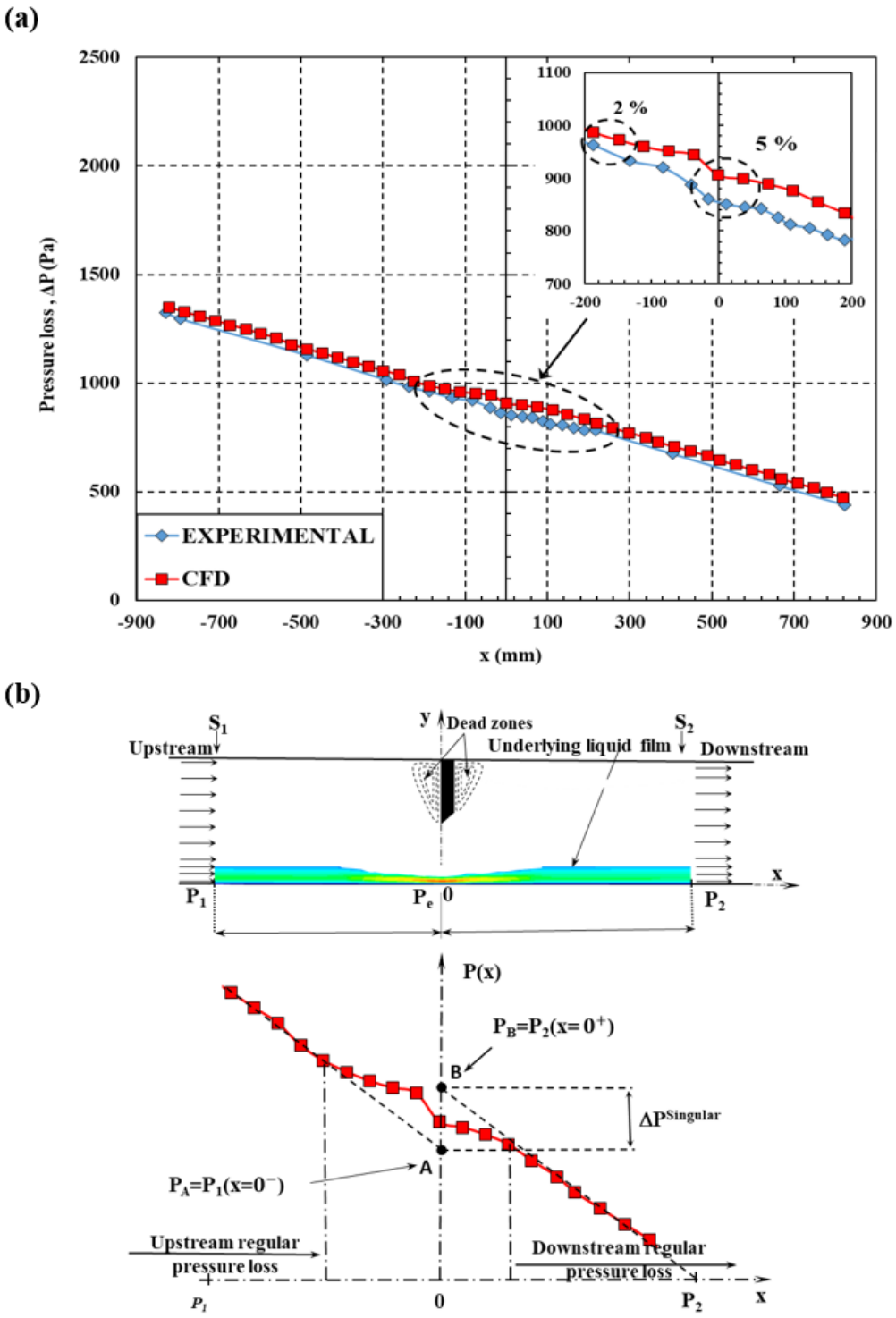

Figure 43. Longitudinal static pressure drop of the foam flow at Re = 32. (a): Evolution of the longitudinal static pressure drop along the test channel. (b): Zoom on the area influenced by the fence.

III.3.2 Singular pressure drop

According to (Aloui and Madani, 2008, 2007), the singular pressure drop caused by the fence and the global wall friction against the wall in the vicinity of the fence can be written as:

$$\Delta P_{Singular} = P_2(x = 0^+)_{downstream} - P_1(x = 0^-)_{upstream} \quad (18)$$

$$\Delta P_{friction} = \Delta P_{tot} - \Delta P_{singular} \quad (19)$$

where $\Delta P_{singular} = \frac{1}{2}.\xi.\rho_f.U^2$ can be considered as the singular pressure due to the kinetic effects of the fence. The singular pressure drop coefficient (ξ) is equal to 8.52 (Aloui and Madani, 2008), and P_1 and P_2 are the pressure in the upstream and downstream of the fence respectively.

In the case of *Re* = 32, and for a foam quality of 65%, the singular pressure drop was estimated *as* $\Delta P_{singular} \simeq$ 58 Pa (determined by extrapolating the regular pressure evolution downstream and upstream of the fence as shown in Figure 43 (b)). This numerical result has a slightly larger value than the experimental one (≃40 Pa). This means that the foam flow adapts faster than the Herschel-Bulkley fluid to the section change and its behaviour is less affected by the fence. Besides, the results obtained show that foam flow under a fence is the exact opposite of the flow of a Newtonian liquid single-phase. The contribution of the pressure loss by friction in the global singular pressure drop is about 98%. This means that the energy loss in this condition of foam flow under the fence is not dominated by any kinetic effects of the fence ($\Delta P_{singular}$=1.15 Pa), but by the friction near the fence ($\Delta P_{friction} \simeq$ 57 Pa).

III.3.3 Local averaged velocity fields

To determine the behaviour of Herschel-Bulkley fluid under the fence, it appears necessary to visualize the velocity fields and the deformation of their profiles, by giving a comparison of the numerical simulation results with the experimental ones. Figure 44 represents an example of a velocity field for the numerical simulations of the CFD Herschel-Bulkley fluid.

The presence of the fence disrupts the flow by forcing the foam to bypass it, inducing the creation of stagnant areas around the fence (absence of velocity vectors on both sides in the vicinity of the fence as shown in Figure 44 (a)). The visualization of the velocity field through the horizontal plane at *y* =19 mm (Figure 44 (b)), confirms the direction of the flow. Thus, the upstream dead zone is longer than that one downstream ($l_1 > l_2$, where l_1 (≃0.47d_h) and l_2 (≃0.23d_h) are respectively the lengths of the appearance of dead zones immediately upstream and downstream of the fence).

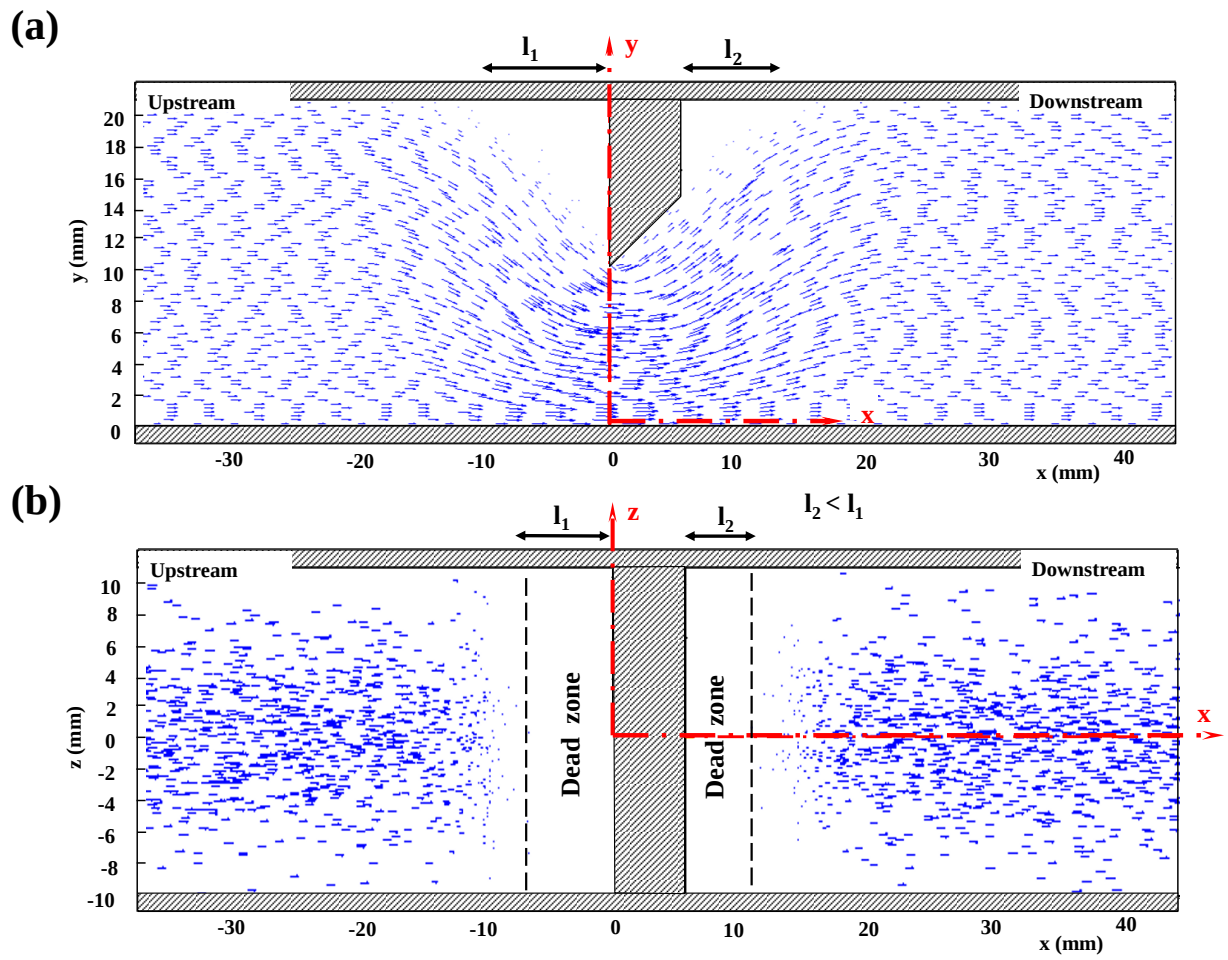

Figure 44. Example of velocity field obtained under the fence at the middle axis of the duct by CFD simulation using the Herschel-Bulkley model (foam at Re = 32). (a): Lateral view. (b): Top view at y =19 mm.

The comparison between these numerical and experimental results shows a close concordance (Supplementary data 3- Figure 45 (Averaged u-axial component (a) and v-vertical component velocity field (b) of experimental foam flow and the Herschel-Bulkley model under the fence).

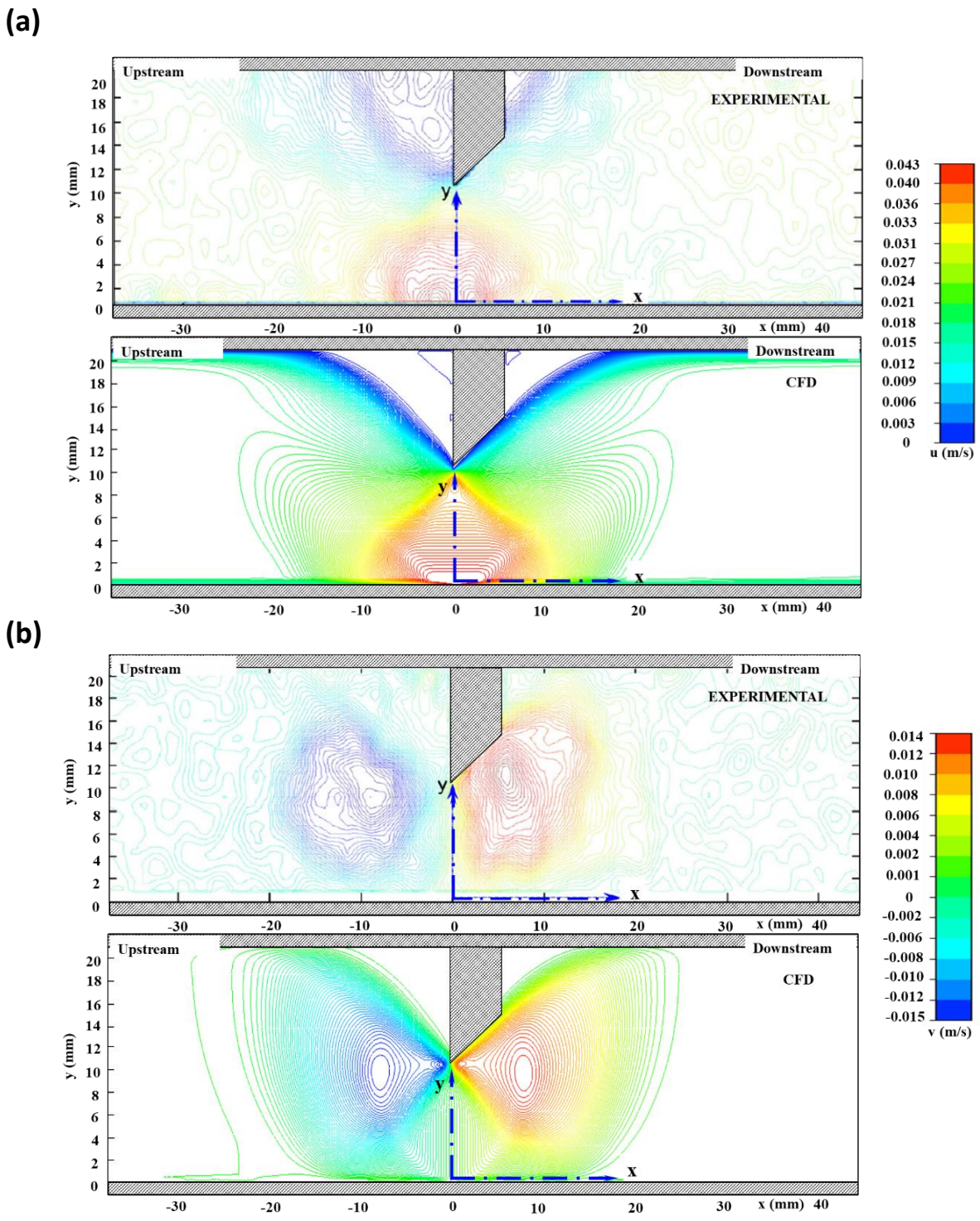

Supplementary data 3- Figure 45. Averaged u-axial component (a) and v-vertical component velocity field (b) of experimental foam flow and the Herschel-Bulkley model under the fence.

The effect of the fence can be quantified by plotting the evolution of the axial and vertical components' velocity profiles along the x-coordinate near the fence for different positions upstream and downstream of the fence (Figure 46). These velocity profiles allow a better

comparison between the foam flow, the Bingham model proposed by (Chovet et al., 2014) and our proposed model, namely the Herschel-Bulkley law.

A close similarity between the experimental and the CFD results were thus observed with the Herschel-Bulkley CFD model results showing less deviation than the Bingham model ones.

As mentioned above, simulating a complex fluid such as foam is a challenge because of the presence of several phenomena. For instance, it is difficult for the software code to reproduce incidents such as the slip and deformation of bubbles, coalescence, and foam drainage (Golemanov et al., 2008). The Herschel-Bulkley model, based on the hypothesis of a pseudo-fluid, can describe the behaviour of the foam flow more reasonably than the Bingham model. Hence, Axial velocity component results by the Bingham model show a discrepancy of between 21% and 37% between the foam flow experiments and the CFD simulations, while Herschel-Bulkley only shows a difference of 8% to 21%. For both models, vertical velocity component profiles show the greatest deviation, where the foam deformation increases near the fence (at x=-5mm), entailing its maximum deviation of 50%. It should be noted that contrary to CFD results, the experimental data indicate a slip at the walls. While accepting its limits, this study has shown that the rheological Herschel-Bulkley fluid model is capable of satisfactorily describing the behaviour of flowing foams under a fence.

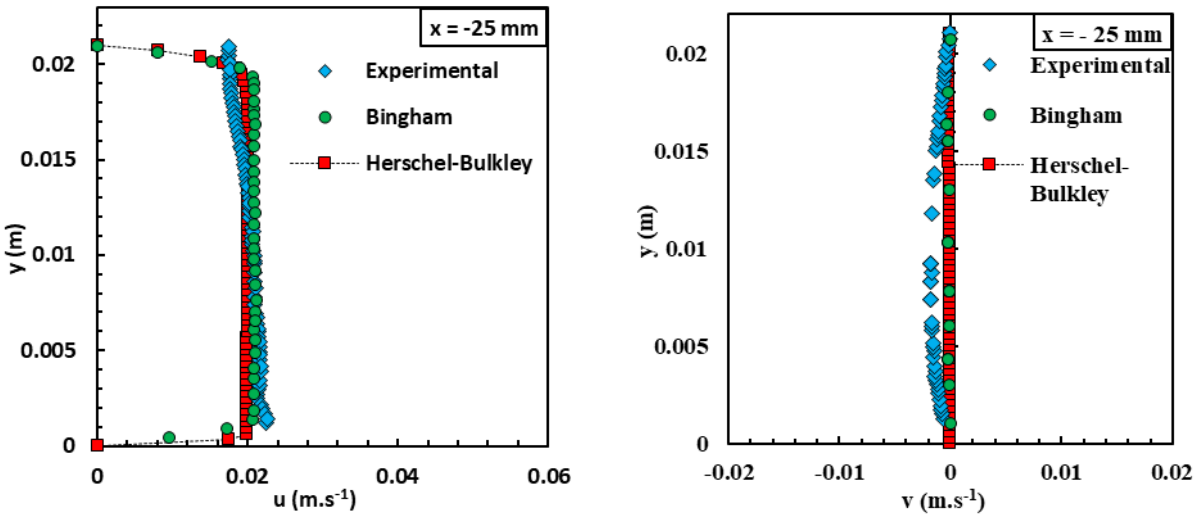

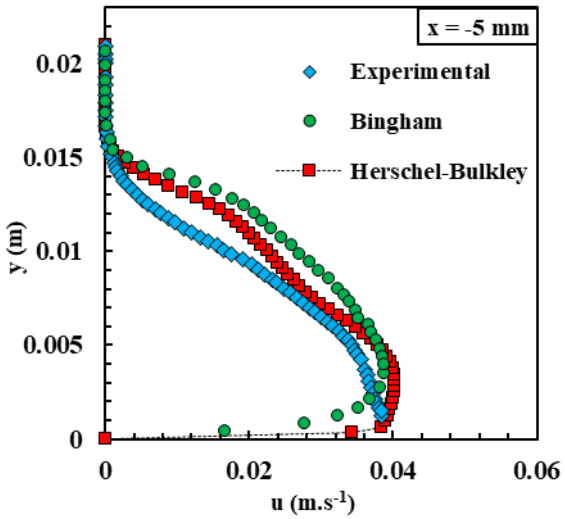
x = -5 mm
Experimental
Bingham
Herschel-Bulkley
y (m)
u (m.s-1)
0
0.005
0.01
0.015
0.02
0.04
0.06

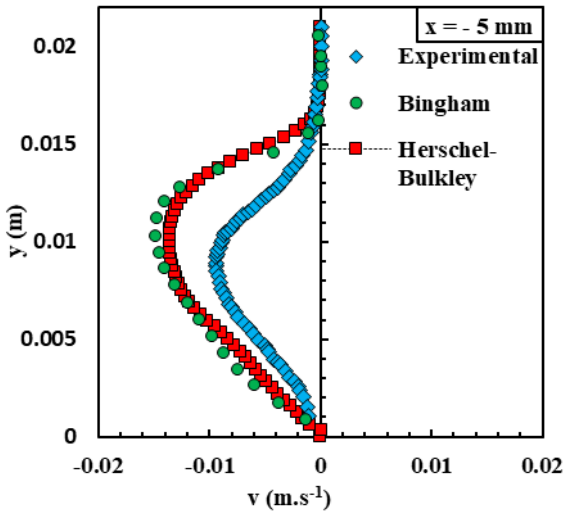
x = - 5 mm
Experimental
Bingham
Herschel-Bulkley
y (m)
v (m.s-1)
-0.02
-0.01
0
0.01
0.02

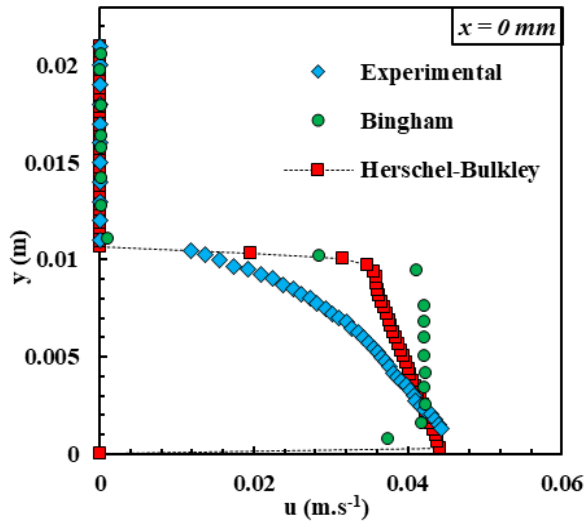
x = 0 mm
Experimental
Bingham
Herschel-Bulkley
y (m)
u (m.s-1)
0
0.005
0.01
0.015
0.02
0.04
0.06

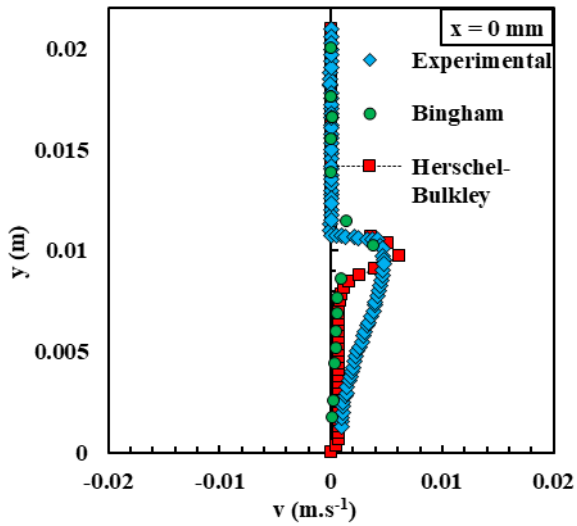
x = 0 mm
Experimental
Bingham
Herschel-Bulkley
y (m)
v (m.s-1)
-0.02
-0.01
0
0.01
0.02

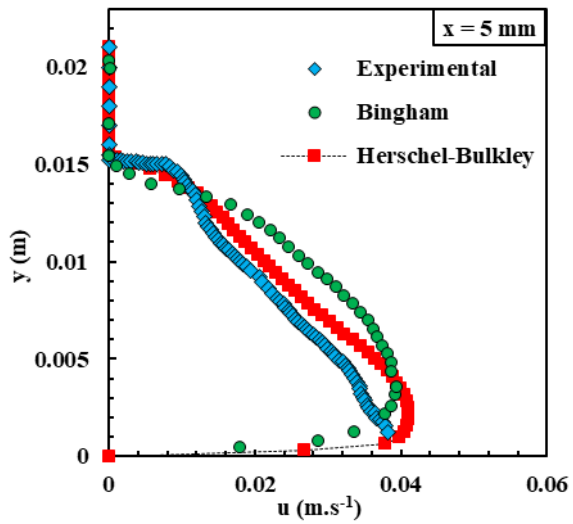
x = 5 mm
Experimental
Bingham
Herschel-Bulkley
y (m)
u (m.s-1)
0
0.005
0.01
0.015
0.02
0.04
0.06

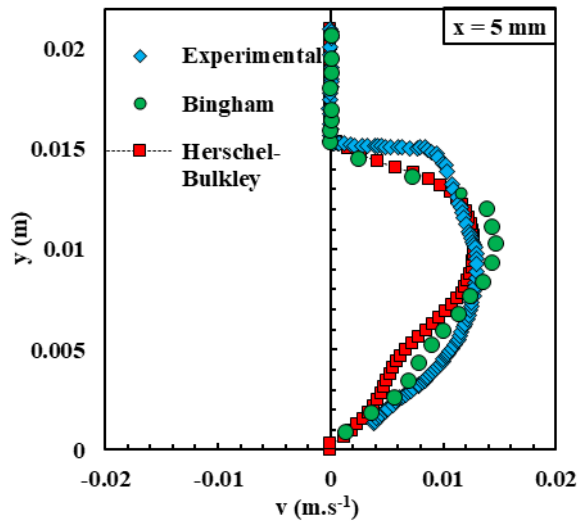
x = 5 mm
Experimental
Bingham
Herschel-Bulkley
y (m)
v (m.s-1)
-0.02
-0.01
0
0.01
0.02

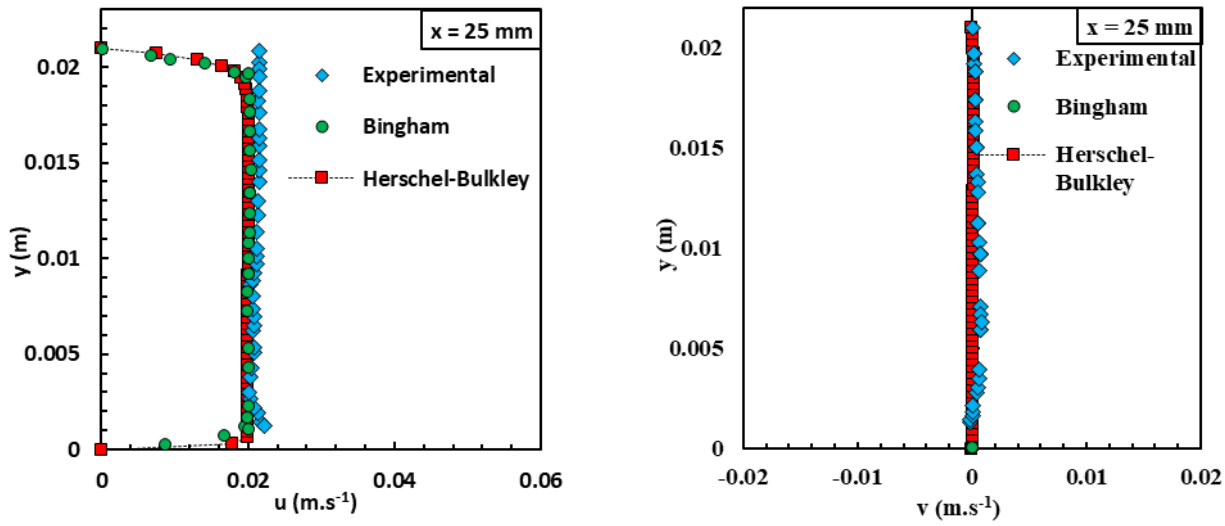

Figure 46. Lateral averaged axial (u) and vertical (v) mean component velocity profiles for different positions near the singularity, for the case of foam at Re of 32.

Supplementary Data 4- Figure 47 illustrates the velocity profiles on the upper part in three planes along x-z axes: at the top of the channel (y = 19 mm), in the middle (y = 10.5 mm), and at the bottom (contact with the underlying liquid film, for y = 2mm). This was achieved by numerical simulations to define and to present the evolution in foam flow's behaviour along the x-coordinate near the fence at different locations. It should be noted that the experimental results did not investigate the velocity fields inside the foam and far from walls, as the opacity of the foam limited the PIV technique's capacity to visualize the flow. In such cases, CFD studies are of distinct benefit.

It is clear, that the foam flow behaves like plug flow, hence as a unidirectional regime. Therefore, these results confirm the presence of dead areas at the top of the channel (at y = 19 mm and -15 mm < x < 15 mm), where the velocity is nil and that the maximum acceleration occurs at the location of the fence when x = 0 mm and y = 10.5 mm.

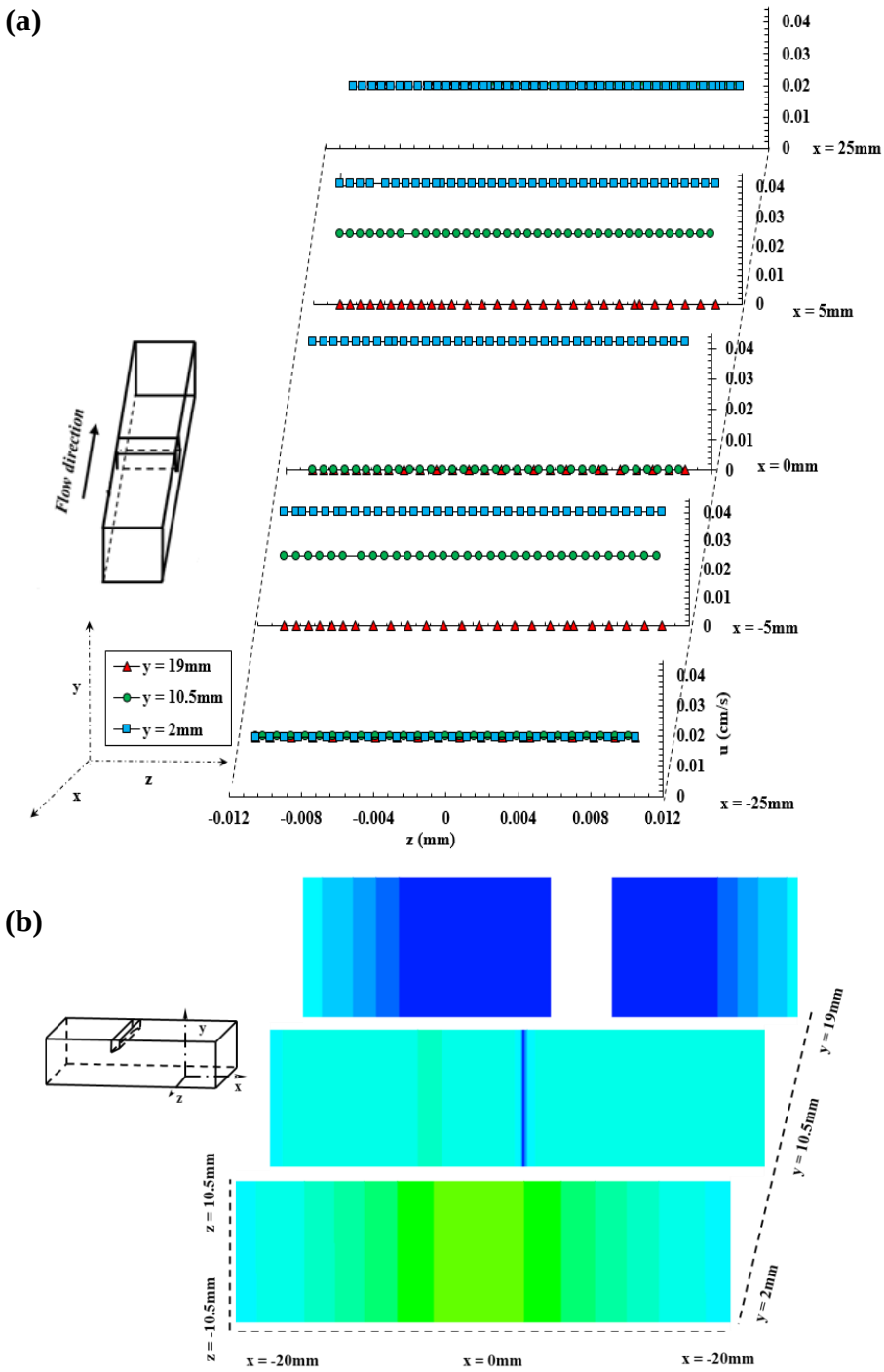

Supplementary data 4- Figure 47. CFD spanwise (top side) axial velocity at different locations in the vicinity of the singularity for case 1. (a): averaged axial velocity component profiles. (b): Axial velocity component distribution for three horizontal planes located at: y = 2, 10.5, and 19 mm.

III.3.4 Underlying film thickness in the vicinity of the fence

Wet foam flows also create liquid films along the bottom surface of the duct. This thickness can affect the dynamic behaviour of the flow. Previous works have also shown that the thickest liquid film is formed at the bottom of a channel arranged horizontally under the gravitational

force effects and more specifically under the foam drainage (drainage of the liquid through the plateau borders or bubbles' contours) (Tisné et al., 2004).

Despite the experimental data available, the model was not able to accurately reproduce this phenomenon. This is the reason why a liquid (water) film was imposed at the bottom channel as a second inlet condition, unlike previous attempts to model the foam flow using CFD tools (Chovet et al., 2014). Figure 48 (a) presents the velocity evolution of the underlying liquid film. We noted that the velocity of the liquid film increased when approaching the fence to reach a maximum value caused by the narrowing of the section (velocity of 3.3 cm.s^{-1} at x = 0 mm). After the fence, the velocity of the film liquid increased gradually to recover its initial value of 2.1 cm.s^{-1}.

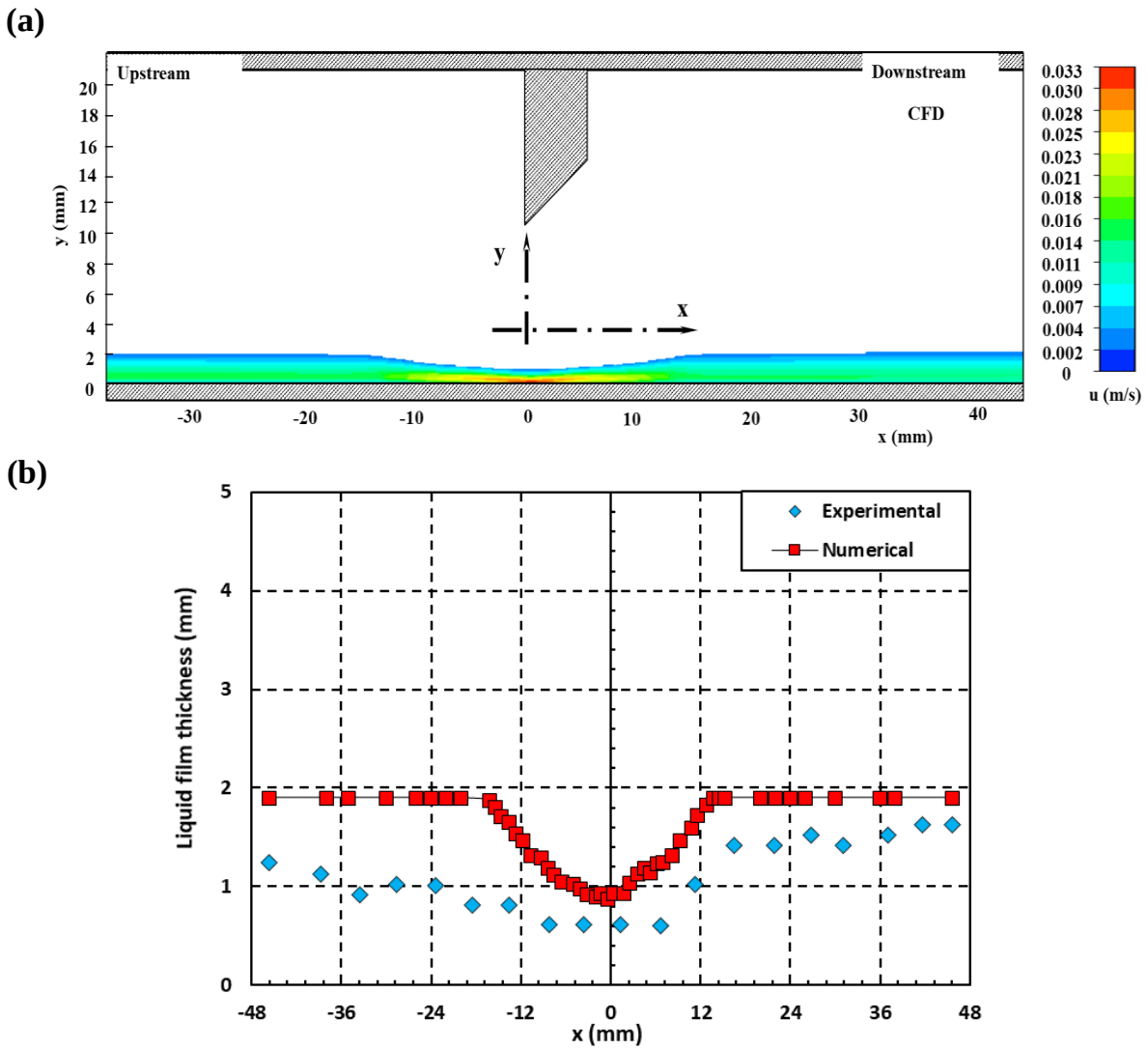

Figure 48. Underlying liquid film located at the bottom of the horizontal duct. (a): Averaged axial velocity field. (b): Comparison of experimental (blue diamonds) and numerical simulation (red squares) underlying liquid film thickness. The foam in this simulation was defined by Hershel-Bulkley model.

To better understand the deviations and the disturbance caused by the fence, Figure 48 (b) represents the thickness evolution of the underlying liquid layer. The underlying liquid film thickness remained constant and had no pronounced fluctuations upstream or downstream of the fence. It was stable and its thickness was about 1.9 mm. However, this thickness gradually decreased below the fence and reached its minimum value, which was about 0.9 mm. This modification was mainly due to the abrupt acceleration of the outgoing flow through the reduced cross-section passage, which then exerted compression on the underlying liquid film.
This evolution studied by CFD is only an approximation of the underlying liquid film thickness. However, it does present a discrepancy of about 45% from the experimental results given by the conductimetric method. These show the same evolution except that the liquid film is 20% thicker downstream than upstream of the fence. This thickness difference is mainly due to the foam drainage phenomenon, which increased with the acceleration of the foam flow and after the reorganization of the bubbles (Golemanov et al., 2008; Marchand et al., 2020). The experimental results again indicate that the fence induced some changes in the foam flow structure.

III.4 Case of foam flow at higher velocity (Re = 97)

The main goal was to test the ability of the rheological model proposed to reproduce the physical phenomena response of high Reynolds numbers, where the yield shear stress is exceeded. Figure 49 illustrates the evolution of axial and vertical velocity components along the *x* and *y* coordinates at different distances from the fence.
The validation of the CFD results is based on the experimental measurements provided by the PIV technique, in order to investigate the foam flow velocity components' profiles under the same conditions.
The comparison between experimental and numerical results shows an agreement, despite the observed deviations for the Herschel-Bulkley model (from 19% to 47% for the axial velocity component and from 30% to 74% for the vertical velocity component). On the other hand, it shows to what extent the Bingham model describes the sheared condition of the foam flow (from 30% to 100% difference for the axial and vertical velocity components). The greatest deviation that occurred for the vertical velocity component profiles is at x=-5mm. This difference is partly due to the use of a laminar regime instead of the turbulent regime, causing the underlying liquid layer to slide and secondly, due to the compressibility of the foam gas phase (experimental fluid) and to its resistance to the narrowing of the duct cross-section, thereby generating a viscoelastic response by the foam.

The Herschel-Bulkley model proposed is written as the sum of a yield stress τ_0 and a viscous stress τ_v. First, as discussed above, the experimental identification of the threshold stress under dynamic conditions is a challenge due to experimental artefacts. On the other hand, the capillary pressure of the bubbles, the adsorption of the surfactant layer on the surfaces of the bubbles and the viscous friction between the bubbles and the wetting walls provide a scale for the viscous stress (Borkowski et al., 2020; Denkov et al., 2005). As the foam in this work is identified as a pseudo-fluid which does not reflect the real identity of the foams i.e. a dispersion of gas bubbles in liquids containing surfactants according to (Langevin, 2017), it is difficult for Herschel-Bulkley to represent these phenomena and accurately reproduce the experimental behaviour of high-velocity foam flow. Thus, according to several previous studies (Messelmi, 2019; Moreno et al., 2016), some limitations of this model should be studied and experiments performed in future works using a slip wall condition, in order to focus on a simulation of the shape, trajectory, and interaction of bubbles on the walls (Ge and Liu, 2021).

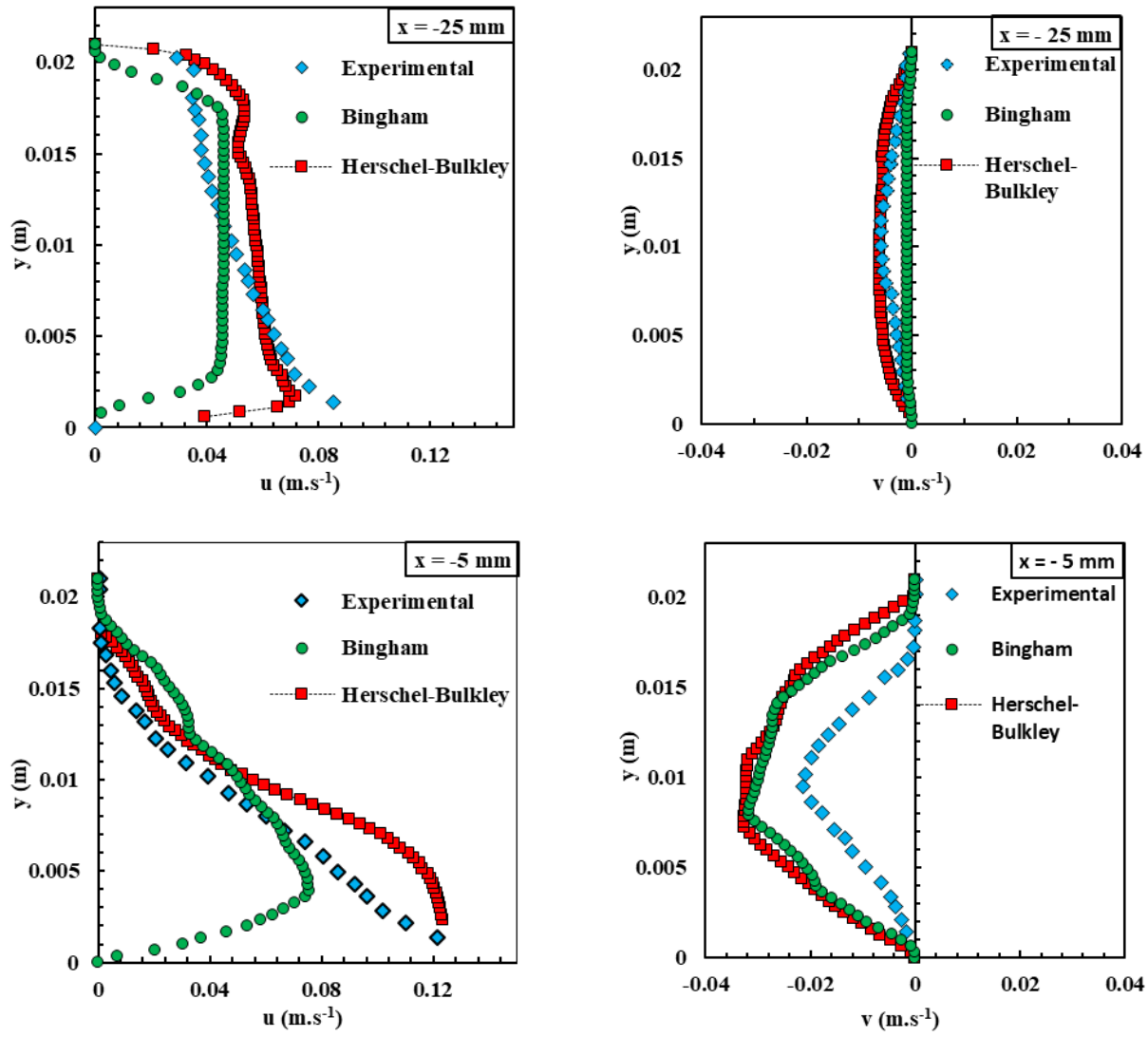

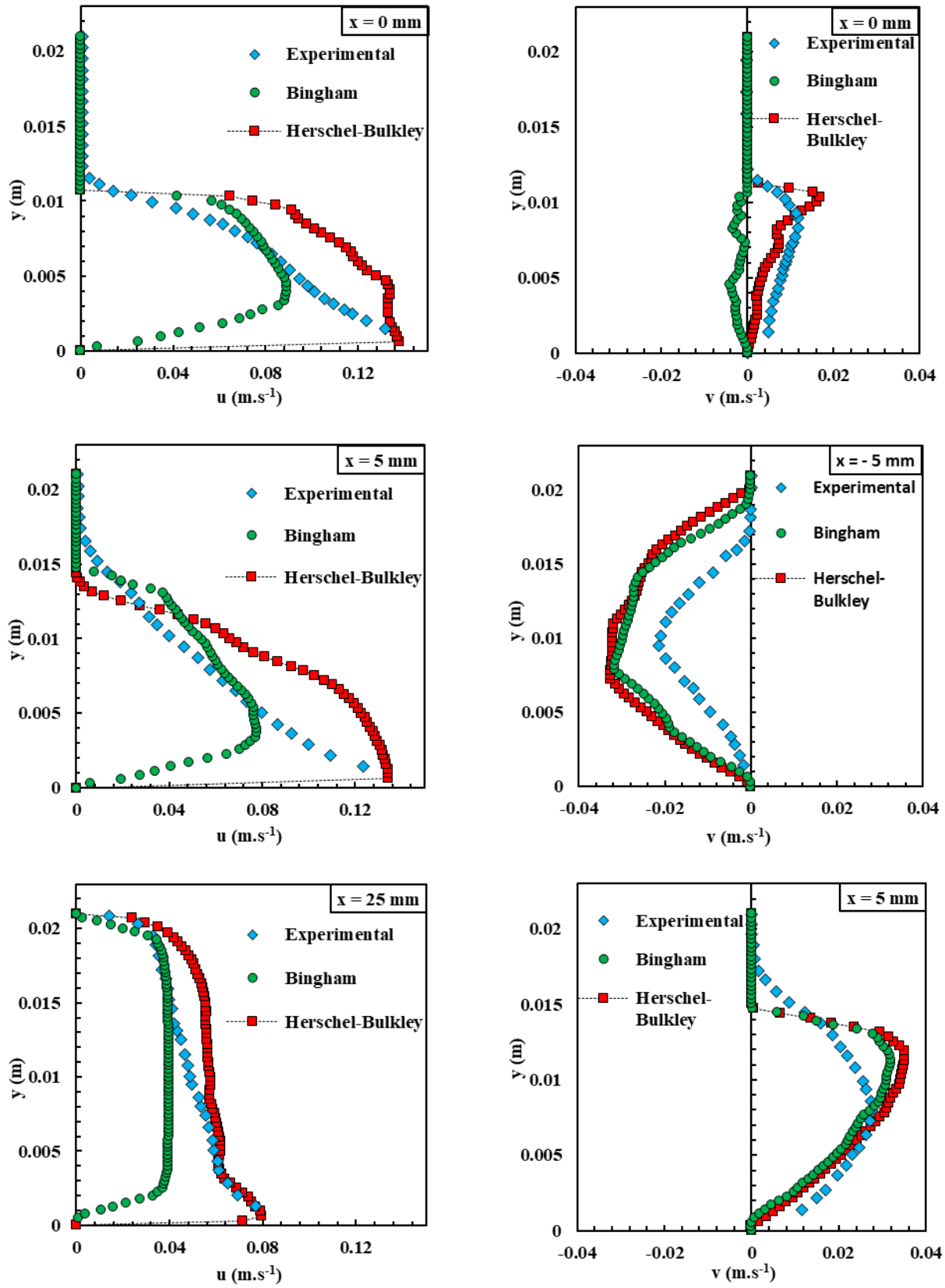

Figure 49. Lateral averaged axial (u) and vertical (v) mean component velocity profiles for different positions near the singularity, for the case of foam at Re = 97 and different rheological models.

Concerning the foam flow behaviour on the spanwise plane, the velocity fields are not accessible experimentally using the PIV technique because of the opacity of the foam, as already mentioned. Figure 50 shows the evolution of the velocity profiles thanks to CFD, along the z-coordinate near the fence, plotted in three horizontal planes: at the bottom of the channel (x, y = 2 mm, z), in the middle (x, y = 10.5 mm, z), and at the top (x, y = 19 mm, z).

In contrast to the first case (Re = 32), the shear stress in the channel far exceeds the yield stress inducing velocity profiles with parabolic shapes of the as shown in Figures 50 (a), and 50 (b). In addition, there is a great contrast comparing the foam velocities at the top (low velocities) and at the bottom (high velocities) of the channel.

(a)

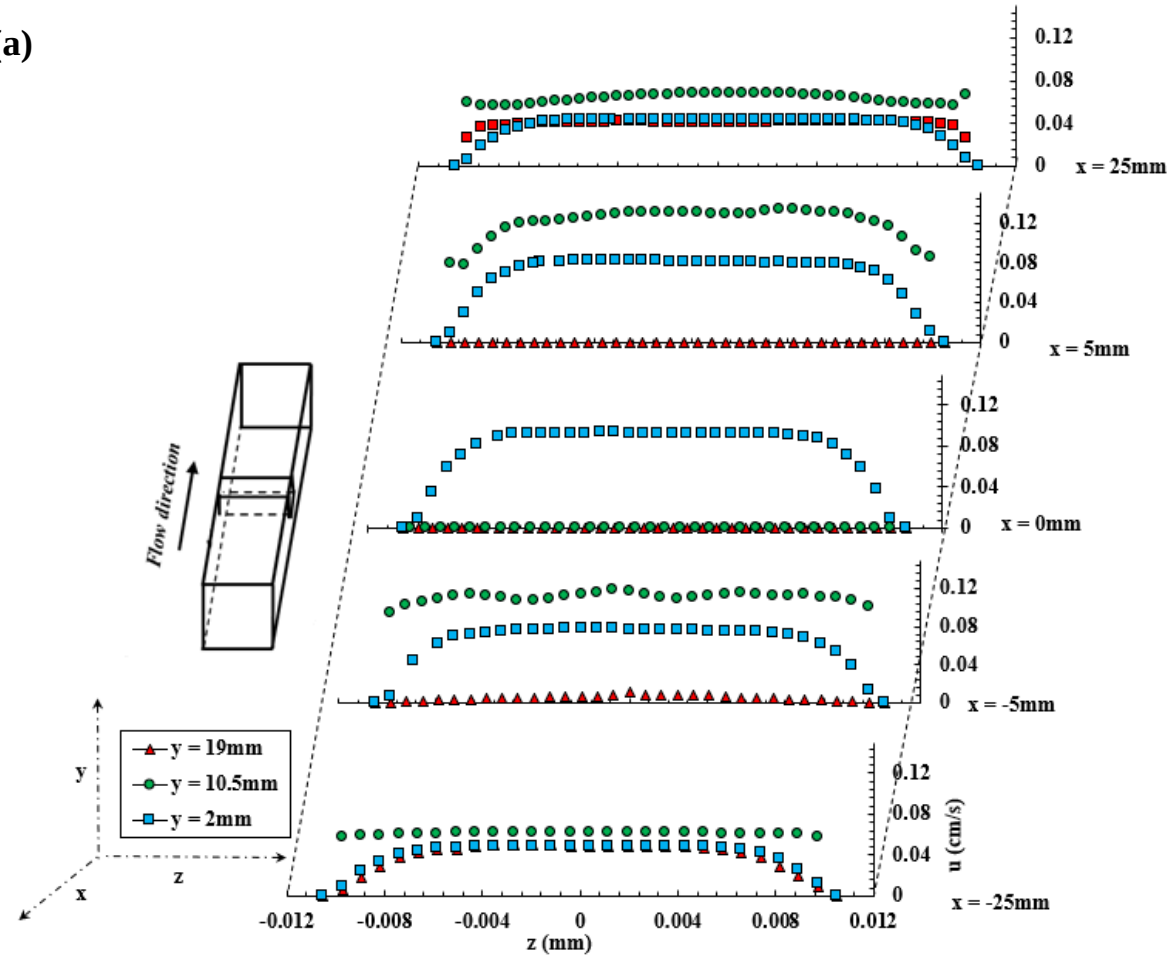

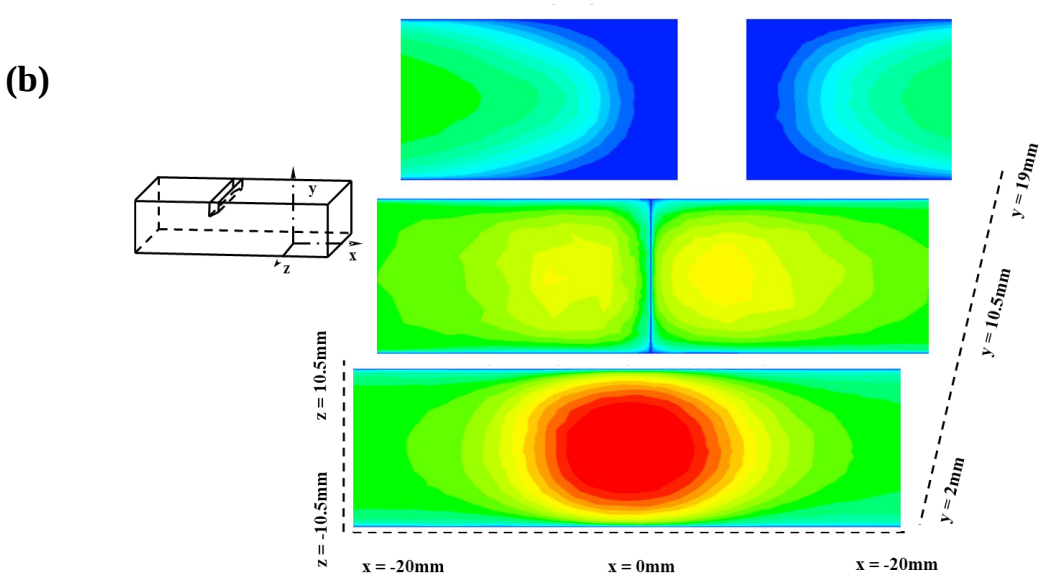

Figure 50. CFD spanwise (top side) axial velocity at different locations in the vicinity of the singularity for case of foam at Re = 97. (a): averaged axial velocity component profiles. (b): Axial velocity component distribution for three horizontal planes locate at: y = 2, 10.5, and 19 mm.

IV. Conclusions

In this work, the effect of the fence both on the characteristics of the foam flow, as well as on the different phenomena observed, has been studied using both experimental and CFD simulation approaches, giving original results.

Different measurements were made including liquid film thickness, foam structure and its flow behaviour. This allowed us to clearly understand the deformation of the foam in the vicinity of the fence, where it displays marked elasticity. CFD results were directly compared to those obtained experimentally under the same flow conditions. Attention was focused on the velocity component profile evolution upstream and downstream of the fence. The CFD simulations and the experimental results showed the same trends. The Herschel-Bulkley rheological model can better describe the foam flow for all regimes (3 cases studied), than the Bingham rheological model. As for the lower Reynolds number, the two fluids behave like a plug-type flow presenting a mean deviation of 15%. In contrast, in the case of higher Reynolds number (Case 3), some greater deviations appear near to the fence, which can reach more than 50% with Hershel-Bulkley and be completely different for Bingham. This considerable discrepancy reflects the higher sensitivity of the chosen model (pseudo-fluid flow) and its limits in presenting this type of foam flow deformation and the bubbles' reorganization. This is probably related to the actual rheological properties of the foam modelled here by a quite simple Herschel-Bulkley pseudo-fluid model. However, some likely important phenomena should be

taken into account in the future such as the compressibility of the foam gas phase and the slipping of the foam bubbles on the channel walls (phenomena existing at the bubble-bubble and bubble-liquid film interfaces) highlighted by the different experimental methods.

Despite the complexity of the proprieties involved in the physics of foams (border stability plateau, effect of surface tension, drainage of liquid, bubble movements, coarsening, ripening, coalescence, compressibility), the non-Newtonian fluid model with threshold stress gives a quite good approximation of the foam's flow behaviour and its deformation on encountering a fence.

In a previous work, we have demonstrated that compared to the standard cleaning-in-place, the use of foam flow to remove bacterial contamination (spores and biofilms) can improve the cleaning efficiency and dramatically reduce the consumption of water and energy (Al Saabi et al., 2021). However, this enhancement of cleaning was closely related to the foam proprieties such as void fraction, shear stress, liquid film thickness, bubble size, and its stabilities (Schad et al., 2021). Modification of the ducts geometries and the presence of specific equipment (valves, fences in heat exchangers, corners or other obstacles) in agro-food processing industries would thus significantly change the foam structure and the flow organization and eventually, reduce the efficiency of foam cleaning (Al Saabi et al., 2020). Computational Fluid Dynamic approaches in a first step assist in identifying the temporal evolution of the flow parameters in complicated situations where experimental definition is difficult. Consequently, their use helps to improve cleaning efficiency when modeling and designing industrial equipment and installing its accessories, thereby ensuring high foam stability and a fast recovery of the flow regime due to a better flow organization. Further studies could investigate the impact of such singularities on the removal kinetics of static bacterial biofilms under foam flow cleaning regimes.

ACKNOWLEDGMENT

This work was supported by the National Institute for Agricultural Research INRAE (Villeneuve d'Ascq, France, laboratory UMET UMR 8207) and the LAMIH CNRS UMR 8201 (Polytechnic University Hauts-de-France, INSA Hauts-de-France, France). The authors wish to express their gratitude to the Interreg V, GoToS3, Vegitec project (EU) and to the Erflow-Engineering (Nantes, France) for the support and funding provided for this research.

References

Al Saabi, A., Dallagi, H., Aloui, F., Faille, C., Rauwel, G., Wauquier, L., Bouvier, L., Bénézech, T., 2021. Removal of Bacillus spores from stainless steel pipes by flow foam: Effect of the foam quality and velocity. J. Food Eng. 289, 110273. https://doi.org/10.1016/j.jfoodeng.2020.110273

Al Saabi, A.-A., Benezech, T., Faille, C., Aloui, F., Rauwel, G., 2020. Foam flow for cleaning of closed equipment contaminated by Bacillus cereus spores or Pseudomonas fluorescens biofilms. Lille, France.

Aloui, F., Madani, S., 2008. Experimental investigation of a wet foam flow through a horizontal sudden expansion. Exp. Therm. Fluid Sci. 32, 905–926. https://doi.org/10.1016/j.expthermflusci.2007.11.013

Aloui, F., Madani, S., 2007. Wet foam flow under a fence located in the middle of a horizontal duct of square section. Colloids Surf. Physicochem. Eng. Asp. 309, 71–86. https://doi.org/10.1016/j.colsurfa.2007.01.009

AlQuaimi, B.I., Rossen, W.R., 2019. Characterizing foam flow in fractures for enhanced oil recovery. J. Pet. Sci. Eng. 175, 1160–1168. https://doi.org/10.1016/j.petrol.2018.06.020

Badve, M., Barigou, M., 2020. Local description of foam flow, deformation and pressure drop in narrow constricted channels. Int. J. Multiph. Flow 103279. https://doi.org/10.1016/j.ijmultiphaseflow.2020.103279

Benzenine, H., Saim, R., Abboudi, S., Imine, O., 2010. Numerical simulation of the dynamic turbulent flow field through a channel provided with baffles: comparative study between two models of baffles: transverse plane and trapezoidal 14.

Blondin, E., Doubliez, L., 2002. Particle imaging velocimetry of a wet aqueous foam with an underlying liquid film. Exp. Fluids 32, 294–301. https://doi.org/10.1007/s003480100318

Borkowski, M., Kosior, D., Zawala, J., 2020. Effect of initial adsorption coverage and dynamic adsorption layer formation at bubble surface in stability of single foam films. Colloids Surf. Physicochem. Eng. Asp. 589, 124446. https://doi.org/10.1016/j.colsurfa.2020.124446

Buzza, D.M.A., D. Lu, C.-Y., Cates, M.E., 1995. Linear Shear Rheology of Incompressible Foams. J. Phys. II 5, 37–52. https://doi.org/10.1051/jp2:1995112

Calvert, J.R., 1988. The flow of foam through constrictions. Int. J. Heat Fluid Flow 9, 69–73. https://doi.org/10.1016/0142-727X(88)90032-X

Calvert, J.R., Nezhati, K., 1986. A rheological model for a liquid-gas foam. Int. J. Heat Fluid Flow 7, 164–168. https://doi.org/10.1016/0142-727X(86)90016-0

Cantat, I., 2013. Liquid meniscus friction on a wet plate: Bubbles, lamellae, and foams. Phys. Fluids 25, 031303. https://doi.org/10.1063/1.4793544

Cappello, J., Sauret, A., Boulogne, F., Dressaire, E., Stone, H.A., 2015. Damping of liquid sloshing by foams: from everyday observations to liquid transport. J. Vis. 18, 269–271. https://doi.org/10.1007/s12650-014-0250-1

Chandran Suja, V., Rodríguez-Hakim, M., Tajuelo, J., Fuller, G.G., 2020. Single bubble and drop techniques for characterizing foams and emulsions. Adv. Colloid Interface Sci. 286, 102295. https://doi.org/10.1016/j.cis.2020.102295

Chen, L., Huang, M., Li, Z., Liu, D., Li, B., 2020. Experimental study on the characteristics of foam flow in fractures. J. Pet. Sci. Eng. 185, 106663. https://doi.org/10.1016/j.petrol.2019.106663

Chen, S., Liu, H., Yang, J., Zhou, Y., Zhang, J., 2019. Bulk foam stability and rheological behavior of aqueous foams prepared by clay particles and alpha olefin sulfonate. J. Mol. Liq. 291, 111250. https://doi.org/10.1016/j.molliq.2019.111250

Chovet, R., Aloui, F., Keirsbulck, L., 2015. Wall Shear Stress Generated by Aqueous Flowing Foam, in: Volume 1: Symposia. Presented at the ASME/JSME/KSME 2015 Joint Fluids Engineering Conference, American Society of Mechanical Engineers, Seoul, South Korea, p. V001T14A001. https://doi.org/10.1115/AJKFluids2015-14039

Chovet, R., Aloui, F., Keirsbulck, L., 2014. Gas-Liquid Foam Through Straight Ducts and Singularities: CFD Simulations and Experiments, in: Volume 1B, Symposia: Fluid Machinery; Fluid-Structure Interaction and Flow-Induced Noise in Industrial Applications; Flow Applications in Aerospace; Flow Manipulation and Active Control: Theory, Experiments and Implementation; Multiscale Methods for Multiphase Flow; Noninvasive Measurements in Single and Multiphase Flows. Presented at the ASME 2014 4th Joint US-European Fluids Engineering Division Summer Meeting collocated with the ASME 2014 12th International Conference on Nanochannels, Microchannels, and Minichannels, American Society of Mechanical Engineers, Chicago, Illinois, USA, p. V01BT14A003. https://doi.org/10.1115/FEDSM2014-21190

Çoşkun, Ş., Hazaveh, H.A., Uzol, O., Kurç, Ö., 2017. Experimental investigation of wake flow field and wind comfort characteristics of fractal wind fences. J. Wind Eng. Ind. Aerodyn. 168, 32–47. https://doi.org/10.1016/j.jweia.2017.05.001

Cukurel, B., Selcan, C., Stratmann, M., 2015. Convective heat transfer investigation of acoustically excited flow over an isolated rib obstacle. Int. J. Heat Mass Transf. 91, 848–860. https://doi.org/10.1016/j.ijheatmasstransfer.2015.07.043

Dallagi, H., Al Saabi, A., Faille, C., Benezech, T., Augustin, W., Aloui, F., 2019. CFD Simulations of the Rheological Behavior of Aqueous Foam Flow Through a Half-Sudden Expansion, in: Volume 1: Fluid Mechanics. Presented at the ASME-JSME-KSME 2019 8th Joint Fluids Engineering Conference, American Society of Mechanical Engineers, San Francisco, California, USA, p. V001T01A030. https://doi.org/10.1115/AJKFluids2019-4650

Dallagi, H., Gheith, R., Al Saabi, A., Faille, C., Augustin, W., Benezech, T., Aloui, F., 2018. CFD Characterization of a Wet Foam Flow Rheological Behavior, in: Volume 3: Fluid Machinery; Erosion, Slurry, Sedimentation; Experimental, Multiscale, and Numerical Methods for Multiphase Flows; Gas-Liquid, Gas-Solid, and Liquid-Solid Flows; Performance of Multiphase Flow Systems; Micro/Nano-Fluidics. Presented at the ASME 2018 5th Joint US-European Fluids Engineering Division Summer Meeting, American Society of Mechanical Engineers, Montreal, Quebec, Canada, p. V003T20A004. https://doi.org/10.1115/FEDSM2018-83338

Denkov, N.D., Subramanian, V., Gurovich, D., Lips, A., 2005. Wall slip and viscous dissipation in sheared foams: Effect of surface mobility. Colloids Surf. Physicochem. Eng. Asp. 263, 129–145. https://doi.org/10.1016/j.colsurfa.2005.02.038

Deshpande, N.S., Barigou, M., 2001a. Foam fow phenomena in sudden expansions and contractions. Int. J. Multiph. Flow 15.

Deshpande, N.S., Barigou, M., 2001b. The fow of gas-liquid foams through pipe fttings 8.

Dollet, B., Raufaste, C., 2014. Rheology of aqueous foams. Comptes Rendus Phys. 15, 731–747. https://doi.org/10.1016/j.crhy.2014.09.008

Dong, Z., Luo, W., Qian, G., Lu, P., Wang, H., 2010. A wind tunnel simulation of the turbulence fields behind upright porous wind fences. J. Arid Environ. 74, 193–207. https://doi.org/10.1016/j.jaridenv.2009.03.015

Du, D., Li, Y., Chao, K., Wang, C., Wang, D., 2018. Laboratory study of the Non-Newtonian behavior of supercritical CO2 foam flow in a straight tube. J. Pet. Sci. Eng. 164, 390–399. https://doi.org/10.1016/j.petrol.2018.01.069

Endres, L.A.M., Möller, S.V., 2001. On the fluctuating wall pressure field in tube banks. Nucl. Eng. Des. 203, 13–26. https://doi.org/10.1016/S0029-5493(00)00293-4

Fang, F., Ueng, J., Liu, C., Soong, P., 1999. Dynamic response of an elastic fence under wind action. J. Chin. Inst. Eng. 22, 469–478. https://doi.org/10.1080/02533839.1999.9670485

Farahmandfar, R., Asnaashari, M., Taheri, A., Rad, T.K., 2019. Flow behavior, viscoelastic, textural and foaming characterization of whipped cream: Influence of Lallemantia royleana seed, Salvia macrosiphon seed and carrageenan gums. Int. J. Biol. Macromol. 121, 609–615. https://doi.org/10.1016/j.ijbiomac.2018.09.163

Firoze Akhtar, T., Ahmed, R., Elgaddafi, R., Shah, S., Amani, M., 2018. Rheological behavior of aqueous foams at high pressure. J. Pet. Sci. Eng. 162, 214–224. https://doi.org/10.1016/j.petrol.2017.12.050

Ge, Y., Liu, T., 2021. Numerical simulation on bubble wall shape evolution and uniformity in poly(ethylene terephthalate) foaming process. Chem. Eng. Sci. 230, 116213. https://doi.org/10.1016/j.ces.2020.116213

Golemanov, K., Tcholakova, S., Denkov, N.D., Ananthapadmanabhan, K.P., Lips, A., 2008. Breakup of bubbles and drops in steadily sheared foams and concentrated emulsions. Phys. Rev. E 78, 051405. https://doi.org/10.1103/PhysRevE.78.051405

Gorlier, F., Khidas, Y., Pitois, O., 2017. Coupled elasticity in soft solid foams. J. Colloid Interface Sci. 501, 103–111. https://doi.org/10.1016/j.jcis.2017.04.033

Hatsehek, V.E., 1907. Die Viskositiit der Dispersoide. 6.

Höhler, R., Cohen-Addad, S., 2005. Rheology of liquid foam. J. Phys. Condens. Matter 17, R1041–R1069. https://doi.org/10.1088/0953-8984/17/41/R01

Hwang, J.J., Lia, T.Y., Liou, T.-M., 1998. Effect of fence thickness on pressure drop and heat transfer in a perforated-fenced channel. Int. J. Heat Mass Transf. 41, 811–816. https://doi.org/10.1016/S0017-9310(97)00169-5

Jabarkhyl, S., Barigou, M., Badve, M., Zhu, S., 2020. Rheological properties of wet foams generated from viscous pseudoplastic fluids. Innov. Food Sci. Emerg. Technol. 102304. https://doi.org/10.1016/j.ifset.2020.102304

Kabla, A., Debrégeas, G., 2003. Local Stress Relaxation and Shear Banding in a Dry Foam under Shear. Phys. Rev. Lett. 90, 258303. https://doi.org/10.1103/PhysRevLett.90.258303

Khan, S.A., Armstrong, R.C., 1987. Rheology of foams: II. Effects of polydispersity and liquid viscosity for foams having gas fraction approaching unity. J. Non-Newton. Fluid Mech. 25, 61–92. https://doi.org/10.1016/0377-0257(87)85013-9

Kraynik, A.M., Reinelt, D.A., 1996. Linear Elastic Behavior of Dry Soap Foams. J. Colloid Interface Sci. 181, 511–520. https://doi.org/10.1006/jcis.1996.0408

Langevin, D., 2017. Aqueous foams and foam films stabilised by surfactants. Gravity-free studies. Comptes Rendus Mécanique 345, 47–55. https://doi.org/10.1016/j.crme.2016.10.009

Liu, B.T., Muller, S.J., Denn, M.M., 2002. Convergence of a regularization method for creeping flow of a Bingham material about a rigid sphere. J. Non-Newton. Fluid Mech. 102, 179–191. https://doi.org/10.1016/S0377-0257(01)00177-X

Marchand, M., Restagno, F., Rio, E., Boulogne, F., 2020. Roughness-Induced Friction on Liquid Foams. Phys. Rev. Lett. 124, 118003. https://doi.org/10.1103/PhysRevLett.124.118003

Messelmi, F., 2019. On the blocking limit of steady-state flow of Herschel–Bulkley fluid. Math. Mech. Complex Syst. 7, 63–73. https://doi.org/10.2140/memocs.2019.7.63

Moreno, E., Larese, A., Cervera, M., 2016. Modelling of Bingham and Herschel–Bulkley flows with mixed P1/P1 finite elements stabilized with orthogonal subgrid scale. J. Non-Newton. Fluid Mech. 228, 1–16. https://doi.org/10.1016/j.jnnfm.2015.12.005

Ozbayoglu, E.M., Akin, S., 2005. Foam Characterization Using Image Processing Techniques 8.

Panckow, R.P., McHardy, C., Rudolph, A., Muthig, M., Kostova, J., Wegener, M., Rauh, C., 2021. Characterization of fast-growing foams in bottling processes by endoscopic imaging and convolutional neural networks. J. Food Eng. 289, 110151. https://doi.org/10.1016/j.jfoodeng.2020.110151

Parikh, D., Wu, Y., Peterson, C., Jarriel, S., Mooney, M., Tilton, N., 2019. The coupled dynamics of foam generation and pipe flow. Int. J. Heat Fluid Flow 79, 108442. https://doi.org/10.1016/j.ijheatfluidflow.2019.108442

Pierre, J., Leroy, V., 2016. ACOUSTICAL PROPERTIES OF LIQUID FOAMS 2.

Saugey, A., Drenckhan, W., Weaire, D., 2006. Wall slip of bubbles in foams. Phys. Fluids 18, 053101. https://doi.org/10.1063/1.2196912

Schad, T., Preisig, N., Blunk, D., Piening, H., Drenckhan, W., Stubenrauch, C., 2021. Less is more: Unstable foams clean better than stable foams. J. Colloid Interface Sci. 590, 311–320. https://doi.org/10.1016/j.jcis.2021.01.048

Schramm, L.L. (Ed.), 2000. Surfactants: fundamentals and applications in the petroleum industry. Cambridge University Press, Cambridge, U.K. ; New York.

Sherif, T., Ahmed, R., Shah, S., Amani, M., 2015. Rheological behavior of oil-based drilling foams. J. Nat. Gas Sci. Eng. 26, 873–882. https://doi.org/10.1016/j.jngse.2015.07.022

Stevenson, P. (Ed.), 2012. Front Matter, in: Foam Engineering. John Wiley & Sons, Ltd, Chichester, UK, pp. i–xv. https://doi.org/10.1002/9781119954620.fmatter

Sullivan, E., Yee, J., 1984. The viscosity of a foam (air in water emulsion) 6.

Tandiroglu, A., 2006. Effect of flow geometry parameters on transient heat transfer for turbulent flow in a circular tube with baffle inserts. Int. J. Heat Mass Transf. 49, 1559–1567. https://doi.org/10.1016/j.ijheatmasstransfer.2006.01.018

Tcholakova, S., Denkov, N.D., Golemanov, K., Ananthapadmanabhan, K.P., Lips, A., 2008. Theoretical model of viscous friction inside steadily sheared foams and concentrated emulsions. Phys. Rev. E 78. https://doi.org/10.1103/PhysRevE.78.011405

Tisné, P., Aloui, F., Doubliez, L., 2003. Analysis of wall shear stress in wet foam flows using the electrochemical method. Int. J. Multiph. Flow 29, 841–854. https://doi.org/10.1016/S0301-9322(03)00038-7

Tisné, P., Doubliez, L., Aloui, F., 2004. Determination of the slip layer thickness for a wet foam flow. Colloids Surf. Physicochem. Eng. Asp. 246, 21–29. https://doi.org/10.1016/j.colsurfa.2004.07.014

Weaire, D., Fu, T. -L., 1988. The Mechanical Behavior of Foams and Emulsions. J. Rheol. 32, 271–283. https://doi.org/10.1122/1.549972

Wilson, J.D., 1987. On the choice of a windbreak porosity profile. Bound.-Layer Meteorol. 38, 37–49. https://doi.org/10.1007/BF00121553

Zoheidi, L., Chin, H., Rauh, C., Delgado, A., 2017. Flow Characterization of Milk Protein Foam Transport in Horizontal Channels: FLOW CHARACTERIZATION OF MILK PROTEIN FOAM. J. Food Process Eng. 40, e12450. https://doi.org/10.1111/jfpe.12450

CHAPTER 3: FOAM FLOW CLEANING PROCESS

Contents

Objectives, main approaches, and progress

The previous chapter consisted of experimental and numerical studies to identify the rheological behaviour of the foam under different velocity conditions in different duct geometries. This study revealed that changes in geometry could lead to significant changes in the structure of the foam, sometimes resulting in the generation of high parietal shear stress despite rather low values of the mean flow velocities. Thus, it seemed interesting to study how this type of fluid could be an interesting alternative for cleaning in the food industry.

Before the official start of my thesis, I was recruited on a short-term contract in the PIHM team. During this period and during the first months of my thesis, I was involved in a preliminary study on the physical characterization of flowing foams. More concretely, I was in charge of the implementation and development of the pilot rig as well as the installation of the required sensors to control and characterize the different flow conditions of the foam. The results were integrated in Ahmad al-Saabi's dissertation thesis and in a recently published article (Al Saabi et al., 2021).
This study (Publication I) investigated the removal kinetics of *B. amyloliquefaciens* 98/7 and *B. cereus* 98/4 spores from stainless steel surfaces using foam flow. The respective roles of the foam quality (air/water balance), and of the flow rate were analyzed by modeling removal kinetics.
As for the results reported in the literature for the cleaning of adherent spores in CIP, a rapid removal of adherent spores during the first phase (1 min) was followed by a second phase of slow spore removal. The removal of the contamination was dependent on the foam quality (50%, 60%, and 70% of air), the foam velocity (2 to 6 cm/s), and the cleaning time (up to 20 min). The wetter the foam, the better the efficiency during the first detachment phase lasting less than 1 min. However, this trend was not clearly observed during the second phase possibly more effective with a dryer foam. As an example, the detachment after 1 min of wet foam cleaning (qualities of 50%) was 1.8 log reduction, while it was 0.5 log reduction for the case of foam at a quality of 70%. However, after 20 min of cleaning the spore detachment achieved 2, and 1 log reduction for the 50% and 70% foam respectively. When the authors have compared the best option of foam (50% at the lower velocity) to the standard cleaning in place at a shear stress of 5 Pa, the removal of spores using foam was 0.3 and 0.5 log higher than that using CIP. The effect of foam flow cleaning was then tested with hydrophobic spores (*B. cereus* 98/4) showing a strong reduction in the cleaning efficiency considering the same foam flow conditions. Based on studies reported in the literature mainly on flows bubbles in capillaries, it has been hypothesized that the efficiency of foam cleaning could be related to the bubbles' sizes, capillary forces, and the variation of the wall liquid film at the walls.

My work then concerned the investigation of the potential role of the foam properties on the effectiveness to clean surfaces contaminated with *B. subtilis* spores (hydrophilic Bs PY79 or hydrophobic Bs PY79 *spsA*), and by more complex structures, the biofilms (*Escherichia coli* SS2, *B. cereus* 98/4, and *Pseudomonas fluorescens* Pf1). These studies were performed in

straight pipes, with 50% foam at different velocities, (shear stresses ranging from 2.2 to 13.2 Pa).

The first part of the publication II presents a detailed characterization of the foam in different flow conditions and the efficiency of spore cleaning in the different tested conditions. Different methods were first performed such as polarography to measure the local shear stress, conductimetry to measure the liquid film thickness at the walls, and image analysis for the bubble size distributions. These various analyses revealed that the variation of the foam velocity and bubble size (0.18-0.4 mm) resulted in variations in the magnitude and frequency of fluctuations in wall shear stress and in the liquid film thickness. The consequences in terms of cleaning efficiency of adherent hydrophilic and hydrophobic spores were then investigated. The results first showed differences in cleaning efficiency directly related to the hydrophobicity of the spores, with increased resistance to detachment for the hydrophobic one. More interesting, the size of the bubbles and the mean velocity of the foam flow played a major role in the removal of both spores. Indeed, smaller bubbles have higher wall shear stress and remove impurities when it swept the surface. The flow rate can improve this process, but it can also cause an unfavorable growth of the air bubbles, thus weakening the cleaning effect. In other words, the synergy of high shear stress and small bubbles size was needed for enhancement of the cleaning efficiency. This increase in efficiency appeared to be due to a conjunction of different mechanisms such as fluctuating shear stress and capillary forces for the detachment and/or wiping and imbibition in the foam of the detached contaminants. Lastly, for both strains, foam flow cleaning showed a better removal efficiency than conventional cleaning in place considering the same average shear stress conditions

Publication III aimed to test the ability of the foam flow to remove more complex contamination patterns, i.e. biofilms developed on stainless steel surfaces. Coupons were immersed horizontally for 24 h in a nutrient media containing suspensions of three bacteria previously demonstrated at PIHM to be able to grow in biofilms: *E. coli* SS2, *B. cereus* 98/4, and *P. fluorescens* Pf1 and held at 30°C for 24 h. Then they were subjected to the different cleaning procedures described in publication II. Results of the enumeration of the cultivable cells showed that the growth of the biofilm and its resistance to detachment depended strongly on the strains. The largest amount of biofilm was produced by Pf1, then *E. coli* SS2 and Bc 98/4. However, a complete detachment of *E. coli* was observed even under the mildest cleaning conditions (wall shear stress of 2.2 Pa), while the maximum detachment rate was of 2.2 log CFU cm^{-2} for *Pf1* and Bc 98/4 at 13.2 Pa. These results were confirmed by the observation of the biofilm structure using epifluorescence and confocal laser microscopes. After cleaning of Bc 98/4 biofilm with foam, the number of small clusters and isolated cells was highly reduced while the larger clusters seemed to have resisted more to the detachment. Concerning Pf1 biofilms, microscopic observations suggest that the clusters are disaggregated, while only very few cells of *E. coli* were observed on the coupons after the cleaning procedure. Unlike the case of spores' removal in the publication II, the statistical analysis showed that only the shear stress has a significant role in the improvement of the efficiency of the biofilm removal. Increasing the shear stress improved the cleaning efficiency. However, it was interesting to observe that foam is still more effective than the CIP process regardless of the contamination pattern. Then, a life cycle assessment (LCA) of the cleaning procedures, SDS surfactant-containing foam, SDS

surfactant-containing CIP, and NaOH-containing CIP more in line with industrial CIP conditions, using SimaPro software, was performed in order to investigate the environmental impacts. It was found that the CIP steps containing NaOH contribute the most to the environmental impacts, with the highest water and electricity consumption while the foam flow impacts on energy consumption and wastewater emissions showed significant benefits.

Highlights

Compared to conventional cleaning-in-place, foam flow effectively removed *Bacillus subtilis* spores as well as Bc-98/4, Ec-SS2, and Pf1 biofilms from stainless steel surfaces.

The synergy between high wall shear stress and reduced bubble size leads to efficient cleaning of stainless steel surfaces contaminated with bacterial spores.

Biofilms were less affected by the bubbles' size and the consequences in terms of fluctuation of the mechanical action in our experimental conditions but a clear improvement was observed when increasing the mean wall shear stress.

Mechanisms such as capillary imbibition, foam drainage, and fluctuation of wall shear stress induced by bubbles' passage were investigated and were related to the removal mechanisms.

Foam flow cleaning is a suitable technique to reduce water and energy consumption presenting less environmental impacts than CIP processes.

Publication I: Removal of Bacillus spores by flowing foam from stainless steel pipes: effect of the foam quality and velocity

https://doi.org/10.1016/j.jfoodeng.2020.110273

Ahmad Al Saabi [1], Heni Dallagi [1], Fehti Aloui[2], Christine Faille [1], Gaétan Rauwel[3], Laurent Wauquier[1], Laurent Bouvier[1] and Thierry Bénézech [1,*]

[1] Univ. Lille, CNRS, INRAE, ENSCL, UMET, F-59650, Villeneuve d'Ascq, France
[2] Polytechnic University Hauts-de-France, LAMIH CNRS UMR 8201, Campus Mont-Houy, F-59313 Valenciennes Cedex 9, France ; Fethi.Aloui@uphf.fr
[3] Anios-Ecolab, Sainghin-en-Mélantois, France ; gaetan.rauwel@anios.com
*****Correspondence: Thierry.benezech@inrae.fr

Highlights

- Foam flow: a promising new technology for cleaning surfaces contaminated by microorganisms.
- Foam flow allows efficient removal of bacterial contaminants at low velocities inducing high wall shear stress and fluctuations.
- Foam flow allows efficient cleaning with low energy and water consumption.

Abstract

Effective cleaning operations in food industries are considered mandatory to mitigate the risk of remaining unwanted contamination without jeopardizing any further disinfection steps. However, such operations consumed large amount of water, chemicals and energy. In this work an attempt was made to study the cleaning potencies of flowing foams to eliminate *Bacillus* spores from stainless steel surfaces. An original set-up was designed to allow the formation of wet foams to be flown under three flow regime conditions without modifying the foam structure. However, a bubbles' size rearrangement was observed while increasing the velocity affecting the cleaning efficiency visible with the driest foams. The best option was observed with foam at 50% air/water and low velocities to remove 2 log of the initial contamination of *B. amyloliquefaciens* spores being comparable to similar CIP conditions. Removal kinetics were modelled with a simple exponential two-phase kinetics showing in the most favorable cases very high constant rates during the first phase. Hence, comparing with the literature, it was possible to highlight roles on such efficient cleaning to the local high wall shear stress fluctuations and to the presence of capillary forces (low velocities, favorable bubbles size repartition and for the hydrophilicity of bacteria spores).

Keywords:

Flowing foam; wall shear stress; Cleaning; *Bacillus* spores; hygiene

I. Introduction

In agro-food industrial environments, surfaces have been reported to be contaminated by a range of microorganisms, including pathogenic and spoilage bacteria (Srey et al., 2013). Once introduced, if environmental conditions are suitable, many bacteria are able to persist on the contaminated surfaces or even to form biofilms. Indeed, despite cleaning and disinfection procedures, some bacteria are still commonly found on the surfaces of food processing lines, mostly in the form of adherent spores, e.g. *Bacillus* spores in closed equipment (Peng et al., 2002) or in the form of biofilms, e.g. *Pseudomonas spp* (Dogan and Boor, 2003).

Cleaning in place (CIP) leading to residue removal from inner surfaces of processing lines without disassembling, has been a crucial factor in guaranteeing the safety and quality of food. If not done properly, consequences can be devastating, especially in the case of pathogen surface contamination (Pietrysiak et al., 2019; Ribeiro et al., 2019). In order to clean rapidly, CIP aims to combine the advantages of the high temperature, detergent and the mechanical action generated by the turbulent flow (or the impact of the spray) (Moerman et al., 2014). The mechanical effect is created by the flow rate and it is generally admitted that high flow rates result in high removal rates because of the high shear forces on the deposit layer. However some works have detailed the role of hydrodynamics and in particular of the mean wall shear stress and the major role played by its fluctuations (Blel et al., 2013, 2010). This was very recently judged to be mandatory for any CIP improvement (Li et al., 2019).

The addition of foaming surfactants or even gas-stabilized foam means the cleaning solution can be applied as a foam, which can increase the retention time, e.g. on vertical surfaces. Foam is widely used in static conditions throughout the food industry for the cleaning of large open surfaces (floor, conveyors, workshops and equipment). To clean open surfaces, foam requires specific qualities, namely density, foamability, stability and void fraction-based quality. However, foam cleaning agents could also be used for cleaning some closed equipment such as filtration modules (Gahleitner et al., 2013). Despite its widespread use, very little work has been carried out on the elimination of surface deposits using flowing foam, essentially gas-liquid two-phase flows in capillaries (Kondjoyan et al., 2009) and to our knowledge none have dealt with the elimination of microorganisms.

Almost nothing is known about the potential of foam flow to conduct cleaning operations using much less energy (very low velocity) and much less water. Aqueous foams are non-Newtonian complex fluids consisting of concentrated dispersions of gas bubbles in a soapy liquid. Depending on the amount of water they contain, they can be either wet or dry. The air fraction defines the so-called foam β quality (Tisné et al., 2004). Foams have original mechanical properties which rely on their low density and high surface area combined with their ability to elastically respond to low stresses and to flow like a viscous liquid with large distortions.

Foams admit an unexpected and nonlinear rheological behavior (shear thinning and yielding), where the properties of the liquid and gas, that compose it, have an influence on it. Their rheological behavior can be compared with some non-Newtonian models such as, power law, Bingham, and Herschel–Bulkley. Recently it was demonstrated that the foam rheological behavior can be better described by Herschel-Bulkley model (Dallagi et al., 2019, 2018).

Among the consequences of foam flow, the mechanical action exerted on the contact-surface depends on the velocity, foam composition (air/liquid) and the ability of the system (foam,

geometry and surface properties of the equipment to be cleaned) to maintain a thin liquid film between the solid surface (wall) and the foam flow.
Wall shear stress, especially due to this thin liquid film located between the wall and the foam flow, plays an important role in the characterization of the rheological properties of this foam, depending mainly on the bubble size and particularly on the volume fraction of the liquid (Chovet, 2015; Chovet et al., 2014). These properties can be used to understand the microorganism detachment phenomena, such as spores from solid surfaces. Therefore, foam flows would constitute a true novelty in surface hygiene, as low water load and high mechanical actions under moderate temperatures would permit highly cleaning, which can easily be combined with disinfection.
This study investigates the removal kinetics of *B. amyloliquefaciens* 98/7 and *B. cereus* 98/4 spores using foam flow. The respective roles of the foam quality (importance of air/water balance), and of the flow rate were analyzed by means removal kinetics modeling. Results were then compared to spore removal under mild cleaning in place conditions. We then investigated some foam properties (the flow regime and the mean foam flow velocity, bubble-size distribution, bubble-passage frequency, foam quality and mean wall shear stress).

II. Materials and Methods

II.1 Bacterial strains and solid surfaces

In this study, two bacterial strains isolated from dairy processing lines forming spores of very different surface energies one hydrophobic and the second hydrophilic (Faille et al., 2019, 2016, 2010) were used: *B. cereus* CUETM 98/4 (BC-98/4) and *B. amyloliquefaciens* CUETM 98/7 (formerly known as *B. subtilis* 98/7). *Bacillus* spores were produced as previously described (Faille et al., 2019). Before any experiment, two further washes were performed and spores were subjected to a 2.5-min ultra-sonication step in an ultrasonic cleaner (Bransonic 2510E-MT, 42 kHz, 100 W, Branson Ultrasonics Corpo-ration, USA) to limit the presence of aggregates. In order to evaluate the hydrophobic character of spores, Microbial Affinity to Hydrocarbons tests (MATH) were performed as previously described (Faille et al., 2019b).
The material, used in the form of rectangular coupons (45 mm x 15 mm), was AISI 316 stainless steel with pickled (2B) finish (kindly provided by APERAM, Isbergues, France). Prior to each experiment, coupons were cleaned and disinfected using a standard protocol used at UMET. Coupons was first cleaned using pure alkaline detergent (RBS T105, Traitements Chimiques des Surfaces, France). They were then subjected to a 10 min immersion in a 5% RBS T105 at 60 °C, followed by thorough rinsing with tap water, then with softened (reverse osmosis) water for 5 min each. 24 h before the experiments, stainless steel coupons were treated in a dry heat oven at 180°C for 1 h.

II.2 Surface soiling and cleaning

The soiling suspensions were prepared with ultra-purified sterilized water and a concentration of spore suspension of around 10^6 CFU/mL. The coupons were vertically immersed in a Beaker containing 250 ml of the soiling solution, then kept at room temperature for 4 hrs.
Coupons were then inserted into a 23 10^{-2} m long stainless steel test duct with a 1.5 x 1 10^{-2} m rectangular cross-section. The geometry of the rectangular test ducts used for the experiments

was previously described (Cunault et al., 2015). The three central coupons out of the five installed in the ducts were soiled and further analyzed after cleaning.

The production foam prototype was built according to previous work (Chovet and Aloui, 2016; Tisné et al., 2003a). The experimental set-up, with an open foam flow circuit, was designed to allow the foam flow to develop within horizontally-placed square ducts, with the coupons to be cleaned at the top. The test ducts were situated after a transparent Plexiglas rectangular duct, of identical inner size, to visualize the foam flow. To allow steady state flow conditions, the test ducts were placed at intervals exceeding 80 times the hydraulic diameter of the vein inlet (i.e. 1.5 m).

The prototype is presented in Figure 51. The rig includes a mother tank (capacity: 100 L) filled with Sodium Dodecyl Sulfate (Sigma-Aldrich ReagentPlus®, over 98.5% purity) dissolved in osmosed water (0.15% ww). The SDS solution is pumped into the feeding tank (50 L) located at a height of 3 m using a positive displacement pump (VARMECA 21TL055, Leroy-Somer). This set-up creates a constant flow rate in the foam generators due to gravity.

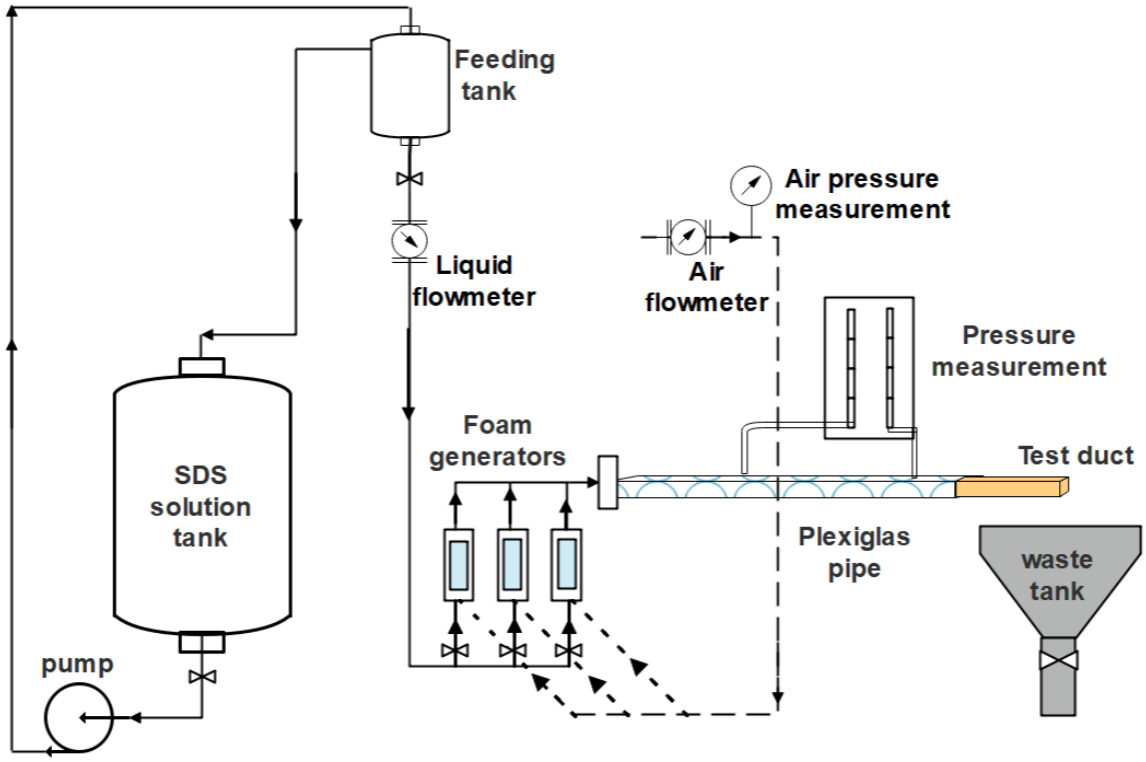

Figure 51. Scheme of foam cleaning in place prototype

Three foam generators were designed as previously described (Tisné et al., 2003a). The foam is generated by injection of pressurized air through a porous medium (DURAN®, pore sizes ranging from 1 to 1.6 µm, Dislab, Lens, France), inside cylindrical containers filled with the SDS solution. The foam quality describing the air/water content of the foam was calculated as follows (Equation 1) according to (Chovet and Aloui, 2016) where Q_g and Q_l are respectively the gas and liquid flow rates:

$$\beta = \frac{Qg}{Qg+Ql} \quad (1)$$

The three independent parallel generators allowed us to increase the bulk velocity without affecting the foam structure. Three foam qualities were chosen for the cleaning experiments 50%, 60% and 70%. The mean velocity was calculated taking into account the global flow rate (Q_l+Q_g) divided by the cross-section area S of the test duct. The Reynolds number was calculated according to Equations (2) and (3), taking into account the density of both gas and liquid phases. Foam viscosity was calculated using the relationship based on a heuristic model of concentrated emulsions (Equation 4).

$$Re = \frac{\rho_f . \bar{v} . d_h}{\mu_f} \quad (2)$$

$$\rho_f = (1 - \beta) . \rho_l + \beta . \rho_g \quad (3)$$

$$\mu_f = \frac{\mu_l}{1 - {\mu_l}^{1/3}} \quad (4)$$

Three liquid/air flowmeters enabled the adjustment of the flow rate from 0 to 35 l h^{-1} and 0 to 70 l h^{-1} respectively.

Flowing from the generators, the foam passes through a transparent Plexiglas pipe of 1.1 m length. The transparent pipe enables the visualization of the foam texture, bubble size and foam velocity measurement. Two pressure outlets allow the connection of 2 manifold tubes placed over a scaled plate that measures on a length L of 1m the pressure drop ΔP to calculate the mean wall shear stress $\bar{\tau}$ (d_h ΔP / 4 L). For each cleaning experiment, only one test duct containing the soiled coupons was clamped to the transparent pipe.

The different test ducts were thus cleaned with three foam qualities at 20°C, at foam mean velocities ranging from 2.1 to 6.7 m s-1, for 15 and 35 s, 1, 3, 5, 10 and 20 min and other experiments were carried out to mimic CIP conditions. The test ducts were connected to a CIP pilot rig (Jullien et al., 2008) and a simple CIP procedure was then carried out under the same conditions as those used for the foam tests, i.e. SDS concentration, temperature, cleaning times. The flow rate was selected to generate a mean wall shear stress of 5 Pa, falling within the range of the mean wall shear stress conditions induced by the flowing foam as described in the Results Section. After the cleaning process, the coupons were removed from the test tubes and rinsed by dipping in a beaker containing one liter of sterile ultrapure water. The residual spore contamination was then analyzed as follows.

To determine the number of adhering spores before (N0) or after the (Nresid) cleaning procedure, coupons were subjected to an ultrasonication step in 10 ml of 2% Tween 80 (v/v) in peptone water without indole 0.015 g/L (Biokar), diluted to 1L with ultra-purified sterilized water (5 min, Ultrasonic bath, Branson 2510, 40 Hz). This treatment has been previously shown, in our laboratory, to remove more than 99% of the adherent spores (Tauveron et al., 2006). The detached spores were enumerated on nutrient agar composed of 1.3% w/v nutrient broth (Biorad, France) and 1.5% w/v bacteriological agar type E (Biokar Diagnostics, France) after 48 h at 30°C. The percentage of residual spores after cleaning was then calculated [(Nresid/N0) * 100].

For microstructure examination, some rinsed coupons were first dried at 20 °C for at least 1 hour to prevent spore detachment during the staining procedure. The coupons were then stained with orange acridine (0.01%) for 15 min at 20°C, gently rinsed with softened water and allowed to dry before observation. Finally, the surface contamination organization was observed using an epifluorescence microscope (Zeiss Axioskop 2 Plus, Oberkochen, Germany) at magnification 1000X.

II.3 Foam flow visualisation

The method is based on the observation of the displacement of moving bubbles at the walls of the pipe, for a given interval. Measurements were carried out at the last part of the pipe where the foam flow could be considered as established. The velocity of the bubbles was measured by marking the Plexiglas pipe wall by two thin marks spaced at a known distance. For both the lateral and the top walls of the pipe, three locations were chosen: two at 1 mm from the edges and one in the middle of the observed wall. The time taken for a bubble to pass between the two marks was recorded to calculate the its velocity. The smallest easily-visible bubbles (0.3 mm) were considered for tracking and 10 successive measurements were carried out. Mean values were then calculated. These could be considered as representative of the local velocity at the wall whatever the bubble size (Tisné et al., 2003). This method gives an approximation of the bubbles' speed. A selection of photos of the foam flow (camera Panasonic LUMIX DMC-FZ62, High speed video [HS], at a speed of up to 200 frames / second) were analyzed using Piximètre 5.1 R1540 image analysis software. The clearest two images in terms for each flow condition induced by the generators and for the three foam qualities were filtered to better observe the borders of the bubbles. It was thus possible to evaluate the bubble size distribution in all the cases studied.
An optical probe (© RBI instrumentation, Meylan, France) based on the discrete variation of the refractive indicator optics between the two-phase flow (air/liquid) was used to evaluate the void fraction and the air bubbles' passage frequency at the wall top (at 0.5 mm from the top). Data were analysed using the ISO software provided by RBI.

II.4 Kinetics modelling

A two-phase kinetics model was used to fit the data as previously proposed for the detachment kinetics of biofilms during CIP (Benezech and Faille, 2018). The fitting was performed using GInaFIT (Geeraerd et al., 2005) using a biphasic model composed of two first order kinetics (Dallagi et al., 2018b, 2019).

II.5 Statistical analysis

At least 3 repetitions were carried out for the quantitative analysis of the residual contamination after foam cleaning. Data were analysed by general linear model procedures using SAS V8.0 software (SAS Institute, Gary, NC, USA). Variance analysis was performed to determine how the bacteria removal described by the kinetic parameters (residual contamination at different cleaning times and model parameters were affected by the cleaning conditions tested.

III. Results

III.1 Foam flow organization and mechanical action induced by the foam

Three foam qualities were prepared with a concentration of SDS of 0.15 % w/w in order to exceed the Critical Micelle Concentration (CMC). The SDS as an anionic surfactant is a good representative of the "sulphate" surfactants largely used in formulated detergents. The SDS is known to be highly soluble and easy to rinse and is largely used in academic studies (Mai et al., 2016). Anionic surfactants are recognized for their cleaning, foaming and emulsifying properties. The foam generated was found to be very stable (no changes were observed in terms of foam drainage and bubble size over one hour – data not shown).

Table 5. Flow conditions for the foam flow and the CIP

Liquid flow rate ($l.h^{-1}$)	Air flow rate ($l.h^{-1}$)	Foam quality β	Mean velocity ($cm.s^{-1}$)	$\bar{\tau}w$ (Pa)	Re
6	6		2.0	2.2	43
9	9	50%	4.0	4.2	87
13.5	13.5		6.1	5.9	130
4.2	6.3		2.4	2.2	51
8.4	12.6	60%	4.9	4.4	101
12.6	18.9		7.3	6.0	151
4.2	9.8		2.9	2.4	67
8.4	19.6	70%	5.7	5.1	135
12.6	29.4		8.6	6.4	202
650	-	0 (no foam)	120	5.1	14500

Top wall

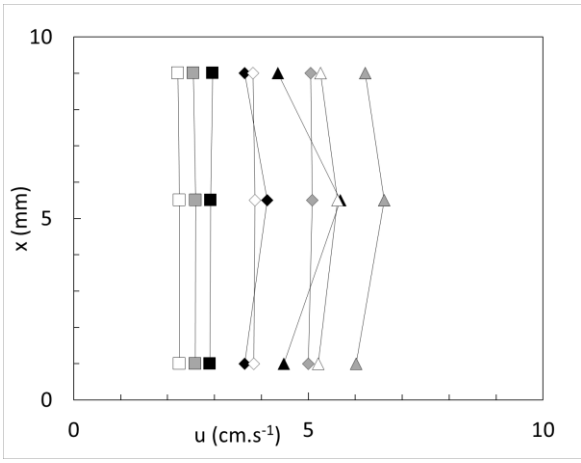

Lateral wall

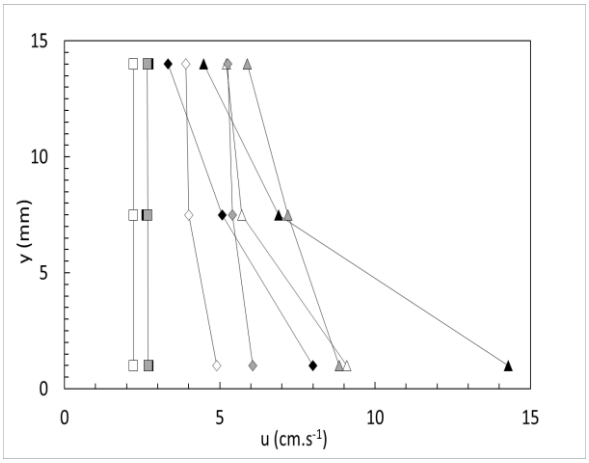

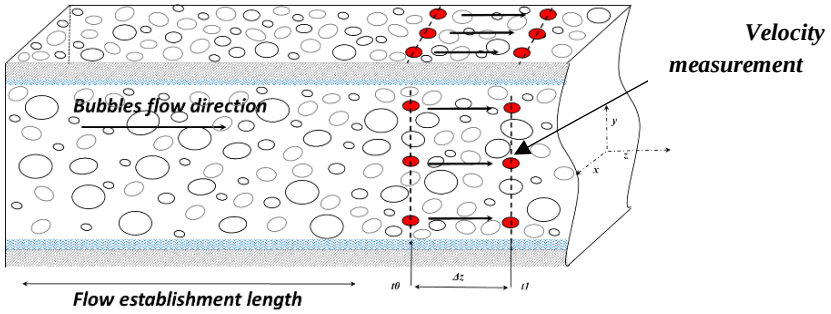

Figure 52. Bubbles velocities measured at the top and lateral walls of the transparent duct measured at three positions (in red) in relation with the number of generators (one: square, two: diamond, three: triangle) and with the foam qualities (white: 50%, grey: 60% and black: 70%).

We also checked that the use of one, two or three generators in parallel failed to modify the foam structure significantly, despite the differences in the foam velocity. Thanks to the transparent Plexiglas tube, placed upstream of the test duct with the soiled coupons subjected to the cleaning procedure, it was possible to visualise the foam flow through the rig and to take images or videos. Observations were made from one side and from through the top.

The bubble velocity was first measured as shown in Figure 52 in three locations on each selected duct wall (top and lateral). As shown in Figure 52, depending on the experimental conditions (number of generators, foam quality), the velocity profiles were quite different. As the mean velocity increased, a difference in the flow velocity of the bubbles appeared depending on their position in the duct. Indeed, when a single generator was used, bubble velocity was generally constant and the foam flow therefore behaved like a plug flow. The increase induced by two generators showed no change at the top of the duct, except for the foam quality of 70%. Conversely, the bubble velocities increased from the top to the bottom of the duct as shown in Figure 52 B. This is due especially to the underlying liquid film, which pulls the foam in contact because its velocity increases. At the top wall, bubble velocities were highest at the centre of the side, and thus decreased as the flow approached the duct edges. All conditions used are summarized in Table 5.

The foams' flow conditions varied from 2.0 to 8.6 cm s^{-1}, whilst for the CIP conditions the velocity was significantly higher at 120 cm s^{-1} and the flow regime was turbulent (Re > 14500). The mean wall shear stress (WSS) condition for the CIP was chosen to fall within those induced by the foam, i.e. ranging from 2.2 to 6.4 Pa, allowing comparison between the CIP mechanical action and the use of foam flow. One can note that the plug flow regime with constant foam velocity profile corresponding to 1 generator flow (all foam qualities) related to a Reynolds number maximum of 67. At over 100, the foam flow velocity profile at the top wall could not be considered as constant (Figure 52A).

In Figure 53, an example of photos of the foam flow arrangement at the top surface of the transparent duct is shown.

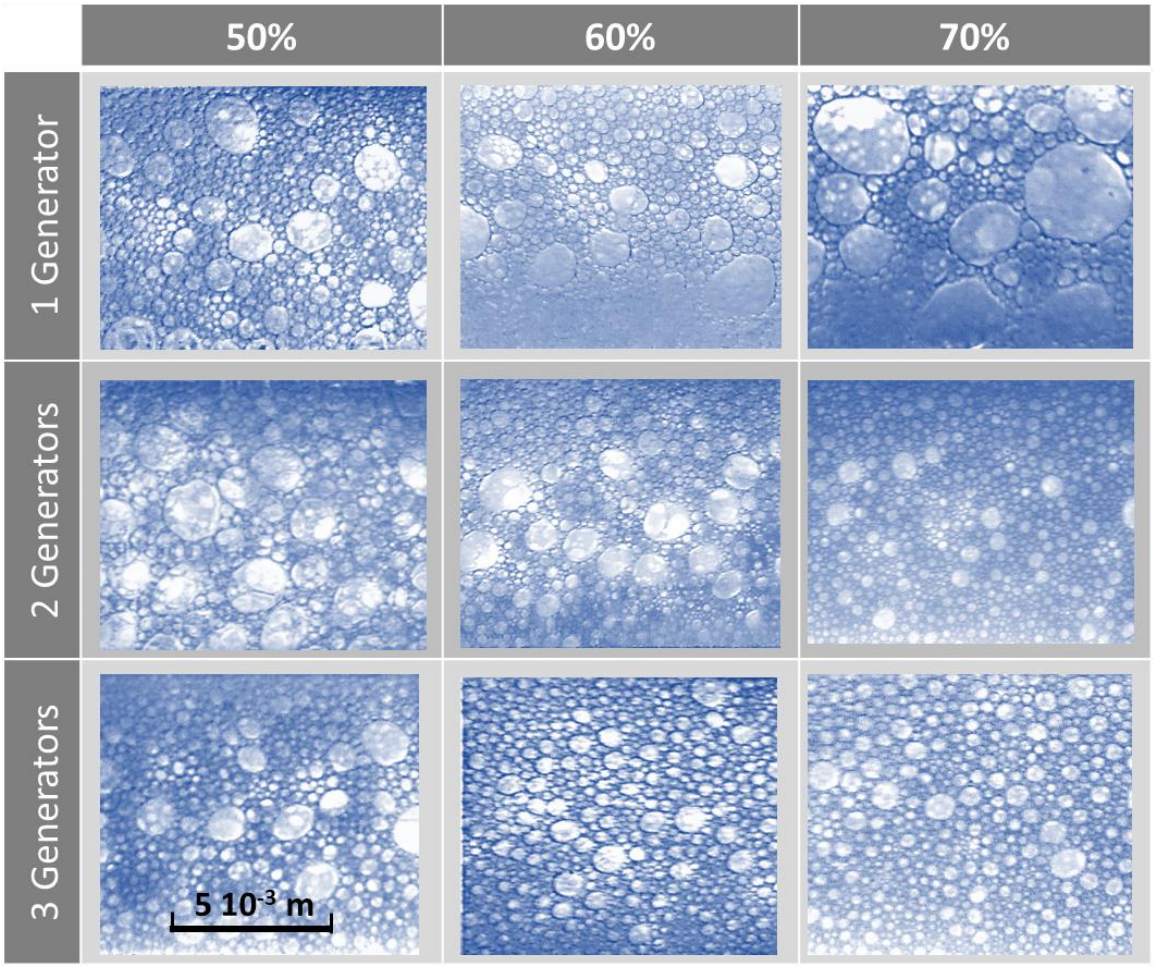

Figure 53. Foam visualization at the top wall of the Plexiglas duct just before the test ducts for the three foam qualities and the foam flow conditions**.**

In order to identify the distribution of bubble size within the foam under different conditions, photos were taken at the top wall of the Plexiglas duct (Figure 53). The size distribution appeared to be affected by both velocity and foam quality. For example, the greater the velocity at the top wall, the smaller the bubbles.

The bubble sizes were then measured and the data are given in Figure 45. When only one generator was used, the bubble sizes were more heterogeneous than those obtained with two or three generators, whatever the foam quality. Moreover, a significant number of big bubbles (between 1 mm and 10 mm in size) was also observed. The increase in the velocity was thus more conducive to smaller bubbles. In accordance with Figure 53, some larger bubbles (size > 1mm) could still be measured with 2 and 3 generators for the foam flow where $\beta = 50\%$ and with 2 generators for the foam flow where $\beta = 60\%$.

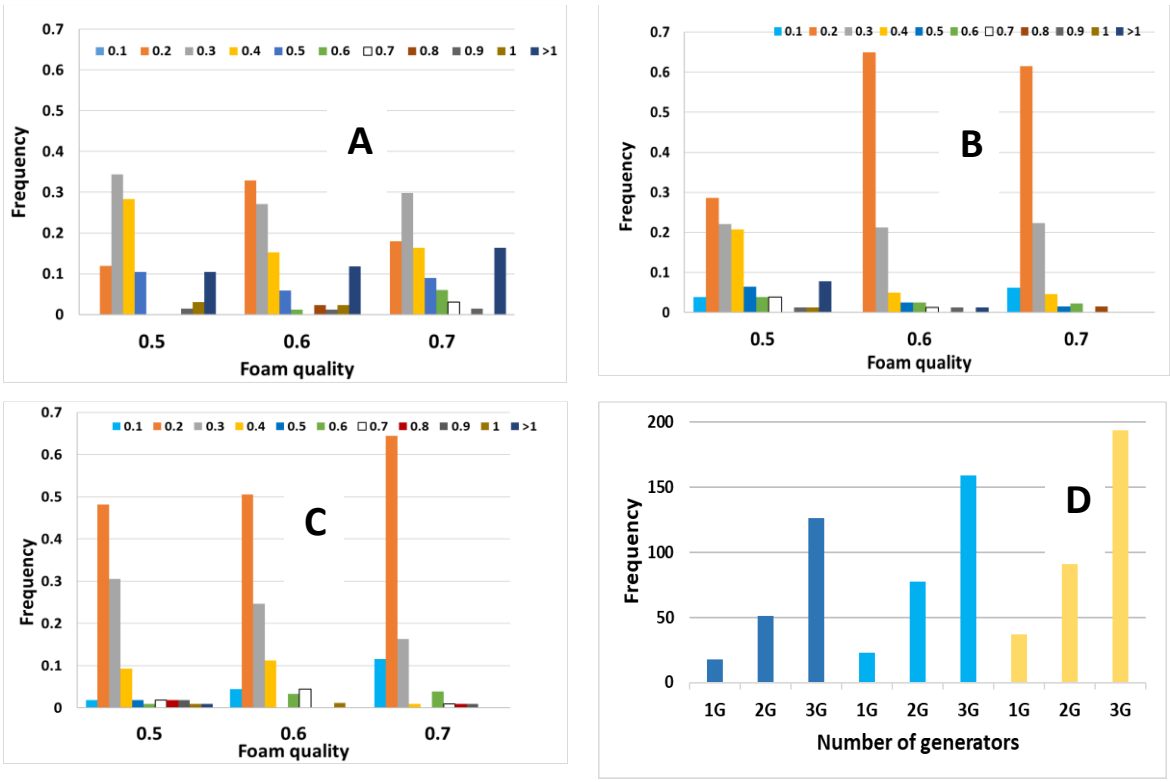

Figure 54. Bubble size (mm) repartition; A: one generator, B: 2 generators & C: 3 generators and frequency of passage of bubbles in front of the optical probe (D) at the top wall for the three foam qualities: 0.5 (dark blue), 0.6 (light blue), 0.7 (yellow).

The mean frequencies of the bubbles' passage observed by the optical probe (Figure 54, D) near the top wall increased with the number of generators. However, this increase could not be explained solely by the mean velocity, but is apparently also linked to the reduction in the bubble sizes e.g. for the foam 50%, the doubling or the tripling of the mean velocity induced an increase in the frequency by factors of respectively 2.9 and 7.1.

III.2 Spores' detachment under the different flowing conditions

Spore adhesion to the stainless-steel coupons (Ra: 0.08 µm) was 5.6 ± 0.4 log CFU.cm^{-2} for *B. amyloliquefaciens* and 5.4 ± 0.3 log CFU.cm^{-2} for *B. cereus*. Before any detachment experiments, we checked that spore incubation in SDS 0.15% did not result in any significant viability loss (data not shown). The detachment of *B. amyloliquefaciens* spores was investigated under all the flow conditions with each of the three foam qualities. In Figure 55, only the mean values of the remaining contamination at the different kinetic times were presented. In all cases, the detachment curves clearly showed two distinct phases.

Both phases appeared to be exponential and therefore were quite accurately described by the biphasic model, with R2 ranging from 0.62 to 0.98 and mostly over 0.80.

During the first detachment phase (less than 1 min), the spore detachment was very fast, with a 0.6 to 1.8 log decrease in the population of surface-attached spores. Large differences were observed according to the number of generators used with the 50%, foam quality whereas the number of generators had little effect on the detachment of the other two foams (60% and 70%). Taking into account all the conditions used, it appears that spore detachment during this first

phase was much more efficient with the 50% foam quality when 1 or 2 generators were used. After this first step, the detachment continued for at least 20 minutes, i.e. the duration of the cleaning procedure, though more slowly. Here again, the spore detachment rate seemed dependent on the experimental conditions (number of generators, foam quality). The cleaning kinetics with foam were compared to a CIP using the SDS 0.15% and a mean wall shear stress of 5 Pa (Figure 55D). The first detachment step was close to the most efficient one with foam, i.e. allowing the detachment of over 1.5 log CFU, close to the one observed when 1 or 2 generators were used with the □ = 50% foam. Conversely, no further detachment occurred after this first phase, indicating that a plateau value had been reached.

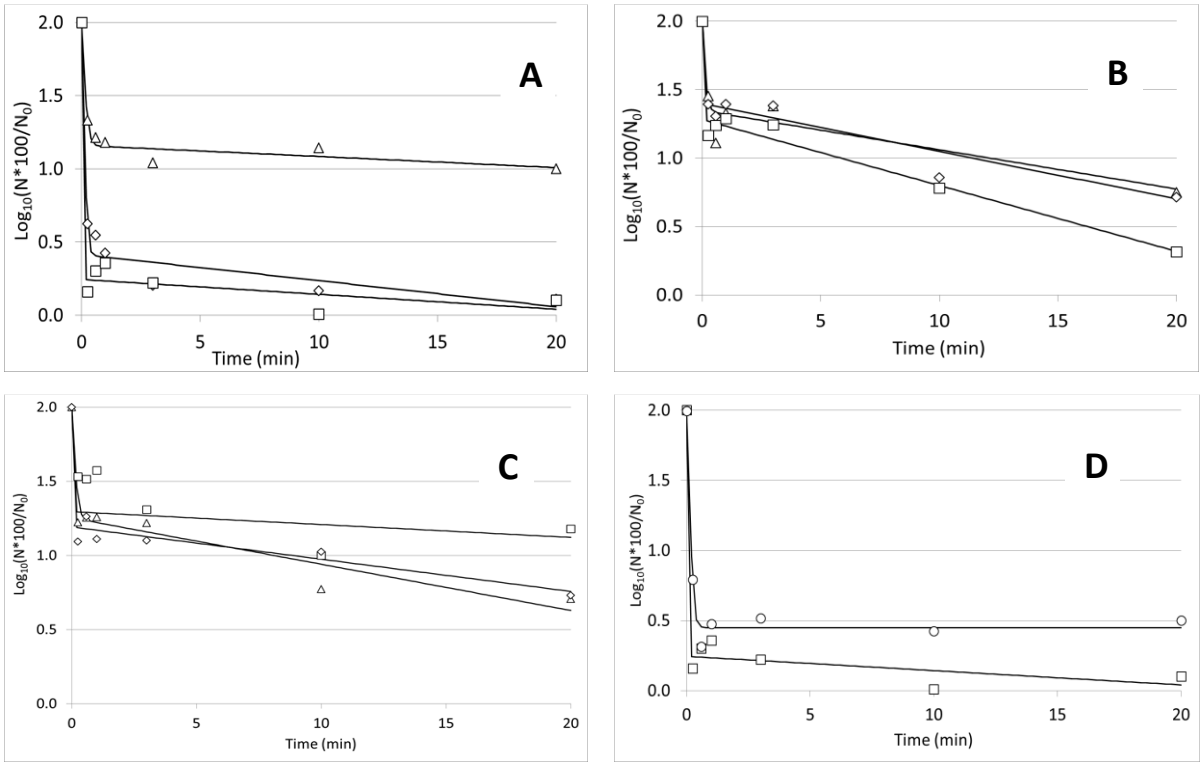

Figure 55. Removal kinetics of *B. amyloliquefaciens 98/7* spores under different flowing conditions: 1 generator (square), 2 generators (diamond), 3 generators (triangle) for the foam qualities of 50% (A), 60% (B) and 70% (C); Removal kinetics with the foam 50%, one generator compared to CIP (D).

The decimal reduction at 20 min, i.e. the end of the second phase of the cleaning kinetics, was statistically analysed to compare the role of the flow rates conditions induced by the generators, the different foam qualities and by the CIP conditions. At 20 min, cleaning efficiencies observed were comparable between CIP and the flow rates induced by one and two generators (letter A, Tukey's grouping) as shown in Figure 56. In addition, the cleaning efficiency induced by the 50% and 60% foam qualities appeared significantly better than the 70% foam (different letters according to the Tukey's grouping).

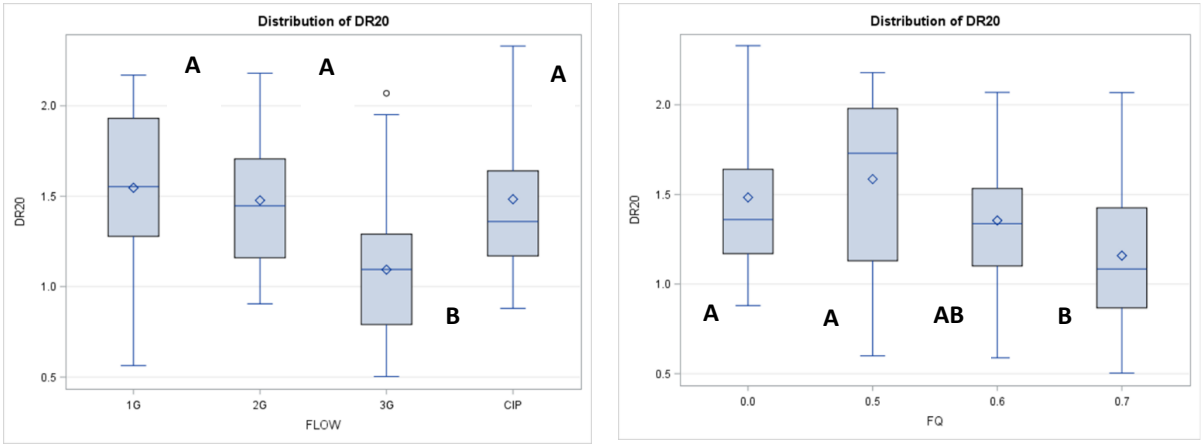

Figure 56. Decimal reduction of the *B. amyloliquefaciens* spores induced by different flowing conditions at 20 min cleaning time: comparison of the combined effects of the flow conditions and the foam quality including CIP conditions ("foam quality" being equal to zero in that case).

Focusing on the cleaning conditions with foam, the variance analysis confirmed that the variability observed on the three kinetics parameters (f, kmax1, and kmax2), was significantly related to the flow rate induced by the foam generators. However, some discrepancies should be noted (see Figure 57). Considering the potential combined effects of the foam quality and the flow rate (one, two and three generators) on the parameter f (f is the poorly adherent fraction of the population and/or less resistant to detachment), the variance analysis gave a p value of 0.027. The Tukey's grouping as shown in Figure 57, highlighted a slight effect of the flow rate: f being higher under the lowest flow rate conditions and higher with the foam where β=50%, compared to the foam with β=70% (no common letters, Tukey's grouping). More visible was the role of the flow rate on the constant rate Kmax1 (p=0.001), the lowest flow rate clearly being the most efficient condition for spore removal under this first phase: Kmax1 was multiplied by a factor up to 300. Foam quality appeared to play a role as the Tukey's grouping highlighted that Kmax1 values for the β=70% foam were very low compared to 50% and 60% foams. While taking into account data obtained with the CIP conditions, as also shown in Figure 57, flow conditions were still highly significant (P=0.0012) and three classes were defined by Tukey's grouping (A, AB and B). In this case, CIP conditions gave an intermediate mean value of 55 for Kmax1 compared to 87 with one generator and 6.7 or 1.3 respectively for two or three generators.

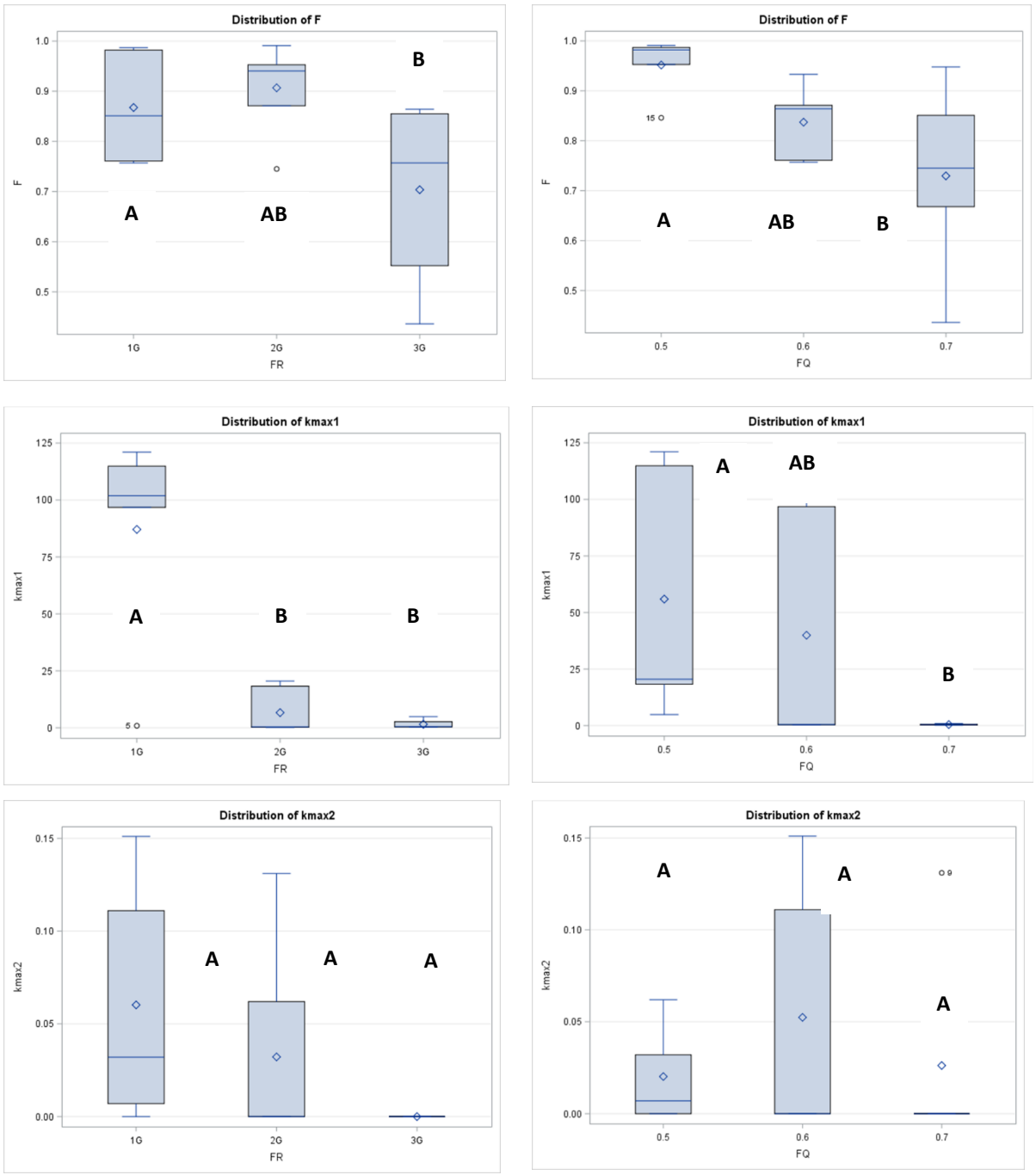

Figure 57. Variations induced by the combination of the foam quality (including CIP conditions for the two last graphs) and the flow rate induced by one, two or three generators on the kinetics parameters f, Kmax1 and Kmax2. According to the Tukey's grouping letters were indicated with potentially three classes A, AB and B.

The effect of cleaning using foam flow, was tested with another *Bacillus* species. In Figure 58 the two kinetics appeared very similar with a quick detachment in less than one minutes followed by a second phase, with about 0.5 log removal in both cases. Such a cleaning condition was chosen as the most efficient, according to the results described above. The main difference lied in the Kmax1 values, *B. cereus* spores being more difficult to remove than *B. amyloliquefaciens* ones at the initial phase of the kinetics. Conversely, the removal during the

second phase of the kinetics appeared very similar and this was confirmed by close values of the detachment rate Kmax2 for the two bacteria.

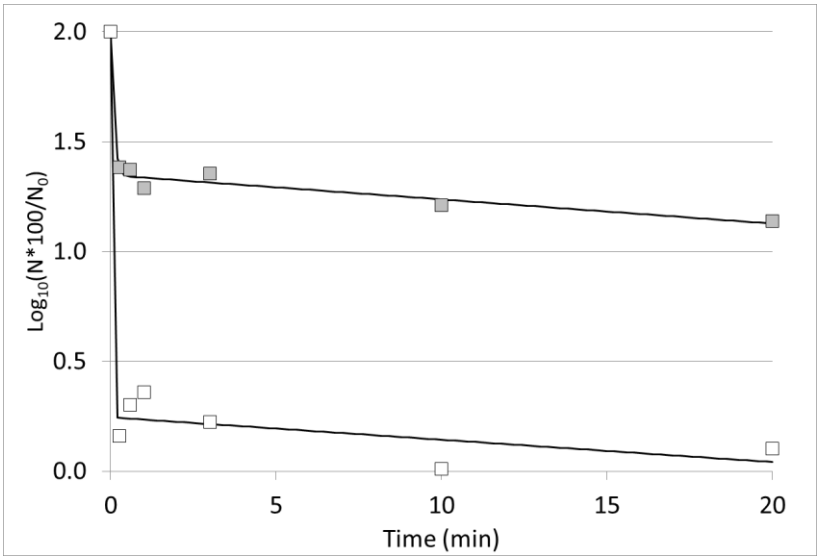

Figure 58. Comparison between the removal of *Bacillus amyloliquefaciens* and *Bacillus cereus* spores: cleaning with foam of β=50% and one generator.

The microscopic observations showed the spores distribution on the coupons before and at different cleaning times. Only times 0 (fouling), 15 s, 3 minutes and 20 minutes were considered for comparison between foam cleanings (0.5 and 1 generator), one of the most effective foam cleanings observed and CIP. Microscopic observation showed that *B. amyloliquefaciens 98/7* spores formed some clusters as shown in Figure 58, but these spores were mainly evenly distributed on the steel surface after the 4 hours soiling. Clusters were limited by the sonication of the spore suspensions prior to the soiling step and these were rapidly removed after only 15 s by both CIP and foam flow. Yet, according to Figure 59, removal was visibly greater with foam flow than CIP. The difference observed here (almost one log) is less than the one given by the removal kinetics (Figure 55B; 0.5 log difference), which considers viable and cultivable bacteria. However, the variability (up to 0.5 log) between trials could easily explain this discrepancy.

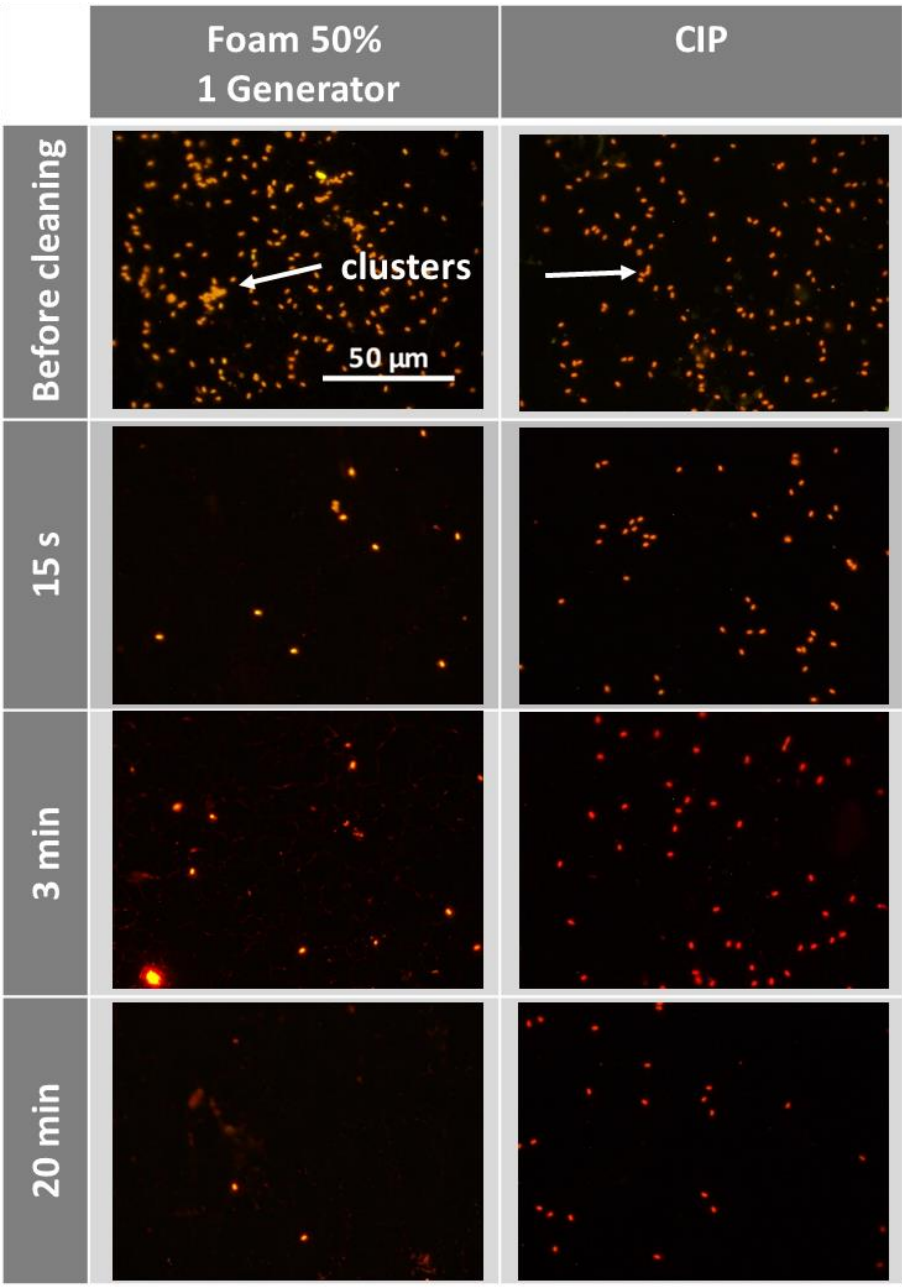

Figure 59. Observations of the stainless-steel coupons before cleaning and after 15 s, 3 min and 20 min with a foam flow where β=50% and using one generator and with CIP.

IV. Discussion

Foam is a two-phase gas-liquid fluid, in which gas is the dispersed phase and liquid is the continuous phase, where the volume of gas greater than that of liquid. In this work, only wet foam was used, meaning that foam is formed only of spherical bubbles, as observed at the top wall as previously described (Chovet and Aloui, 2016; Tisné et al., 2004) . Each mean velocity induced by one, two or three generators engendered a different flow regime. Indeed, for the lowest mean velocity, the axial component was uniform over the entire cross-section, thereby corresponding to the mono-dimensional flow regime or plug foam flow regime. For the mean velocity of 4 cm s^{-1}, the flow appeared partially sheared with a sliding at the walls, the axial velocity component no longer being uniform, depending on the ordinate and corresponding to

the two-dimensional (2D) foam flow regime. One can notice that the top wall velocity remained constant (foam at β=50% and β=60%) or was only slightly modified at the center of the top wall (foam at β=70%) under our experimental conditions. For the highest mean velocities, the foam flow was completely sheared with a sliding at the walls and could therefore be considered as three-dimensional (3D), with the underlying liquid film at the bottom of the duct flowing at a higher velocity, pulling the foam flow above and therefore inducing a significant increase in the bubbles' velocity directly in contact with this thick liquid film. This phenomenon is accompanied by a rearrangement of bubble sizes, with the largest bubbles being mostly moved up the pipe. Such a phenomenon was already described by (Tisné et al., 2003). In this work, the cleaning of surfaces by the foam was evaluated at the top wall as a first evaluation of the role of flowing foam in the removal of surface contaminations (bacteria spores). In parallel, even if the experimental conditions were supposed to maintain the foam structure with the increase in the mean velocity, it appeared that the bubble size repartition at the top wall varied with the foam quality tested, meaning that bubble rearrangement had occurred: the increase in the mean velocity induced a reduction in the bubble size at the top wall.

Furthermore, it has been demonstrated that the variation at the top wall of the the thin liquid film between the bubbles and the wall is directly affected by the bubbles passage and depends on their size (Tisné et al., 2004), which could have an effect on the effectiveness of adherent bacteria removal. The thickness fluctuations thus induced under their experimental 1D flow conditions varied between 5 µm and 35 µm with a foam quality of 70%. Under 1D flow conditions for a foam quality of 55%, conditions close to our experimental conditions Chovet and Aloui, 2016 , observed fluctuations at the top of the channel liquid film varying from 2 µm to 40 µm. In addition, this amplitude decreased with the increase in the foam quality, probably due to a change in the bubble size arrangement at the wall.

Microscopic scale studies (Tisné et al., 2004), reveal that it is possible to rely on studies of bubble flows inside circular capillaries, which will help in understanding the underlying phenomena (Bretherton, 1961). Assuming that there was no tangential shear stress at the fluid–fluid interface, he predicted that the film thickness was dependent on four parameters: the tube radius r, the liquid viscosity μ_L, the surface tension γ and the bubbles' velocity V_b. The film thickness is as follows:

$$e = 1.337\ r\ Ca^{2/3} \quad (5)$$

where Ca represents the capillary number defined as:

$$Ca = \mu_L\ V_b / \gamma \quad (6)$$

In relation to Bretherton's approach, r was assimilated to the radius of the bubble. Tisné et al., 2004 representing the evolution of the measured contact film thickness versus $Ca^{2/3}$ observed a close agreement with the Bretherton law (Bretherton, 1961), the bubble size considered being 0.5 mm. Our experiments are in a capillary number range of $11\ 10^{-4} < Ca < 44\ 10^{-4}$ ($0.011 < Ca^{2/3} < 0.026$) falling within the range proposed by these authors, $3.10^{-4} < Ca < 28.10^{-4}$ ($0.005 < Ca^{2/3} < 0.02$). Given the agreement observed with the Bretherton law, the contact liquid film thickness in our experimental conditions would have ranged from 7 to 18 µm given a mean

bubble radius of 0.5 mm, the thinnest liquid films being observed at the lowest velocities. Such a range of variation is in agreement with previous works (Chovet and Aloui, 2016; Tisné et al., 2004).

In parallel, it was shown (Tisné et al., 2003) that the wall shear stress was lower in the liquid film between each bubble and the wall. The wall friction was especially concentrated at the two ends of the bubbles; the wall shear stress fluctuations' amplitude being linked to the bubble size. When compared with the spore detachment kinetics, the greatest detachment efficiency appeared to be obtained with larger bubble size, notably when their diameter exceeded 0.1 mm, as clearly observed with the foam qualities of 0.5 (1D and 2D foam flow conditions) and 60% (1D foam flow condition) during the first step. Under CIP conditions, the detachment rate appeared to be comparable to the best foam cleaning conditions tested for comparable mean WSS conditions. In both cases the cleaning agent was the SDS under cold conditions (20°C). Previous work (Faille et al., 2018), highlighted the significant role of the fluctuation in the local wall shear stress on the cleaning efficiency under CIP conditions. One can draw a parallel here with these previous observations (Chovet and Aloui, 2016; Tisné et al., 2003), as the presence of the WSS fluctuations induced by the foam at the top wall appeared to play a role in the detachment mechanism and was clearly visibly under the 1D flow regime. However, for the 70%, foam quality, larger sized bubbles were observed at the top wall, which failed to ensure cleaning efficiency. Conversely, the increase in foam velocity meant a re-arrangement of the bubble sizes at the top wall (smaller bubbles). This phenomenon appeared to be unfavorable for efficient cleaning, as despite an increase in mean WSS, fluctuation amplitude decreased. Local wall shear stress decreases dramatically while bubble passes and increases to a maximum between bubbles (Tisné et al., 2003). Therefore, the frequency of fluctuation of the local wall shear stress with large bubbles is less than the fluctuation with small bubbles but the amplitude is higher and would explain the differences in the spores' removal.

The kinetics of bacteria spore detachment in the different flow and foam quality conditions were investigated and modelled according to previous work (Benezech and Faille, 2018) on biofilm removal under CIP conditions. An identical simple two-phase model was found to be suitable for describing biofilm removal kinetics. The first bacterial removal phase corresponded to a quick removal of biofilm matrix with embedded cells, while the second phase accounted for the removal of cells directly attached to the steel surface. For bacterial spores removed by foam flow, the mechanisms appeared to be totally different, as the bacteria were evenly distributed on the stainless steel surfaces with very few clusters. This is unlikely to explain the quick and strong removal at the very beginning of the cleaning (less than 1 min). The parameter f corresponding to the part of the spore's population easily affected by the foam flow appeared to be significantly higher at the lowest velocities and for the wettest foam (β=50%). This also corresponded to the highest values of the Kmax1 constant rate, i.e. the first phase of the removal kinetics. However, the second kinetic phase did not significantly improve the cleaning efficiency as a whole, whatever the conditions. For biofilms, it was observed that the chemical action contrarily to the mechanical action induced by the foam flow, was only involved in the first removal kinetic phase. The addition of chemicals such as NaOH during CIP conditions would largely improve this initial kinetics removal phase (Benezech and Faille, 2018). The difficulty in removing the remaining spores during the second phase of the kinetics was probably due to the stainless steel surface finish 2B used, which was proven to be less hygienic

than other finishes, such as bright annealed 2R, as it presents boundary grains where spores can accumulate. The fluctuations in the liquid film thickness and/or of the wall shear stress appeared to impact the detachment phenomenon to a lesser extent.

A comparison with previous work on particles detachment by bubbles moving in a capillary duct, will allow the potential role of the capillary forces in the bacterial detachment to be taken into account. Two types of particles in terms of surface energy (hydrophobic and hydrophilic) of a size comparable to the Bacillus spores were used (Kondjoyan et al., 2009b), the entire air–liquid interface was modelled and the time-variation of the capillary force during transit of the bubble at the surface was determined. The particle detachment curve was thus predicted from near zero velocity to the highest velocity value, at which capillary force was supposed to vanish. The approach was validated using latex particles 2µm in diameter. The bell-shaped detachment curves experimentally obtained showed a width dependent on the value of the contact angle of the particles, the curve being narrower for hydrophilic particles than for hydrophobic ones. The effective contact angle values of the particles could thus be deduced directly from the width of the detachment curves. *B. amyloliquefaciens* 98/7 spores according to previous work were highly hydrophilic (Faille et al., 2010) with a contact angle to water of 20.5° (data not shown). For hydrophilic particles (Kondjoyan et al., 2009b), the detachment occurred at bubble velocities of around 3 cm s^{-1} and dramatically decreased at 5 cm s^{-1}. As far as a direct comparison is conceivable, such a velocity range corresponded to the variation range (2.2 – 5 $cm.s^{-1}$), where the greatest detachment rate was observed, as illustrated by high Kmax1 constant rate values under 1D flow conditions. For hydrophobic particles, the bell-shaped detachment rate was wider and detachment started at greater bubble velocities, starting at 3 $cm.s^{-1}$ and peaking at around 7 cm s^{-1}. This could partly explain the very low cleaning efficiency of surfaces soiled by the *Bacillus cereus* 98/4 spores by the best foam cleaning conditions observed for *B. amyloliquefaciens*. *B. cereus* spores presented a high contact angle value (111.1°) as described recently (Faille et al., 2019a), largely over the value of 59° for the hydrophobic particles deduced from the bell-shaped curve (Kondjoyan et al., 2009b). With *B. cereus* spores, greater foam velocities should be tested, while conserving the bubble pattern obtained in this work under 1D flow conditions.

Time-variations relating to the capillary forces as an inlet condition in a modified adhesion and dynamic model were suggested as a way of predict the nano- and micro-movements of particles during their detachment from a surface (Kondjoyan et al., 2009). These movements are probably emphasized by the shear force fluctuations in our experimental conditions, which differ greatly to capillary flow conditions.

V. Conclusions and perspectives

This work constitutes a cornerstone for future work on the implementation of foam flow cleaning. This requires further activities on foam flow characterisation in order to be able to design a new efficient cleaning foam structure (less drainage phenomenon, increase of the wall shear stress at the bottom of the ducts), which would take into account both the surfactant used (more profitable and usable industrially) than the SDS and the temperature of the foam. The decrease of the temperatures seemed to play a significant role in its cohesion strengths (data not shown) potentially corresponding to food processing sectors working under positive cold conditions e.g. fresh-cut or frozen vegetable and fruit industries. The novelty of this concept is

to clean complex equipment while using far less potable water, at a lower energy consumption level.

Acknowledgments
This work was supported by the project Veg-I-Tec (programme Interreg V France-Wallonia-Flanders GoToS3), ANIOS laboratories and the European Regional Development fund via the Hauts-de-France region.

References

Benezech, T., Faille, C., 2018. Two-phase kinetics of biofilm removal during CIP. Respective roles of mechanical and chemical effects on the detachment of single cells vs cell clusters from a Pseudomonas fluorescens biofilm. J. Food Eng. 219, 121–128. https://doi.org/10.1016/j.jfoodeng.2017.09.013

Blel, W., Legentilhomme, P., Bénézech, T., Fayolle, F., 2013. Cleanabilty study of a Scraped Surface Heat Exchanger. Food and Bioproducts Processing 91, 95–102. https://doi.org/10.1016/j.fbp.2012.10.002

Blel, W., Legentilhomme, P., Le Gentil-Lelièvre, C., Faille, C., Legrand, J., Bénézech, T., 2010. Cleanability study of complex geometries: Interaction between B. cereus spores and the different flow eddies scales. Biochemical Engineering Journal 49, 40–51. https://doi.org/10.1016/j.bej.2009.11.009

Bretherton, F.P., 1961. The motion of long bubbles in tubes. Journal of Fluid Mechanics 10, 166. https://doi.org/10.1017/S0022112061000160

Chovet, R., 2015. Experimental and numerical characterization of the rheological behavior of a complex fluid: application to a wet foam flow through a horizontal straight duct with and without flow disruption devices (FDD). Université de Valenciennes et du Hainaut-Cambresis.

Chovet, R., Aloui, F., 2016. Liquid Film Thickness: Study and Influence over Aqueous Foam Flow. J. Appl. Fluid Mech. 9, 39–48.

Chovet, R., Aloui, F., Keirsbulck, L., 2014. Gas-Liquid Foam Through Straight Ducts and Singularities: CFD Simulations and Experiments. https://doi.org/10.1115/FEDSM2014-21190

Cunault, C., Faille, C., Briandet, R., Postollec, F., Desriac, N., Benezech, T., 2018. Pseudomonas sp. biofilm development on fresh-cut food equipment surfaces – a growth curve – fitting approach to building a comprehensive tool for studying surface contamination dynamics. Food and Bioproducts Processing 107, 70–87. https://doi.org/10.1016/j.fbp.2017.11.001

Dallagi, H., Al Saabi, A., Faille, C., Benezech, T., Augustin, W., Aloui, F., 2019. Cfd Simulations of the Rheological Behavior of Aqueous Foam Flow Through a Half-Sudden Expansion, in: Proceedinge of the Asme/Jsme/Ksme Joint Fluids Engineering Conference, 2019, Vol 1. Amer Soc Mechanical Engineers, New York, p. UNSP V001T01A030.

Dallagi, H., Gheith, R., Al Saabi, A., Faille, C., Augustin, W., Benezech, T., Aloui, F., 2018a. CFD Characterization of a Wet Foam Flow Rheological Behavior, in: Volume 3: Fluid

Machinery; Erosion, Slurry, Sedimentation; Experimental, Multiscale, and Numerical Methods for Multiphase Flows; Gas-Liquid, Gas-Solid, and Liquid-Solid Flows; Performance of Multiphase Flow Systems; Micro/Nano-Fluidics. Presented at the ASME 2018 5th Joint US-European Fluids Engineering Division Summer Meeting, ASME, Montreal, Quebec, Canada, p. V003T20A004. https://doi.org/10.1115/FEDSM2018-83338

Dallagi, H., Gheith, R., Al Saabi, A., Faille, C., Augustin, W., Benezech, T., Aloui, F., 2018b. CFD Characterization of a Wet Foam Flow Rheological Behavior, in: Volume 3: Fluid Machinery; Erosion, Slurry, Sedimentation; Experimental, Multiscale, and Numerical Methods for Multiphase Flows; Gas-Liquid, Gas-Solid, and Liquid-Solid Flows; Performance of Multiphase Flow Systems; Micro/Nano-Fluidics. Presented at the ASME 2018 5th Joint US-European Fluids Engineering Division Summer Meeting, ASME, Montreal, Quebec, Canada, p. V003T20A004. https://doi.org/10.1115/FEDSM2018-83338

Dogan, B., Boor, K.J., 2003. Genetic diversity and spoilage potentials among Pseudomonas spp. isolated from fluid milk products and dairy processing plants. Appl. Environ. Microbiol. 69, 130–138.

Faille, C., Bihi, I., Ronse, A., Ronse, G., Baudoin, M., Zoueshtiagh, F., 2016. Increased resistance to detachment of adherent microspheres and Bacillus spores subjected to a drying step. Colloids and Surfaces B: Biointerfaces 143, 293–300. https://doi.org/10.1016/j.colsurfb.2016.03.041

Faille, C., Cunault, C., Dubois, T., Benezech, T., 2018. Hygienic design of food processing lines to mitigate the risk of bacterial food contamination with respect to environmental concerns. Innov. Food Sci. Emerg. Technol. 46, 65–73. https://doi.org/10.1016/j.ifset.2017.10.002

Faille, C., Lemy, C., Allion-Maurer, A., Zoueshtiagh, F., 2019. Evaluation of the hydrophobic properties of latex microspheres and Bacillus spores. Influence of the particle size on the data obtained by the MATH method (microbial adhesion to hydrocarbons). Colloid Surf. B-Biointerfaces 182, UNSP 110398. https://doi.org/10.1016/j.colsurfb.2019.110398

Faille, C., Lequette, Y., Ronse, A., Slomianny, C., Garénaux, E., Guerardel, Y., 2010. Morphology and physico-chemical properties of Bacillus spores surrounded or not with an exosporiumConsequences on their ability to adhere to stainless steel. International Journal of Food Microbiology 143, 125–135. https://doi.org/10.1016/j.ijfoodmicro.2010.07.038

Gahleitner, B., Loderer, C., Fuchs, W., 2013. Chemical foam cleaning as an alternative for flux recovery in dynamic filtration processes. Journal of Membrane Science 431, 19–27. https://doi.org/10.1016/j.memsci.2012.12.047

Geeraerd, A.H., Valdramidis, V.P., Van Impe, J.F., 2005. GInaFiT, a freeware tool to assess non-log-linear microbial survivor curves. International Journal of Food Microbiology 102, 95–105. https://doi.org/10.1016/j.ijfoodmicro.2004.11.038

Jullien, C., Benezech, T., Gentil, C.L., Boulange-Petermann, L., Dubois, P.E., Tissier, J.P., Traisnel, M., Faille, C., 2008. Physico-chemical and hygienic property modifications of stainless steel surfaces induced by conditioning with food and detergent. Biofouling 24, 163–172. https://doi.org/10.1080/08927010801958960

Kondjoyan, A., Dessaigne, S., Herry, J.-M., Bellon-Fontaine, M.-N., 2009a. Capillary force required to detach micron-sized particles from solid surfaces—Validation with bubbles

circulating in water and 2μm-diameter latex spheres. Colloids and Surfaces B: Biointerfaces 73, 276–283. https://doi.org/10.1016/j.colsurfb.2009.05.022

Li, G., Tang, L., Zhang, X., Dong, J., 2019. A review of factors affecting the efficiency of clean-in-place procedures in closed processing systems. Energy 178, 57–71. https://doi.org/10.1016/j.energy.2019.04.123

Mai, Z., Butin, V., Rakib, M., Zhu, H., Rabiller-Baudry, M., Couallier, E., 2016. Influence of bulk concentration on the organisation of molecules at a membrane surface and flux decline during reverse osmosis of an anionic surfactant. J. Membr. Sci. 499, 257–268. https://doi.org/10.1016/j.memsci.2015.10.012

Moerman, F., Rizoulières, P., Majoor, F.A., 2014. 10 - Cleaning in place (CIP) in food processing, in: Lelieveld, H.L.M., Holah, J.T., Napper, D. (Eds.), Hygiene in Food Processing (Second Edition). Woodhead Publishing, pp. 305–383. https://doi.org/10.1533/9780857098634.3.305

Peng, J.-S., Tsai, W.-C., Chou, C.-C., 2002. Inactivation and removal of Bacillus cereus by sanitizer and detergent. Int. J. Food Microbiol. 77, 11–18.

Pietrysiak, E., Kummer, J.M., Hanrahan, I., Ganjyal, G.M., 2019. Efficacy of Surfactant Combined with Peracetic Acid in Removing Listeria innocua from Fresh Apples. J. Food Prot. 82, 1959–1972. https://doi.org/10.4315/0362-028X.JFP-19-064

Ribeiro, M.C.E., Fernandes, M. da S., Kuaye, A.Y., Gigante, M.L., 2019. Influence of different cleaning and sanitisation procedures on the removal of adhered Bacillus cereus spores. Int. Dairy J. 94, 22–28. https://doi.org/10.1016/j.idairyj.2019.02.011

Srey, S., Jahid, I.K., Ha, S.-D., 2013. Biofilm formation in food industries: A food safety concern. Food Control 31, 572–585. https://doi.org/10.1016/j.foodcont.2012.12.001

Tauveron, G., Slomianny, C., Henry, C., Faille, C., 2006. Variability among Bacillus cereus strains in spore surface properties and influence on their ability to contaminate food surface equipment. Int. J. Food Microbiol. 110, 254–262. https://doi.org/10.1016/j.ijfoodmicro.2006.04.027

Tisné, P., Aloui, F., Doubliez, L., 2003. Analysis of wall shear stress in wet foam flows using the electrochemical method. International Journal of Multiphase Flow 29, 841–854. https://doi.org/10.1016/S0301-9322(03)00038-7

Tisné, P., Doubliez, L., Aloui, F., 2004. Determination of the slip layer thickness for a wet foam flow. Colloids and Surfaces A: Physicochemical and Engineering Aspects 246, 21–29. https://doi.org/10.1016/j.colsurfa.2004.07.014

Publication II: Wet foam flow: a suitable method for improving surface hygiene in the food industry

https://doi.org/10.1016/j.fbp.2021.12.009

Heni DALLAGI[a], Christine FAILLE[a], Laurent BOUVIER[a], Maureen DELEPLACE[a], Thomas DUBOIS[a], Fethi ALOUI[b], Thierry BENEZECH[a]*

[a] Univ. Lille, CNRS, INRAE, Centrale Lille, UMET, F-59000 Lille, France
[b] Polytechnic University Hauts-de-France, LAMIH CNRS UMR 8201, Campus Mont-Houy, F-59313 Valenciennes, France

***Corresponding Author:** Thierry BENEZECH, INRAE, UMET, 369 rue Jules Guesde, F-59650 Villeneuve d'Ascq, France. thierry.benezech@inrae.fr

Highlights

- Foam flow cleaning would be enhanced by small bubble sizes at high shear stress.
- Hydrophobic spores are more resistant than hydrophilic spores against foam flow.
- Foam flow being more effective than the corresponding CIP conditions for spores.
- Foam cleaning could be an interesting option for environmental friendliness.

ABSTRACT

In the food industry, the cleaning of contaminated surfaces requires new strategies to be adopted which can provide greater cleaning efficiency with minimal energy and water consumption. The use of wet foams was proposed to clean stainless steel surfaces contaminated by droplets containing *Bacillus* spores. Methods such as polarography, conductimetry and foam structure identification were used. Foam flow conditions with varying wall shear stresses and bubble sizes were observed to measure their impacts on surface contaminant removal kinetics. Compared to conventional cleaning-in-place method, foam flow more effectively removed both hydrophilic and hydrophobic spores. The combination of high shear stress and small bubble sizes (<0.2 mm) showed promise for improving the cleaning efficiency of the foam. Mechanisms such as fluctuation in local stresses, or in the liquid film thickness between the bubbles and the steel wall induced by bubble passage, foam imbibition, and liquid film drainage were then investigated.

Keywords
Flow foam cleaning; *Bacillus* spores; conductimetry; polarography; bubble size; shear stress

I. Introduction

In the agro-food industrial environment, avoiding surface contamination by unwanted microorganisms is of crucial importance (Alvarez-Ordonez et al., 2019; Farag et al., 2021). Indeed, contaminated surfaces can recontaminate food in contact (cross-contamination), with sometimes disastrous consequences in terms of food spoilage, but also in terms of transmission of pathogens that can be the cause of large-scale epidemics. For example, surface contamination with microorganisms would have accounted for more than 50% of the collective foodborne illnesses (CFTI) in France between 2006 and 2008 (Delmas et al., 2010). Nowadays, cleaning-in-place (CIP) is a routine method in the food and pharmaceutical industries to ensure the equipment hygiene and the quality of product. The effect of the hydrodynamics of the cleaning fluid on CIP efficiency has been the subject of numerous studies (Li et al., 2019; Piepiórka-Stepuk et al., 2021). Particular interest has been shown in parameters such as the mechanical action exerted by the flow in creating wall shear stress (Bénézech and Faille, 2018) or the impact of Reynolds number (Fan et al., 2018). Their results showed that turbulence affects the cleaning process, as an increase in the presence of turbulent structures generated at the walls could improve the cleaning efficiency, but up to a certain limit. The use of non-stationary flows, such as pulsed flows and intermittent jet flows, would appear to increase CIP efficiency. Indeed, these kinds of flows affect both the mean and fluctuating components of the wall shear stress and consequently reduce the residual contamination (Absi and Azouani, 2018; Blel et al., 2013). Gas-liquid two-phase flows (air bubbles in liquid or foam), which are also non-stationary flows, are likely to be of similar interest to pulsed flows. Indeed, liquid containing gas bubbles (non-foaming solution) had been shown to efficiently remove from surfaces both particles (Kondjoyan et al., 2009) and bacteria (Kriegel and Ducker, 2019). Recently, the efficiency of foam flow to remove *Bacillus* spores from stainless steel surfaces has been investigated by (Al Saabi et al., 2021) and the use of aqueous unstable foams has also been proposed for cleaning the sensitive surfaces of artistic and cultural assets (Schad et al., 2021). It should also be noted that foam in static conditions, is widely used in the food industry for cleaning open surfaces (floors, conveyor belts, worktops and equipment) (Mierzejewska et al., 2014).

Aqueous foam could be considered as a non-Newtonian fluid consisting of gas dispersion in liquid containing surfactants. Depending mainly on the liquid fraction, the foam could be ranked as wet (small and spherical bubbles) or dry (large and polyhedral bubbles). A liquid-rich layer may be formed near a solid surface due to the bubble migration, thereby giving a slip effect between the foam and the wall (Tisné et al., 2003). Given this complexity, the rheological behavior of foam can follow the shear-thinning Herschel-Bulkley model, which states that under strong mechanical stresses, foam behaves as a viscous liquid, while under low stresses it behaves as a solid whose structure can be deformed and return to its initial state (Dallagi et al., 2019). Moreover, very wet foam flow (liquid fraction = 0.5) was found to clean hydrophilic spores better than dryer foam (liquid fraction between 0.3 to 0.4) (Al Saabi et al., 2021). However, the maximum of the shear stress that they used was 6 Pa, and the work lacks the explanation of the cleaning process.

The aim of this study was to investigate the potential role of the foam velocity and their structure (described by air/water content of the foam and size of air bubbles) in efficiently removing *Bacillus subtilis* spores. In this respect, different flow conditions of wet foam (liquid fraction

= 0.5), by varying the shear stress (from 2 up to 13.2 Pa) and the foam structure, were carried out to test its efficiency. All cleaning conditions were tested on two *Bacillus* spore strains which differ only in their hydrophilic/hydrophobic character. Another originality of this present work is the detailed physical analysis of the dynamic behavior of foam and its structure and consequences at the wall to identify the underlying mechanisms of the bacterial spores' removal and choose the foam flow condition leading to optimal cleaning. The foam cleaning effectiveness was then compared to a standard CIP procedure.

II. Materials and Methods

II.1 Foam preparation

The foam production prototype was built according to a previous work (Al Saabi et al., 2021). The prototype is presented in Figure 60. Briefly, foam was produced by pressurized air injection through a porous medium (pore sizes ranging from 1 to 1.6 µm) into an SDS surfactant (Sodium Dodecyl Sulfate (over 98.5% purity) dissolved in osmosed water (0.15% w/w) to avoid any unwanted interactions with ions contained in the standard tap water.

The physical properties of the foaming solutions used were a 1 Bar atmospheric pressure and 20°C standard temperature, a 997.9 kg.m^{-3} density (ρ_l), a 0.94 10^{-3} Pa.s dynamic viscosity (μ_l) and a 26.2 10^{-3} N.m^{-1} surface tension (σ). The foam quality (β) describing the air/water content of the foam was calculated as follows (Equation 1) where Q_g and Q_l are respectively the gas and liquid flow rates.

$$\beta = \frac{Q_g}{Q_l + Q_g} \quad (1)$$

A foam quality of 0.5 was chosen in this work by varying the shear stress and the capillary forces. The capillary force of the bubble $F_c = \sigma 2\pi r$ is defined as the force due to surface tension that acts between the two halves of the bubble (Al-Qararah et al., 2013) with respect to the capillary pressure ($P_c = \frac{\sigma}{r}$) (Schad et al., 2021), where r is the bubble radius. The balance between the viscous drag forces versus surface tension forces of the foam can be represented by the non-dimensional capillary number $Ca = \frac{\mu_l v}{\sigma}$. μ_l and v are the dynamic viscosity of the liquid solution and the foam velocity, respectively.

Therefore, the first part presents a detailed characterization of these foam flow conditions in order to understand the mechanism by which the foam detached the spores, to identify the key parameters and then to test these new foam conditions on cleaning of stainless-steel coupons contaminated by *Bacillus* spores. Table 6 (in Result section) summarizes all the FFC conditions (quality of 0.5) and CIP. The foam mean velocity ($\bar{v}$) and the Reynolds number (Re) are determined from the following equations:

$$Re = \frac{\rho_f . \bar{v} . d_h}{\mu_f} \quad d_h \text{ being the hydraulic diameter} \quad (2)$$

$$\bar{v} = \frac{Q_l + Q_g}{S} \quad (3)$$

$\rho_f = (1-\beta).\rho_l + \beta.\rho_g$ ρ_l being the liquid density (4)

$\mu_f = \frac{\mu_l}{1-\mu_l{}^{1/3}}$ (5)

The foam flow velocity varied from 1.5 to 13.5 cm/s. The three first cases correspond to the conditions used in a previous work (Al Saabi et al., 2021). Cases 4 and 5 have the highest velocities, which were generated using three parallel generators. CIP has the highest velocity, while the mean shear stress was similar to that in case 4.

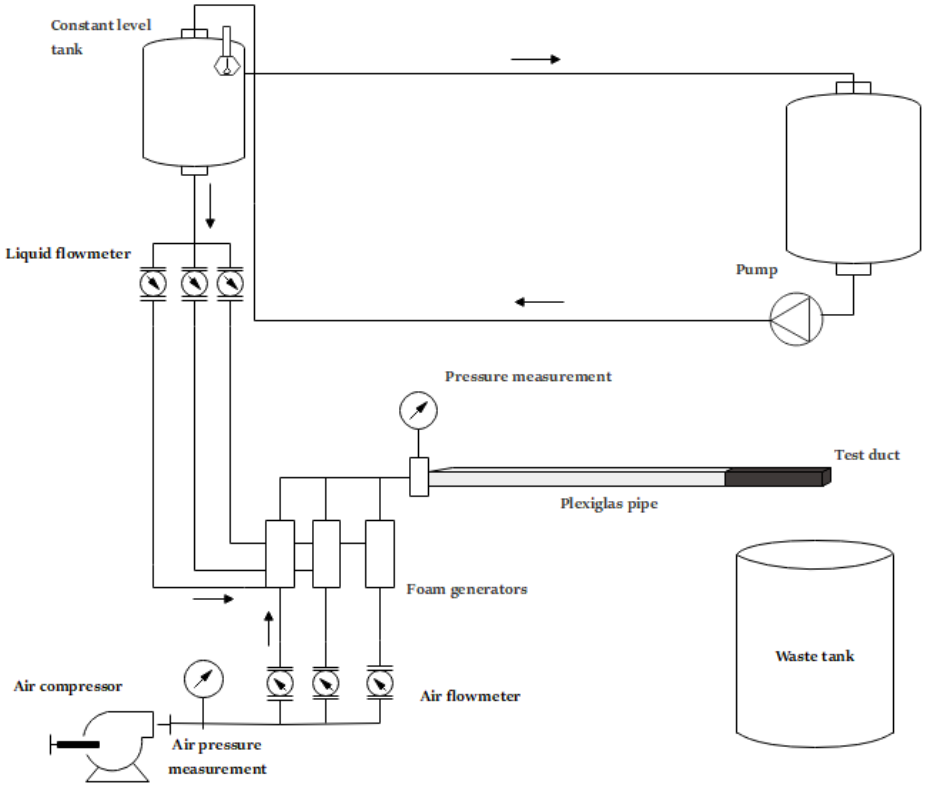

Figure 60. Experimental set-up for studying the foam cleaning in place process.

II.2 Foam characterization

II.2.1 Foam morphology

Foam flow was visualized in order to observe the bubble's displacement at the channel walls, for a given interval. A Nikon D850camera, equipped with an AF-S Micro NIKKOR 60 mm f/2.8 G ED with a resolution of 8256 x 5504 pixels, was used to record foam microtexture and its associated bubble size distribution. For each foam flow condition, three images were captured then analyzed using Piximètre 5.1 R1540 software. First, the chosen images were calibrated, then were subjected to different image processing features (local threshold, filters…) to reduce the noise in order to better observe its contours. The bubble size distribution was then calculated according to usual granulometric distributions. To evaluate the heterogeneity/uniformity of this distribution, different parameters were identified such as *F0.05*, and *F0.2* corresponding to the percentage of the bubbles with a diameter of less than 0.05 and 0.2 mm respectively.

II.2.2 Thin film thickness

The conductimetry technique was used to measure the thickness of the thin film. This is based on the measurement of the impedance of the liquid volume located between the liquid-foam interface and two outcropping electrodes at the duct wall. A generator provided an alternating sinusoidal voltage to power these electrodes. The frequency was 50 kHz to avoid any polarization phenomena. The calibration of the conductimetric probe was carried on using the calibrated Mylar sheets. The estimated error was 8%.

II.2.3 Wall shear stress

When foam flowed, mean shear stress was calculated based on the measurement of the static pressure along the channel. The power loss measurements were carried out using a differential pressure sensor Shlumberger, type 8D. Two pressure outlets allow the connection of 2 manifold tubes placed over a scaled plate that measures on a length L of 1m the pressure drop placed after 1.5 m from the entry of the foam in the duct. Indeed, to allow steady state flow conditions, the test ducts were placed at intervals exceeding 80 times the hydraulic diameter of the vein inlet (i.e. 1.5 m). The mean wall shear stress can thus be computed as:

$$\bar{\tau} = \frac{\Delta P}{\Delta x}\frac{d_h}{4} \quad (6)$$

where $\frac{\Delta P}{\Delta x}$ is the pressure gradient.

The local shear stress at the top wall where coupons were placed, was measured using the polarography method. This technique allows the determination of the local velocity gradient at the walls by measuring the mass transfer coefficient of the electrodes. Briefly, based on the simplified assumptions for the resolution of the convection-diffusion equation proposed by (Mitchell, 1965), the wall shear stress calculation was obtained from the velocity gradient (Lévêque solution and Sobolic correction). Details of the method used here were given previously (Tisné et al., 2003).

From a theoretical point of view, the polarographic signal is related to the slip layer thickness and foam velocities. The diffusion limit current can be represented as the Sherwood number form (*Sh*) or directly as the wall shear stress (τ_w). Spectral analysis of the time signals appears necessary in order to understand the underlying mechanisms and to trace back to the flow characteristics near the wall duct. The method used for spectral representation is based on the processing of the signal acquired by the Fourier transform (*FT*) with Matlab software. This was proposed by (Ioana et al., 2007). It expresses the frequency distribution of the amplitude, the power spectral density, as well as the fluctuation rate of the considered signals. These specters revealed peaks obtained at characteristic frequencies corresponding to the passage frequencies of bubbles respective to each foam condition and their harmonics.

It was found that the SDS did not support the addition of electrochemical products (Ferri-ferrocyanide potassium) for the use of the polarography method. In fact, a reaction other than oxidation-reduction was produced, destabilizing the foam. For this reason, we replaced the SDS with a non-anionic surfactant: Lauramine oxides (Ammonyx® LO (Stephan) = 0.8 ml/L). To ensure the presence of the same phenomena for the same flow conditions, the thickness of the liquid film and of the conductivity signals produced with that of the SDS solution was verified.

The same behavior and signal variation with SDS or Ammonyx® surfactant was observed, which is in line with previous works (Tisné et al., 2003), where another surfactant (Amonyl®) replaced the SDS for the same reason.

II.3 Bacterial strains and materials

Two *Bacillus subtilis* strains were used throughout this study. *Bacillus subtilis* PY79 (subsequently named Bs PY79) is a laboratory strain producing hydrophilic spores surrounded by a mucous layer called crust. A Bs PY79 recombinant strain deleted in *spsA* (Dubois et al., 2020), subsequently named Bs PY79 *spsA*, which produces hydrophobic spores modified in their crust properties, was also used throughout this study. Both *Bacillus* strains were tagged with green fluorescent proteins to make the spores more fluorescent. Spores were produced as previously described (Faille et al., 2019) on Spo8-agar at 30°C. When over 95% of spores were obtained, they were harvested by scraping the surface, washed five times in sterile water, and stored in sterile water at 4°C until use. In order to limit the presence of spore aggregates, the spore suspensions were subjected to an ultrasonication step (Bransonic 2510E-MT, Branson Ultrasonics Corporation, USA) before each experiment.

All experiments were carried out on AISI 316 stainless steel with pickled (2B) finish coupons (provided by APERAM, Isbergues, France) in the form of rectangular coupons (45 mm × 15 mm). In order to have surface properties similar to those used in the dairy industry, the stainless-steel coupons were subjected to a conditioning procedure consisting of 15 runs of soiling and cleaning both to mimic what might occur in food processing lines and to stabilize their surface properties. The soiling step was achieved by immersing the coupons in milk in semi-skimmed reconstituted milk (150 g/L milk powder) for 30 min at room temperature. After a quick rinse, soiled coupons were cleaned by immersion in sodium hydroxide at 0.5% w/w for 30 min at 70°C. Before each experiment, coupons were cleaned using an alkaline detergent (RBS T105, Traitements Chimiques des Surfaces, France). Each coupon was first rubbed vigorously with pure RBS and then immersed for 10 minutes in 5% RBS at 60°C. Coupons are thoroughly rinsed for 5 min with tap water, and then with softened (reverse osmosis) water for another 5 min. One day before experiments, coupons were sterilized in a dry heat oven at 180°C for 1h.

The hydrophilic character of the cleaned and disinfected coupons was estimated using a goniometer (Digidrop, GBX, France). A water contact angle (θ_{water}) of 66° was measured, which reflects the relatively hydrophilic character of this material.

II.4 Surface soiling and cleaning

For both strains, the concentration of the spore suspensions was set at 10^8 CFU ml^{-1}. Five 1 µL droplets of the spore suspension were placed on each coupon and evaporated for 1h at 30°C. The procedure was schematically illustrated Figure 61. Some coupons were analyzed to control the initial contamination level (5 10^5 spores per coupon) and to observe the droplet architecture under the microscope (Supplementary- Figure 61 in the Supporting Information). Then, sets of 4 coupons were placed inside a rectangular stainless-steel duct (1.5 10^{-2}m high × 1 10^{-2}m width), subjected to a cleaning procedure and analyzed again for residual contamination (three coupons) for enumeration and deposit architecture (one coupon).

In this work, as previously (Al Saabi et al., 2021), the foam cleaning phenomenon was evaluated at the top wall because the wall shear stress and the thin liquid film thickness would be considered to show constant variations in this zone according to previous work (Tisné et al., 2004, 2003). This position was selected in order to facilitate the interpretation of the role of foam flow in the cleaning process.

The resistance of the spore deposits to a cleaning procedure was performed as follows. The test ducts were connected to the pilot rig and then were subjected to the cleaning process. Experiments were carried out on foam flow cleaning (FFC) under different conditions (by varying the foam shear stress and the foam/bubble structure) for 15 and 35 s, 1, 3, 5, 10, and 20 min. Other experiments were carried out on cleaning in place (CIP) under the same conditions to compare the relative effectiveness of FFC and CIP. Details are provided in the Results section. After the cleaning process, the coupons were removed from the test duct, then rinsed by immersion in sterile ultrapure water to remove the rest of the foam. In order to investigate the possible role of the presence of SDS surfactant on spore detachment, further experiments were performed in static conditions by dipping a set of coupons in pure water or in SDS 0.15% (w/w) for 20 min (data not shown). It should be noted that *B. subtilis* spore incubation in SDS did not result in any significant viability loss.

To determine the quantity of spores on the coupons before and after cleaning, each coupon surface was sampled using a dry cotton swab (Copan, Brescia, Italy). The swabs were placed in a tube containing 5 ml of sterile ultrapure water and vortexed for 1 min at 2400 rpm. The suspensions containing the detached spores were enumerated on TSA (Tryptone Soy Agar, Biokar, France) after 48h at 30°C. For microstructure examination, the observation of some deposits was performed before and after cleaning, using an epifluorescence microscope (Zeiss Axioskop 2 Plus, Oberkochen, Germany). The observations were first made at low magnification (x50) in order to observe the whole deposit resulting from the drying of a droplet. Further observations were carried out at higher magnification (x400) to determine the fine structure of the densest parts of these deposits (clusters, peripheral rings…), including any 3D organization.

After cleaning, the deposits were mostly weakly fluorescent, which made them difficult to observe. It was therefore necessary to stain them before observation. For that purpose, dried coupons were stained with orange acridine (0.01%) for 15 min. In order to ensure that the deposits were not removed during this staining step, some deposits were observed before and after the staining step. No significant difference was observed.

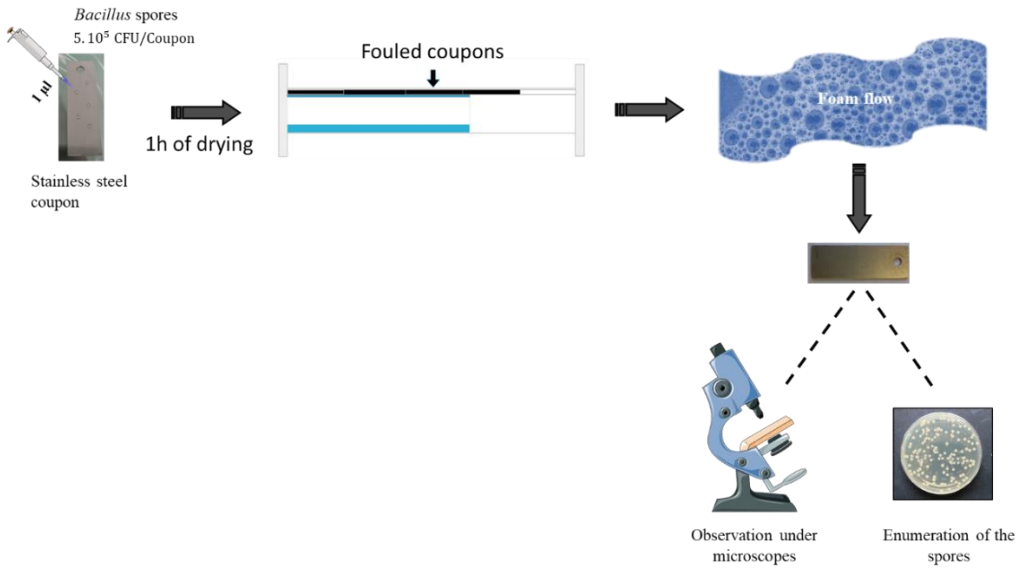

Supplementary- Figure 61. Schematic drawing of technique of the surface soiling and cleaning with foam flow.

II.5 Kinetics modeling

The removal kinetic profiles of the percentage of residual spores were fitted according to previous work (Bénézech and Faille, 2018), using GInaFIT. A two-phase model was selected (Equation 4), which presents the existence of two subpopulations characterized by different removal behaviors.

$$\frac{N}{N_0} = f\, e^{(-k_{max1}t)} + (1-f)e^{(-k_{max2}t)} \quad (4)$$

Where N_0 is the initial bacteria count, f is the poorly adherent fraction of the population (less resistant to detachment), $(1-f)$ is the more adherent fraction, and k_{max1} and k_{max2} [s^{-1}] are the specific detachment rates of the two sub-populations.

II.6 Statistical analysis

All the experiments were carried out in triplicate. Statistical analyses were performed by general linear model procedures using SAS V8.0 software (SAS Institute, Gary, NC, USA). For each cleaning condition, variance analyses were performed to determine the possible role of the shear stress and the foam structure on the removal kinetics of spores (f, k_{max1}, and k_{max2}) and the effectiveness of the cleaning by foam flow compared to the CIP process.

III. Results

III.1 Foam flow characterization

III.1.1 Bubbles size distributions

Figure 62 shows top views of the foam at the top wall for the different flow conditions. For all foam flow conditions, the bubbles had a roughly spherical shape and were separated by thick

liquid films (lamellae). Different foam granulometries were observed. Indeed, when the velocity increased from 1.5 to 9 cm/s, a clear decrease in the bubble size was observed. However, no additional decrease could be observed between 9 and 13.5 cm. s^{-1}.

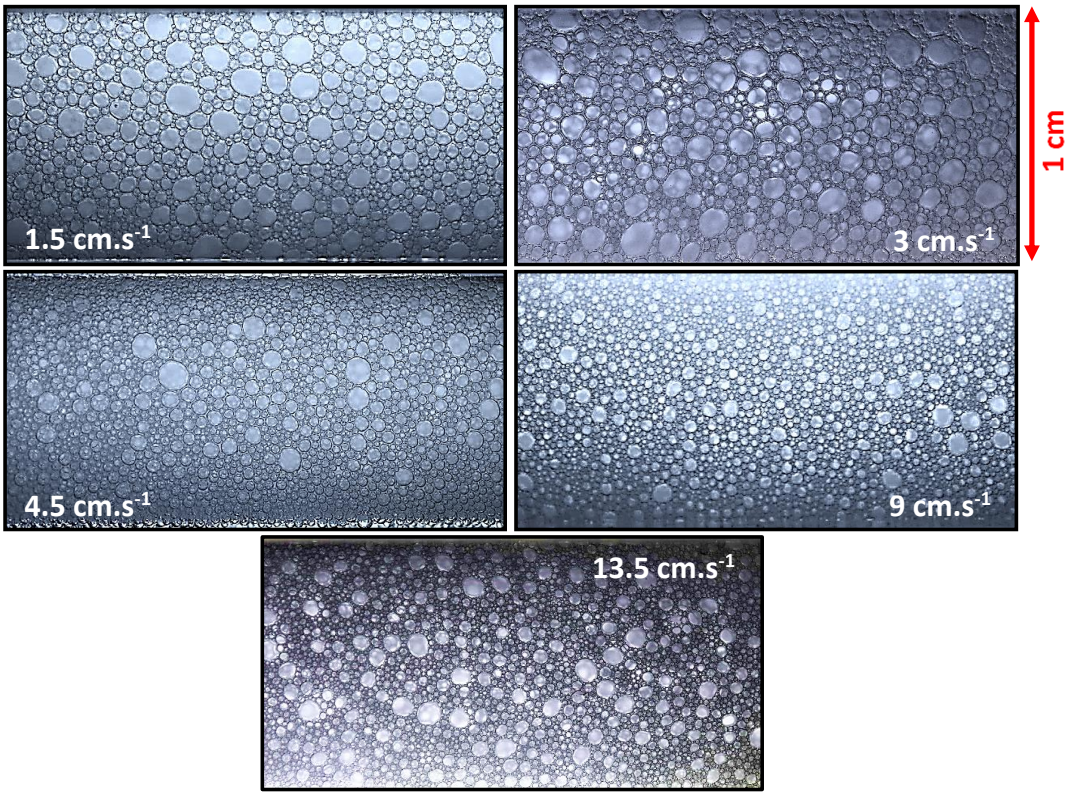

Figure 62. Top view of foam visualization at the wall of the transparent pipe (the entire width, 1 cm) upstream the test ducts for the different foam flow conditions.

Bubble sizes were then measured for these different conditions and the curves of the cumulative fraction of the bubble size distributions are presented in Figure 63. First, the distribution of the bubble size in all conditions was fitted by a lognormal function (R^2 ranging from 0.89 to 0.97) to better visualize the differences between the conditions tested. Variation of velocity causes a change in foam structure and bubble size distribution. As the foam velocity increased (Table 6), the mean diameter of bubbles decreased (from 0.34 down to 0.18 mm, for foam at 1.5 and 9 cm/s respectively) and the distribution became more homogeneous, except for foam at 13.5 cm/s where the mean diameter was 0.21 mm. While the number of small bubbles (less than 0.05 mm in diameter) was very close at 9 and 13.5 cm. s^{-1}, intermediate-sized bubbles (between 0.2 and 0.6 mm in diameter) were more abundant at 9 cm/s than at 13.5 cm/s. Therefore, the cumulative bubble size number at 0.2 mm (*F02*) was 0.68 and 0.60 respectively for 9 and 13.5 cm/s, as indicated in Table 6 and were found to be statistically different ($Pr < 0.0001$). These differences were much greater when comparing the highest velocities to the lowest ones. Indeed, considering bubbles with a diameter ≤ 0.05 mm (see fraction *F005*, Table 6), at 13.5 cm/s the cumulative fraction was more than 20 times higher than that for the lowest foam velocities, at 1.5 cm/s.

Table 6. Description of the different flow conditions carried out. The FFC and CIP represent the foam flow conditions and the cleaning-in-place that has been processed for removal of Bacillus spores from stainless steel surfaces, respectively.

Flow conditions	u (cm/s)	Ca [10^{-3}]	τ (Pa)	Dmean (mm)	F005	F02	RFS (%)	f (Hz)
FFC	1.5	0. 5	2.2	0.34	0.002	0.29	957	20
	3	1.1	4.2	0.30	0.006	0.36	688	39
	4.5	1.6	5.9	0.28	0.013	0.44	491	45
	9	3.3	9.8	0.18	0.022	0.68	130	70
	13.5	4.8	13.2	0.21	0.043	0.60	193	76
CIP	180	----	10	----------				

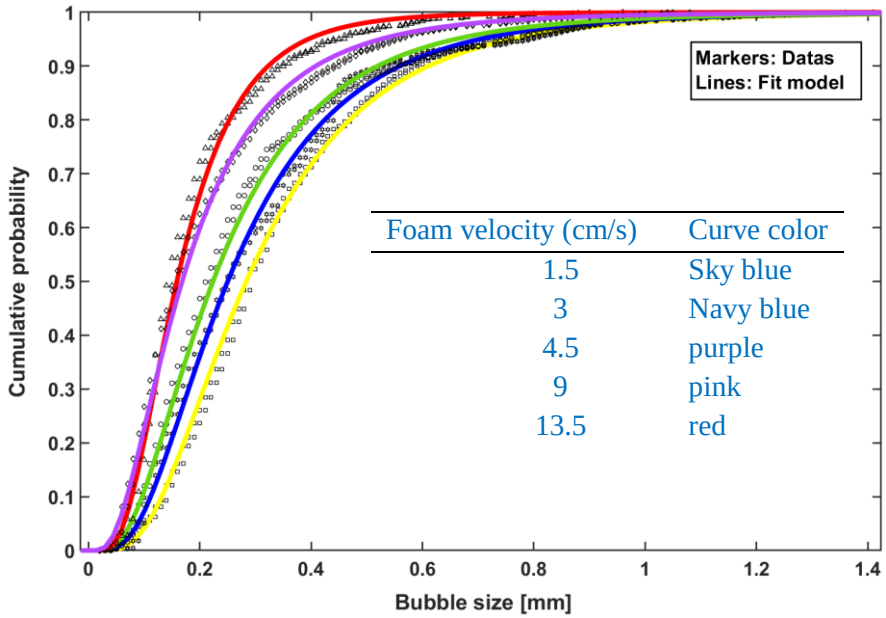

Figure 63. Cumulative fraction of the bubble size distribution for all the foam flow conditions. The markers present the brut data and the lines represent the Lognormal model fitted to each condition.

III.1.2 Upper liquid film thickness

Foam is not in direct contact with the wall surface, but bubbles are slipping over a thin liquid film layer (a few micrometers width). Variations of the liquid film thickness (from 11 up to 13 µm) measured at the top wall are shown in Figure 64 (left) for three foam mean velocities of 1.5, 3, and 4.5 cm/s, bearing in mind the limitations of our experimental set-up up essentially due to the inability to access sufficiently high foam flow rates as it was possible for the cleaning experiments.

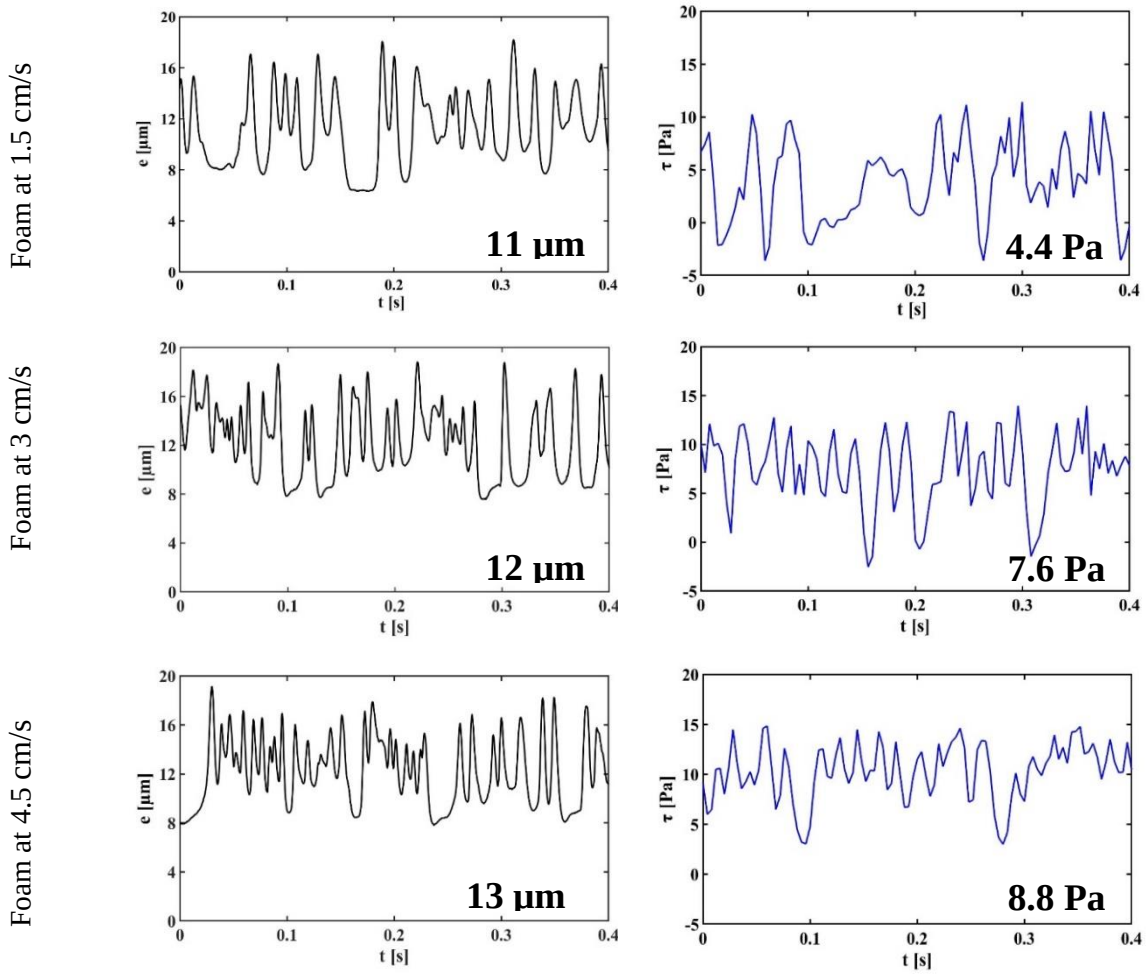

Figure 64. Example of the evolution of wall film thickness (left) and wall shear stress (right) given by the temporal signals of conductimetry and polarography over the top wall for the three cases, respectively. The values indicated in the images show the mean thickness and the mean wall shear stress during 40 seconds of acquisition.

The film thickness was affected by the bubble passage as shown in Figure 64 (left) with an example of the observed temporal evolution of the signal at the middle of the test section. It should be noted that whatever the position of the probe the signal was observed as similar either on the sides or in the middle of the duct. In the three cases, conductimetry signals presented high fluctuations reflecting the non-uniformity of this liquid film. Indeed the signals showed an instantaneous variation of 72 and 54% relative to the mean thickness value which varied from 5 to 21 µm, and from 8 to 22 µm for foam at 1.5 and 4.5 cm/s, respectively. In addition, the profiles obtained appeared to be very different within the three cases. The higher is the velocity the higher is the frequency of the signal (variation from 45 to 72.5 Hz for cases of foam at 1.5 and 4.5 cm/s, respectively), and the lower is the amplitude (variation from 9.8 up to 6, respectively). These variations were directly linked to the frequency of passage of the bubbles and to the size variations leading to the shape of the signal. Indeed, the maximum thickness of the liquid film (peaks of the signal) corresponds to the film thickness between two following bubbles passage, minimum thickness (signal hollows) corresponding to the presence of the bubble, the bigger bubble the lower film thickness could be stated from Figure 62. It should be noted that conductimetry results, for both tested surfactants SDS and Ammonyx, have shown

the same instantaneous evolution and presented the same phenomena at the walls. A variation of 61 and 42% relative to the mean thickness and an increasing of frequency from 37.5 to 77.5 Hz for cases of foam at 1.5 and 4.5 cm/s respectively, are shown in Supplementary- Figure 65 in the Supporting Information.

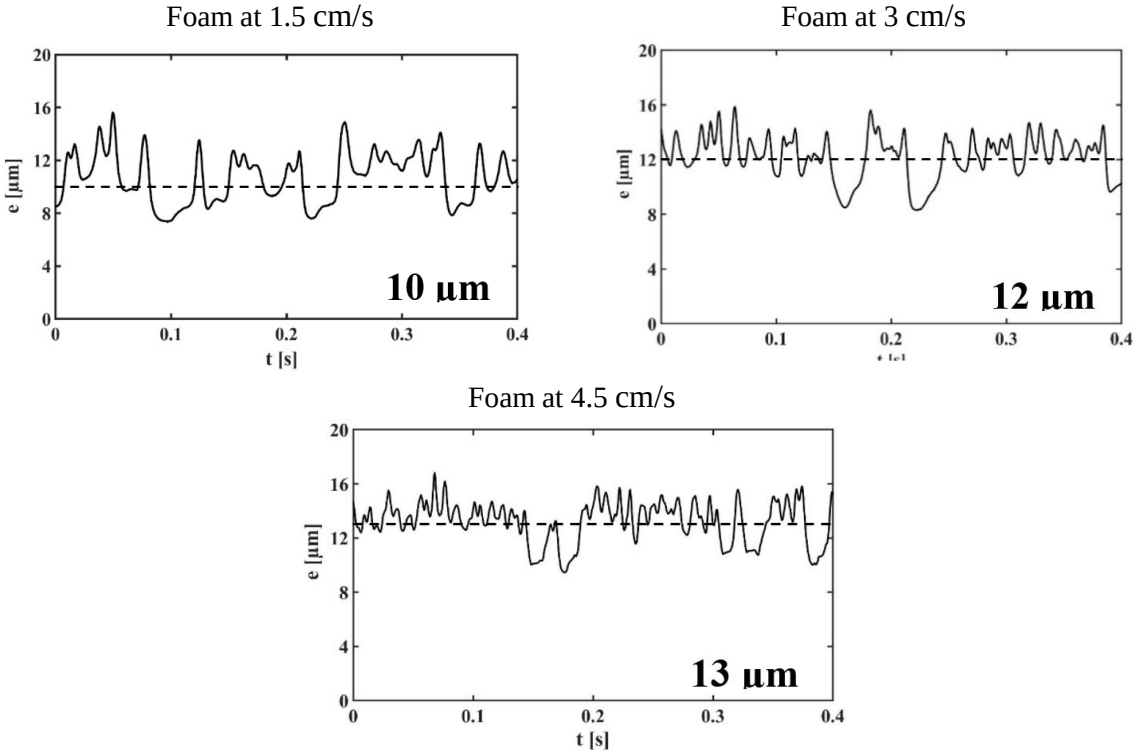

Supplementary- Figure 65. Example of the evolution of wall film thickness given by the temporal signals of conductimetry over the top wall for the three cases, using Ammonyx surfactant. The values indicated in the images show the mean thickness during 40 seconds of acquisition.

III.1.3 Wall shear stress

To highlight the effect of the passage of a bubble on the shear rate at the wall, temporal signals from the frequency response of the polarography probe located in the middle of the channel have been plotted (Figure 64, right).

The wall shear stresses on the upper region of the pipe appeared larger and approximately double the value of the average stress measured on the section (data not shown). This is in relation to the low thickness of the liquid film at this location. The average shear stress increases slower than the foam flow velocity but increases from 4.3 Pa at 1.5 cm/s to 7.2 and 8.1 Pa for velocities of 3 and 4.5 cm/s, respectively. More interesting were the temporal variations of the wall shear stress at the top wall as shown in Figure 64 (right), the signal varies periodically with a more homogeneous pattern with velocity increase but a clear decrease in amplitude but a decrease in amplitude is clearly visible at 4.5 cm/s. The rate of fluctuation of the wall shear (*RFS*) related to the signal amplitude decreases as the foam velocity increases reaching 957, 688, and 491% for the three foam velocities tested, 1.5, 3, and 4.5 cm/s respectively. The passage of bubbles, as seen in the film thickness variations, causes these variations in local shear stress. These fluctuations are therefore characterized by a frequency that corresponds directly to the frequency of bubble sliding on the upper wall.

Observing the spectral densities of the wall velocity gradient, all the curves had almost the same shape of which spectrums obtained with the probes gave a low energy level (Figure 66 in the Supporting Information). The frequencies of bubbles are 20, 39, and 45 Hz for the first three cases respectively. For the other foam conditions, the frequency and the *RFS* were determined by the extrapolation of these experimental results and the theoretical correlations between the frequency and foam parameters (where $f_{bi} = \frac{\beta.v}{d_{bi}}$, $A_{bi} = \frac{v}{f_{bi}}$, and d_{bi} are the frequency, amplitude, and diameter of i bubble). As was expected, foam at higher velocities (9 and 13.5 cm/s) had the highest frequency (76 Hz) with a strong decrease in the wall shear fluctuation rate (130% for foam at 9 cm/s). All results are reported in Table 6.

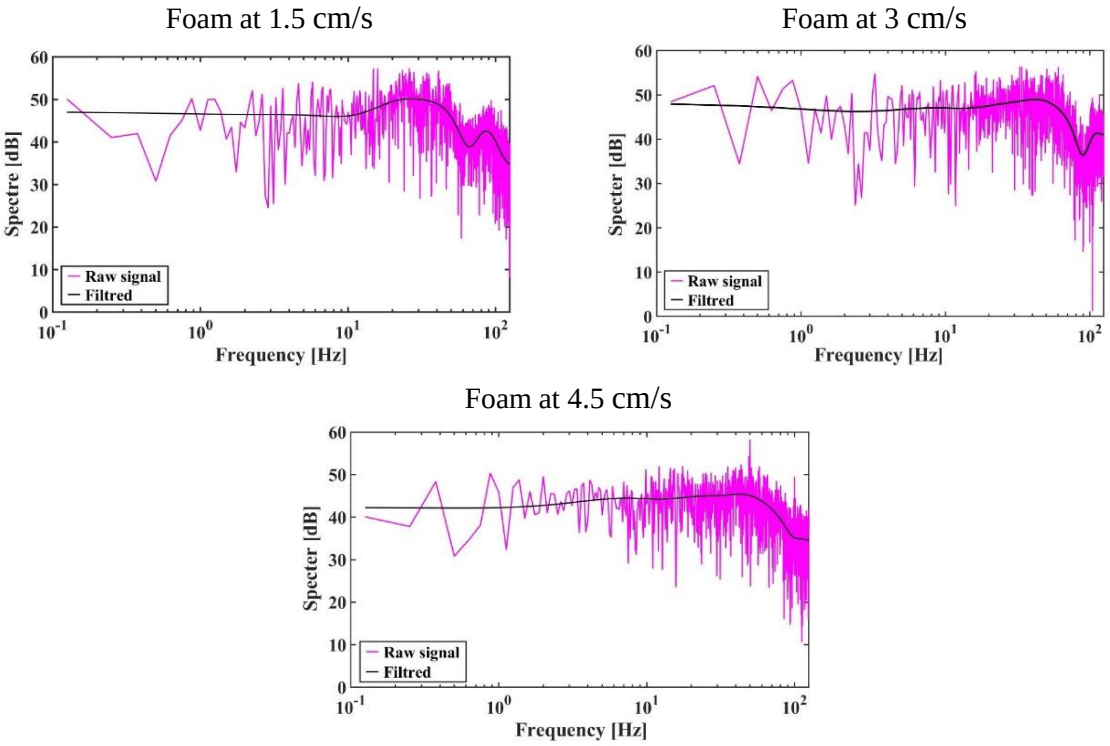

Supplementary- Figure 66. Example of spectral densities of the velocity gradient measured using polarography method for the three cases. This spectrum presentation provides for the identification of the characteristic frequencies corresponding to the passage frequencies of bubbles using Py. (1990) method.

III.2 Spores' detachment

III.2.1 Resistance to cleaning procedures

The cleaning kinetics for the two bacterial spores are presented in Figure 67 based on the evolution of the mean values of the logarithmic reduction of adherent spores with the cleaning time. In all cases, the detachment curves clearly showed two distinct phases. Both phases appeared to be exponential and therefore were quite accurately described by the biphasic model, with R^2 ranging from 0.84 to 0.97. Whatever the flow conditions, the first detachment phase lasted less than 1 min, and the duration of this phase depended on the flow conditions of the foam (shorter at low velocity, for the two spores), but especially on the strain. At 1 min, the resulting log reduction of the adherent spores during this first phase ranged between 1.94 and 2.6, and between 0.95 and 1.33 for *B. subtilis* PY79 and *B. subtilis* PY79 *spsA*, respectively.

The second phase was much longer and would probably continue over 20 min. The detachment rate of the hydrophilic spores (*B. subtilis* PY79) during this second phase was quite low at 1.5, 4.5, and 13.5 cm/s resulting in an additional 0.15-0.28 log reduction of the adherent spores, whereas at 9 cm/s the reduction reached around 1.15 log. A similar trend was observed for the hydrophobic spores with 0.2-0.3 log reduction at 1.5, 4.5, and 13.5 cm/s and 0.45-0.57 log reduction at 9, and 13.5 cm/s.

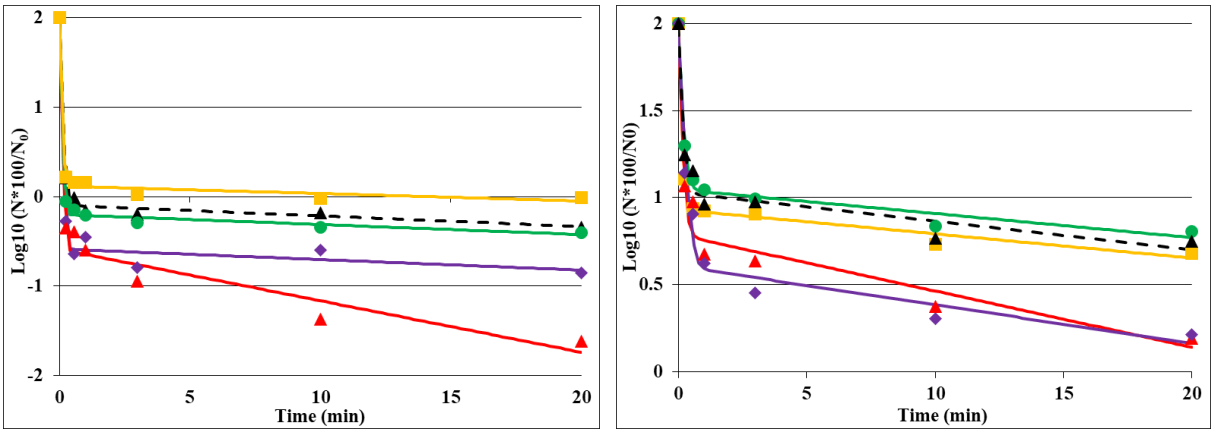

Figure 67. Removal kinetics of *B. subtilis* PY79 (left) and *B. subtilis* PY79 spsA spores under the different flow conditions. Markers showed the data of three repetitions, and the line represents the biphasic fitted model fit to each condition: 1.5 cm/s (yellow square), 4.5 cm/s (green circle), 9 cm/s (red triangle), 13.5 cm/s (purple diamond), and CIP (black triangle).

The role of the flow parameters and strains on the three kinetics parameters (f, k_{max1}, and k_{max2}) was then investigated. When comparing the two strains, the influence of the strains on the removal efficiency during the first phase represented by the two parameters f (poorly adherent fraction of the population) and k_{max1} (first kinetics constant rate) was highly significant as confirmed by the variance analysis ($Pr < 0.0001$ for both parameters). According to Tukey's groupings, f was significantly affected by the strain, with mean values of 0.92 and 0.998 for *B. subtilis* PY79 *spsA* and *B. subtilis* PY79 respectively as shown in Figure 68. The initial detachment rate (k_{max1}) also was largely dependent on the strain (from 1.7 up to 3.4 times higher for hydrophilic spores), while the second detachment rate (k_{max2}) was not affected and was quite similar for the two strains (Figure 68, no significant differences).

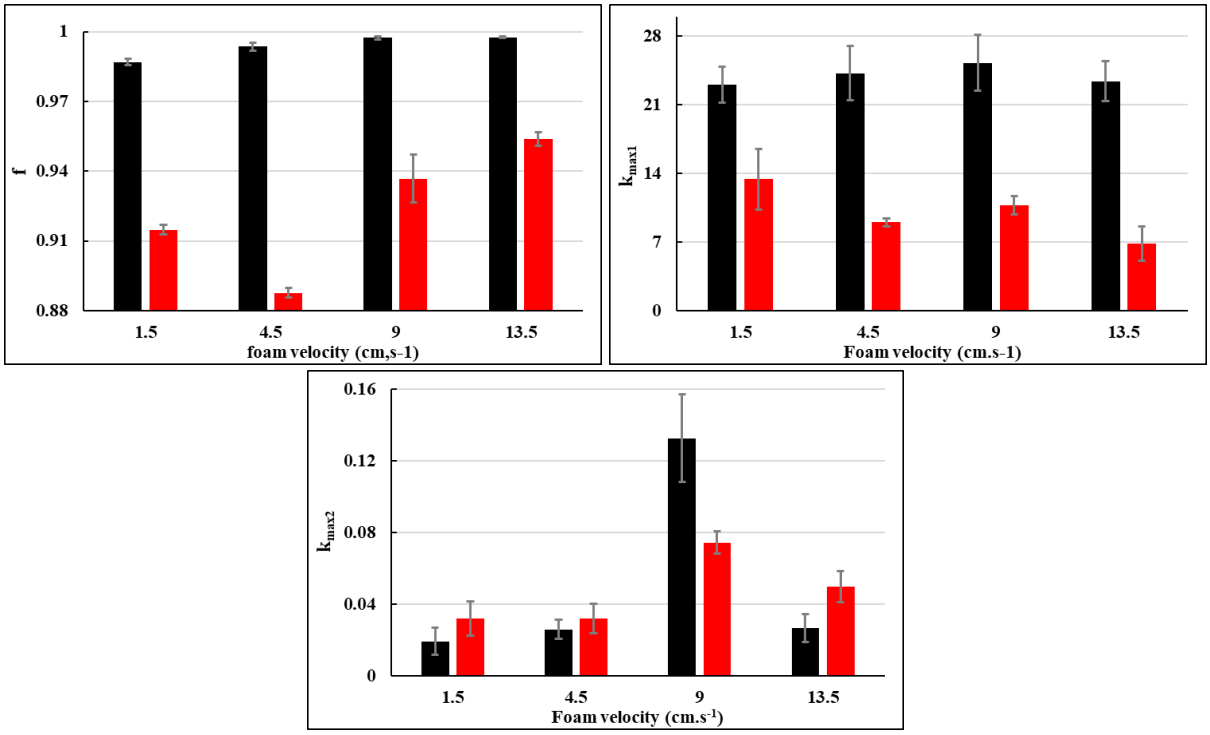

Figure 68. Kinetics parameters f, Kmax1, and Kmax2 for *B. subtilis* PY79 (black color) and *B. subtilis* PY79 *spsA* (red color) spores under different flow conditions.

The role of the flow parameters as the shear stress (mean value, frequency, and *RFS*) and/or to the distribution of bubbles (mean diameter and *F02*) on the three kinetics parameters (*f*, k_{max1}, and k_{max2}) was then investigated (Table 7 and Figure 69 in the Supporting Information). Whatever the parameter in relation to the flow and the bubble size arrangement the Tukey's grouping tests gave the same ranking between the 4 velocities tested (Table 7) and can be visualized clearly in Figure 69, the two groups of parameters as the ones related to the wall shear stress and the ones related to the bubbles' size influencing, in the same way, the removal kinetics. However, differences between the two strains could be stated. For *B. subtilis* PY79, the first kinetics phase rate constant k_{max1} was similar for all the studied cases (no difference according to the Tukey' test) but an effect was observed on *f* with a significant difference between the lowest and the highest velocities (1.5 and 4.5 compared to 9 and 13.5 cm/s) leading however to an improvement while increasing the velocity (Figure 69, black dots in the Supporting Information). Conversely, k_{max2} was significantly higher in the case of foam at 9 cm/s comparatively to the other cases whatever the strains. Some differences could be seen with the hydrophilic spores, according to Tukey's grouping in Table 7 and Figure 69 red dots in the Supporting Information. Indeed, the maximum foam velocity tested induced a significantly higher value of *f* ($Pr < 0.0001$), a phenomenon more marked than with hydrophilic spores, as for k_{max1}, it was significantly higher at this velocity than at the lowest velocity tested ($Pr > 0.013$). However, k_{max2} variation trend with the velocity was similar to those of the hydrophilic strain and also highly significant ($Pr > 0.0007$), the velocity of 9 cm/s being the best option. It should be noted that it was not the highest mean shear stress tested (13.2 Pa), but it has the lowest bubble sizes (mean diameter of 0.18 mm and *F02* of 0.68).

Cleaning with foam was then compared to a CIP procedure (pink and black curves in Figure 67) using the SDS solution at a shear stress of 9.8 Pa, shown to be the most efficient condition

with foam. Concerning hydrophilic spores, the first detachment's phase in the case of CIP was shorter than for foam cleaning and the removal was 0.5 log CFU less efficient. In addition, very few spores were detached in the second phase, resulting in about 2 log CFU reduction after 20 min cleaning compared to around 4 log CFU with foam. The same trend was observed with hydrophobic spores but at a lesser extent, the use of foam allowing an improvement in detachment efficiency of only 0.5 log in 20 min compared to CIP. The variance analysis confirmed that whatever the strains significant differences could be observed between CIP and FFC considering the two kinetics parameters f and k_{max2} (Pr > 0.034 and less than 0.001 respectively), k_{max1} being apparently not significantly modified (Figure 69 in the Supporting Information).

Table 7. Tuckey grouping for PY79 and spsA spores.

Mean Velocity of FFC conditions (cm/s)	f		Kmax1		Kmax2	
	PY79	*spsA*	PY79	*spsA*	PY79	*spsA*
1.5	C	C	A	A	B	B
4.5	B	D	A	AB	B	B
9	A	B	A	AB	A	A
13.5	A	A	A	B	B	B

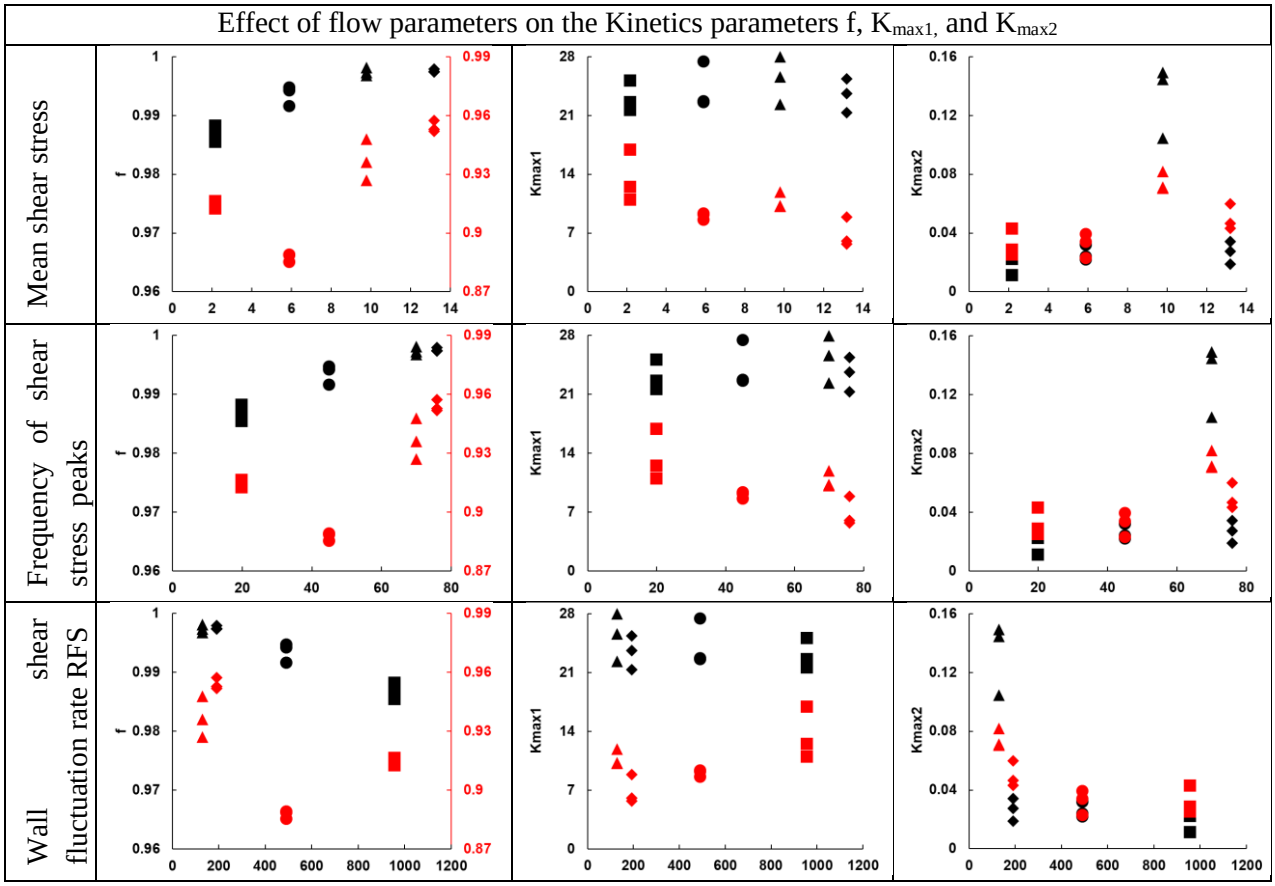

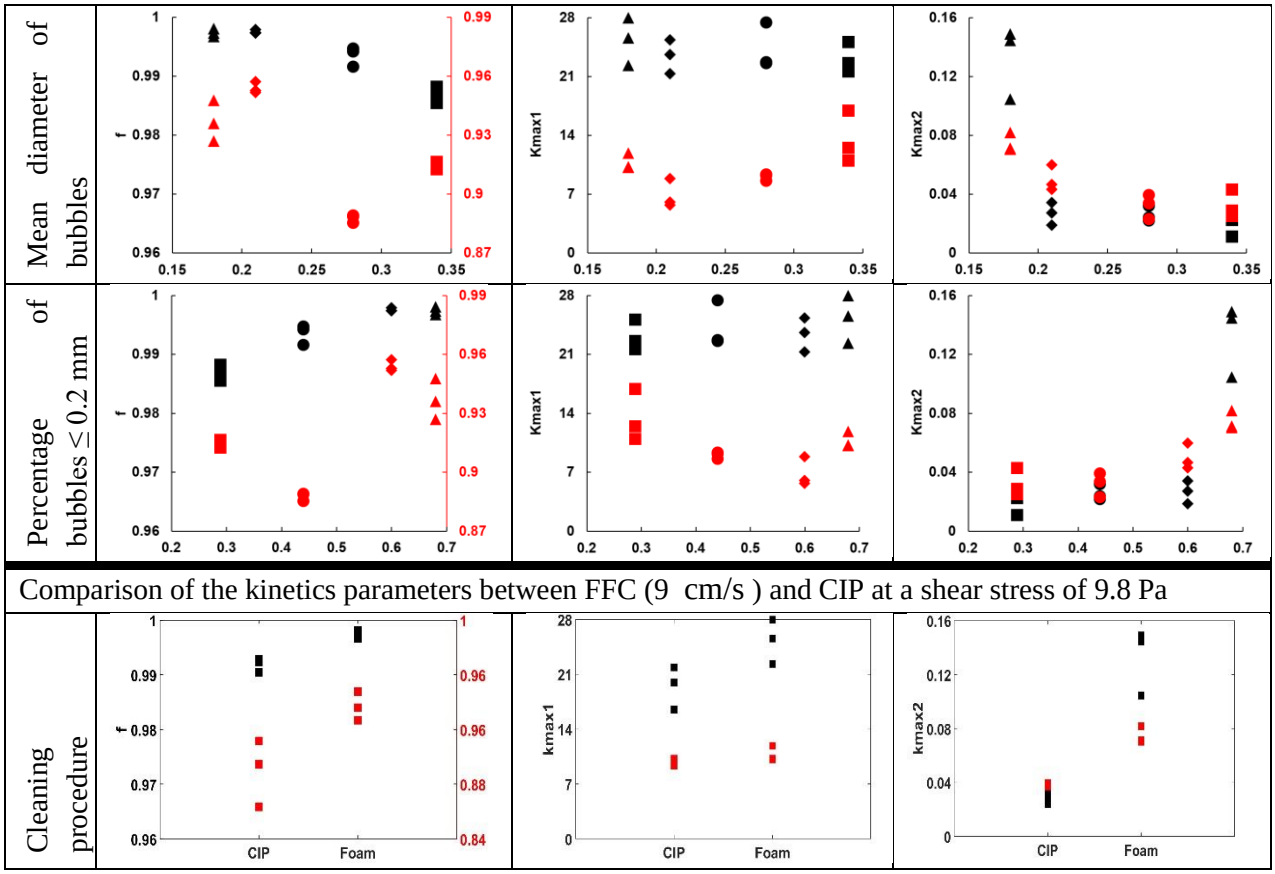

Figure 69. Variations induced on the kinetics parameters f, Kmax1 and Kmax2 for *B. subtilis* PY79 (black color) and *B. subtilis* PY79 *spsA* (red color) spores under different flow conditions: 1.5 cm/s (square), 4.5 cm/s (circle), 9 cm/s (triangle), 13.5 cm/s (diamond), and CIP.

III.2.2 Deposition patterns before and after cleaning

In order to observe whether the different areas of the dried drops were more or less easily removed during the cleaning procedures, the dried deposits were observed before cleaning and after 15 seconds and 20 minutes of cleaning. Two different deposition patterns were observed in epifluorescence microscopy (Supplementary- Figure 70 in the Supporting Information).

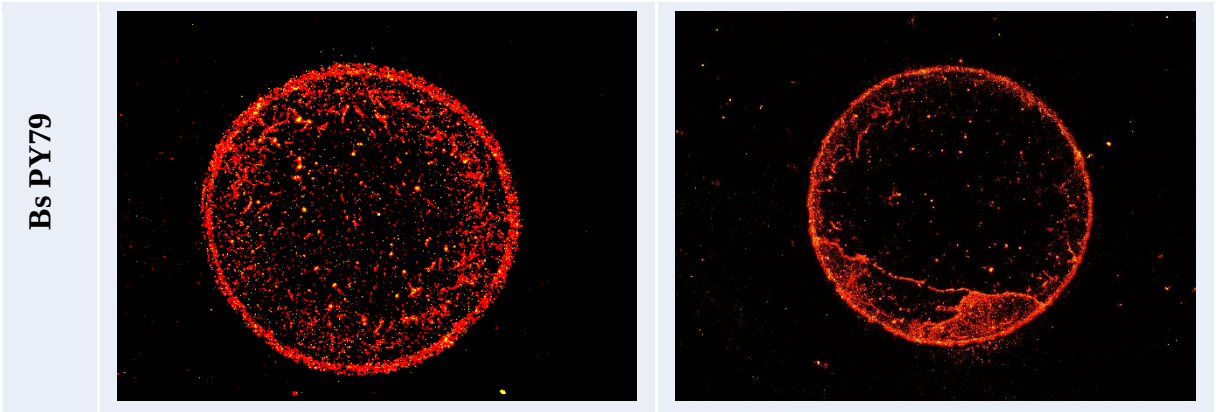

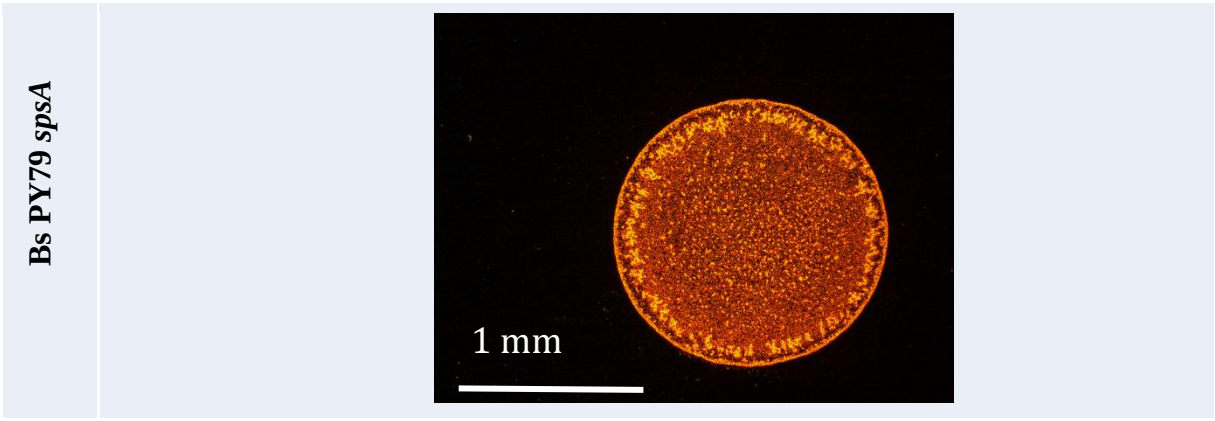

Supplementary- Figure 70. Deposition patterns of *Bacillus* spores before the cleaning procedures, examined by epifluorescence with a Zeiss Axioskop 2 plus microscope (x50).

Whatever the spores, a regular round peripheral ring, often referred to as the "coffee ring" was clearly observed. For *B. subtilis* PY79 spores, this external coffee ring shape was thick with relatively few adhered spores within the ring. Depending on the trial, the internal deposition was more or less regular, as if the contact line remained fixed or detached and then reattached, resulting in one or more small contaminated areas. Conversely, with the hydrophobic spores *B. subtilis* PY79 *spsA*, a diffuse peripheral deposit was often observed, within which single spores but also spore clusters are present over the whole surface.

After cleaning, the observation of the residual patterns shown a good agreement with the enumeration results (Figure 71). First, *B. subtilis* PY79 spores seemed to be removed in a higher extent compared to *B. subtilis* PY79 *spsA* spores. In the case of *B. subtilis* PY79 spores after 15 s, the peripheral ring was partially removed by the cleaning procedure and this was particularly noticeable at 13.5 cm/s, but especially at 9 cm/s. After 20 min of cleaning, the ring had completely disappeared at 9 and 13.5 cm/s and to a lesser extent at 4.5 cm/s. However, spores were still visible on the inner area of the deposits except for foam after 20 min at 9 cm/s. Regarding the cleaning of *B. subtilis* PY79 *spsA* spores, spores, and small clusters seemed to be greatly removed while the larger clusters seemed to have better resisted the detachment, and the peripheral ring was partially removed only after 20 min. For both strains, removal was visibly greater with foam flow at 9 cm/s than CIP. At 15 seconds, the cleaning of the deposits of hydrophobic spores *B. subtilis* PY79 *spsA* seemed to induce a slid of the contamination along the surface in the direction of the flow showing a quite scattered pattern visible with foam flow cleaning and CIP (blue arrows on Figure 71). This sliding phenomenon was absent in the case of hydrophilic spores *B. subtilis* PY79.

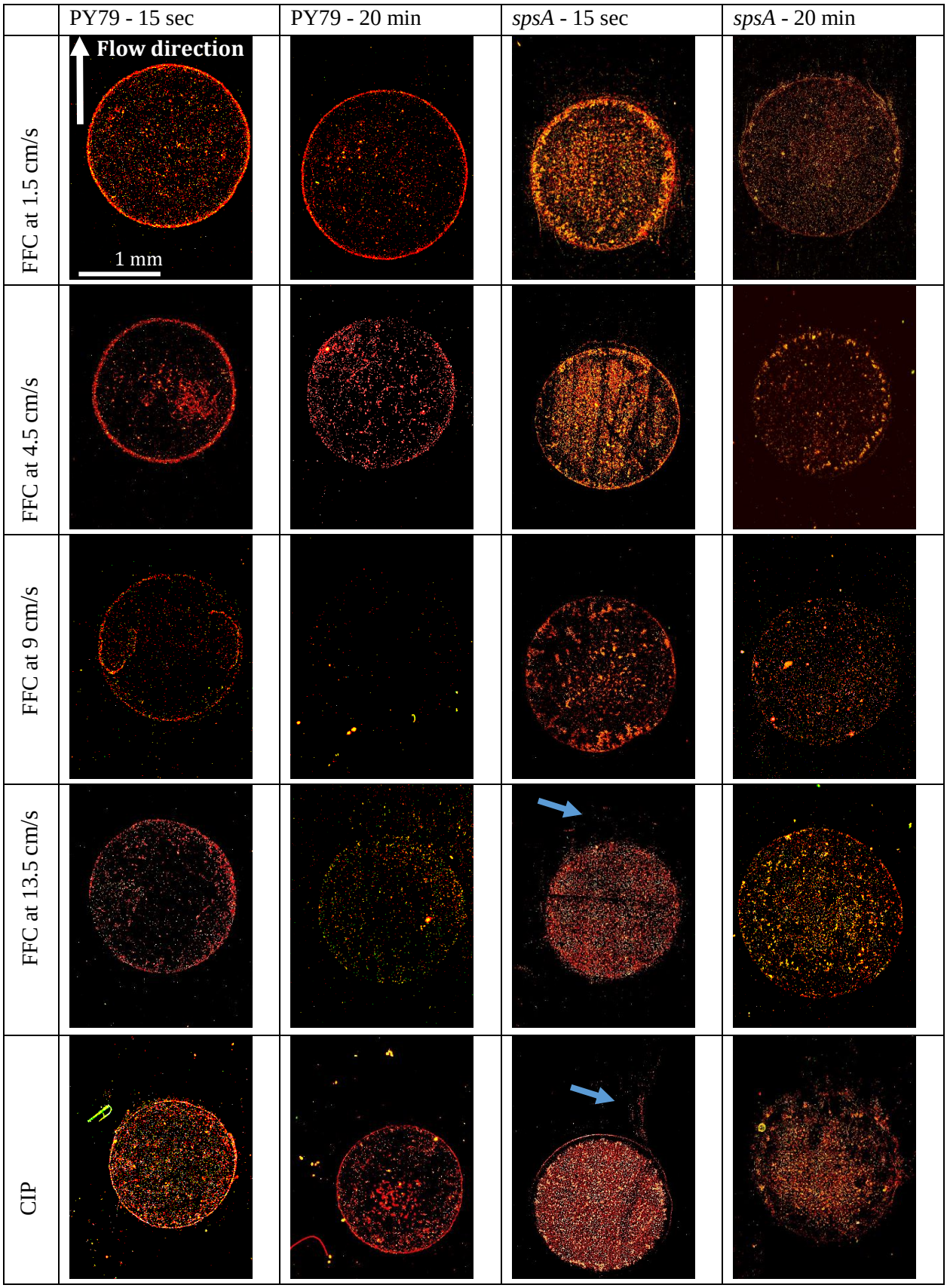

Figure 71. Residual deposition patterns of droplet contaminated with *B. subtilis* spores after complete evaporation and further subjected to 5 seconds and 20 minutes of FFC and CIP

procedures, examined by epifluorescence with a Zeiss Axioskop 2 plus microscope (x50). Blue arrows indicated the sliding of the spores observed at 15 s for *B. subtilis* PY79 spsA.

IV. Discussion

Foam has been considered as a non-Newtonian fluid and the Herschel–Bulkley model can predict its flow behavior as previously described (Dallagi et al., 2019). At low shear stress (2.2 Pa) the foam flow behaved as a plug flow in one direction, the velocity of the foam being uniform over the entire section (1 Dimensional regime). When the wall shear stress exceeded 4.2 Pa the plug behavior remained only at the top side of the duct (2D regime), and at shear stresses greater or equal to 5.9 Pa, the foam became completely sheared (3D regime) (Al Saabi et al., 2021). The rheological behavior of foams is controlled by processes that occur within the microstructures such as the rearrangement of bubble size, liquid film, and Plateau borders. A slight modification on the pressure or the shear stress applied could lead to deformation on the foam state. In previous studies on the rheology of emulsion and foam, authors have demonstrated the deformation of the bubble as a function of the capillary number (Llewellin and Manga, 2005). Their results show that as the capillary number increases, bubbles start to deform and the film separating bubbles either thicken or shrink trends to maintain the minimal surface energy. However, this deformation can result in developing anisotropy in foams properties if the capillary number exceeds a critical value which is not the case here: for all studied cases *Ca* was lower than 0.1 and the bubbles remained almost spherical with isotropy of the foam nearly preserved.

It should be noted that except for the three foam conditions at 1.5, 3, and 4.5 cm/s obtained using 1, 2, or 3 generators with the same surfactant, flow rate, and air pressure content, the increase of the foam velocity up to 9 and 13.5 cm/s was obtained by increasing the surfactant flow rate and air pressure and content in the foam generators. It was demonstrated that the pressure significantly affects the foam texture, and its stability with a potential change in bubble size distributions, liquid drainage, and bubble coalescence (Al-Qararah et al., 2013), a reduction in the average radius of bubbles was observed with the increase of the pressure. These authors reported that the bubble size decreases with the increasing of the rotation speed up to a certain limit under axial mixing in a Becher. At a rotation lower than 5500 RPM (revolution per minute), the foam remains stable since the air is well homogenized in the surfactant solution. Conversely, above 5500 RPM, because of the saturation of air content, the interactions between bubbles were more numerous which favored their coalescence. Thus, their size increases, resulting in a decrease in interfacial stability. The observation of the foam at the highest velocity (13.5 cm/s) allowed to suggest that the large bubbles are more likely the consequence of a movement inside the foam (3D flow regime) allowing the larger bubbles indeed less dense to rise towards the upper wall rather than a coalescence of the bubbles explained by the high speed of the foam. This behavior was probably enhanced by the fact that the foam is quite wet with a quality of 0.5.

Furthermore, the conductimetry and polarography results (Figure 64) demonstrated a significant impact of the velocity of the bubbles and their sizes on the fluctuation of the liquid film thickness between bubbles and the top wall and on the local wall shear stress increases significantly between two consecutive bubbles (Plateau borders). These variations would directly affect bacteria present at the surface influencing the removal phenomenon. The

displacement of the bubbles leads to sudden increases in the Sherwood number due to shear stress peaks, appearing in a harmonic manner directly related to the bubble passage frequency. Comparing foams at 1.5, 3, and 4.5 cm/s, as the velocity increased, the bubbles became smaller with an F02 of 0.29, 0.36, and 0.44. The frequency of the shear stress increased in parallel from 20 up to 45 Hz while amplitude decreased in agreement with previous works (Tisné et al., 2003). Hence, foam at 9 cm/s having a higher amount of small bubble sizes presented the lowest *RFS* (*RFS* of 130 %) with the high frequency (*f* of 70 Hz) related to the thin liquid film height variation measurements. The peaks of the shear stress were clearly observed at the two ends of the bubbles, the bubble front, and the back. As an example, the wall shear stress value between the bubbles is about 15 Pa while it remains lower than 2 Pa under the bubbles, for foam at 4.5 cm/s. These values corresponded therefore to the maximum and minimum film thickness observed, respectively. In the literature, CFD simulations, as well as experimental studies in two-phase gas-liquid slug flow, e.g. in capillary membranes (Kumari et al., 2018), suggested that the major contribution to the wall shear stress came from the bubbles ends and could be attributed to the Laplace pressure difference caused by the surface tension. (Tisné et al., 2004) revealed that it was possible to relate foam flow study to studies of a long bubble moving in capillaries, and they observed that the bubbles moved as flattened bubbles in a Hele-Shaw cell confirming the localization of the shear stress on the Plateau borders.

When compared with spore removal kinetics, parameters in relation to the shear stress and bubble size variations seemed to play a significant role in the cleaning efficiency of foam flow. For both *B. subtilis* strains, the increase of the mean shear stress roughly leads to an improvement in the cleaning efficiency. However, it was not true for the foam at 13.5 cm/s [1], which showed a reduction in cleaning efficiency, compared to 9 cm/s. This result suggests that other parameters than the mean shear stress were involved in the FFC efficiency and therefore the variation of the local wall shear stress as discussed above in relation to the size and the velocity of the bubbles could play a major role. These results are consistent with previous works in literature. Silva et al. highlighted the significant role of the wall shear stress fluctuation on the cleaning efficiency using pulsed flow (Silva et al., 2021). Results showed that shorter periods promoted higher removal of raw milk cells due to the occurrence of the annular effect and its important frequency. A higher frequency of peaks wall shear stress was needed to make turbulent pulse flow effective to remove tomato deposits (Absi and Azouani, 2018). The authors explained obtained results by the fact that at higher frequency the surfaces are submitted more often to the phenomenon caused by peaks. Hence, as the foam has a higher amount of small bubbles, the contamination will be more subjected to the pick of wall shear stress and perhaps also to the viscous dissipation in the narrow Plateau borders between consecutive bubbles since smaller bubbles possess a higher Laplace pressure.

Whatever the FFC conditions, the removal kinetics showed a strong detachment rate at the beginning of the cleaning process (less than 1 min), followed by a second kinetic phase described by a slow detachment rate. Previous works on biofilm removal under CIP (Bénézech and Faille, 2018) and bacteria spores under different foam qualities (Al Saabi et al., 2021) have reported similar observations. Neither the shear stress nor the bubble size has affected the first kinetic phase rate of removal with *B. subtilis* PY79 spores, while high shear stress induced low k_{max1} with *B. subtilis* PY79 *spsA*. For both strains, as the shear stress increased, the *f* parameter increased (the spore population detached more easily). The synergy between high shear stress

and small bubbles (foam at 9 cm/s) would explain the highest k_{max2} and a better cleaning efficiency. To prove or disprove this suggestion, a new foam flow condition was produced at 9 cm/s, using a single generator. The air pressure in the generator in this condition was 3 times more than that for the 9 cm/s foam, produced by three parallel generators. As was expected, the mean shear stress was 9.8 Pa, while the bubble size increased (mean diameter of 0.19 mm with a presence of large bubbles (Supplementary- Figure 72 in the Supporting Information). When comparing the second detachment phases, foam with the smallest bubbles was more efficient for PY79 spores, by 1 log CFU over 20 min. k_{max2} was 1.5 times higher (with 9.8 Pa foam and small bubble size) than that in the alternative condition tested. For *B. subtilis spsA* spores, k_{max2} seems to be similar in these two conditions.

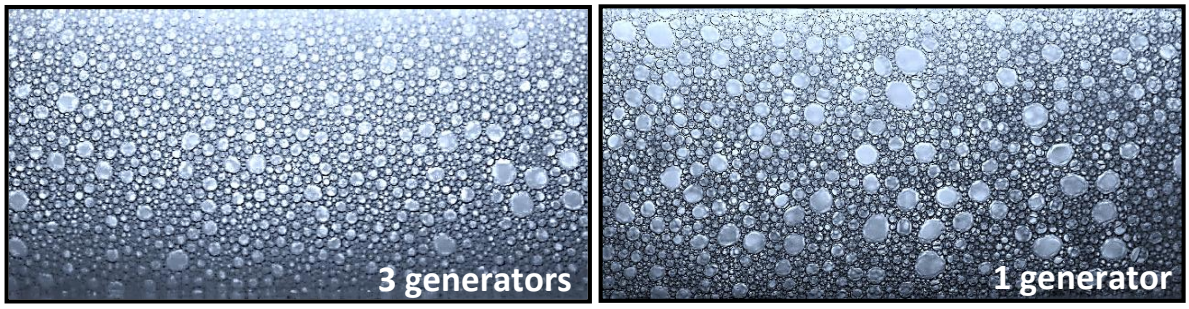

Supplementary- Figure 72. Top view of foam visualization at the wall of the transparent pipe upstream the test ducts for foam flow at 9 cm/s, using simultaneously 3 generators (left) or a single generator (right).

According to (Kondjoyan et al., 2009), the role of capillary forces is not negligible and depends on the size of the bubbles and their speed. In (Al Saabi et al., 2021), the detachment of the hydrophilic spores of *Bacillus amyloliquefaciens* 98/7 occurred at bubble velocities of around 3 cm/s and dramatically decreased at 5 cm/s in line with the work of (Kondjoyan et al., 2009), where the greatest detachment rate was observed, as illustrated by high k_{max1} constant rate values. In this work, no visible changes could be seen for the first kinetic phase with the increase in the foam velocity from 9.5 up to 13.5 cm/s, but the second kinetic phase showed a significant decrease in the removal efficiency. For hydrophobic particles, according to (Kondjoyan et al., 2009), the detachment rate would start at higher bubble velocities. In this work, the increase in the foam velocity indeed was accompanied by an increase in the detachment efficiency during the first minutes of the foam cleaning, which corresponds to an increase in the *f* parameter, resulting in a more rapid and efficient spore removal.

Other phenomena would occur under the combination of the drainage and the imbibition effects (Figure 73). It is known that under gravity and capillarity, the liquid flows through drainage networks called Plateau borders. This phenomenon has been demonstrated in previous works (Maestro et al., 2013). Thus, as discussed before, the spores present in the thin liquid film between the bubble and the solid surface are prone to be absorbed within the Plateau borders under the imbibition effect. This mechanism is driven by the capillary forces. Indeed, these Plateau borders have a curvature that creates a capillary under-pressure in the liquid phase. Owing to this pressure difference, the foam was able to absorb the spores (which were in small size,1 µm), just as a sponge would. It has been proven in the literature that the imbibition

mechanism was highly dependent on the bubble size, which is the strongest for foam with a smaller bubble size (Maestro et al., 2013; Mensire et al., 2015). On the other hand, such a mechanism could help in understanding the difference in the results obtained by the two strains of spores. Unlike hydrophilic spores which can be easily trapped by the liquid film, absorbed into the Plateau border and then flushed out of the pipe, the hydrophobic character of *B. subtilis* PY79 *spsA* gives spores a strength to oppose the imbibition effect. They mostly remain in the liquid film and then due to bubble fluctuations, some of them are able to re-adhere to the solid surface. To highlight this phenomenon, the ability of hydrophobic spores to adhere to sterile coupons was tested at a distance of around 10 cm downstream of the contaminated area. Whatever the flow conditions, results showed that 1.3% of the detached hydrophobic spores after 20 min of cleaning were able to re-adhere to the surface. Comparatively, the re-adhesion of hydrophilic spores was found to be negligible, at less than 0.1% of the detached spores after 20 min. Otherwise, due to the continuous fluctuations of the shear stress and the liquid film thickness induced by the bubble passage, some spores that were strongly attached to the surface were pushed to other locations, thereby causing a sliding phenomenon. This phenomenon was more visible in the case of hydrophobic spores than for hydrophilic ones. This could be explained by the strongly hydrophobic character of *B. subtilis* PY79 *spsA*. Recently, Schad et al. have shown that foams with small bubble sizes are more efficient in cleaning glass surfaces contaminated with fluorescent oil (Schad et al., 2021). The authors explained the cleaning by an interplay of imbibition, drainage, and wiping mechanisms. Imbibition and drainage of oil into the Plateau borders of foams were found to be the strongest with small bubbles, which is in concordance with our results. However, the wiping mechanism, i.e., shifting of the contact line between foam, oil and glass was found to be more efficient with unstable foam than with a stable one. This is not surprising since they used static foam. Given similar conditions, unstable foams clearly clean better than stable foams, being continuously in motion and accelerating the re-arrangements of their bubbles with time which leads, as they explained, to violent wiping motions between the foams and the interface. Consequently, these are not completely irrelevant with our work since in our study foams were used in a dynamic form and the movement/flow was imposed, leading to forceful wiping. However, the instability of foam can reduce the cleaning efficiency through the generation of large bubbles (as observed in the case of foam at 9 cm/s).

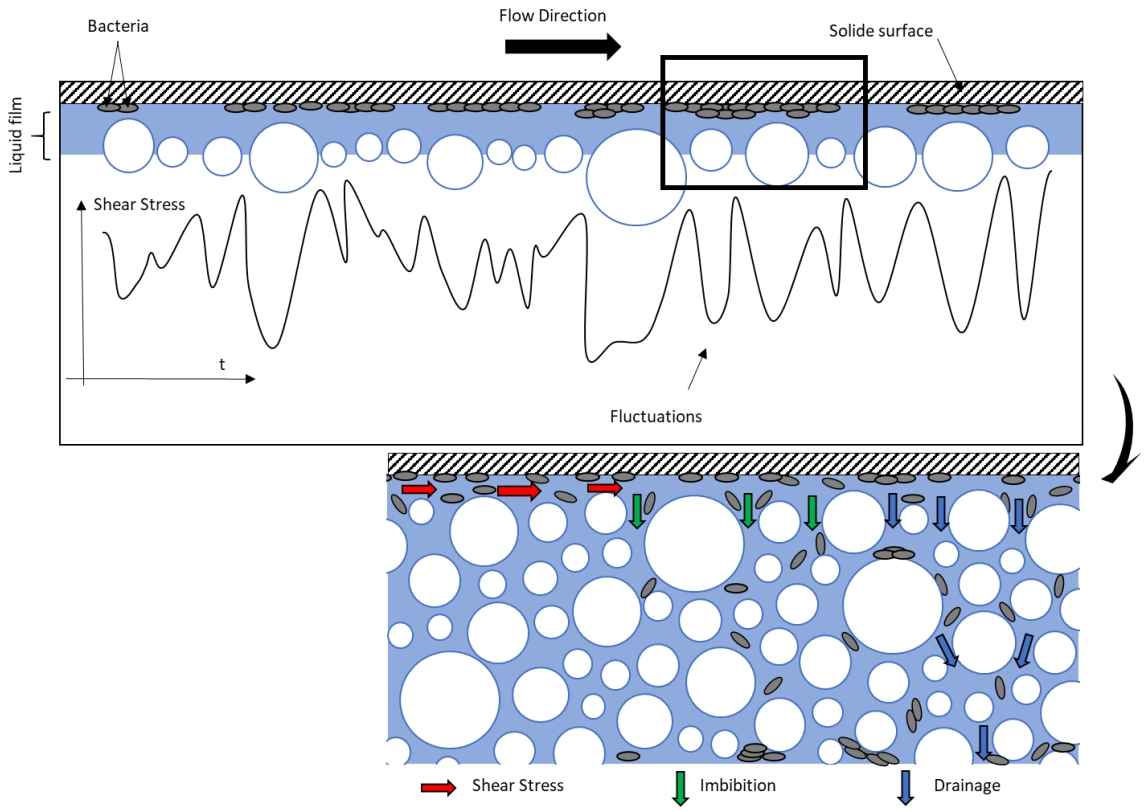

Figure 73. Schematic of the suggested cleaning mechanisms using foam flow.

V. Conclusion

In this study, we analysed the ability of wet foam flow to remove *Bacillus subtilis* spores from dried droplets on stainless steel surfaces. Two strains, *B. subtilis* PY79 and *B. subtilis* PY79 *spsA*, of different hydrophobicities were used. Regardless of the strain, the foam flow showed a better removal capacity than conventional cleaning in place at the same average shear stress. Optimisation and improvement of cleaning efficiency using foam flow requires a quantification of the key parameters, such as bubble size, liquid film thickness and wall shear stress. Analyses obtained from polarography, conductimetry and bubble size quantification have shown that the magnitude and frequency of fluctuations in wall shear stress and liquid film thickness are related to bubble size and flow velocity. These phenomena are most likely to be the cause of spore removal, as described in the literature, although to a lesser extent, for cleaning with liquid solutions. In contrast, with foam, the particularity of fluctuations at the wall (liquid film thickness and shear stress) in relation to the bubble sizes and their velocities, combined with other probable phenomena such as imbibition and drainage of the liquid film within the foam, favours not only the release of contaminants, but also their entrapment. This leads to the conclusion that a combination of high wall shear stress, and the presence of small bubbles (<0.2 mm) indeed improves surface biocontamination cleaning efficiency. Further studies would be interesting to test the ability of this process to clean actual industrial equipment, which is frequently of complex design. Further research could also be carried out into the removal of other types of microbial fouling by these flowing foams, such as into biofilm contaminations developed on the surfaces of materials other than steel, such as polymers, which are sometimes rougher and often more hydrophobic. The implementation of such a foam cleaning technology

for CIP cleaning would request an effective foam removal during the rinsing step. Future work could be envisaged to solve this problem using stimuli-responsive surfactants allowing at request a complete disappearance of the foam.

ACKNOWLEDGMENTS

The authors are grateful to Christelle Lemy and Laurent Wauquier from UMET, for their valuable technical assistance.

FUNDING

This work was supported by the region Hauts-de-France through their funding of the Interreg Veg-I-Tec project (Programme Interreg V France-Wallonia-Flanders, GoToS3) and the ANR (Agence Nationale de la Recherche) for funding of the FEFS project (contract number ANR-18-CE21-0010).

References

Absi, R., Azouani, R., 2018. Toward automatic cleaning of industrial equipment: pulsed flow-induced wall shear stress. Procedia CIRP 78, 359–363. https://doi.org/10.1016/j.procir.2018.10.001

Al Saabi, A., Dallagi, H., Aloui, F., Faille, C., Rauwel, G., Wauquier, L., Bouvier, L., Bénézech, T., 2021. Removal of Bacillus spores from stainless steel pipes by flow foam: Effect of the foam quality and velocity. Journal of Food Engineering 289, 110273. https://doi.org/10.1016/j.jfoodeng.2020.110273

Al-Qararah, A.M., Hjelt, T., Koponen, A., Harlin, A., Ketoja, J.A., 2013. Bubble size and air content of wet fibre foams in axial mixing with macro-instabilities. Colloids and Surfaces A: Physicochemical and Engineering Aspects 436, 1130–1139. https://doi.org/10.1016/j.colsurfa.2013.08.051

Alvarez-Ordonez, A., Coughlan, L.M., Briandet, R., Cotter, P.D., 2019. Biofilms in Food Processing Environments: Challenges and Opportunities. Annu. Rev. Food Sci. Technol. 10, 173–195. https://doi.org/10.1146/annurev-food-032818-121805

Bénézech, T., Faille, C., 2018. Two-phase kinetics of biofilm removal during CIP. Respective roles of mechanical and chemical effects on the detachment of single cells vs cell clusters from a Pseudomonas fluorescens biofilm. Journal of Food Engineering 219, 121–128. https://doi.org/10.1016/j.jfoodeng.2017.09.013

Blel, W., Legentilhomme, P., Bénézech, T., Fayolle, F., 2013. Cleanabilty study of a Scraped Surface Heat Exchanger. Food and Bioproducts Processing 91, 95–102. https://doi.org/10.1016/j.fbp.2012.10.002

Dallagi, H., Al Saabi, A., Faille, C., Benezech, T., Augustin, W., Aloui, F., 2019. CFD Simulations of the Rheological Behavior of Aqueous Foam Flow Through a Half-Sudden Expansion, in: Volume 1: Fluid Mechanics. Presented at the ASME-JSME-KSME 2019 8th Joint Fluids Engineering Conference, American Society of Mechanical Engineers, San Francisco, California, USA, p. V001T01A030. https://doi.org/10.1115/AJKFluids2019-4650

Deleplace, M., Dallagi, H., Dubois, T., Richard, E., Ipatova, A., Bénézech, T., Faille, C., 2021. Structure of deposits formed by drying of droplets contaminated with Bacillus spores

determines their resistance to rinsing and cleaning. Journal of Food Engineering 110873. https://doi.org/10.1016/j.jfoodeng.2021.110873

Delmas, G., Jourdan da Silva, N., Pihier, N., Weil, F.-X., Vaillant, V., De Valk, H., 2010. Les toxi-infections alimentaires collectives en France entre 2006 et 2008 6.

Dubois, T., Krzewinski, F., Yamakawa, N., Lemy, C., Hamiot, A., Brunet, L., Lacoste, A.-S., Knirel, Y., Guerardel, Y., Faille, C., 2020. The sps Genes Encode an Original Legionaminic Acid Pathway Required for Crust Assembly in Bacillus subtilis. mBio 11, e01153-20, /mbio/11/4/mBio.01153-20.atom. https://doi.org/10.1128/mBio.01153-20

Faille, C., Lemy, C., Allion-Maurer, A., Zoueshtiagh, F., 2019. Evaluation of the hydrophobic properties of latex microspheres and Bacillus spores. Influence of the particle size on the data obtained by the MATH method (microbial adhesion to hydrocarbons). Colloids and Surfaces B: Biointerfaces 182, 110398. https://doi.org/10.1016/j.colsurfb.2019.110398

Farag, M.A., Mesak, M.A., Saied, D.B., Ezzelarab, N.M., 2021. Uncovering the dormant food hazards, a review of foodborne microbial spores' detection and inactivation methods with emphasis on their application in the food industry. Trends in Food Science & Technology 107, 252–267. https://doi.org/10.1016/j.tifs.2020.10.037

Ioana, C., Mansour, A., Quinquis, A., Radoi, E., 2007. Le traitement du signal sous Matlab: Pratique et applications, Hermes Science.

Kondjoyan, A., Dessaigne, S., Herry, J.-M., Bellon-Fontaine, M.-N., 2009. Capillary force required to detach micron-sized particles from solid surfaces—Validation with bubbles circulating in water and 2μm-diameter latex spheres. Colloids and Surfaces B: Biointerfaces 73, 276–283. https://doi.org/10.1016/j.colsurfb.2009.05.022

Kriegel, A.T., Ducker, W.A., 2019. Removal of Bacteria from Solids by Bubbles: Effect of Solid Wettability, Interaction Geometry, and Liquid–Vapor Interface Velocity. Langmuir 35, 12817–12830. https://doi.org/10.1021/acs.langmuir.9b01941

Kumari, S., Kumar, N., Gupta, R., 2018. Effect of gas–liquid ratio on the wall shear stress in slug flow in capillary membranes. Asia-Pac J Chem Eng 13, e2258. https://doi.org/10.1002/apj.2258

Llewellin, E.W., Manga, M., 2005. Bubble suspension rheology and implications for conduit flow. Journal of Volcanology and Geothermal Research 143, 205–217. https://doi.org/10.1016/j.jvolgeores.2004.09.018

Maestro, A., Drenckhan, W., Rio, E., Höhler, R., 2013. Liquid dispersions under gravity: volume fraction profile and osmotic pressure. Soft Matter 9, 2531. https://doi.org/10.1039/c2sm27668b

Mensire, R., Piroird, K., Lorenceau, E., 2015. Capillary imbibition of aqueous foams by miscible and nonmiscible liquids. Phys. Rev. E 92, 053014. https://doi.org/10.1103/PhysRevE.92.053014

Mierzejewska, S., Masłowska, S., Piepiórka-Stepuk, J., 2014. Evaluation of the efficiency of removing protein deposits from various surfaces by foam cleaning. Agricultural Engineering 131–137. https://doi.org/10.14654/ir.2014.149.014

Mitchell, J.E., 1965. Investigation of wall turbulence using a diffusion-controlled electrode. University of Illinois.

Schad, T., Preisig, N., Blunk, D., Piening, H., Drenckhan, W., Stubenrauch, C., 2021. Less is more: Unstable foams clean better than stable foams. Journal of Colloid and Interface Science 590, 311–320. https://doi.org/10.1016/j.jcis.2021.01.048

Silva, L.D., Filho, U.C., Naves, E.A.A., Gedraite, R., 2021. Pulsed flow in clean-in-place sanitization to improve hygiene and energy savings in dairy industry. J Food Process Eng 44. https://doi.org/10.1111/jfpe.13590

Tisné, P., Aloui, F., Doubliez, L., 2003. Analysis of wall shear stress in wet foam flows using the electrochemical method. International Journal of Multiphase Flow 29, 841–854. https://doi.org/10.1016/S0301-9322(03)00038-7

Tisné, P., Doubliez, L., Aloui, F., 2004. Determination of the slip layer thickness for a wet foam flow. Colloids and Surfaces A: Physicochemical and Engineering Aspects 246, 21–29. https://doi.org/10.1016/j.colsurfa.2004.07.014

Publication III: Is foam flow cleaning effective and environmentally friendly in controlling the hygiene of surfaces contaminated with biofilms?

Heni DALLAGI[a], Christine FAILLE[a], Cosmin GRUESCU[a], Fethi ALOUI[b], Thierry BENEZECH[a*]

[a] Univ. Lille, CNRS, INRAE, Centrale Lille, UMET, F-59000 Lille, France
[b] Polytechnic University Hauts-de-France, LAMIH CNRS UMR 8201, Campus Mont-Houy, F-59313 Valenciennes, France

*Corresponding Author: Thierry BENEZECH, INRAE, UMET, 369 rue Jules Guesde, F-59650 Villeneuve d'Ascq, France. thierry.benezech@inrae.fr

Highlights

- Wall shear stress increase improved the cleaning efficiency of foam flow likely explained by the increase in the local wall shear stress frequency and amplitude at the same time.
- According to the biofilm structure, the action of the foam flow could differ but the largest biofilms' clusters remained difficult to be removed
- Foam flow being more effective than the corresponding CIP conditions for biofilm removal.
- Foam cleaning could decrease water/energy consumption with less environmental impacts.

Abstract
The aim of this work was to investigate the capacity of foam flow of the detachment kinetics of biofilms from stainless steel surfaces. Three bacterial strains (*Escherichia coli* SS2, *Bacillus cereus* 98/4, and *Pseudomonas fluorescens* Pf1) were grown 24h in a horizontal position. Different foam flow conditions were performed, by varying the shear stress and the bubble size of a wet foam (liquid fraction of 0.5). Whatever the bacterial strain, foam flow cleaning was more efficient on biofilm detachment than the conventional cleaning in place. The increase of the wall shear stress has improved the cleaning efficiency. Then, a Life Cycle Assessment study was performed to investigate the environmental impacts of the foam flow cleaning process. Compared to CIP processes (using NaOH, or SDS surfactant) foam flow cleaning showed significant benefits on the environmental impacts with a drastic reduction of water and energy consumptions.

Keywords
Flow foam cleaning; cleaning-in-place; Biofilm; detachment kinetics; Life Cycle Assessment; environmental impacts; shear stress

I. Introduction

Biofilms are a major challenge for the food industry due to their ability to attach to surfaces. Their formation is affected mainly by the surface properties of the materials (such as physiochemistry and roughness) and bacterial strains, as well as by the flow arrangements, and position of surfaces (Bouvier et al., 2021; Jha et al., 2020a, 2022). These biofilms are often resistant to the hygiene procedures implemented in the food industries, and can therefore be responsible for cross-contamination of food in contact with insufficiently cleaned or disinfected surfaces (Brooks and Flint, 2008). The consequences of these cross-contaminations can be disastrous for the industry as they can lead to food spoilage, but also to gastroenteritis epidemics since these biofilms can harbor pathogenic bacteria such as *Listeria monocytogenes*, *Salmonella spp*., *Vibrio spp*. Indeed, a 1995 WHO survey in Europe (Reij et al., 2004) indicated that nearly 25% of foodborne outbreaks could be attributed to recontamination. A recent example concerned an outbreak of *L. monocytogenes* in South Africa between 2017 and 2018 (1060 confirmed cases, 216 deaths). The origin of the contamination was shown to be a delicatessen factory of the Enterprise Group, where poor hygiene conditions were found. The possibility of such contamination in the food industry imposes strict prevention and removal/disinfection measures to be taken. Nowadays, cleaning-in-place (CIP) is a routine method in the food and pharmaceutical industries. It is an automated process that consists of cleaning, without having to remove or disassemble pipe works and equipment in processing lines, by circulating either water or detergents including the use of high-pressure spray impingement specifically for tanks. According to Sinner's Circle, the accurate combination of the influencing factors such as time, temperature, chemistry, as well as the mechanical action generated by the fluid flow, tends to make cleaning a reliable and optimized process (Grandillo and Tatianchenko, 2020; Holah, 2014).

In particular, several works were performed to study the effect of the hydrodynamics of the cleaning fluid on the efficiency of biofilm removal. The objective was to identify the detachment behavior of bacterial contamination from surfaces by varying the shear forces applied to the wall. For some studies, the wall shear forces allow detachment or at least disruption of the biofilms. Others have defined threshold stress, below which the detachment of a biofilm can be achieved. However, exceeding this shear stress value, a compression of biofilms could occur. The use of pulsed or jet flows demonstrated the beneficial effect of increasing the wall shear stress and its fluctuations on the enhancement of bacterial removal (Blel et al., 2013, 2007; Silva et al., 2021). Diphasic flow, as foam or air bubbles in a liquid, were found to improve the removal efficiency of bio-contamination (Al Saabi et al., 2021a; Charlène, 2018; Toquin et al., 2020).

For example, a recent study on the removal of *Chlorella Vulgaris* biofilms from the surfaces of a photobioreactor using bubbles showed that the surface layers of the biofilm are considered to be the least adherent were periodically detached. The first layers of the biofilm were more resistant to detachment and the soiled surfaces were suitable for the recruitment of new cells. Increasing the fluctuation of shear stress at the wall was a means of increasing detachment rates and this phenomenon was mainly related to bubble size (Charlène, 2018). In addition, wet foam flow showed promising results in removing Bacillus spores from stainless steel surfaces. Compared to a related CIP process, foam flow cleaning was found to be more effective due to

fluctuating wall shear stress, liquid drainage, and capillary imbibition. However, no information is still available regarding the removal of biofilms by foam flows, and biofilms are considered as complex structures e.g. extracellular polymeric substances (EPS) act as a binder between cells (Crouzet et al., 2014).

It is widely recognised that these CIP procedures are very energy, potable water and detergent intensive. For example, in the dairy industry, hygiene procedures are responsible for about 28% of total water consumption (van Buuren and Prasad, 2005) and almost 14% of energy consumption (Piepiórka-Stepuk et al., 2017). Additionally, this sector accounts for around 10, 5, and 4% of the potential for eutrophication, global warming, and photochemical ozone creation of the total European, respectively (Böhringer et al., 2009).

Today, many efforts are needed to better control and properly optimize the sustainability of food processing, whether by increasing the productivity of each unit process, or by reducing its demands for water and energy, and hence less environmental impacts. There have been a few publications assessing the environmental impacts of the manufacturing process in food industries with a detailed assessment of the contributions of individual unit processes (Gésan-Guiziou et al., 2019; Tsai et al., 2021). This type of assessment at the unit process level could clarify the critical phases that require an appropriate intervention. To this end, Life cycle assessment (LCA) is a mandatory approach for any new proposed processes.

Foam flow cleaning has therefore been proposed as an alternative method to improve the hygiene in food industry and to save the energy used in cleaning phases. To this end, we have recently initiated a new line of research to identify the effectiveness of foam flow cleaning in place, as this procedure would result in significant savings in energy, water and detergents (Dallagi et al., 2022).

This work aimed to evaluate the capacity of foam flow to remove biofilm contaminations from stainless-steel surfaces. The removal kinetics of three biofilm strains (*Escherichia coli* SS2, *Bacillus cereus* 98/4, and *Pseudomonas fluorescens* Pf1) were investigated under different flow conditions (foam at 2.2, 5.9, 9.8, 13.2 Pa, and CIP at 10 Pa). Then an LCA was presented to compare the environmental impact of different cleaning methods, foam flow and CIP (using SDS surfactants) and conventional CIP (using NaOH).

II. Materials and methods

II.1 Bacterial strain

In this study, three bacterial strains previously shown to form biofilms (Jha et al., 2022) were used as model microorganisms. *Pseudomonas fluorescens* 1 (subsequently named Pf1) isolated by ANSES from cleaning-in-place wastewater, *Escherichia coli* SS2 (Ec-SS2) expressing a green fluorescent protein (Gomes et al., 2017), and lastly *Bacillus cereus* 98/4 (Bc-98/4) isolated from a dairy processing line.

II.2 Soiled material and Biofilm formation

Biofilms were produced on AISI 316 stainless steel coupons (45 mm × 15 mm) with a pickled (2B) finish (kindly provided by APERAM, Isbergues, France). In order to have surface properties relevant to those found in food processing lines, the stainless-steel coupons were subjected to a conditioning procedure using milk and sodium hydroxide, as was previously

described (Dallagi et al., 2022). Then, before each experiment, they were cleaned using alkaline detergent (RBS T105, Traitements Chimiques des Surfaces, France). 24 h before the experiments, coupons were disinfected in a dry heat oven at 180 °C for 1 h.
In this study, the biofilm formation was performed as follows. The cleaned and disinfected coupons were immersed horizontally in Petri-dishes of 14 cm diameter containing 50 mL of the bacterial suspensions consisting of 1/10 TSB inoculated with 24 h-cultures of each strain (concentration of about ± 10^7 CFU.mL^{-1}). After a 24 h incubation at 30 °C, soiled coupons were gently rinsed with ultra-purified water to remove loosely attached cells. The coupons were left at room temperature to dry for 1 hour.

II.3 Resistance to cleaning

In order to determine the foam cleaning efficiency on the bacterial biofilm, the dried coupons were placed into rectangular stainless-steel ducts ($1.5 \times 1\ 10^{-2}$ m), connected to the pilot rigs (Dallagi et al., 2022). Then, they were subjected to cleaning processes involving wet foam (50% of air and 50% of SDS surfactant (Sodium dodecyl sulfate, over 98.5% purity, 0.15% w/w)), at foam mean velocities ranging from 1.5 to 13.5 cm.s^{-1}, Table 8. The time of the cleaning kinetics were 15 and 35 s, 1, 3, 5, 10, and 20 min. Other cleaning experiments were carried out in a CIP rig using a fluid made of 0.15% SDS at 10 Pa and the residual biofilms were analyzed after the same cleaning times. The residual biofilms were analyzed as described below. All the conditions are presented briefly in Table 8. Further tests were performed in static conditions by immersing the soiled coupons in water or SDS 0.15% w/w for 20 min at room temperature to investigate the possible detachment in presence of the SDS solution (chemical action alone).

Table 8. The different conditions of the foam flow and the cleaning-in-place carried out for removal of biofilms from stainless steel surfaces.

Flow conditions	Velocity (cm.s^{-1})	Shear stress (Pa)	Mean diameter (mm)
FFC	1.5	2.2	0.34
	4.5	5.9	0.28
	9	9.8	0.18
	13.5	13.2	0.21
CIP	180	10	----------

II.4 Biofilm analyses

To quantify the number of cultivable cells within biofilms, half of the soiled coupons were subjected two times to a 2.5 min of ultra-sonication step in 10 ml of 0.5% Tween 80 (Bransonic 2510E-MT, 100 W, Branson Ultrasonics Corpo-ration, USA) and vortexed for 25 seconds between each sonication step (at maximal speed, 2400 rpm). This treatment has been validated previously and it can remove more than 99% of the adherent contaminations (Tauveron et al., 2006). The detached bacteria were plated on TSA (Tryptone Soy Agar, Biokar, France) and the colony-forming units (CFU) were enumerated after 48 h at 30°C.
The organization of the biofilms was observed under a microscope. For this purpose, coupons were dried at room temperature, covered with acridine orange (0.01%), and kept in the dark for

15 minutes, then gently rinsed with softened water and allowed to dry before any observation. Observation of biofilm microstructure was first performed with an epifluorescence microscope (Zeiss Axioskop 2 Plus, Oberkochen, Germany, x50 and 1000 magnification) to investigate the spatial organization of the biofilms. The 3-D organization was then analyzed by confocal laser scanning microscope (CSLM, Zeiss, LSM780, Oberkochen, Germany, x400 magnification).

II.5 Kinetics modeling and Statistical analysis

A two-phase kinetics model was used to fit the data. The fitting was performed using GInaFIT (Geeraerd et al., 2005) using a biphasic model composed of two first order kinetics two subpopulations characterized by different removal behavior (Bénézech and Faille, 2018).

$$\frac{N}{N_0} = f\, e^{(-k_{max1}t)} + (1-f)e^{(-k_{max2}t)} \quad (1)$$

where;

- f poorly adherent fraction,
- kmax1 [s^{-1}] detachment rates of the first population
- kmax2 [s^{-1}] detachment rates of the second population.

At least three repetitions were carried on (with three coupons for each one) for all the experiments. Statistical analyses of Data were performed using SAS V8.0 software (SAS Institute, Gary, NC, USA). For each cleaning condition, variance analyses were made to determine the impact of the biofilm strains, the mean shear stress, and the foam structures on the efficiency of the cleaning by foam flow compared to the CIP process. Further analyses were performed as multiple comparison tests using Tukey's test (Alpha level = 0.05).

II.6 Environmental impact

Life cycle assessment (LCA) is a standardized quantitative method ((ISO 14040, 2006), and (ISO 14044, 2006)) to assess the environmental impacts associated with an industrial process and to quantify the contribution of each step in the process in order to identify eco-design approaches or to improve the environmental performance of the process. Four points were examined: definition of purpose and scope, inventory analysis, impact assessment, and analysis.

II.6.1 Goal and scope definition

The LCA study was carried out by considering only one unit of the manufacturing process addressing the food industry sector, using the LCA software SimaPro 8.3 and the ecoinvent v3.0 database. For this purpose, the production and transport phases have not been considered here, while the attention was only focused on the cleaning operations. The objective was to analyze the environmental impacts of the proposed foam cleaning method, by comparing this alternative process to two CIP conditions, one using the same foaming surfactant and one using a commonly used alkaline chemical (NaOH). The results illustrate how such a technological proposal leads to improved cleaning with water and energy savings and more generally favorable environmental impacts.

The functional unit (FU) of this work was defined as monthly cleaning of 27 cm^2 of stainless-steel surfaces. The amount of resources and chemical products required to clean these

contaminated surfaces w summarized in Table 9. It should be noted that these data are related to pilot-scale experiments, as was explained in the section of biofilm removal section.

Table 9. Life cycle inventory of the cleaning processes.

PARAMETERS	PROCESS A	PROCESS B	PROCESS C	Unite
Soft water	19000	7000	1040	kg
Compressed air	0	0	9.27	m^3
Electricity	45	15	1.98	kWh
Natural gas (heat treatment)	440	0	0	kwh
Sodium Dodecyl Sulfate (SDS)	0	4.5	0.36	kg
Sodium Hydroxide (NaOH)	15	0	0	kg
Sulfite (heat treatment)	10	0	0	kg

II.6.2 Inventory analysis

Figure 74 outlines respectively the different phases included in this analysis. The process (A) corresponding to a 5 min of rinsing with softened water at 300 L/h flow rate at room temperature, followed by 20 min of cleaning with 0.5% NaOH water at 650 L/h at 60°C, and lastly a second rinsing stage for 5 min with softened water at 300 L/h flow rate at room temperature. The two processes (B and C) are the CIP and foam cleaning conditions used in this paper (first section), for 20 min at 10 Pa at room temperature. A 5 min of two rinsing steps with softened water at room temperature were performed before and after each cleaning process. It should be noted that for the rinsing stage after foam cleaning, given our experimental system of using the osmosis water supply directly, there is no need for a specific pumping system. However, in the case of both CIP conditions, the centrifugal pump used for cleaning is obviously also used for rinsing. The consumption of energy (pumps, compressor, and boiler for the heating of fluids), water, and chemical substances (SDS, NaOH, and sulfite (used for the boiler during heating process)) during one month of cleaning is summarized in Table 9. All input data were extracted from the ecoinvent database v3.0. can be considered the most up-to-date, comprehensive, reliable and accessible source of CMI data, and a data are considered of an outstanding quality (Kapur et al., 2012). However, the SDS surfactant was not included in the database. Therefore, it was defined as 40% sodium carbonate and 60% fatty alcohol sulfate as reported in a recent LCA study (Van Lieshout et al., 2015).

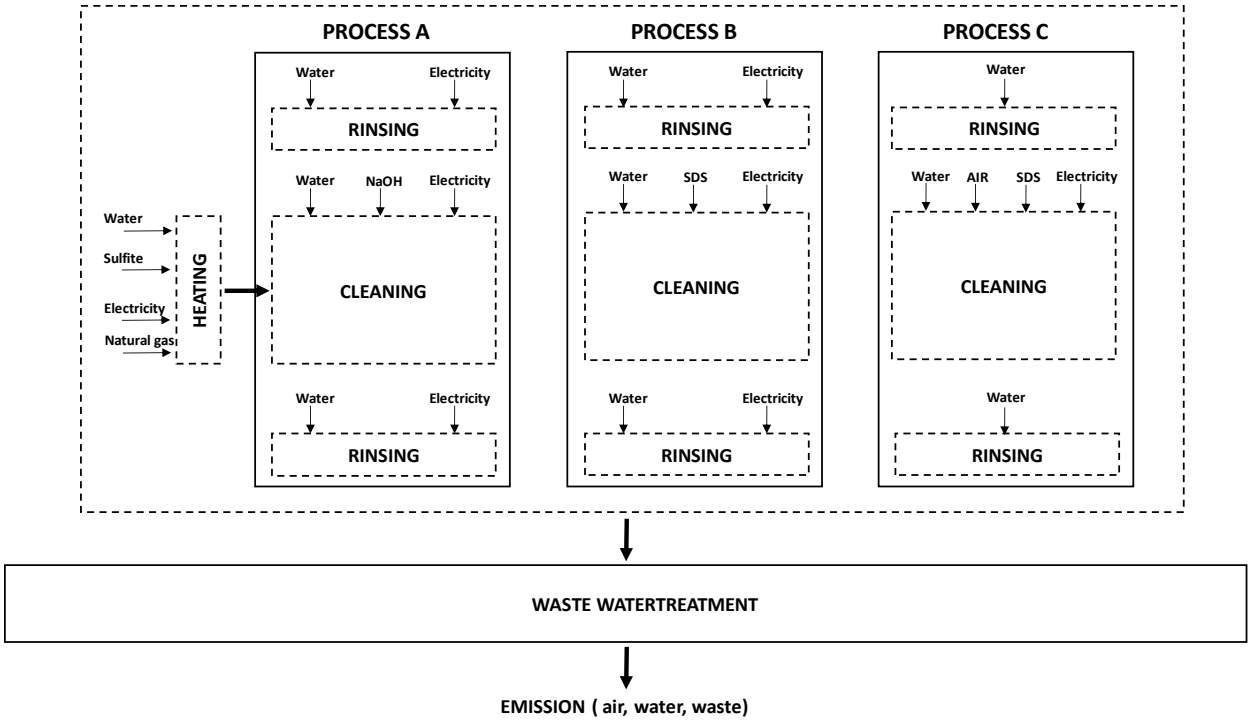

Figure 74. Flow diagram of the cleaning processes involved in this study.

II.6.3 Impact assessment

In this study, environmental impacts were quantified using two different endpoint indicators, ReCiPe Endoint (E) v1.09 and IMPACT 2002+ v2.11 which represent different approaches to determining the categorical environmental impacts, and the global warming potential and respectively. These approaches represent a recent and comprehensive method for impact assessment and have been widely used for this type of analysis (Gésan-Guiziou et al., 2019; Tsai et al., 2021). Secondly, various indicators have been reported in this study as they have been identified by previous LCA studies as the most important environmental impacts associated with food processing in which CIP processes have neen considered (Gésan-Guiziou et al., 2019; Zouaghi et al., 2019). The modeling of the processes was presented in Supplementary- Figure 75.

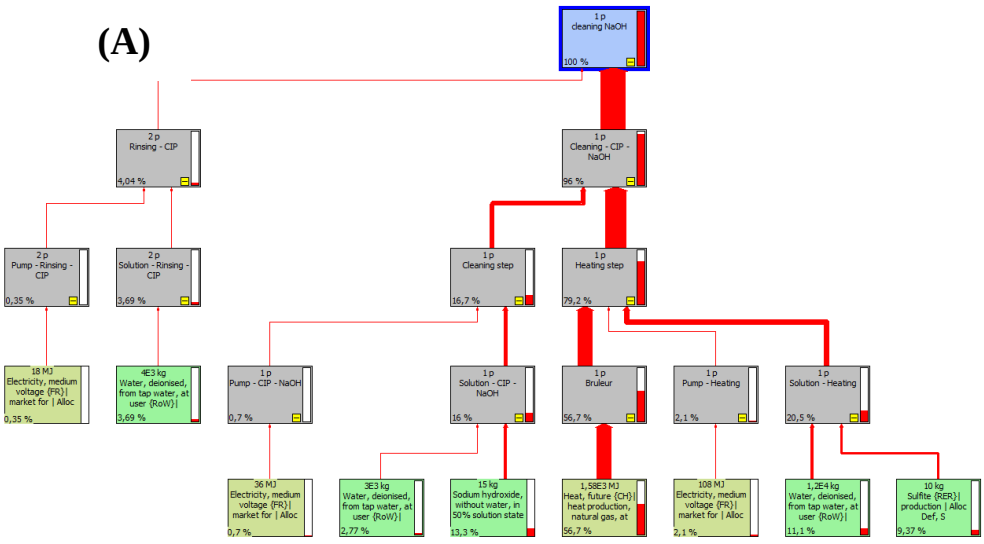

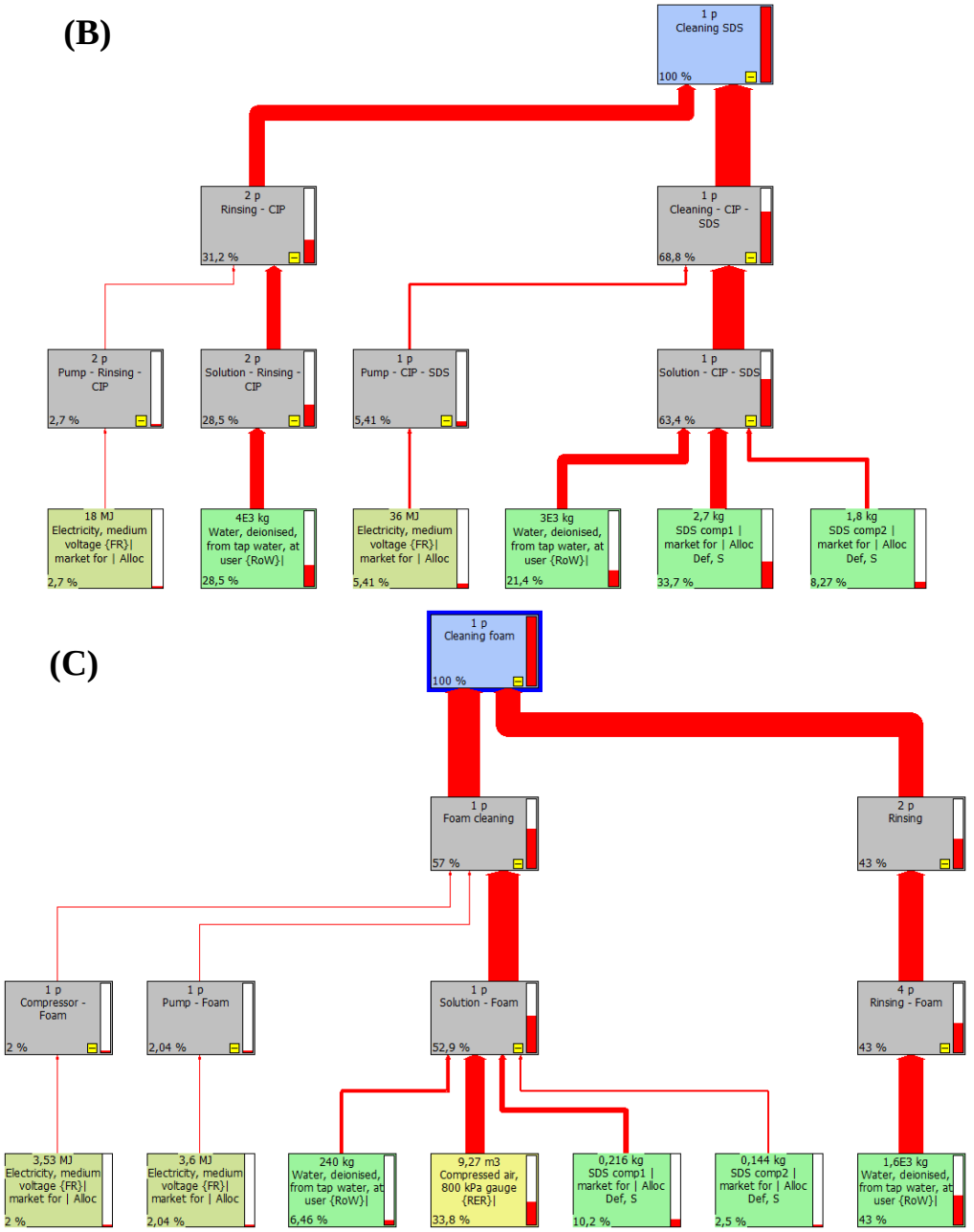

Supplementary- Figure 75. Modeling of the cleaning processes using SimaPro software.

III. Results

III.1 Biofilm formation

The numbers of the cultivable cells within the biofilms are given in Figure 76. As expected, great differences were observed between strains. The highest amount was observed for Pf1 with around 8 log CFU cm^{-2}, the two other strains Ec-SS2 and Bc-98/4 being at around 10^6 CFU cm^{-2} (3 and 8 10^6 respectively). However, some variations could be seen within the stainless-steel coupons with one log variation at the highest for Pf1 (between 3 10^7 and 3 10^8 CFU cm^{-2}). After staining the contaminated coupons with orange acridine, the distribution and

structure of the 24h biofilms were observed by epifluorescence microscopy at x50 magnification. (Figure 76). The surface coverage levels were consistent with the enumeration results. The Pf1 biofilm was tightly packed in large and dense clusters on the overall surface of the coupons, while the biofilms formed by the two other strains were composed of medium-sized clusters separated by less contaminated areas with many single cells and small clusters. The observation by confocal microscopy shows that the clusters of Bc-98/4 and Ec-SS2 have a 3D structure whereas the large Pf1 clusters are relatively flat, although they appear to be formed of several layers. Furthermore, observations by epifluorescence microcopy at x1000 magnification (Supplementary- Figure 82) clearly demonstrated the presence of spores (stained green) within the biofilms of Bc-98/4 (10-30 %).

	Bc-98/4	**Ec-SS2**	**Pf1**
Surface contamination	3.10^6 CFU cm^{-2} (from $9\ 10^5$ to $6\ 10^6$)	8.10^6 CFU cm^{-2} (from $4\ 10^6$ to $1\ 10^7$)	1.10^8 CFU cm^{-2} (from $3\ 10^7$ to $3\ 10^8$)
Epifluorescence microscope at x50 magnification	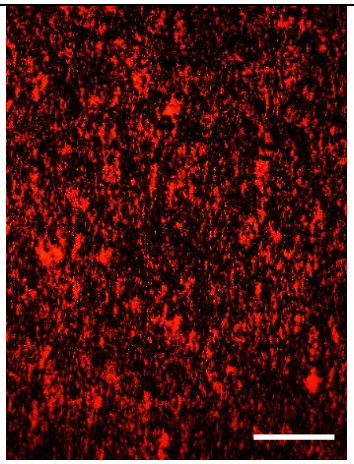	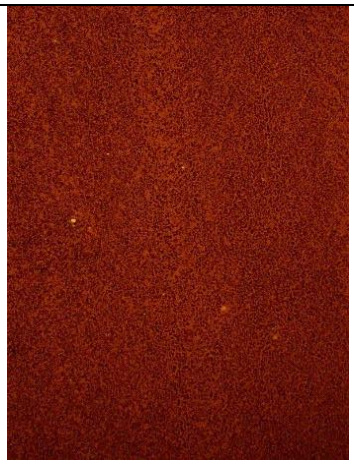	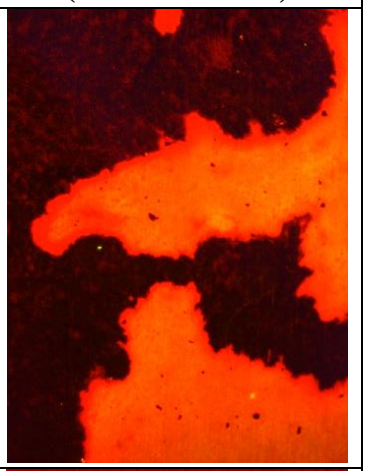
Confocal scanning laser microscope at x400 magnification.	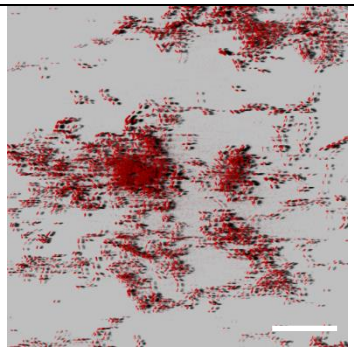	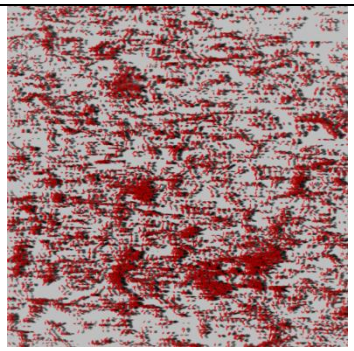	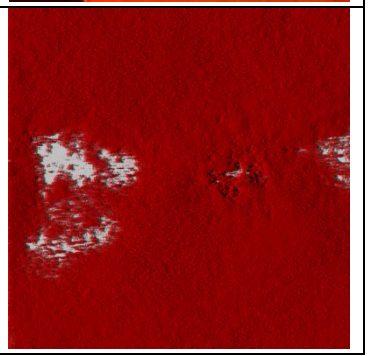

Figure 76. Biofilm formed on stainless steel surfaces stained with orange acridine, exanimated with Epifluorescence and confocal laser microscopes. White bar = 50 and 5 µm, for Epifluorescence and confocal images respectively.

III.2 Resistance to cleaning

III.2.1 Detachment kinetics of biofilm

We first investigated the possible detachment of biofilms when coupons were dipped in water and SDS in static conditions for 20 min (Supplementary- Figure 77).

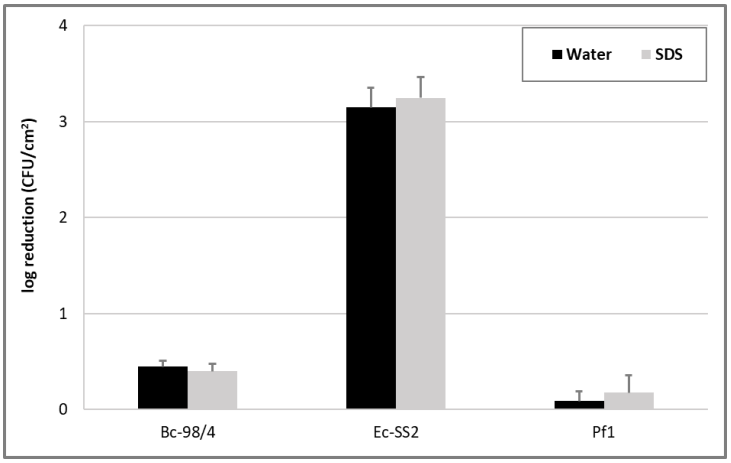

Supplementary- Figure 77. Reduction of the number of log CFU/cm2 under static conditions (20 min of dipping in water or SDS 0.15) of Bc-98/4, Ec-SS2, and Pf1 Biofilms.

Whatever the strain, no significant difference could be demonstrated between water and SDS. Conversely, great differences were observed between strains. Almost no effect was observed on Pf1 biofilm with only 0.2 log reduction, less than 0.5 log reduction for Bc-98/4, while Ec-SS2 was particularly sensitive with more than 3 log reduction. Furthermore, the Ec-SS2 biofilms were poorly resistant to foam flow cleaning. Indeed, at 2.2 Pa, a 4 to 5 log decrease in the number of adherent bacteria was detected after 15 seconds of cleaning, and no residual bacteria could be detected after 3 minutes of cleaning. This strain was therefore not retained for the remainder of this study on the effectiveness of foam flow cleaning procedures. The removal kinetics of the two other strains in terms of the percentage of residual cultivable cells are presented in Figure 78. In all cleaning conditions, the detachment curves clearly showed two distinct phases. Both phases appeared to be exponential and therefore were nicely described by the biphasic model, with R^2 ranging from 0.88 to 0.99. Whatever the flow condition and the strain, the curves showed a first very short phase (less than 1 min), characterized by a rapid detachment of the biofilms, followed by a far less efficient second phase observed during the remaining 20 min of the cleaning time. The first phase was shorter for Bc-98/4 than for Pf1 biofilms (less than 35 sec and around 1 min, respectively). Moreover, for Bc-98/4 biofilms, the duration of this phase was similar regardless of the cleaning condition, while the detachment rate after 30 s cleaning increased with the shear stress (between 1.1 and 1.7 log reduction). During the second phase, an additional decrease close to 0.3 log was observed, whatever the cleaning condition. For Pf1, the initial detachment rate was fastest at 13.2 Pa, slowest at 2.2 Pa, and the duration of the first phase was longer at 2.2 Pa than in other cleaning conditions. The amount of residual biofilm continues to decrease during the second phase, but much less at 2.2 Pa than under the other cleaning conditions.

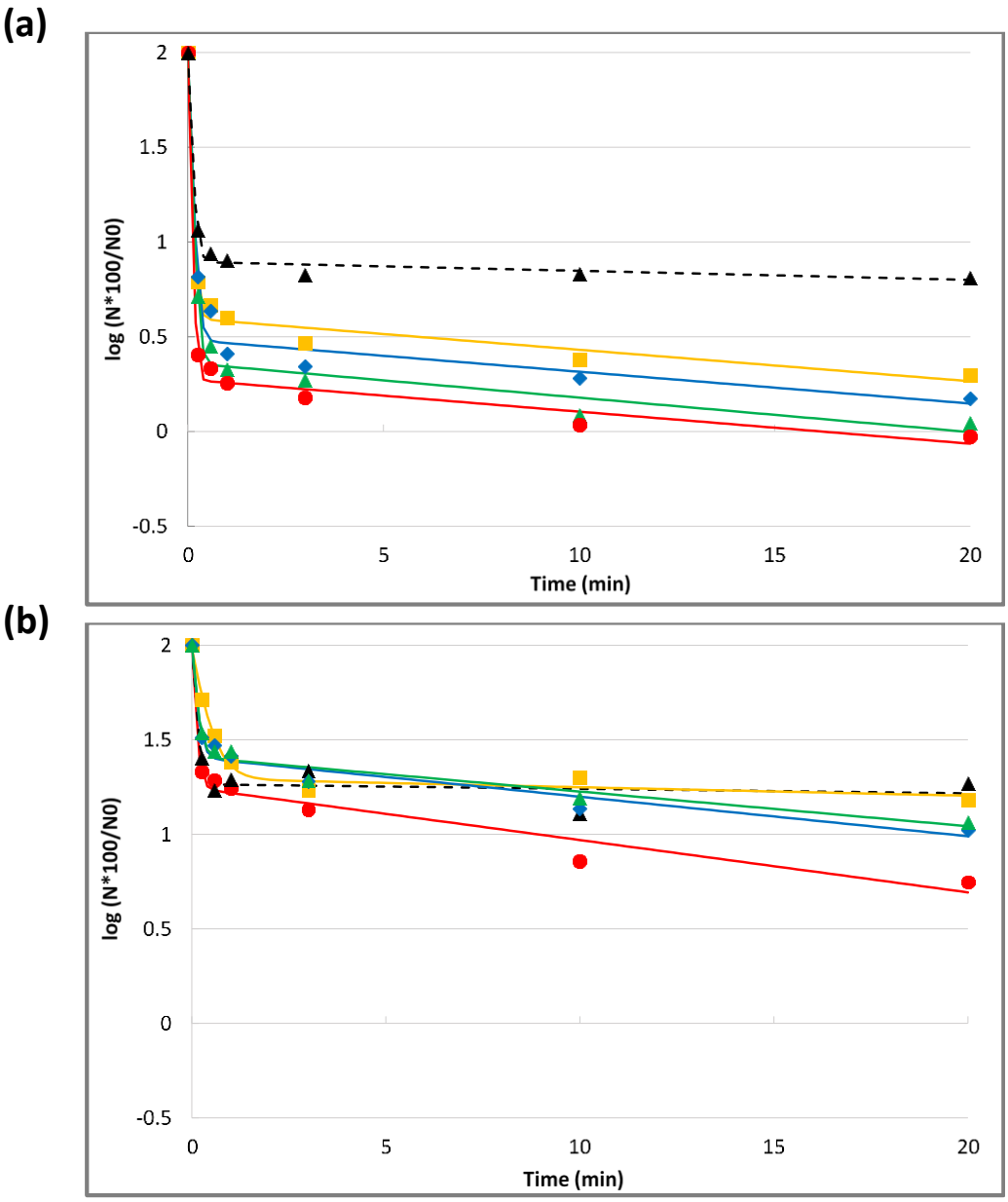

Figure 78. Detachment kinetics of Bc-98/4 (a) and Pf1 (b) under the different flow conditions. Markers showed the data of three repetitions, and the line represents the biphasic fitted model fit to each condition: 2.2 Pa (yellow square), 5.9 Pa (blue diamond), 9.8 Pa (green triangle), 13.2 Pa (red circle), and CIP 10 Pa (black triangle).

The role of the foam shear stress and the bacterial strain on the kinetics parameters (fraction of the biofilm released during the first phase *f*, first kinetics constant rate *kmax1*, and the second kinetics constant rate *kmax2*) was then investigated. As clearly observed in Figure 79, the kinetics parameters were strongly affected by the strain and to a lesser extent by the cleaning conditions. First, the role of the strain was very pronounced on the parameters *f* and K*max1* ($Pr<0.0001$ for both parameters). Indeed, *f* was systematically higher than 0.96 for Bc-98/4 biofilms, and lower than 0.82 for Pf1 biofilms. As for K*max1*, it was clearly higher for Bc-98/4 biofilms in all cleaning conditions (between 1.6 and 5 times higher). On the other hand, the results were more nuanced with respect to *Kmax2*. While the values of this parameter were

close to 0.04 s^{-1} in all cleaning conditions for the Bc-98/4 biofilms, they clearly increased overall with shear stress for the Pf1 biofilms. Consequently, at 2.2 Pa, *Kmax2* of Bc-98/4 biofilms was 3.8 times lower than that of Pf1 biofilms and almost 2 times higher at 13.2 Pa.
Comparing the role of shear stress on the kinetics parameters for Bc-98/4 biofilms, the increase in shear stress leads to an increase in the two parameters *f* and *Kmax1*, which results in a cleaning efficiency of this phase that increases with the shear stress. Conversely, no significant influence of the shear stress on the parameter *Kmax2* could be identified according to the Tukey test. For Pf1 biofilms, the values of the parameters *f* and *Kmax1*, but also of *Kmax2*, increased overall with the shear stress, except for *f* at 2.2 Pa, which had an intermediate value.
We then investigated the efficiency of a CIP procedure with SDS at 10 Pa (Figures 78 and 79). After 20 min cleaning, this procedure was much less effective than all the procedures involving foam on Bc-98-4, but similar to cleaning at 2.2 Pa (the least effective procedure with foam) on Pf1 biofilms. Moreover, the detachment of the two biofilms occurs mainly during the first phase, which was confirmed by the *Kmax2* values (0.011 and 0.005 for Bc-98/4 and Pf1 biofilms, respectively).

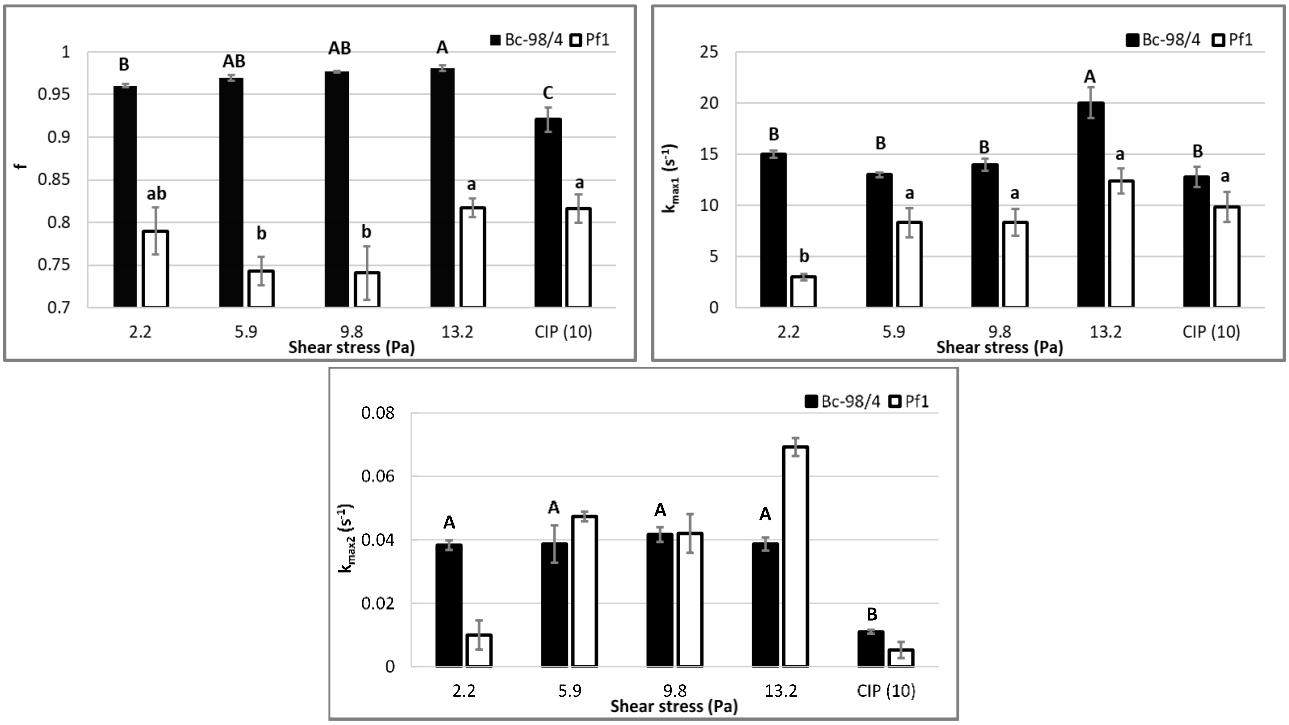

Figure 79. Kinetics parameters f, Kmax1, and Kmax2 for Bc-98/4 and Pf1 biofilms under different flow conditions. Following Tukey's grouping, conditions with no common letter are significantly different.

III.2.2 Structure of the residual biofilm after the cleaning process

As in the case of biofilms before cleaning, the coupons were viewed by epifluorescence (Figure 80) and confocal microscopy (Supplementary- Figure 81) after 1 min and 20 min of cleaning under the different conditions tested.

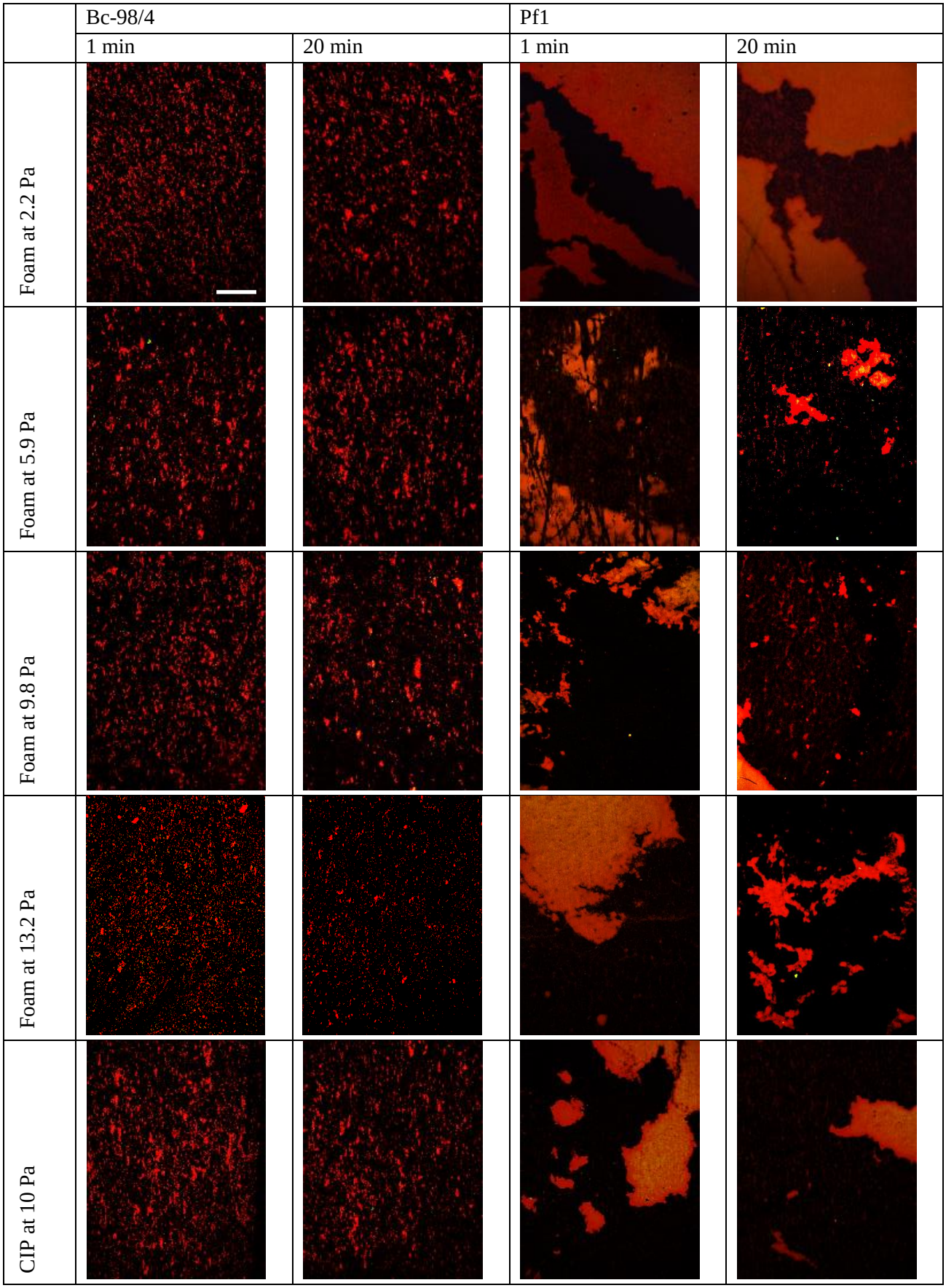

Figure 80. Microscopic images of residual biofilm under different flow conditions. Exanimated with epifluorescence microscopy at x50 magnification. White bar = 50 µm.

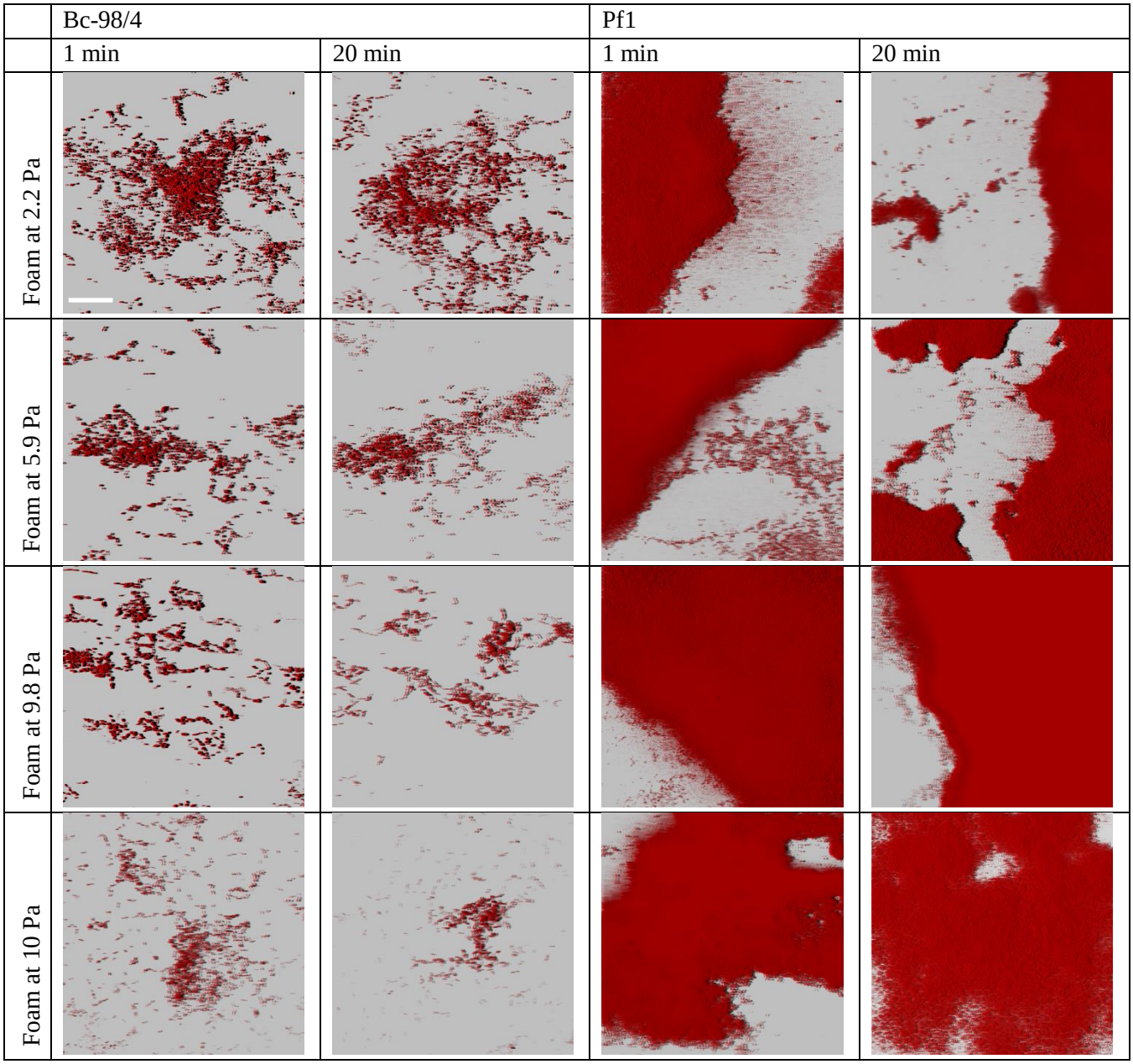

Supplementary- Figure 81. 3D structure of residual biofilm under different foam flow conditions. Exanimated with confocal laser microscopes at x400 magnification. White bar = 50 µm.

First of all, no clear differences between cleaning procedures (foam cleaning and CIP) could be observed. After cleaning of Bc-98/4 biofilm with foam, the number of small clusters and isolated cells was highly reduced, even after a one-minute cleaning, while the larger clusters seemed to have better resisted to the detachment. The structure of the residual Bc-98/4 biofilms did not appear to be more affected by longer cleaning times. Whatever the cleaning conditions, residual spores were still observed within biofilms after 20 min cleaning (Supplementary-Figure 82).

Concerning Pf1 biofilms, the first cleaning phase also resulted in the detachment of many isolated cells, but also in the disintegration of part of the large clusters. Indeed, the residual clusters were often smaller than before cleaning, and the whole surface covered by the biofilms

was significantly reduced. An additional reduction of the covered surface was also observed after 20 min cleaning.

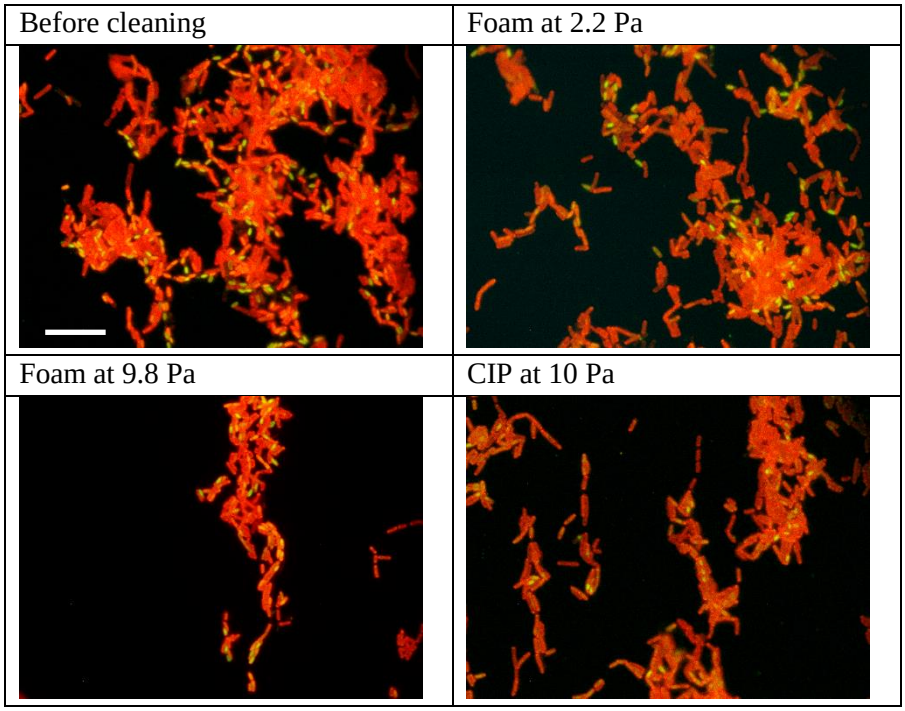

Supplementary- Figure 82. Observation of spores within Bc-98/4 biofilms, exanimated with epifluorescence microscopy at x1000 magnification. White bar = 2 µm.

III.3 Life Cycle Assessment

All inputs considered were summarized in Table 9. The water and energy consumption of the cleaning processes were significantly different. For example, the CIP process using NaOH at 60°C required the largest amount of water and electricity by 1.9 10^4 kg and 45 kWh respectively. However, more than 63% of these consumptions came from the heating step not including the use of 440 kWh of natural gas. On the other hand, foam flow cleaning required respectively 6.7 and 7.6 times less water and electricity respectively than the SDS-containing CIP while in the latter conditions it consumed about 18.3 and 22.7 times less than NaOH-containing CIP. It should be noted that the two rinsing steps in all the processes (A, B, and C respectively) account for about 21, 57, and 77% of the total water used in each process. The consumption of SDS surfactant was very high (12.5 times more) in CIP than foam cleaning.

When comparing the environmental impact of these processes, CIP using NaOH (A) was the most harmful process, followed by CIP using SDS (B) and then the foam cleaning process (C). Indeed, the damage to human health and ecosystem quality caused by foam cleaning method, mainly due to the emission of the surfactant and compressed air production, does not exceed 6.6%, and 14.2% of that caused by process B. However, the damage caused by Process B was 18.6% and 41.7% of that caused by process A. The high human toxicity score for process A is related to SO_x and NO_x emissions during the combustion step (heating of the solution).

The results of the IMPACT 2002+ characterization are presented in Figure 83 (a) and Table 10. Process A appears to be significantly less favorable on all indicators, except the one corresponding to land use. This was mainly due to the heat treatment and the use of NaOH. In

almost all aspects reflecting the total environmental impact, both process B, and C did not exceed 20% of the environmental impact of process A. A specific comparison between processes B and C is presented in Supplementary- Figure 84. Compared to CIP using the same surfactant (SDS), foam cleaning reduced the environmental impacts in all aspects by about 70%, with the lowest effect on the impact for terrestrial ecotoxicity (by 20%, 244 kg TEG soil). The largest reduction was in land occupation (reduction by 90%), ionizing radiation, respiratory organics (C_2H_4 eq), and global warming (CO_2 eq). However, due to the production of compressed air, foam cleaning was less favorable than CIP on aquatic eutrophication and mineral extraction by an increase of 20% and 45% respectively.

Table 10. Contribution of the unit process to the total environmental impact of the cleaning processes per impact category according to the impact assessment methods IMPACT 2002+.

Impact category	Unit	Process A	Process B	Process C
Carcinogens	kg C_2H_3Cl eq	3.31E+00	6.81E-01	2.00E-01
Non-carcinogens	kg C_2H_3Cl eq	1.47E+00	3.30E-01	3.30E-01
Respiratory inorganics	kg PM2.5 eq	1.30E-01	2.35E-02	7.81E-03
Ionizing radiation	Bq C-14 eq	5.80E+03	1.53E+03	2.78E+02
Ozone layer depletion	kg CFC-11 eq	4.03E-05	5.07E-06	1.24E-06
Respiratory organics	kg C_2H_4 eq	4.63E-02	1.21E-02	2.06E-03
Aquatic ecotoxicity	kg TEG water	1.05E+05	3.78E+04	1.04E+04
Terrestrial ecotoxicity	kg TEG soil	1.54E+03	3.07E+02	2.44E+02
Terrestrial acid/nutri	kg SO_2 eq	1.85E+00	3.76E-01	1.10E-01
Land occupation	m^2org.arable	1.26E+00	3.62E+00	3.58E-01
Aquatic acidification	kg SO_2eq	8.14E-01	1.22E-01	4.50E-02
Aquatic eutrophication	kg PO_4 P-lim	1.92E-02	4.22E-03	5.13E-03
Global warming	kg CO_2 eq	1.47E+02	1.91E+01	5.05E+00
Non-renewable energy	MJ primary	3.00E+03	4.90E+02	1.01E+02
Mineral extraction	MJ surplus	5.62E+00	1.21E+00	2.40E+00

(a)

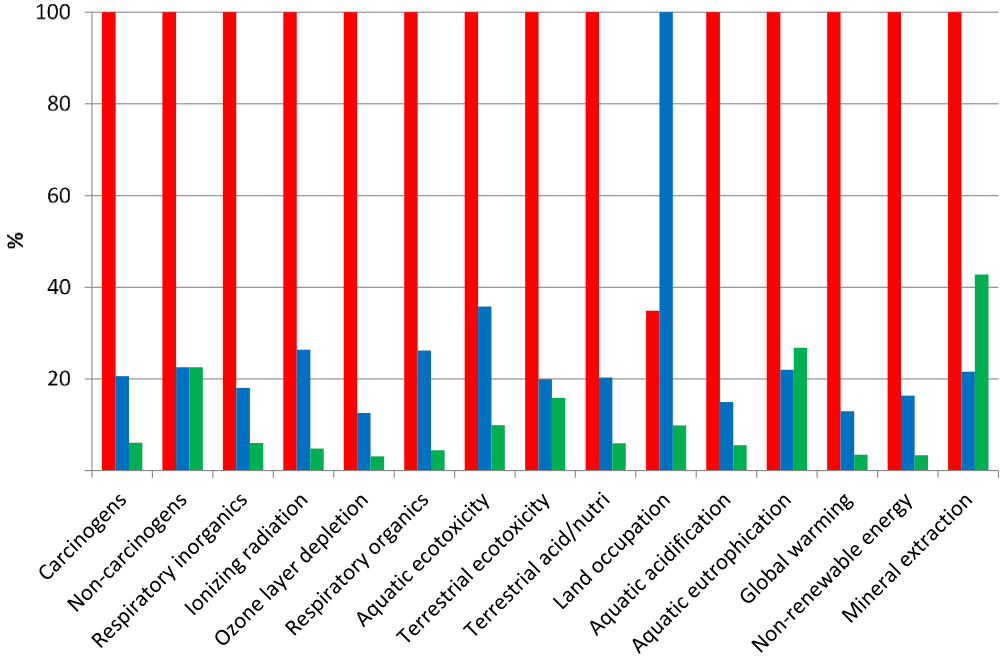

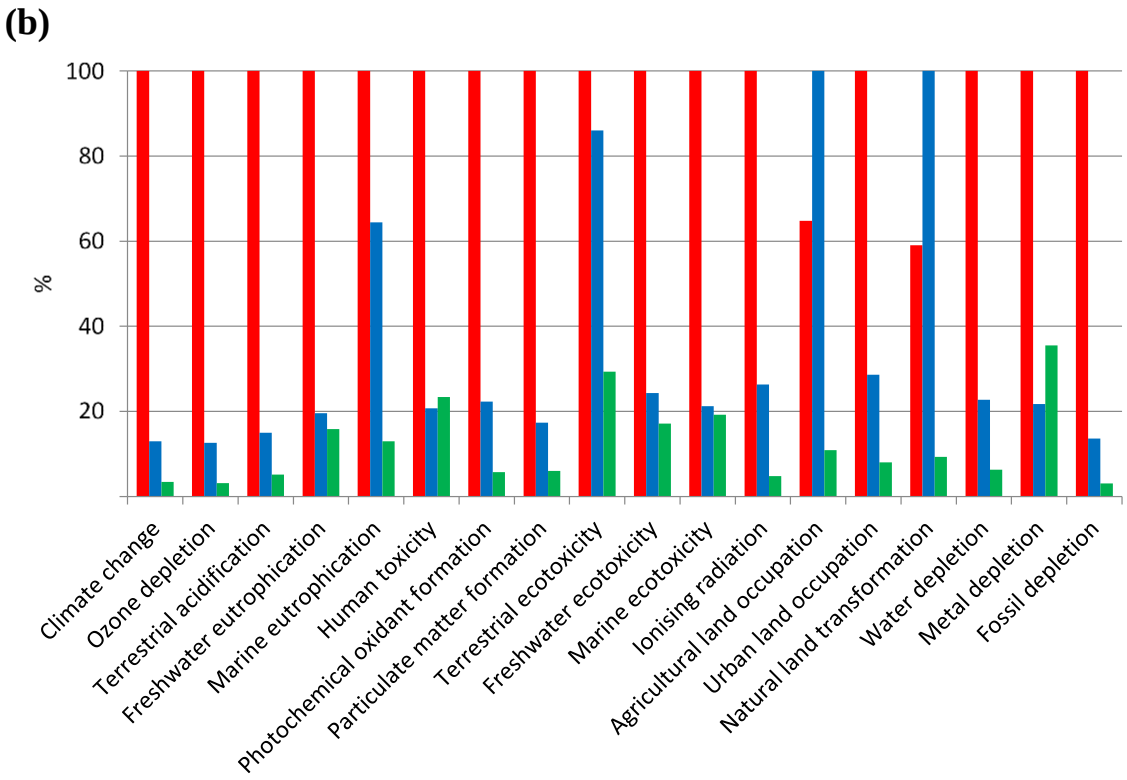

Figure 83. Environmental impact profiles of cleaning processes according to the impact assessment methods IMPACT 2002+ (a) and ReCiPe (b) midpoints. Process A (red color), Process B (blue color), and Process C (green color).

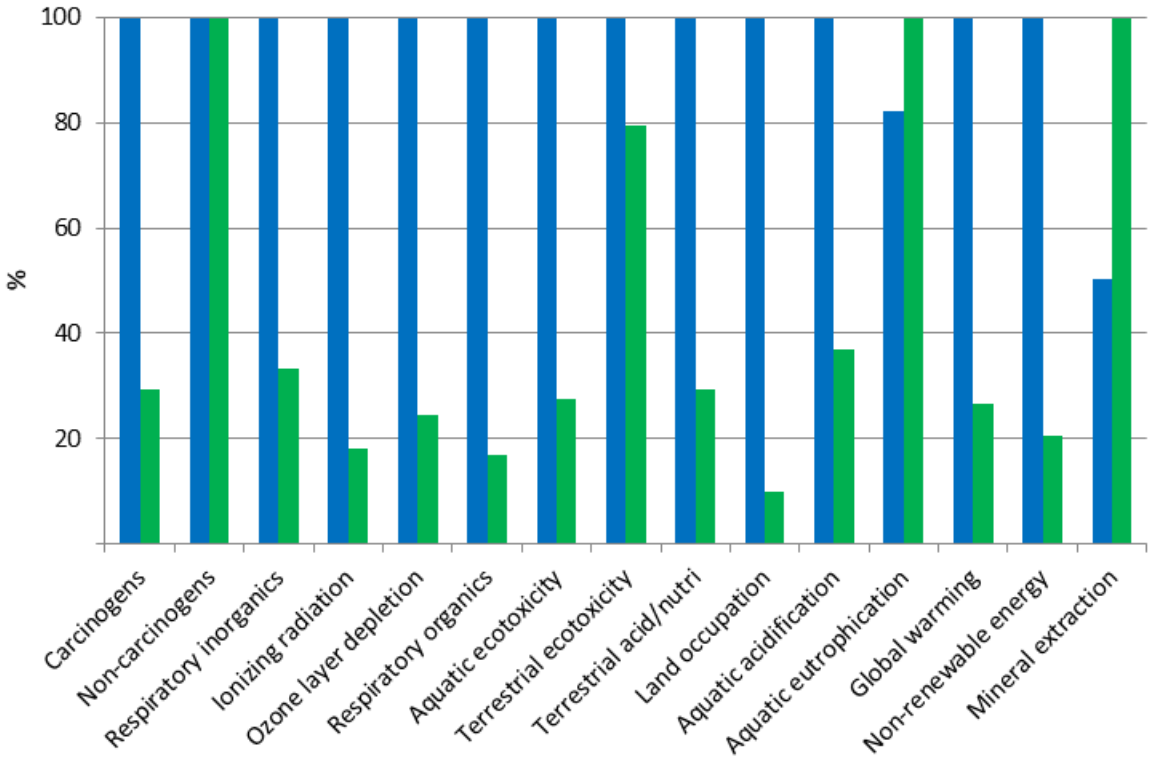

Supplementary- Figure 84. Comparison of the environmental impact profiles of cleaning processes B (blue) and C (green) according to the impact assessment methods IMPACT 2002+.

For more details, Figure 85 highlights the main substances contributors to the three impact aspects as global warming, non-renewable energy, and aquatic eutrophication for all the cleaning processes. Carbon dioxide (CO_2) and other greenhouse gas emissions such as methane (CH_4), sulfur hexafluoride (SF_6), and dinitrogen monoxide (N_2O) were found to be the main contributors to climate changes in this study. CO_2 contributes to more than 90% of the total emission for all the cleaning processes, followed by CH_4 and SF_6 with about 5 and 1% respectively. The use of natural gas in process A (57% of the total kg CO_2 eq emitted), deionized water, and SDS surfactant in process B (respectively 50% and 42% of the total kg CO_2 eq emitted) and the production of deionized water and compressed air in process C (respectively 50% and 34% of the total kg CO_2 eq emitted) were found to be the potential source to global warming. In addition, the excessive use of natural gas, deionized water, SDS, and electricity was the main source of non-renewable energy depletion in all cleaning processes, while the production of compressed air contributes to 86% of the aquatic eutrophication for process C (equivalent to the amount of phosphate and phosphorus to imbalances the aquatic system).

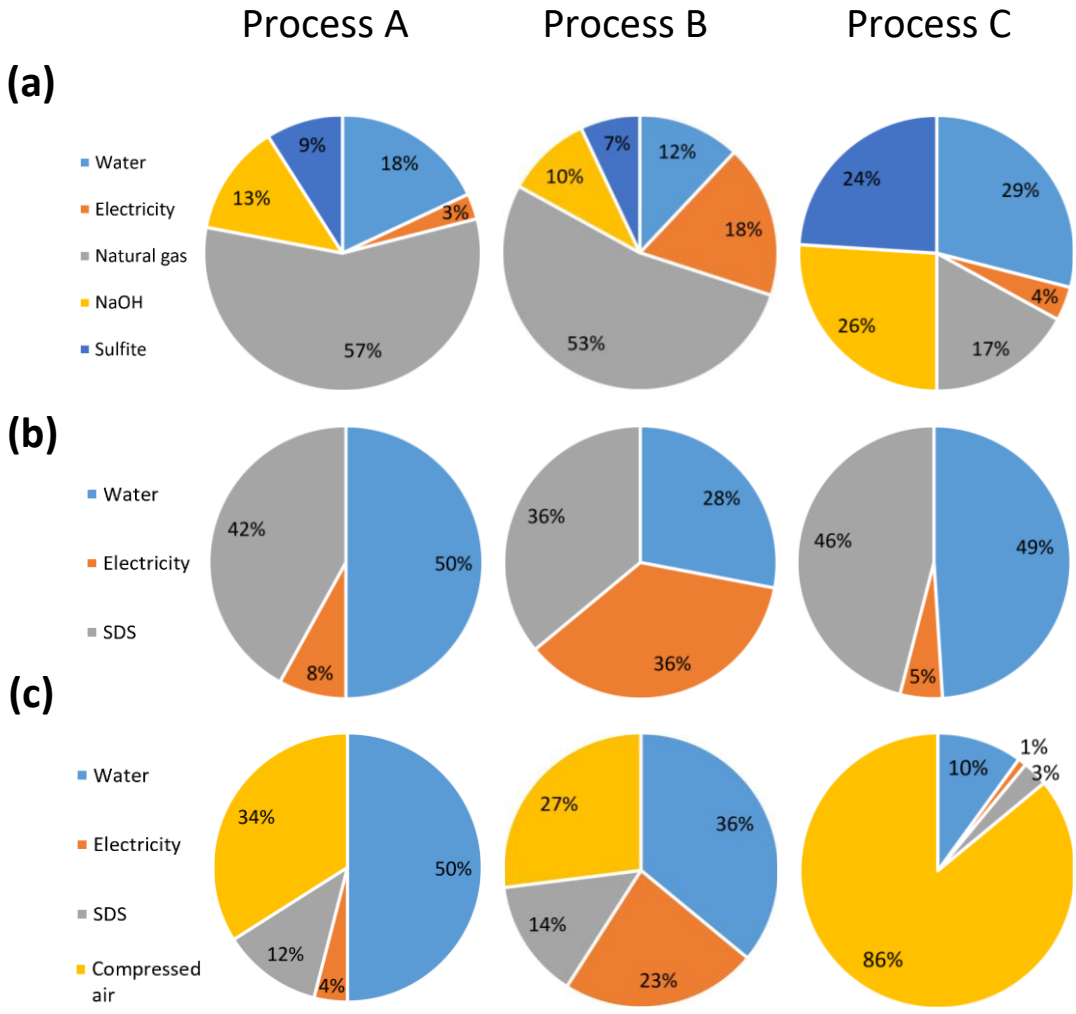

Figure 85. Contributors for three impact categories of the cleaning processes according to the impact assessment methods IMPACT 2002+. (a) global warming, (b) non-renewable energy, and (c) aquatic eutrophication.

On the other hand, the results obtained by ReCiPe (Figure 85 (b), Table 11) suggest a larger contribution of process B to the total environmental impact compared to that obtained by IMPAC T2002+. As shown in Table 11, the score of process B for marine eutrophication and terrestrial ecotoxicity was 65% and 85% of that of process A respectively. In addition, process B contributed the most to agricultural land occupation (3.8 m^2a) and natural land transformation (0.0456 m^2). The SDS surfactant, especially fatty alcohol sulfate component, contributed 89-96%. The foam cleaning process resulted in a 90% reduction in score (0.412 m^2a for agricultural land occupation and 0.00423 m^2 for natural land transformation). In this case, the SDS contribution was 65-83%, due to the fatty alcohol sulfate component.

Table 11. Contribution of the unit process to the total environmental impact of the cleaning processes per impact category according to the impact assessment methods ReCiPe.

Impact category	Unit	Process A	Process B	Process C
Climate change	kg CO_2 eq	1.46E+02	1.89E+01	5.00E+00
Ozone depletion	kg CFC-11 eq	4.04E-05	5.09E-06	1.26E-06
Terrestrial acidification	kg SO_2 eq	8.00E-01	1.20E-01	4.10E-02
Freshwater eutrophication	kg P eq	3.59E-02	7.02E-03	5.68E-03
Marine eutrophication	kg N eq	1.96E-02	1.26E-02	2.55E-03
Human toxicity	kg 1,4-DB eq	1.62E+03	3.37E+02	3.80E+02
Photochemical oxidant formation	kg NMVOC	3.46E-01	7.70E-02	1.97E-02
Particulate matter formation	kg PM10 eq	2.44E-01	4.23E-02	1.46E-02
Terrestrial ecotoxicity	kg 1,4-DB eq	6.56E-02	5.64E-02	1.92E-02
Freshwater ecotoxicity	kg 1,4DB eq	1.19E+00	2.88E-01	2.03E-01
Marine ecotoxicity	kg 1,4-DB eq	1.20E+03	2.55E+02	2.31E+02
Ionising radiation	kBq U235 eq	5.72E+01	1.51E+01	2.74E+00
Agricultural land occupation	m^2a	2.46E+00	3.80E+00	4.12E-01
Urban land occupation	m^2a	1.05E+00	2.99E-01	8.36E-02
Natural land transformation	m^2	2.69E-02	4.56E-02	4.23E-03
Water depletion	m^3	5.59E+02	1.27E+02	3.51E+01
Metal depletion	kg Fe eq	6.74E+00	1.46E+00	2.39E+00
Fossil depletion	kg oil eq	4.86E+01	6.60E+00	1.48E+00

IV. Discussion

In this paper, we look for the removal of biofilm contamination using foam flow. Three strains were investigated, Bc-98/4, Ec-SS2, and Pf1. The choice of these strains was based on their extensive occurrence in the food industry and their ability to adhere and contaminate the

equipment surfaces. Indeed, all three strains are commonly associated with food spoilage leading to food outbreaks. For example, in a flavored yogurt manufacturing plant, the presence of *Escherichia coli* at the pumps may have caused an outbreak (Morgan et al., 1993). *Pseudomonas fluorescens* is among the more dominant species on food contact surfaces that are highly resistant to cleaning and disinfection operations (Fagerlund et al., 2017; Maes et al., 2019). It has a marked occurrence in food processing plants since it is able to form biofilms in different environmental conditions (Jara et al., 2021; Meliani and Bensoltane, 2015; Stellato et al., 2017). Even if this species was not pathogenic, it might behave as a "helper" for further pathogenic bacteria to persist in food facilities, mainly using its matrix as cover and/or as an anchoring surface (Puga et al., 2018). Lastly, *Bacillus cereus* strain has a high potential for biofilm formation on steel surfaces in the dairy industry (Ostrov et al., 2019; Sharma and Anand, 2002) which is related to physicochemical properties, notably the hydrophobicity of the spore surface (Simmonds et al., 2003; Tauveron et al., 2006). In addition, this strain is known to form a heat-resistant endospore that can complicate the removal of biofilm from the equipment surface, whatever the cleaning procedure applied as seen in Supplementary- Figure 82. This phenomenon was widely reported in the literature (Carrascosa et al., 2021; Shaheen et al., 2010), suggesting that generally, Gram-positive strains seem to better resist cleaning and disinfection procedures than Gram-negative strains (Bridier et al., 2011). On the other hand, the presence of spores embedded in the biofilm of *Bacillus cereus* soiled on a stainless steel surface modified the properties of the biofilm, such as the interaction forces and consequently the enhancement of the resisting to the disinfection (Ryu and Beuchat, 2005). As was expected, all the strains were able to form a large amount of biofilm on stainless-steel surfaces but with different structures (mainly on the sizes of clusters and the 3D organization seen in Figure 76). This result was consistent with (Jha et al., 2022) work, who explains the formation of biofilm on horizontal surfaces by the sedimentation phenomenon. However differences have been observed between strains in term of contamination levels and biofilm structures which potentially play a role in their resistance to cleaning procedures.

The impact of the shear stress on biofilm detachment was investigated by varying the mean shear stress of foam flow from 2.2 to 13.2 Pa. When comparing biofilm removal under the different foam flow conditions, it was found that the increase of the mean wall shear stress could have an important role in the cleaning efficiency. Indeed, an increase in the mean shear stress was followed by an improvement in the cleaning efficiency of the two strains Bc-98/4 and Pf1. As an example, after 20 min cleaning with foam at 13.2 Pa (the highest shear stress) exceeded 2 and almost 1.5 log CFU reduction for Bc-98/4 and Pf1 respectively showing an additional 0.5 log reduction compared to foam at 2.2 Pa. The same trend was observed during the first detachment phase (before 1 min). This observation is in line with a recent work performed in our laboratory on Pf1 under a water flow (40°C) at different shear stress (0.14-19.99 Pa), as the shear stress increased, the number of residual cells of *Pseudomonas* biofilm on the surfaces decreased (Bénézech and Faille, 2018). These results are not surprising since the improvement of biofilm detachment with increasing shear stress has already been observed in the literature (Fernandes et al., 2021; Li et al., 2019). For example, the removal of *Pseudomonas* biofilm from stainless steel surfaces using CIP containing a chlorinated alkaline detergent was reported (Grinstead, 2009). Indeed, the authors have increased the mechanical action by the increase of the velocity of the cleaning solution. This resulted in a significant

decrease of the residual biofilm after cleaning operations, from 68% to 94% at 0.3 and 1.5 m s^{-1}. In addition, several studies have noted similar trends on the removal of another bio-contaminants as just adhered spores using CIP or foam cleaning. In this previous study (Dallagi et al., 2022), foam flow at 9.8 and 13.2 Pa showed better efficiency in the removal of *Bacillus subtilis* spores with over than 4 log reduction after 20 min cleaning while only about 2 log reduction at 2.2 or 5.8 Pa. In the same way, the increase of the shear stress from 30 to 500 Pa in a rinsing-in-place procedure has a positive effect to remove *Bacillus cereus* 94/4 (from 9% to 85%) and *Bacillus subtilis* 98/7 (from 1% to 76%). Contrarily, other authors have defined a yield stress value, over which the detachment of a biofilm cannot be achieved. In other words, the statement that the higher the shear stress the better the cleaning cannot be considered as such: *Acinectobacter calcoaceticus* biofilms exposed to intermediate stresses (7 and 14 Pa) were more prone to be removed with an efficiency of 18-20%, while shear stresses of 2 and 23 Pa only resulted in 9-10% biofilm removal (Gomes et al., 2018). Another example concern the cleaning of *Bacillus cereus* and *Pseudomonas fluorescens* biofilms from high-density polyethene was reported in (Gomes et al., 2021). For a set of flow conditions with shear stress ranging between 0.7 and 17.7 Pa, a lower value of 1.66 Pa caused the highest biofilms detachment while a higher value of 17.7 Pa seemed to compress the biofilm allowing it a higher resistance against the shear forces. The authors explained that as the biofilms were gradually compressed by the shear forces, the porosity of the biofilm shifted, and its mechanical stability and detachment processes were also deeply affected. In our case, the optimum value for the mean wall shear stress was not reached or possibly the efficiency of the flow mechanical action is not solely due to the mean shear stress value but as demonstrated previously is largely dependent to the local wall shear stress variations induced by the bubbles 'passage and to their different sizes (Dallagi et al., 2022). Such effect of the fluctuations was largely demonstrated in previous works (Absi and Azouani, 2018; Blel et al., 2009).

Microscopy images (epifluorescence and confocal) suggested that the foam flow strongly affected the detachment of the clusters where cells were frequently embedded in the EPS matrix. For the Bc-98/4 strain, as the shear stress increased, the number of small clusters and isolated cells had diminished while the larger clusters seemed to have resisted more to the detachment within the first 1 min of cleaning. This could explain that f and k_{max1} were significantly affected at 13.2 Pa, the highest shear stress condition tested. Furthermore, after 20 min (second detachment phase) the largest clusters with visibly 3D structures appeared more or less reduced in size and occurrence.

The specificity of the Pf1 biofilm structure, with probably a thick layer of cells covering a large part of the surface of the coupons, does not allow conclusions to be drawn so easily from simple microscopic observations. However, naked eye observation of the whole coupons gives the impression that the large biofilm mats were greatly reduced after 20 min of cleaning under high shear stress (data not shown).

Concerning *E. coli* SS2 strain, biofilms were found to be too sensitive to the cleaning using foam flow. Indeed, foam flow condition at 2 Pa was sufficient to remove more than 4 log CFU before 1 min and at least 6 log CFU after 20 min. Microscopy images in Figure 86 confirmed this observation where few cells were remaining on the coupons after the cleaning procedure. This was not surprising since the cleaning in static condition (dipping in water or SDS solution for 20 min) was able to remove almost 3 log CFU. The resistance of *E. coli* to cleaning

procedures has already been observed (Furukawa et al., 2010; Jha et al., 2022, 2020). (Furukawa et al., 2010) demonstrated that strong acidic and strong alkaline CIP cleaning agents were significantly effective for cleaning *Staphylococcus aureus* and *E. coli* biofilms from stainless steel surfaces with more than 7 log reduction while water rinsing was able to remove 1 log for *E. coli* and has no effect on *S. aureus* biofilms. More recently, a study of the formation of Bc-98/4, Pf1, and Ec-SS2 at air-liquid-wall interface (ALW interface) on different materials (stainless steels with 2R or 2B finishes, polypropylene, and glass) showed the obtaining of an excessively dense biofilm with a clear 3D structure (Jha et al., 2020). When these biofilms were exposed to CIP containing 0.5% NaOH at 60°C at a shear stress of 3.6 Pa, cultivable cells in the remaining contamination indicated around 1.7 log reduction for Bc-98/4biofilms, at least 5 log for Pf1 biofilms, and only 4 log for Ec-SS2. Microscopy images show that the remaining contamination still suggesting the presence of many viable but not culturable cells within the residual biofilms mainly due to the NaOH effect.

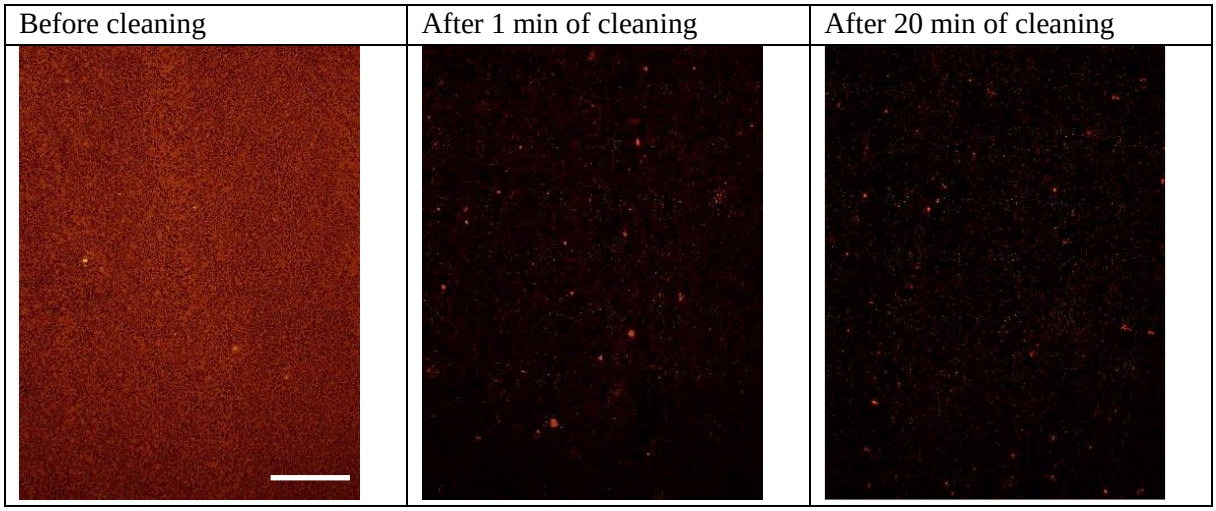

Figure 86. Comparison between E. coli-SS2 biofilm before cleaning and after foam flow cleaning, exanimated with Epifluorescence at x50 magnification. White bar = 50 µm.

In this study, the comparison between foam flow cleaning and CIP at 10 Pa (containing SDS surfactant) showed that foam flow was more efficient to remove biofilm contaminations. As seen in Figure 78, no improvement in the cleaning efficiency during the second detachment phase could be observed. Almost all the removed contaminations were observed before 1 min which reflected the low values of K_{max2} for the CIP compared to the corresponding foam flow condition. Microscopy images confirmed this observation, as almost no difference could be detected after 1 or 2 min of CIP. Large as well as medium size of biofilm clusters (clearly observed on Bc-98/4) remained even after 20 min of cleaning. The same behavior of detachment with CIP was observed in previous work (Dallagi et al., 2022; Al Saabi et al., 2021). However, as reported in (Bénézech and Faille, 2018; Grinstead, 2009), the addition of a chemical agent to the CIP solution or an increase of the temperature could lead to an enhancement of the cleaning efficiency during the second phase allowing the destruction of the large clusters.

Regarding the fact that the two procedures used in this study have the same mean shear stress but gave different results proved that the mean shear stress is not the only key parameter to

control the removal phenomenon. In the previous study on the removal of Bacillus spores, foam flow showed a better efficiency of cleaning. By a detailed characterization of the foam (such as the bubbles size distribution, thickness of the liquid film, and the wall shear stress), authors have tried to explain the removal mechanism. Capillary imbibition, liquid drainage, and fluctuation of the shear stress at the walls were hypothesized to be involved. Authors have concluded that a synergy of small bubble size and high shear stress could improve the cleaning efficiency of spores. However, in this study, the bubble size did not show a strong effect in the enhancement of cleaning since the condition of foam flow at 9.8 Pa which has the smallest bubble size (mean diameter of 0.18 mm) was not the most efficient condition. However, the frequency and the amplitude of wall shear stress might also explain the biofilm removal which also increased with the foam velocity (from 20 to 76 Hz, for the case of foam at 2.2 and 13.2 Pa respectively). While the fluctuation rate of the shear stress decreases with the foam velocity, from 957 to 193% for foam at 2.2 and 13.2 Pa respectively. Furthermore, it should be noted that the local shear stress generated by the foam could exceed more than three times its mean values. As an example, it was demonstrated using the polarography method that the wall shear stress of the foam at 2.2 or 5.9 Pa achieve a maximum value of 10 or 15 Pa respectively (Dallagi et al., 2022). In addition, the effect of the wall shear stress and its fluctuations on the cleaning efficiency was reported in the literature. The use of pulsed flow in turbulent regime was shown to increase the mean and fluctuating shear rates and a consequent enhancement of *Bacillus cereus* spores removal rates from surfaces (Blel et al., 2009; Lelièvre et al., 2002), which corresponds to twice that obtained for the steady condition at high Reynolds number (Re of 35000). A higher frequency of the wall shear stress has also shown a relevant role to remove a backed tomato deposit (Absi and Azouani, 2018). In both cases, the authors explained that this increase in the local velocity gradient at the surface (in other words the wall shear stress) played a relevant role in convective mass and heat transfer inducing a weakening and breaking of the bonds between the contaminations and the solid surface. Another study on the elimination of *Chlorella vulgaris* biofilms fouled on the surfaces of a photobioreactor was performed using different bubbles sequences (Charlène, 2018). Their results showed that the surface layers of the biofilm considered as the loosely bound were periodically detached, but the first layers of the biofilm which remained provided a nice bonding surface for new cells recruitment from the photobioreactor medium. The wall shear stress was mainly dependent on the bubble sizes. Indeed, the flow subjected to an injection of big bubbles was found to be less effective in removing the superficial layers of the *Chlorella vulgaris* biofilms.

In food industries, the cleaning stage consumes a huge amount of water and energy which reflecting its negative contribution to environmental impacts, requiring the adoption of a new eco-friendly process. Despite great efforts in this regard, few studies have been conducted in the literature on the environmental impact of manufacturing processes in food industries. Recently, an LCA study of a milk protein transformation process was carried out involving the contribution of the cleaning phase on the environmental impacts (Gésan-Guiziou et al., 2019). Their results showed that the production and cleaning phases were the most impacting steps with a contribution of 65% and 31% of the total impact of the whole manufacturing process. It was recently demonstrated (Tsai et al., 2021) that pasteurization of egg yolk in powder manufacturing plants, using standard CIP, consumed more than 34.4% of total water and energy consumption which is in agreement with other studies (Krokida et al., 2016).

In this study, as well as in the previous one (Dallagi et al., 2022) foam flow cleaning was found to be more efficient than CIP (considering the same wall shear stress conditions and with the same surfactant) in the cleaning of surfaces contaminated by spores and biofilms. The effects of this method on environmental performance were assessed by a comparative analysis with standard CIP processes, but at a laboratory scale. As was expected, CIP using NaOH at 60°C was the least favorable process in almost all environmental impact indicators such as global warming, ionizing radiation, aquatic ecotoxicity, human health, and non-renewable energy. The high scores were due to the excessive consumption of chemicals, water, electricity, and gas natural mainly during the heating process.

These results are in line with those obtained previously in the literature when CIP using NaOH at high temperatures has been reported (Eide et al., 2003; Gésan-Guiziou et al., 2019; Tsai et al., 2021). Although this process is the best option for cleaning surface contaminations (Jha et al., 2020b), attention should be paid to its potentially harmful impacts. On other hand, foam flow cleaning not only improved the cleaning efficiency, however not as the same extent than NaOH cleaning when comparing to its efficiency on *Pseudomonas fluorescens* biofilms (Benezech and Faille, 2018), but reduced most of the impacts by about 70% of those caused by CIP using the same surfactant. Water and electricity consumption was reduced up to 7 times less since foam can generate high shear stress at a very low air-liquid flow rate. As the LCA results shown, foam flow cleaning reduced almost all impacts by more than 60%. However, the production of surfactant (SDS) was a dominant contributor to climate change (42% and 13%, for CIP and foam flow cleaning respectively), marine eutrophication (80% and 32%), terrestrial ecotoxicity (84% and 20%), agricultural occupation (90% and 60%) and natural land transformation (96% and 82%).

These results are not surprising since the fatty alcohol sulfate contained in the SDS contributes significantly to these impacts. In LCA studies on green cleaning products (Kapur et al., 2012; Van Lieshout et al., 2015), the majority of the environmental impacts of SDS are attributed to the fatty alcohol sulfate raw material. The authors indicated the need to focus on this ingredient. To avoid this impact, the SDS surfactant could be replaced by an eco-friendly surfactant such as biosurfactants, surface-active biomolecules of microbial origin. Indeed, these types of surfactants have a low toxicity and a degradable nature which make it to be environmentally friendly (Paraszkiewicz et al., 2021).

In conclusion, foam flow cleaning was able to remove a significant part of one-day biofilms grown on stainless steel surfaces. Amongst the three bacteria species tested, Ec-SS2 biofilms were the least resistant presenting a complete removal at a mean wall shear stress of only 2 Pa, while the removal of Pf1 and Bc-98/4reached more than 2 log CFU cm^{-2} after 20 min cleaning at 13.2 Pa. A clear positive effect of increasing the average shear stress on cleaning efficiency was thus observed. But in the same time, the increase in frequency and amplitude of the local wall shear stress could probably better explain this efficiency and leading to draw hypothesis on the specific cleaning mechanisms for biofilms elimination by foam flow. In addition, the detachment of biofilms using foam flow was largely more efficient than conventional cleaning-in-place The life cycle assessment study showed that the foam flow process reduces environmental impacts mainly explained by reduced water and energy consumption, compared

to CIP using the same surfactant or a more widely used cleaning solution such as sodium hydroxide at a higher temperature (here 60°C).

ACKNOWLEDGMENTS

The authors are grateful to Christelle Lemy and Laurent Wauquier from UMET, for their valuable technical assistance.

FUNDING

This work was supported by the region Hauts-de-France through their funding of the Interreg Veg-I-Tec project (Programme Interreg V France-Wallonia-Flanders, GoToS3) and the ANR (Agence Nationale de la Recherche) for funding of the FEFS project (contract number ANR-18-CE21-0010).

References

Absi, R., Azouani, R., 2018. Toward automatic cleaning of industrial equipment: pulsed flow-induced wall shear stress. Procedia CIRP 78, 359–363. https://doi.org/10.1016/j.procir.2018.10.001

Al Saabi, A., Dallagi, H., Aloui, F., Faille, C., Rauwel, G., Wauquier, L., Bouvier, L., Bénézech, T., 2021a. Removal of Bacillus spores from stainless steel pipes by flow foam: Effect of the foam quality and velocity. Journal of Food Engineering 289, 110273. https://doi.org/10.1016/j.jfoodeng.2020.110273

Al Saabi, A., Dallagi, H., Aloui, F., Faille, C., Rauwel, G., Wauquier, L., Bouvier, L., Bénézech, T., 2021b. Removal of Bacillus spores from stainless steel pipes by flow foam: Effect of the foam quality and velocity. Journal of Food Engineering 289, 110273. https://doi.org/10.1016/j.jfoodeng.2020.110273

Bénézech, T., Faille, C., 2018. Two-phase kinetics of biofilm removal during CIP. Respective roles of mechanical and chemical effects on the detachment of single cells vs cell clusters from a Pseudomonas fluorescens biofilm. Journal of Food Engineering 219, 121–128. https://doi.org/10.1016/j.jfoodeng.2017.09.013

Bergman, B.-O., Tragardh, C., 1990. AN APPROACH to STUDY and MODEL the HYDRODYNAMIC CLEANING EFFECT. J Food Process Engineering 13, 135–154. https://doi.org/10.1111/j.1745-4530.1990.tb00064.x

Blel, W., Bénézech, T., Legentilhomme, P., Legrand, J., Le Gentil-Lelièvre, C., 2007. Effect of flow arrangement on the removal of Bacillus spores from stainless steel equipment surfaces during a Cleaning In Place procedure. Chemical Engineering Science 62, 3798–3808. https://doi.org/10.1016/j.ces.2007.04.011

Blel, W., Legentilhomme, P., Bénézech, T., Fayolle, F., 2013. Cleanabilty study of a Scraped Surface Heat Exchanger. Food and Bioproducts Processing 91, 95–102. https://doi.org/10.1016/j.fbp.2012.10.002

Blel, W., Legentilhomme, P., Bénézech, T., Legrand, J., Gentil-Lelièvre, C.L., 2009. Application of turbulent pulsating flows to the bacterial removal during a cleaning in place procedure. Part 2: Effects on cleaning efficiency. Journal of Food Engineering 8.

Böhringer, C., Rutherford, T.F., Tol, R.S.J., 2009. THE EU 20/20/2020 targets: An overview of the EMF22 assessment. Energy Economics 31, S268–S273. https://doi.org/10.1016/j.eneco.2009.10.010

Bouvier, L., Cunault, C., Faille, C., Dallagi, H., Wauquier, L., Bénézech, T., 2021. Influence of the design of fresh-cut food washing tanks on the growth kinetics of Pseudomonas fluorescens biofilms. iScience 24, 102506. https://doi.org/10.1016/j.isci.2021.102506

Bridier, A., Briandet, R., Thomas, V., Dubois-Brissonnet, F., 2011. Comparative biocidal activity of peracetic acid, benzalkonium chloride and ortho-phthalaldehyde on 77 bacterial strains. Journal of Hospital Infection 78, 208–213. https://doi.org/10.1016/j.jhin.2011.03.014

Brooks, J.D., Flint, S.H., 2008. Biofilms in the food industry: problems and potential solutions. International Journal of Food Science & Technology 43, 2163–2176. https://doi.org/10.1111/j.1365-2621.2008.01839.x

Carrascosa, C., Raheem, D., Ramos, F., Saraiva, A., Raposo, A., 2021. Microbial Biofilms in the Food Industry—A Comprehensive Review. IJERPH 18, 2014. https://doi.org/10.3390/ijerph18042014

Charlène, T., 2018. Caractérisation de l'hydrodynamique et des transferts gaz-liquide dans un photobioréacteur intensifié : étude de l'effet du bullage sur le développement de biofilm micro-algal.

Eide, M.H., Homleid, J.P., Mattsson, B., 2003. Life cycle assessment (LCA) of cleaning-in-place processes in dairies. LWT - Food Science and Technology 36, 303–314. https://doi.org/10.1016/S0023-6438(02)00211-6

Fagerlund, A., Møretrø, T., Heir, E., Briandet, R., Langsrud, S., 2017. Cleaning and Disinfection of Biofilms Composed of Listeria monocytogenes and Background Microbiota from Meat Processing Surfaces. Appl Environ Microbiol 83, e01046-17, e01046-17. https://doi.org/10.1128/AEM.01046-17

Fernandes, S., Gomes, I.B., Simões, L.C., Simões, M., 2021. Overview on the hydrodynamic conditions found in industrial systems and its impact in (bio)fouling formation. Chemical Engineering Journal 418, 129348. https://doi.org/10.1016/j.cej.2021.129348

Furukawa, S., Akiyoshi, Y., Komoriya, M., Ogihara, H., Morinaga, Y., 2010. Removing Staphylococcus aureus and Escherichia coli biofilms on stainless steel by cleaning-in-place (CIP) cleaning agents. Food Control 21, 669–672. https://doi.org/10.1016/j.foodcont.2009.10.005

Geeraerd, A.H., Valdramidis, V.P., Van Impe, J.F., 2005. GInaFiT, a freeware tool to assess non-log-linear microbial survivor curves. International Journal of Food Microbiology 102, 95–105. https://doi.org/10.1016/j.ijfoodmicro.2004.11.038

Gésan-Guiziou, G., Sobańtka, A.P., Omont, S., Froelich, D., Rabiller-Baudry, M., Thueux, F., Beudon, D., Tregret, L., Buson, C., Auffret, D., 2019. Life Cycle Assessment of a milk protein fractionation process: Contribution of the production and the cleaning stages at unit process level. Separation and Purification Technology 224, 591–610. https://doi.org/10.1016/j.seppur.2019.05.008

Gomes, I.B., Lemos, M., Fernandes, S., Borges, A., Simões, L.C., Simões, M., 2021. The Effects of Chemical and Mechanical Stresses on Bacillus cereus and Pseudomonas fluorescens Single- and Dual-Species Biofilm Removal. Microorganisms 9, 1174. https://doi.org/10.3390/microorganisms9061174

Gomes, I.B., Lemos, M., Mathieu, L., Simões, M., Simões, L.C., 2018. The action of chemical and mechanical stresses on single and dual species biofilm removal of drinking water bacteria. Science of The Total Environment 631–632, 987–993. https://doi.org/10.1016/j.scitotenv.2018.03.042

Grandillo, A., Tatianchenko, S., 2020. Optimization of Clean-In-Place Sanitation Systems for McCain Supply Chain.

Grinstead, D., 2009. Cleaning and sanitation in food processing environments for the prevention of biofilm formation, and biofilm removal, in: Biofilms in the Food and Beverage Industries. Elsevier, pp. 331–358. https://doi.org/10.1533/9781845697167.3.331

Guinée, J.B. (Ed.), 2002. Handbook on life cycle assessment: operational guide to the ISO standards, Eco-efficiency in industry and science. Kluwer Academic Publishers, Dordrecht ; Boston.

Holah, J., 2014. Hygiene in Food Processing and Manufacturing, in: Food Safety Management. Elsevier, pp. 623–659. https://doi.org/10.1016/B978-0-12-381504-0.00024-X

Jara, J., Alarcón, F., Monnappa, A.K., Santos, J.I., Bianco, V., Nie, P., Ciamarra, M.P., Canales, Á., Dinis, L., López-Montero, I., Valeriani, C., Orgaz, B., 2021. Self-Adaptation of Pseudomonas fluorescens Biofilms to Hydrodynamic Stress. Front. Microbiol. 11, 588884. https://doi.org/10.3389/fmicb.2020.588884

Jha, P.K., Dallagi, H., Richard, E., Benezech, T., Faille, C., 2020a. Formation and resistance to cleaning of biofilms at air-liquid-wall interface. Influence of bacterial strain and material. Food Control 118, 107384. https://doi.org/10.1016/j.foodcont.2020.107384

Jha, P.K., Dallagi, H., Richard, E., Benezech, T., Faille, C., 2020b. Formation and resistance to cleaning of biofilms at air-liquid-wall interface. Influence of bacterial strain and material. Food Control 118, 107384. https://doi.org/10.1016/j.foodcont.2020.107384

Jha, P.K., Dallagi, H., Richard, E., Deleplace, M., Benezech, T., Faille, C., 2022. Does the vertical vs horizontal positioning of surfaces affect either biofilm formation on different materials or their resistance to detachment? Food Control 133, 108646. https://doi.org/10.1016/j.foodcont.2021.108646

Kapur, A., Baldwin, C., Swanson, M., Wilberforce, N., McClenachan, G., Rentschler, M., 2012. Comparative life cycle assessment of conventional and Green Seal-compliant industrial and institutional cleaning products. Int J Life Cycle Assess 17, 377–387. https://doi.org/10.1007/s11367-011-0373-8

Krokida, M., Taxiarchou, M., Politis, A., Peppas, A., Kyriakopoulou, K., 2016. LIFE CYCLE ASSESSMENT (LCA) ON EUROPEAN SKIMMED MILK POWDER PROCESSING PRODUCTION PLANT 6.

Lelièvre, C., Legentilhomme, P., Gaucher, C., Legrand, J., Faille, C., BeÃneÃzech, T., 2002. Cleaning in place: e ect of local wall shear stress variation on bacterial removal from stainless steel equipment. Chemical Engineering Science 11.

Li, G., Tang, L., Zhang, X., Dong, J., 2019. A review of factors affecting the efficiency of clean-in-place procedures in closed processing systems. Energy 178, 57–71. https://doi.org/10.1016/j.energy.2019.04.123

Maes, S., Heyndrickx, M., Vackier, T., Steenackers, H., Verplaetse, A., Reu, K.D., 2019. Identification and Spoilage Potential of the Remaining Dominant Microbiota on Food Contact

Surfaces after Cleaning and Disinfection in Different Food Industries. Journal of Food Protection 82, 262–275. https://doi.org/10.4315/0362-028X.JFP-18-226

Meliani, A., Bensoltane, A., 2015. Review of Pseudomonas Attachment and Biofilm Formation in Food Industry. Poult Fish Wildl Sci 03. https://doi.org/10.4172/2375-446X.1000126

Morgan, D., Newman, C.P., Hutchinson, D.N., Walker, A.M., Rowe, B., Majid, F., 1993. Verotoxin producing Escherichia coli O 157 infections associated with the consumption of yoghurt. Epidemiology and Infection 111, 181–188. https://doi.org/10.1017/S0950268800056880

Ostrov, I., Paz, T., Shemesh, M., 2019. Robust Biofilm-Forming Bacillus Isolates from the Dairy Environment Demonstrate an Enhanced Resistance to Cleaning-in-Place Procedures. Foods 8, 134. https://doi.org/10.3390/foods8040134

Paraszkiewicz, K., Moryl, M., Płaza, G., Bhagat, D., K. Satpute, S., Bernat, P., 2021. Surfactants of microbial origin as antibiofilm agents. International Journal of Environmental Health Research 31, 401–420. https://doi.org/10.1080/09603123.2019.1664729

Piepiórka-Stepuk, J., Diakun, J., Jakubowski, M., 2017. The Parameters of Cleaning a CIP System Affected Energy Consumption and Cleaning Efficiency of the Plate Heat Exchanger. Chemical and Process Engineering 38, 111–120. https://doi.org/10.1515/cpe-2017-0009

Puga, C.H., Dahdouh, E., SanJose, C., Orgaz, B., 2018. Listeria monocytogenes Colonizes Pseudomonas fluorescens Biofilms and Induces Matrix Over-Production. Front. Microbiol. 9, 1706. https://doi.org/10.3389/fmicb.2018.01706

Reij, M.W., Den Aantrekker, E.D., ILSI Europe Risk Analysis in Microbiology Task Force, 2004. Recontamination as a source of pathogens in processed foods. Int J Food Microbiol 91, 1–11. https://doi.org/10.1016/S0168-1605(03)00295-2

Ryu, J.-H., Beuchat, L.R., 2005. Biofilm Formation and Sporulation by Bacillus cereus on a Stainless Steel Surface and Subsequent Resistance of Vegetative Cells and Spores to Chlorine, Chlorine Dioxide, and a Peroxyacetic Acid–Based Sanitizer. Journal of Food Protection 68, 2614–2622. https://doi.org/10.4315/0362-028X-68.12.2614

Shaheen, R., Svensson, B., Andersson, M.A., Christiansson, A., Salkinoja-Salonen, M., 2010. Persistence strategies of Bacillus cereus spores isolated from dairy silo tanks. Food Microbiology 27, 347–355. https://doi.org/10.1016/j.fm.2009.11.004

Sharma, M., Anand, S.K., 2002. Characterization of constitutive micro£ora of bio¢lms in dairy processing lines 10.

Silva, L.D., Filho, U.C., Naves, E.A.A., Gedraite, R., 2021. Pulsed flow in clean-in-place sanitization to improve hygiene and energy savings in dairy industry. J Food Process Eng 44. https://doi.org/10.1111/jfpe.13590

Simmonds, P., Mossel, B.L., Intaraphan, T., Deeth, H.C., 2003. Heat Resistance of Bacillus Spores When Adhered to Stainless Steel and Its Relationship to Spore Hydrophobicity. Journal of Food Protection 66, 2070–2075. https://doi.org/10.4315/0362-028X-66.11.2070

Stellato, G., Utter, D.R., Voorhis, A., De Angelis, M., Eren, A.M., Ercolini, D., 2017. A Few Pseudomonas Oligotypes Dominate in the Meat and Dairy Processing Environment. Front. Microbiol. 8. https://doi.org/10.3389/fmicb.2017.00264

Tauveron, G., Slomianny, C., Henry, C., Faille, C., 2006. Variability among Bacillus cereus strains in spore surface properties and influence on their ability to contaminate food surface equipment. International Journal of Food Microbiology 110, 254–262. https://doi.org/10.1016/j.ijfoodmicro.2006.04.027

Toquin, E.L., Faure, S., Orange, N., Gas, F., 2020. New biocide foam containing hydrogen peroxide for the decontamination of vertical surface contaminated with Bacillus thuringiensis spores 26.

Tsai, J.-H., Huang, J.-Y., Wilson, D.I., 2021. Life cycle assessment of cleaning-in-place operations in egg yolk powder production. Journal of Cleaner Production 278, 123936. https://doi.org/10.1016/j.jclepro.2020.123936

van Buuren, N., Prasad, P., 2005. For further information or feedback regarding this report contact: 26.

Van Lieshout, K.G., Bayley, C., Akinlabi, S.O., von Rabenau, L., Dornfeld, D., 2015. Leveraging Life Cycle Assessment to Evaluate Environmental Impacts of Green Cleaning Products. Procedia CIRP 29, 372–377. https://doi.org/10.1016/j.procir.2015.02.063

CHAPTER 4: HYGIENIC DESIGN

Contents

Objectives, main approaches, and progress

This section is concerned with investigating the factors affecting the formation of microbial deposits and their resistance to a rinsing and/or cleaning procedure. These include the material hydrophobicity, the position of surfaces (vertical, horizontal or inclined), air-liquid-material interfaces, as well as surfaces that may be contaminated by aerosols. In this chapter four research papers will be presented, which are related to VEG-I-TEC and FEFS projects. My contribution was mainly related to cleaning in place sections, hydrodynamics investigation, meniscus measurements at the interface air-liquid-material, and movements of particles within droplets during evaporation.

In food industry equipment, many horizontal surfaces are present, such as the bottom of tanks. It seemed likely that the formation of biofilms (quantity, structure, even resistance to a cleaning procedure) could be largely affected by the vertical or horizontal position of the surfaces, in particular because of the possible sedimentation of microorganisms on the horizontal surfaces. This issue was discussed in Article 1 of this chapter. Three bacterial strains (*E. coli*, *Bacillus cereus*, and *Pseudomonas fluorescens*) were analyzed for their ability to form biofilms under static conditions on four materials with different topographic and hydrophilic/hydrophobic properties. The materials used were stainless steel with 2R and 2B finishes, polypropylene, and glass. Whatever the surface position, a great difference was observed between strains in the number of CFU (Ec-SS2 > Pf1 > Bc-98/4), as well as in the biofilm structure. However, no significant differences were observed between materials. Regardless of the strain, biofilms formed in horizontal position was found to be denser than those on vertical surfaces, probably due to the sedimentation of the bacteria on horizontal surfaces. In addition, the resistance to a rinsing procedure of horizontal surfaces was close (E. coli, Pf1) or significantly higher (Bc-98/4) than that of vertical surfaces.
In conclusion, horizontal surfaces are more contaminated and sometimes more difficult to clean than horizontal surfaces, which means that they are particularly at risk in terms of surface hygiene control.

The purpose of Article II was to define equipment design changes that would result in improved surface hygiene. This study focused on 1/ the presence or not of horizontal surfaces, 2/ the presence of angles between walls of 90° or >100°, in fresh-cut food washing tanks. The proposed modifications resulted in a delay in the formation of biofilms by a strain of *Pseudomonas fluorescens* (Pf1), especially in areas at particular risk, such as weld zones, corners and interfaces. For example, in orthogonal vats, the biofilm growth on horizontal welds reached a plateau after 48 hrs and no lag phase was observed. Conversely, the presence of 100° and 132° apertures between walls resulted in a marked change in the lag phase duration, which reached 20 h on the horizontal welds and >30 h on the interfaces air-liquid-wall (ALW). In order to understand the mechanisms underlying these modifications, the flow organization in tanks of different geometries was determined by computational fluid dynamics calculation. This study showed a modification of the flow organization (better mixing in the modified tank with reducing ‘‘dead zones’’ and a quite homogeneous wall shear stress repartition) following the changes in the tank geometry, which resulted in a decrease of the dead zones.

Another area suspected to be favorable to the installation of biofilms in the food industries is the air-liquid-wall interface (ALW), in spite of the warnings issued by some authors about the risk due to these areas on the control of surface hygiene. In fact, ALW interfaces can be found on many surfaces, such as those of partly-filled devices (e.g. tanks, sinks, or washing units) as well as industrial storage and piping systems in areas where some residual liquid has remained after operations.

To investigate the influence of these interfaces on the formation of biofilms and their subsequent resistance to a cleaning procedure (Article III), four bacterial strains (*E. coli*, *Bacillus cereus*, *Pf1*, and *B. subtilis* PY79) were analyzed for their ability to form biofilms under static conditions on three materials with different topographic and hydrophilic/hydrophobic properties (AISI 316 stainless steel with pickled (2B) and bright annealed (2R) finishes, and polypropylene (PP). After one day of incubation in a bacterial suspension, three of the four strains tested produced biofilms at the ALW interface, which were sometimes easily observable with the naked eye. Microscopic observations showed that these biofilms were sometimes thick, especially for Bc-98/4 and Pf1 on the hydrophobic PP. When investigating resistance to a CIP procedure involving 0.5% NaOH at 60°C, large amounts of Bc-98/4 and Pf1 biofilms were still observed by microscopy on the different coupons. Furthermore, most residual cells appeared orange after staining with orange acridine suggesting the presence of many viable cells within the residual biofilms. Yet, enumeration after growth on nutrient agar only detected culturable cells in Bc-98/4 biofilms, probably due to the presence of large amounts of spores within these biofilms (highly resistant to many stresses, including those induced by the presence of NaOH at 60°C).

Nevertheless, this study has shown that the ALW interfaces represent a risk that must not be neglected in the food industry, because these areas are suitable for the formation of biofilms by pathogenic bacteria and bacteria responsible for food spoilage and that these biofilms are sometimes highly resistant to a cleaning procedure.

Finally, in the last publication mentioned in this chapter (Article IV), we investigated the formation of deposits by evaporation of droplets containing hydrophilic and hydrophobic spores on different materials. Indeed, a source of surface contamination in the food industries is the presence of bioaerosols (aerosols containing particles of biological origins) that settle on surfaces and equipment and thus contribute to the food contamination during food preparation and packaging. Spores produced by five *Bacillus* strains were used in this study. These spores are surrounded by a flexible membrane called "exosporium" [spores belonging to the species *B. cereus*] or a mucous layer called "crust" [spores belonging to the species *B. subtilis*]. They are also characterized by different hydrophilic/hydrophobic properties. Droplets were settled on four materials, stainless steel (with 2R and 2B finishes), polypropylene, and glass. Results showed that both spores and material properties play a major role in the kinetics of the droplet shape during the evaporation process and in the architecture and the distribution patterns after drying. Thanks to microscope observation, different processes were proved such as pinning, depinning, and formation of ‘’coffee-ring”. The deposits obtained after complete drying of the droplets were subjected to a rinsing and to a CIP procedure in order to determine their resistance to mechanical and chemical actions. After a single rinsing step, more than 90% of the spores

withstood the removal process which reflects an very high resistance of these deposits to mechanical detachment. Spores within the ring were the most easily removed. The role of the material proprieties on the detachment was not very clean, while hydrophilic B. subtilis PY79 were the least resistant to detachment. When the deposits were subjected to CIP using NaOH, the cleaning efficiency was much better. Role of strain and materials on the detachment were drawn, with the highest on glass and the least for Bs PY79 due to the absence of clusters.
In conclusion, the formation of bio-aerosols that can contaminate surfaces even far from their source, and form deposits particularly resistant to cleaning, especially on hydrophobic materials, are to be considered very seriously in the food industries. Indeed, these newly contaminated surfaces may cause cross-contamination in food processing lines.

Highlights

The vertical/horizontal position of the surface affects biofilm formation. Higher amount of biofilms are found on horizontal surfaces, probably due to the accumulation through sedimentation of bacteria on horizontal surfaces. But these biofilms are often more fragile.

The changes in some geometrical features (no horizontal surfaces and only open angles exceeding 100°) induced a better flow organization reducing ‘‘dead zones’’. This results in a delay in the formation of biofilms, especially in areas at particular risk, such as weld zones, corners and interfaces.

Some bacteria form large amounts of biofilm at air-liquid-wall interface, and these biofilms are highly resistant to cleaning. Their amount and structure is deeply affected by the material hydrophobicity.

Bio-aerosols settled on surfaces form deposits whose structure is affected by the hydrophilic/hydrophobic character of the material. The resistance to detachment (rinsing/cleaning) of the dried droplets is affected the material's and particle's hydrophobicity

Publication I: Does the vertical vs horizontal positioning of surfaces affect either biofilm formation on different materials or their resistance to detachment?

https://doi.org/10.1016/j.foodcont.2021.108646

Contents lists available at ScienceDirect

Food Control

journal homepage: www.elsevier.com/locate/foodcont

Does the vertical vs horizontal positioning of surfaces affect either biofilm formation on different materials or their resistance to detachment?

Piyush Kumar Jha [a], Heni Dallagi [a], Elodie Richard [b], Maureen Deleplace [a], Thierry Benezech [a], Christine Faille [a,*]

[a] Univ. Lille, CNRS, INRAE, ENSCL, UMET, F-59650, Villeneuve d'Ascq, France
[b] Univ. Lille, CNRS, INSERM, CHU Lille, Institut Pasteur de Lille, US 41 - UMS 2014 - PLBS, F-59000, Lille, France

ARTICLE INFO

Keywords:
Biofilm
Rinsing procedure
Vertical/horizontal position
Material
Sedimentation

ABSTRACT

In the food industry, the control of surface hygiene is a major issue. It is therefore essential to identify those parameters that can affect the bacterial contamination of surfaces and the effectiveness of hygiene procedures. Numerous studies have focused on the role of bacteria, flow arrangements or materials, but almost nothing has been reported on the possible impact of vertical or horizontal positioning of surfaces on bacterial contamination. The aim of the current study was firstly to determine the ability of bacterial species usually found in food processing lines to form biofilms on surfaces positioned vertically or horizontally and then to assess the resistance of these biofilms to detachment. The experiments were carried out using three bacterial strains (*Escherichia coli* SS2, *Bacillus cereus* 98/4, and *Pseudomonas fluorescens* Pf1) that produced biofilms on glass, polypropylene and stainless steel (surface finishes 2B and 2R). We first observed that not only did the bacterial strain type impacts its ability to form biofilms (Ec-SS2 > Pf1 > Bc-98/4), but that the vertical vs horizontal position of the surface would also affect biofilm formation, probably due to the accumulation through sedimentation of bacteria on horizontal surfaces. However, the horizontally formed Pf1 biofilms were very fragile and could be partially removed by a gentle rinsing step. Lastly, no significant differences could be found in the ability to form biofilms on the different materials. The resistance to detachment to a standard rinsing process in a pilot rig was also investigated. While both strains and materials significantly affected the amount of biofilm detached, only Bc-98/4 biofilms were impacted by the surface position, with horizontal biofilms showing extreme resistance to shear forces. In conclusion, this study shows that horizontal surfaces in food environments probably represent an increased risk of contamination by bacteria frequently isolated from these environments and should be subjected to increased monitoring.

1. Introduction

Biofilms are often defined as assemblages of surface-associated microbial cells encased in a matrix made of self-produced extra-cellular polymeric substance (EPS). In the food industry, biofilm formation can occur on any surface, whether food contact surfaces including processing lines, slicing machines, washing tanks, cutting boards, or non-food contact surfaces such as walls, floors and drains. They therefore represent a serious threat to both food quality and food safety, especially as the biofilms are often strongly resistant to the cleaning (Faille et al., 2018) and disinfection (Araujo et al., 2011) procedures implemented to control surface contamination. Moreover, all types of materials are affected by contamination, including stainless steel, polymers and even glass. Once biofilms are established on a production or packaging line, it is therefore likely that there will be recurrent problems of cross-contamination of food, causing not only reduction of the shelf life of products (Galié et al., 2018) but also potential outbreak of foodborne diseases (Mazaheri et al., 2021).

It is often accepted that many factors affect the formation of biofilms and their properties, e.g. their structure or their resistance to rinsing and/or cleaning procedures. These include bacteria (Faille et al., 2014), flow arrangements (Bouvier et al., 2021), material's surface properties (Faille et al., 2018), or position of the surface within the processing line such as in fully submerged areas vs. at an air-liquid-wall interface (Jha et al., 2020).

Among these factors, the materials of contact surfaces have been the

* Corresponding author.
E-mail address: christine.faille@inrae.fr (C. Faille).

https://doi.org/10.1016/j.foodcont.2021.108646
Received 4 August 2021; Received in revised form 24 October 2021; Accepted 25 October 2021
Available online 28 October 2021

Publication II: Influence of the design of fresh-cut food washing tanks on the growth kinetics of Pseudomonas fluorescens biofilms

https://doi.org/10.1016/j.isci.2021.102506

iScience

CellPress
OPEN ACCESS

Article

Influence of the design of fresh-cut food washing tanks on the growth kinetics of *Pseudomonas fluorescens* biofilms

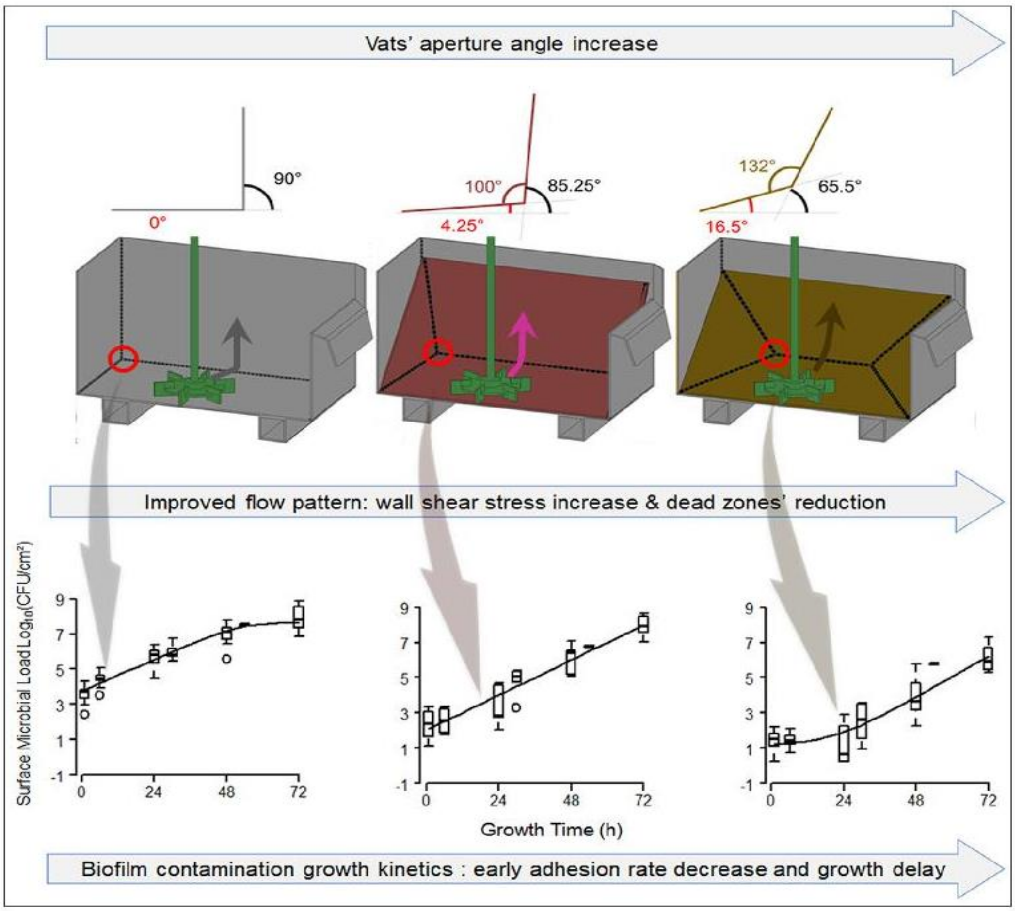

Laurent Bouvier, Charles Cunault, Christine Faille, Heni Dallagi, Laurent Wauquier, Thierry Bénézech

thierry.benezech@inrae.fr

Highlights

Pseudomonas fluorescens biofilm growth kinetics strongly related to the vat design

Improved design lead to 24hr lag time before the biofilm exponential growth phase

Corners, welds, and wetting front areas contamination could be largely mitigated

Bouvier et al., iScience 24, 102506
June 25, 2021
https://doi.org/10.1016/j.isci.2021.102506

iScience

CellPress
OPEN ACCESS

Article

Influence of the design of fresh-cut food washing tanks on the growth kinetics of *Pseudomonas fluorescens* biofilms

Laurent Bouvier,[1] Charles Cunault,[2] Christine Faille,[1] Heni Dallagi,[1] Laurent Wauquier,[1] and Thierry Bénézech[1,3,*]

SUMMARY

Mitigation of cross-contamination of fresh-cut food products at the washing step was studied by investigating how the vat design would affect the biofilm contamination surfaces. Hygienic design features such as no horizontal surfaces and only open angles exceeding 100° were proposed. The flow organization (velocity streamlines, wall shear stresses, and dynamics of the flow) was identified by means of computational fluid dynamics (CFD) calculation. *Pseudomonas fluorescens* PF1 biofilm growth kinetics were then mapped. The change in some geometrical features induced a better flow organization reducing "dead zones". This significantly changed the biofilm growth kinetics, delaying the detection of biofilms from 20 hr to 24 hr. Critical areas such as welds, corners, and interfaces appeared far less prone to strong bacterial development. This would mean milder or less chemicals required at the washing step and faster and easier cleaning.

INTRODUCTION

In agro-food industrial environments, such as breweries, dairies, poultry or meat processing factories, as well as fresh-cut industries, surfaces have been reported to be contaminated by a range of microorganisms, including pathogenic and spoilage bacteria (Srey et al., 2013). Once introduced, many bacteria are able to persist on the contaminated surfaces, or even to form biofilms if environmental conditions are suitable. This may lead to cross-contamination of food and beverages at all food processing stages. For example, it has been proven that an outbreak of *Listeria monocytogenes* in Washington State (USA) was due to the contamination of a milkshake machine (Kase et al., 2017). Indeed, the ability of *L. monocytogenes* to survive cold temperatures or desiccation, together with its capability to form biofilms or to integrate pre-existing biofilms, improves its chances of colonizing and persisting in food processing environments (Pang et al., 2019). This phenomenon has been demonstrated in both dairy (Melero et al., 2019) and ready-to-eat food processing facilities (Henriques et al., 2014). Among the numerous abiotic parameters affecting biofilm formation, equipment design and material surface properties comprising topography and physico-chemistry, would play major roles (Faille et al., 2018). Indeed, biofilms are often found in specific areas including those with surface irregularities (e.g., weld features, groves, and scratches) and those affecting flow patterns (e.g., obstacles, dead ends). When biofilms are formed under dynamic conditions, their 3D structures are deeply affected by the flow pattern (Cunault et al., 2015, 2019; Manz et al., 2005;Simões et al., 2006). More compact and less porous biofilms have been observed under turbulent flows than under laminar flow conditions (Stoodley et al., 1999a; Vieira et al., 1993). In recent work (Cunault et al., 2018, 2019), surface contamination by *Pseudomonas fluorescens* PF1 biofilms has been studied using pilot scale washing tanks with the standard design features encountered in the fresh-cut vegetable processing industry. It has been found that biofilm growth dynamics (Cunault et al., 2018) and structures (Cunault et al., 2019) depend on the location in the tanks, which could range from discontinuous monolayer biofilms to biofilms with large, thick clusters. Poor design features encountered in such tanks make surface contamination difficult to remove. These include horizontal surfaces, right angles, and sometimes, poor quality welds and the presence of closed corners at the vat bottom and are critical in terms of hygiene.

Many efforts have been made to control biofilm development by preventive and curative approaches (Amin et al., 2020; Muhammad et al., 2020; Rajab et al., 2018; Srey et al., 2013; Whitehead et al., 2015). Among the preventive approaches, several strategies have been developed in attempts to prevent biofilm installation,

[1]Univ. Lille, CNRS, INRAE, Centrale Lille, UMR 8207 - UMET - Unité Matériaux et Transformations, F-59000 Lille, France

[2]IATE, Univ Montpellier, INRAE, Institut Agro, Montpellier, France

[3]Lead contact

*Correspondence: thierry.benezech@inrae.fr

https://doi.org/10.1016/j.isci.2021.102506

Publication III: Formation and resistance to cleaning of biofilms at air-liquid-wall interface. Influence of bacterial strain and material

https://doi.org/10.1016/j.foodcont.2020.107384

Contents lists available at ScienceDirect

Food Control

journal homepage: www.elsevier.com/locate/foodcont

Formation and resistance to cleaning of biofilms at air-liquid-wall interface. Influence of bacterial strain and material

Piyush Kumar Jha[a], Heni Dallagi[a], Elodie Richard[b], Thierry Benezech[a], Christine Faille[a,*]

[a] Univ. Lille, CNRS, INRAE, ENSCL, UMET, F-59650, Villeneuve d'Ascq, France
[b] Univ. Lille, CNRS, INSERM, CHU Lille, Institut Pasteur de Lille, US 41, UMS 2014, PLBS, F-59000, Lille, France

ARTICLE INFO

Keywords:
Biofilm
Air-liquid-wall interface
Meniscus
Cleaning in place
VBNC
Bacillus spores

ABSTRACT

Interfaces between air, liquid and walls (ALW interfaces) are known to be conducive to the formation of biofilms, at least in some bacteria, yet little information is available on the influence of material properties on the amount of biofilms formed and their resistance to a cleaning procedure. In this study, we investigated the ability of four bacterial strains (*Pseudomonas fluorescens* [Pf1], *Escherichia coli* [Ec-SS2], *Bacillus cereus* [Bc-98/4] and *B. subtilis* [Bs-PY79]) to form biofilms in static conditions at the ALW interface on four materials with very different topographic and hydrophilic/hydrophobic properties (stainless steels with 2R or 2B finishes, polypropylene and glass). Biofilms were observed after staining with orange acridine visually, by epifluorescence microscopy and by confocal scanner laser microscopy. The number of culturable cells within biofilms was also estimated after growth on agar. After one-day of incubation in a bacterial suspension, three strains (except Bc-PY79) were found to form large amounts of biofilm, easily observable to the naked eye. However, great differences were observed between strains in the number of CFU (between 4.7 and 7.4 log CFU cm^{-2}), as well in the biofilm structure. Furthermore, the material also affected the amount and/or structure of biofilms, and a 3D-biofilm organisation was only observed for two of the four tested strains (Bc-98/4 and Pf1) on PP, a hydrophobic material. After a standard cleaning-in-place treatment involving NaOH 0.5% at 60 °C, cultivable cells were only detected from Bc-98/4 biofilms (growth on agar), while biofilms were also still visible on coupons contaminated with Pf1. Furthermore, most residual biofilms after cleaning appeared orange by epifluorescence microscopy after staining with orange acridine suggesting the presence of many viable but non-culturable cells within the residual biofilms. In Bc-98/4 biofilms, spores were also clearly observed by epifluorescence microscopy. Knowing their ability to survive the conditions encountered during cleaning procedures, this could account for the high level of CFU enumerated after cleaning. Lastly, Bc-98/4 biofilms formed on stainless steel 2R were more resistant to cleaning than on PP and glass. All of these results highlighted the importance of biofilms at the ALW interfaces in the control of surface hygiene, particularly in the food industry. We then investigated whether the shape of the menisci at the interfaces (convex vs concave, kinetics over time) could at least partly explain the shape or even the resistance to detachment of the ALW biofilms.

1. Introduction

Despite the attention currently being paid to hygiene procedures in the food industries, it remains difficult or impossible to produce food free of micro-organisms. Thus, the involvement in food contamination of adherent bacteria, spores, or biofilms on the surface of food processing equipment is widely acknowledged. For the record, biofilms are communities of micro-organisms attached to biotic or abiotic surfaces and embedded in a matrix made of self-produced extracellular polymeric substances (EPS). These biofilms represent a serious challenge to the food industry since their formation is possible on every material, including polymers, stainless steel, thereby compromising food safety and quality. For example, cross-contamination of food by *Listeria monocytogenes* could result from biofilms on food-contact surfaces including slicing machines and cutting boards, as well as on non-food contact surfaces such as floors or drain sinks (Rodríguez-López, Rodríguez-Herrera, Vázquez-Sánchez, & Cabo, 2018). Furthermore, bacteria in biofilms are 100–1000 times more resistant to cleaning (Bénézech & Faille, 2018; Cunault, Faille, Calabozo-Delgado, & Benezech, 2019) and disinfection (Maes et al., 2019) processes than are planktonic cells, rendering them difficult to control them. The slow or incomplete penetration of antimicrobial agents through the EPS matrix

* Corresponding author.
E-mail address: christine.faille@inrae.fr (C. Faille).

https://doi.org/10.1016/j.foodcont.2020.107384
Received 17 April 2020; Received in revised form 23 May 2020; Accepted 28 May 2020
Available online 11 June 2020

Publication IV: Structure of deposits formed by drying of droplets contaminated with Bacillus spores determines their resistance to rinsing and cleaning

https://doi.org/10.1016/j.jfoodeng.2021.110873

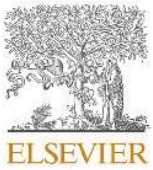

Contents lists available at ScienceDirect

Journal of Food Engineering

journal homepage: www.elsevier.com/locate/jfoodeng

Structure of deposits formed by drying of droplets contaminated with *Bacillus* spores determines their resistance to rinsing and cleaning

Maureen Deleplace [a], Heni Dallagi [a], Thomas Dubois [a], Elodie Richard [b], Anna Ipatova [c], Thierry Bénézech [a], Christine Faille [a,*]

[a] Univ. Lille, CNRS, INRAE, ENSCL, UMET, F-59650, Villeneuve d'Ascq, France
[b] Univ. Lille, CNRS, INSERM, CHU Lille, Institut Pasteur de Lille, US 41 - UMS 2014 - PLBS, F-59000, Lille, France
[c] Univ. Lille, CNRS, UMR 8520 - IEMN, F-59000, Lille, France

ARTICLE INFO

Keywords:
Droplet evaporation
Bacillus spores
Deposition patterns
Material
Hydrophobicity
Surface hygiene

ABSTRACT

The formation of deposits by evaporation of droplets contaminated by *Bacillus* spores was investigated, focusing on the role of spore and material properties. Droplets containing hydrophilic to hydrophobic spores were deposited on materials (stainless steels, polypropylene, glass). The presence of spores within the droplets, as well as material hydrophobicity plays a major role in the kinetics of the droplet shape during drying while the pattern of the dried deposit was affected by both material and spore properties. The resistance to detachment of the different deposits was then investigated. After a single rinsing procedure, a very high resistance to detachment of adherent spores was observed (up to 90% of residual spores). The hydrophilic Bs PY79 spores were the least resistant to removal, while the differences between materials were not pronounced. The ease of cleaning of the dried deposits was much greater. The least resistant spores were still the Bs PY79 ones, while the detachment was 3–100 times more effective on glass than on other materials.

These results highlight the predominant role of hydrophilic/hydrophobic properties of particles and materials on the structure of deposits and their further resistance to rinsing and cleaning procedures.

1. Introduction

In food industries, contamination of equipment surfaces is of concern, as contaminated surfaces can serve as a source of cross-contamination in foods, therefore compromising food quality and safety (Coughlan et al., 2016) and resulting in the rejection of the products, economic losses and even diseases if food-borne pathogens are involved. A source of surface contamination is the presence of bio-aerosols (aerosols containing particles of biological origins) that settle on surfaces and equipment and thus contribute to the food contamination during food preparation and packaging. Indeed, it has long been known that many micro-organisms are present in aerosols in food environments. This is the case, for example, with yeasts in fruit juice production units, molds in cake factories or wheat or rice flour mills, or bacteria in milk processing plants or slaughterhouses (Theisinger and Smidt, 2017).

These bioaerosols can come from ventilation systems and evaporators, as air currents are known to be important vectors for the spread of potentially pathogenic organisms (Eduard et al., 2012). They can also be formed during certain operations during food processing, such as washing fruits and vegetables (high pressure water systems, "bubbling" in tanks with the production of air bubbles). Furthermore, they are also often associated with rinsing or cleaning operations e.g. high pressure cleaning of drains or floors (Faille and Billet, 2020), which causes the dispersion of water droplets over distances sometimes exceeding 2 m in height and 5 m in length (Holah, 2018). One of the major problems posed by these bioaerosols is that some harmful bacteria are able to survive inside droplets or even resist further desiccation. Indeed, it has been shown that *L. monocytogenes*, a non-sporulating bacterium, can survive more than 3 h in aerosols (Spurlock and Zottola, 1991). Furthermore, some food-borne pathogens such as *Salmonella typhimurium* or *L. monocytogenes* and of course bacterial spores, such as *Bacillus* spores, resist a period of desiccation quite well, especially in the presence of food residues (Kuda et al., 2015).

When droplets are deposited on a surface and subjected to a drying step, this will result in the formation of a deposit whose structure is

* Corresponding author. INRAE, UMET, 369 rue Jules Guesde, F-59650, Villeneuve d'Ascq, France.
E-mail address: christine.faille@inrae.fr (C. Faille).

https://doi.org/10.1016/j.jfoodeng.2021.110873
Received 19 July 2021; Received in revised form 29 October 2021; Accepted 31 October 2021
Available online 12 November 2021

GENERAL CONCLUSION & PERSPECTIVES

This study is part of the Interreg VEG-I-TEC project that looks at innovations and technological developments on an industrial scale to reduce the consumption of energy and water and improve the hygiene and the quality of food products. The use of foam flow for cleaning surfaces contaminated by microorganisms was investigated in this project.
Our research was a continuation of the previous works of (Al Saabi et al., 2020; Chovet and Aloui, 2016). It aims to improve and extend the knowledge on the rheological behavior of foam flow and then apply this knowledge in the enhancement of the efficiency of the cleaning process in the food industry. The rheology section consists of determining the foam properties and their flow behavior under different situations. The experimental characterization was intended to develop a robust database in order to validate numerically rheological models allowing to predict the behavior and the reorganization of the foam flow. Then we used this database to explain possible mechanisms involved in the improvement of the cleaning efficiency using foam flow.

The litterature review started with an overview of industrial cleaning procedures in use, identifying parameters affecting cleaning efficiency as well as suggested improvements to optimize these procedures. In fact, microbiological contamination of equipment surfaces can lead to cross-contamination of the product being processed by this equipment, thus causing significant economic problems and even public health issues. In the agri-food industry, microbial contamination possibly growing on surfaces in contact with food throughout the production lines might induce serious foodborne outbreaks. Regardless of the sector involved, to ensure the hygiene of materials in contact with food, cleaning, and disinfection processes are commonly implemented. However, despite the strong enforcement of the conventional cleaning and disinfection processes, each year, alarming statistics are reported by sanitary organizations, emphasizing the need of improving the safety and hygiene of the equipment/products in these sectors. It is in this context that our objectives are related to a better understanding of the potential interests of the use of foam flow for cleaning.

Several key parameters related to foam flow through a horizontal square straight duct were identified such as foam quality, flow velocity, pressure loss, bubble diameter, sliding layer thickness, and wall shear stress. These parameters have been identified through the following experimental methods: polarography methods to measure the wall shear stress, conductimetry to measure the thickness of the slip layer at the walls, Particle Image Velocimetry (PIV) to access to the instantaneous velocity fields, Image analyses to determine the bubble size distribution and thus the void fraction, and different pressure taps along the bottom wall of the channel for pressure loss measurement. All the data thus obtained have allowed an understanding of the hydrodynamic behaviour of the foam flow in a straight channel and its distortion induces by targeted geometry changes (such as half-sudden expansion and fence) under different Reynolds numbers (Re=32, 65, and 97) and foam qualities (0.55, 0.6, 0.65, 0.7, 0.75, 0.88, and 0.85%). Results showed that the rheological behaviour of foams is controlled by processes that occur within the microstructures such as the rearrangement of bubble size, liquid film, and Plateau borders. A slight modification on the pressure or the shear stress applied could lead to deformation on the foam state.

The velocity profiles confirmed that depending on Reynolds number, the foam can flow under different regimes, from a plug flow (1D), to a bi-dimensional (2D) regime, foam being faster at the bottom of the duct than at the top up to a three-dimensional (3D) regime, foam becomes completely sheared foam flow, flows in all directions and the bubbles start to be agitated.
The experimental results confirmed the occurrence of three foam flow regimes (1, 2, and 3D) when investigating the role of a fence or a half-sudden expansion on the foam flow organization. It was observed a significant distortion of the flow and a re-organization of the foam structure near these singularities highlighting the visco-elastic character of the foam, e.g. a noticible change in the static pressure when foam is flowing throught the half-sudden expansion with a slow down of the velocity and the formation of aggregates of reduced-sized bubbles. Simultaneously, these singularities created a "stagnant" cover, altering the velocity of other bubbles passing through them, which leads to a change in the foam structure. Briefly, the decrease of the pressure induced by the section change, foam bubbles are distorted, and the inter-bubble liquid film varies. This deformation induces an increase in the surface energy of the bubbles that consequently store elastic energy in proportion to the surface tension. The foam reveals its elastic character as the low density and the high active surface push the bubbles up into the channel to fill the entire height of the duct's cross-section, to return to its initial equilibrium. Furthermore, this characterization indicated that foam behaves as a non-Newtonian fluid. Under low velocity conditions (small shear stresses under 2 Pa according to our experimental conditions) the foam behaves as a solid. Above this limit, the foam flows like a viscous liquid dissipating energy in relation to the rate of deformation. Indeed, either the foam accumulates its mechanical energy upstream to restore it downstream of the singularity and eventually recover its initial state, or the deformation is irreversible, and the foam within the new geometry retains the same flow regime (plug flow or shear flow).These results confirmed the importance of foam properties in its rheology and physics, demonstrating how sensitive and complex foams are. This information has facilitated our CFD simulation, which aims to predict the viscoelastic character of foam, as for a non-Newtonian fluid, with and without singularities. For this purpose, 3D CFD numerical simulations were performed using the ANSYS CFX code to identify an adequate rheological model that could predict the foam flow behaviour in a straight pipe under different Reynolds numbers and foam qualities, then in presence of the tested singularities. Some hypotheses were proposed in order to simplify such physical problems as the interactions between bubbles and their slides over the liquid films at the walls. The foam was defined as a pseudo-fluid, where its properties depend on those of the air and the liquid in laminar and isothermal conditions. In addition, the presence of the underlying liquid film developed at the bottom of the pipe was well-considered to take into account its stretching effect on the foam. Two rheological models were proposed (Bingham and Herschel-Bulkley).
The identification of the rheological parameters was based on the experimental results (curve flow) and then was adjusted numerically based on the inverse simulation: starting with known experimental results, setting the parameters, and checking the velocity and pressure profiles obtained, then comparing these to the experimental ones. Regardless of the foam quality, the Reynolds numbers, and the type of geometry (with or without singularities) the CFD simulations and the experimental results showed good agreement. In particular, for cases of singularities Herschel-Bulkley rheological model was found to better describe the foam flow for all regimes than the Bingham model. As for the lower Reynolds number, the two fluids

behave like a plug-type flow presenting a mean deviation of 15%. However, at a higher Reynolds number, some greater deviations could appear in the vicinity of the singularities, which can reach more than 50% with Hershel-Bulkley and be completely different for Bingham. This considerable discrepancy reflects the higher sensitivity of the chosen model (pseudo-fluid flow) and its limits in presenting this type of foam flow deformation and the bubbles' reorganization. This is probably related to the actual rheological properties of the foam modeled here by a (too) quite simple Herschel-Bulkley pseudo-fluid model.
In general, CFD simulation provides an approximation of how complex fluids behave, without the requirement of experimental analysis or having access to certain measurements that are difficult to perform experimentally. This goal was achieved by our simulation since we have identified a model that can predict the behaviour of foam under different flow situations and we were able to have access to the velocity fields on the spanwise plane which are not accessible experimentally using the PIV technique because of the opacity of the foam. However, to improve our simulation, some likely important phenomena should be taken into account in the future such as the compressibility of the foam gas phase and the slipping of the foam bubbles on the channel walls (phenomena existing at the bubble-bubble and bubble-liquid film interfaces) highlighted by the different experimental methods. Despite the complexity of the properties involved in the physics of foams (border stability plateau, effect of surface tension, drainage of liquid, bubble movements, coarsening, ripening, coalescence, compressibility), the non-Newtonian fluid model with threshold stress gives a quite good approximation of the foam's flow behaviour and its deformation e.g. when encountering a fence.

The second goal of this research was to study how this type of fluid could be an interesting alternative process for cleaning in the food industry. However, modification of the ducts geometries and the presence of specific equipment (valves, fences in heat exchangers, corners or other obstacles) in agro-food processing industries would thus significantly change the foam structure and the flow organization and probably, affect the foam cleaning process. In this case, our CFD could be of help in improving the cleaning efficiency through and the design improvement of industrial equipment and a better installation of its accessories, thereby ensuring high foam stability and fast recovery of the flow regime due to a better flow organization.
To test the capacity of wet foam flow (foam quality of 0.5, using SDS surfactant (Sodium Dodecyl Sulfate)) to remove the biocontamination from 2B finish stainless-steel surfaces, two different contamination patterns were investigated. The first model consisted of droplets containing *Bacillus subtilis* spores (hydrophilic Bs PY79 and hydrophobic *B. subtilis* PY79 spsA), and biofilms produced horizontally by three bacteria strains encountered in food industry production sites (*Escherichia coli* SS2, *Bacillus cereus* 98/4, and *Pseudomonas fluorescens* Pf1). The choice of these strains was based on their extensive occurrence in the food industry and their ability to adhere and contaminate the equipment surfaces.
It should be noted that all these bacterial strains are commonly associated with food spoilage. In the case of biofilms, the corresponding strains are also very present in food processing plants as they are indeed able to form biofilms under different environmental conditions. However, even if these chosen species are not pathogenic, they can act as "helpers" for pathogenic

bacteria, allowing them to persist in food plants, mainly using the matrix as an anchoring and a protective medium.

To achieve our goal, experiments were carried out on foam flow cleaning (FFC) under different conditions (by varying the foam shear stress from 2.2 to 13.2 Pa, and the bubble size from 0.18 to 0.34) for 15 and 35 sec, 1, 3, 5, 10, and 20 min. Other experiments were carried out using cleaning in place (CIP) under a chosen reference condition (10 Pa, with SDS surfactant) to compare the relative effectiveness of FFC and CIP. Therefore for the used conditions, a detailed characterization of the foam at the walls was performed which aims to understand the detachment mechanisms by the foam, identify the key parameters, then optimize the process by testing news foam conditions on cleaning of stainless-steel coupons. Furthermore, the conductimetry, bubble size distribution, and polarography results demonstrated a significant impact of the bubbles' passage and its size on the fluctuation of the liquid film thickness between the bubbles and the top wall and between bubbles themselves (Plateau borders). This variation directly affects the distribution of the local shears stress, which could influence the efficiency of bacteria removal. The passage of the bubbles leads to an increase in the mass transfer (Sherwood number) represented by peaks of shear stress, which appear in a harmonic approach, and thus informing on the frequency and on the amplitude after the passage of the bubbles. As the velocity increases, the bubbles become smaller, thus the frequency of the shear stress increase, resulting from the increase in the number of passing bubbles, while the amplitude decreases.

On the other hand, we highlighted the effect of 1h evaporation on the disposition pattern of the spores within the droplets using epifluorescence microscopy. For hydrophilic spores Bs PY79, a regular round peripheral ring “called coffee ring” was clearly observed. It was thick with few adhered spores within the ring. The deposition pattern, in this case, was irregular on all the drop surfaces presenting an accumulation of spores on two small areas near the ring. Conversely, a very different soiling pattern was observed with the hydrophobic spores Bs PY79 spsA as they appeared aggregated forming thick clusters resulting in a steady distribution of spores and clusters over the whole contaminated drop area. Noting that the distribution of the patterns of different strains was studied with a lot of details in chapter 4 (hygienic design). Concerning the removal part, the enumeration of residual spores after the cleaning processes showed a strong detachment rate at the beginning of the cleaning process (less than 1 min), followed by a second kinetic phase described by a slow detachment rate. In addition, it showed differences in cleaning efficiency, which is directly related to the hydrophobicity of the spores, with increased resistance to detachment for the most hydrophobic strain tested. This was explained by the remaining clusters in the case of hydrophobic spores, as was observed by microscopy images on the structure of the droplets before and after cleaning. However, for both strains, foam flow cleaning showed a better removal efficiency than conventional cleaning in place considering the same average wall shear stress conditions. This enhancement of cleaning was mainly for the case of hydrophilic spores, where the CIP resulted in about 2 log CFU reduction after 20 min cleaning compared to around 4 log CFU reduction with foam. While the foam was more effective with an additional 1 log reduction for the hydrophobic spores.

When related the experimental results to those of cleaning of spores, different mechanisms such as capillary imbibition, foam drainage, and fluctuation of wall shear stress induced by bubbles’

passage could explain the removal phenomenon. Indeed, as the bubbles progress under the contamination (soiled surface placed upward), important shear forces were applied at the walls with pics at the front and at the back of each bubble. The smallest bubbles generate higher wall shear stress at theirs ends, increasing then the collision frequency with the contamination and inducing the removal from the surfaces. Further, the combination of gravity and surface tension forces intervenes to remove or sweep that contamination into the liquid solution. In addition, this kind of contamination can be sucked into the Plateau borders of the foam under the imbibition effect. The capillary forces drive this mechanism. Indeed, these Plateau borders have a curvature that creates a capillary under pressure in the liquid phase. Owing to this pressure difference, the foam was able to absorb the spores (which have a small size of 1 µm), similar to the behavior of a sponge. Lastly, the synergy between high wall shear stress and reduced bubble size leads to efficient cleaning of stainless steel surfaces contaminated with bacterial spores.

When related these results with those of Ahmad Al Saabi's work published in 2021 with different foam quality, some points could be taken. Indeed, for the same speed, the drier foam showed better removal during the second phase of detachment than the wet foam, while the wetter foam is much more efficient during the first phase of detachment resulting in a much better overall cleaning efficiency.

The characterisation of the foam in Chapter 2 showed that the capillary forces of the wet foam are not sufficient to retain the liquid in the upper part of the pipe. Therefore, this liquid tends to flow through the bubbles and accumulate in the lower part, resulting in a thinning of the liquid in the upper part of the pipe and a thickening in the lower part. This was observed by the evolution of the thickness of the liquid films at the walls using conductimetry methods. It can therefore be assumed that, although this phenomenon is reduced because the foam remains stable over the entire cleaning area, the drainage drives the contamination into the foam and contributes to the cleaning efficiency. On the other hand, the capillary imbibition effect could be a dominant mechanism during the second phase of detachment, which seems to show this better elimination in the case of drier foam. In the literature, foam imbibition can be very high in the case of dry foams explained by the fact that the driving capillary forces are much stronger at the Plateau edges due to the polyhedral shape of the bubbles. This hypothesis does not contradict our work, since for a given foam quality, the decrease in bubble size leads to an increase in the imbibition effect, and thus to an improvement in removal efficiency. This was demonstrated in our work, which shows the effect of small bubbles on the improvement of spore removal during the second phase, whereas no effect was observed for the first phases of detachment. Further characterisation of drier mosses (quality>0.5) is needed to prove or disprove these hypotheses.

Concerning the study on biofilms removal, the obtained results (using enumeration of cultivable cells, or Epifluorescence and confocal laser microscopes) confirmed that the chosen bacterial strain are able to form a biofilm (a minimum of 1 106 CFU/cm2) on a horizontal surface of stainless steel material. However, a difference between the strains were observed. The highest amount was observed for Pf1, then Ec-SS2 and lastly Bc-98/4. In addition,

The Pf1 biofilm was tightly packed in large and dense clusters on the overall surface of the coupons, which appear to be flat and present different layers according to confocal images.

Whereas, the biofilms formed by Ec-SS2 and Bc-98/4 strains were composed of medium-sized clusters (observed on 3D structure) separated by less contaminated areas with many single cells and small clusters.
When the coupons were subjected to cleaning procedures, two phases of detachment have been also observed in the case of Pf1, and Bc-98/4 while complete removal of Ec-SS2 was observed after 3 min of cleaning at the lowest shear stress of foam (2.2 Pa). Indeed, foam flow condition at 2 Pa was sufficient to remove more than 4 log CFU before 1 min and at least 6 log CFU after 20 min where few cells were remaining on the coupons after the cleaning procedure. This was not surprising since the cleaning in static condition (dipping in water or SDS solution for 20 min) was able to remove almost 3 log CFU. On the other hand, foam flow cleaning was able to remove a significant part of Pf1, and Bc-98/4 biofilms grown on stainless steel surfaces.
A clear positive effect of increasing the average shear stress on cleaning efficiency was thus observed for the two detachment phases. Indeed, an increase in the mean shear stress was followed by an improvement in the cleaning efficiency of the two strains Bc-98/4 and Pf1 where the removal at 13.2 Pa exceeded 2 and almost 1.5 log CFU reduction for Bc-98/4 and Pf1 respectively showing an additional 0.5 log reduction compared to foam at 2.2 Pa. The same trend was observed before 1 min of cleaning. However, contrarily to the removal of spores, the bubble size did not show a strong effect in the enhancement of cleaning, but in the same time, the increase in frequency and amplitude of the local wall shear stress could probably better explain this efficiency and lead to draw hypothesis on the specific cleaning mechanisms for biofilms elimination using foam flow. In addition, the detachment of biofilms using foam flow was largely more efficient than conventional cleaning-in-place.

Then a life cycle assessment study was investigated, using SimaPro in order to evaluate the environmental impacts of this alternative cleaning process for the food industry compared to two CIP conditions, one using the same foaming surfactant (SDS) and the other one using a commonly used sodium hydroxide at a higher temperature (60°C). Results showed that the foam flow process reduces environmental impacts mainly explained by reduced water and energy consumption, compared to CIPs procedures. Indeed, foam flow cleaning required respectively 6.7 and 7.6 times less the amount of water and electricity than that used by CIP-containing SDS while it consumes about 18.3 and 22.7 times less than CIP-containing NaOH, which was the harmful process due to the heating step. The SDS surfactant consumption was highly noticeable (12.5 times more) in CIP than foam cleaning. Moreover, compared to CIP using the same surfactant (SDS), foam cleaning was able to reduce the environmental impacts in all aspects by about 70%, with the lowest effect on the impact for terrestrial ecotoxicity (reduction by 20%). The greatest impact reduction was on land occupation (reduction by 90%), ionizing radiation, respiratory organics (C2H4 eq), and global warming (CO2 eq). However, due to the compressed air production, the foam cleaning was less favorable than CIP on aquatic eutrophication and mineral extraction by 20% and 45% more.
The other related activities carried out during the PhD period lead to draw the following conclusions highlighting the utmost importance of the equipment design on the risk of remaining surface contamination after cleaning. The vertical/horizontal position of the surface affects clearly the biofilm formation. Higher amounts of biofilms are found on horizontal surfaces, probably due to the accumulation through sedimentation of bacteria on horizontal

surfaces. But these biofilms are often more fragile. The changes in some geometrical features (no horizontal surfaces and only open angles exceeding 100°) induced a better flow organization reducing ‘‘dead zones’’. This results in a delay in the formation of biofilms, especially in areas at particular risks, such as weld zones, corners, and interfaces. In addition, mandatory to be considered in hygiene is the presence of air-liquid-wall interfaces. Indeed, some bacteria form large amounts of biofilm at air-liquid-wall interface, and these biofilms are highly resistant to cleaning. Their amount and structure are also deeply affected by the material hydrophobicity. Finally, bio-aerosols settled on surfaces form deposits whose structure is affected by the hydrophilic/hydrophobic character of the material. The resistance to detachment (rinsing/cleaning) of dried droplets depends on the hydrophobicity of the material and the particles, which requires specific attention in the context of maintaining hygiene in the food industry.

Future works could be envisaged by considering only the use of flow foams for the cleaning of food equipment. Despite the advances brought by this thesis work, there is still a lot of work to be done on the design of the best foam or at least the most suitable foam for the systems (equipment, processing lines) to be cleaned and under which flow regime. It was demonstrated that the geometry has a strong impact on the organization of the foam and its flow regime and therefore likely its cleaning efficiency. We are particularly concerned by the presence of liquid films which can be thick in the lower parts of the processing lines and which reduce significantly the mechanical action of the foam. Indeed , some attempts were made to study the consequences of the cleaning efficiency of the foam in a pipe after a bend or after a diameter reduction or just after a significant length of pipes (> 4 m). The cleaning efficiency was clearly affected.

Attemps to use other types of surfactants than SDS (e.g. anionic, amphoteric) demonstrated also the great importance of the choice of the surfactant (or of the combination of different surfactants). Working out these aspects is of utmost importance prior to any implementation in the industry. Indeed, one way out of this problem would be to work with other surfactants which would induce foam structures that are more resistant to mechanical stresses without perhaps reducing the mobility of the bubbles between them or the ability of the foam to absorb contamination which is still a hypothesis to explain the cleaning efficiency in this thesis. The new PhD now starting on these aspects will certainly give significant new insights in this area. It thus appears certain that taking into account the Physico-chemical parameters of the foam and the mechanisms induced by the structure and chemical properties of the surfactants are of key importance in order to go further not only in the understanding of the phenomena at the scale of the bubble-liquid film-clogged wall interface system but also in the search for potential technological developments (fields of application: IAA, hospitals) in partnership with industry. The environmental assessment has given us some assurance that the environmental impact will be reduced, but we know that the presence of these surfactant molecules in the environment remains a concern (intensive use of detergents). It would be interesting to consider the use of bio-sourced surfactant molecules that are also biodegradable like the surface-active biomolecules of microbial origin. Within the framework of a circular bioeconomy, the ideal solution would be reuse or use for other applications. Indeed, these types of surfactants exhibit low toxicity and degradable nature, which make it to be environmentally friendly. In addition,

they are able to modify the hydrophobic properties of the bacterial surface, which affects the adhesion properties to the surface leading to an improvement of the foam cleaning. In addition, an adequate treatment of the foam after cleaning (as wastewater) could reduce the environmental impacts of this cleaning process. The possibility of reusing the same foam in another cleaning cycle should not be overlooked but may be required specific treatment. Other ways to improve the cleaning efficiency could be the use of mixt technologies such as cleaning with foam flow containing enzymes, biocides

Title: Numerical and experimental investigations of the rheological behavior of foam flow: Application to the cleaning of surfaces contaminated by microorganisms in the food industries

Abstract: In this research, experimental and numerical characterization of the rheological behavior of an aqueous foam flowing inside a horizontal pipe with and without singularities (presence of half-sudden expansion, and a fence) were investigated. Different conditions of foam flow were studied by varying the foam qualities (from 55% to 85%), and three Reynolds numbers (32, 65, and 97). Measurements of the pressure measurements, and at the wall the local velocity repartition and the thickness of the liquid films using respectively pressure sensors, Particle Image Velocimetry, and a conductimetry technique shown a reorganization of the foam downstream the geometry change, with a thicker liquid film at the duct bottom, larger bubble sizes at the top, as well as a larger foam void fraction increased from the bottom to the top part of the duct section. In addition, foam would present a visco-elastic character comparable to a non-Newtonian monophasic liquid. Computational Fluid Dynamics simulations were undertaken to predict this rheological behavior of the foam, the two models Herschel-Bulkley and Bingham were tested taken into account the presence of an underlying liquid film at the bottom of the channel. Comparison between experimental and numerical results showed that regardless of the foam quality, Herschel-Bulkley model could accurately describe the rheological behaviour of the aqueous foam under the different flow conditions analysed. The second target was to investigate the ability of a wet foam flow (quality of 50%) to clean stainless-steel surfaces contaminated by microorganisms. For this purpose, two different contamination patterns were studied, droplets containing *Bacillus subtilis* spores (either hydrophilic *B. subtilis* PY79 or hydrophobic *B. subtilis* PY79 spsA), and biofilms produced by three bacteria strains encountered in food industry production plants (*Escherichia coli* SS2, *Bacillus cereus* 98/4, and *Pseudomonas fluorescens* Pf1). Different flow conditions were performed by varying the wall shear stresses (2.2 - 13.2 Pa), and bubble sizes (0.18-0.34 mm) in a straight duct with no geometrical changes, in order to identify the mechanisms of contamination release and thus better control and optimize the foam cleaning process. Results show that compared to conventional cleaning-in-place, foam flow effectively removed *B. subtilis* spores as well as Bc-98/4, Ec-SS2, and Pf1 biofilms. Moreover, the combination of high shear stress at the wall and small bubble sizes (<0.2 mm) showed promise for improving the cleaning efficiency of spores. On the other hand, a clear improvement of the biofilm removal was observed when increasing the mean wall shear stress. The characterization of the foam and the interface phenomena (using polarography, conductimetry, and bubble size analysis methods) indicated that mechanisms such as fluctuation in local wall shear stresses, or in the liquid film thickness between the bubbles and the steel wall induced by bubble passage, foam imbibition, and sweeping of the contamination within the liquid film could participate largely to the removal mechanisms. Finally, the life cycle assessment study demonstrated that foam flow cleaning could be a suitable technique to reduce water and energy consumption (7 and 8 times less, respectively) presenting less environmental impacts than CIP processes, with about 70%. Lastly, foam flow cleaning can be an alternative method, which can improve efficiency and reduce environmental impact. Additional activities conducted during the PhD period related to hygienic design are presented highlighting the role of the contaminants (spores and biofilms), the material (other than stainless steel) and the geometry (ducts or more complex design) in hygiene monitoring.

Titre: Investigations numériques et expérimentales du comportement rhéologique de mousses en écoulement: Application au nettoyage des surfaces contaminées par des micro-organismes dans les industries agro-alimentaires

Résumé: La caractérisation expérimentale et numérique du comportement rhéologique d'une mousse aqueuse s'écoulant à l'intérieur d'un tuyau horizontal avec et sans singularités (présence d'une demi-expansion soudaine, et d'une clôture) a été étudiée. Différentes conditions d'écoulement de la mousse ont été étudiées en faisant varier les qualités de mousse (de 55% à 85%), et trois nombres de Reynolds (32, 65, et 97). Les mesures de la pression, de la répartition de la vitesse locale et de l'épaisseur des films liquides au niveau de la paroi à l'aide respectivement de capteurs de pression, de la vélocimétrie par image de particules et d'une technique de conductimétrie ont montré une réorganisation de la mousse en aval du changement de géométrie, avec un film liquide plus épais au fond du conduit, des bulles de plus grande taille au sommet, ainsi qu'une plus grande fraction de vide de la mousse augmentant de la partie inférieure à la partie supérieure de la section du conduit. En outre, la mousse présenterait un caractère visco-élastique comparable à celui d'un liquide monophasique non newtonien. Des simulations de dynamique des fluides par ordinateur ont été entreprises pour prédire ce comportement rhéologique de la mousse, les deux modèles Herschel-Bulkley et Bingham ont été testés en tenant compte de la présence d'un film liquide sous-jacent au fond du canal. La comparaison entre les résultats expérimentaux et numériques a montré que, quelle que soit la qualité de la mousse, le modèle de Herschel-Bulkley pouvait décrire avec précision le comportement rhéologique de la mousse aqueuse dans les différentes conditions d'écoulement analysées. Le deuxième objectif était d'étudier la capacité d'un écoulement de mousse humide (qualité de 50%) à nettoyer des surfaces en acier inoxydable contaminées par des micro-organismes. Pour cela, deux types de contamination ont été étudiés, des gouttelettes contenant des spores de *Bacillus subtilis* (soit hydrophiles *B. subtilis* PY79 ou hydrophobes *B. subtilis* PY79 spsA), et des biofilms produits par trois souches de bactéries rencontrées dans les usines de production de l'industrie alimentaire (*Escherichia coli* SS2, *Bacillus cereus* 98/4, et *Pseudomonas fluorescens* Pf1). Différentes conditions d'écoulement ont été réalisées en faisant varier les contraintes de cisaillement de la paroi (2.2 - 13.2 Pa), et la taille des bulles (0.18-0.34 mm) dans un conduit droit sans changement géométrique, afin d'identifier les mécanismes de libération de la contamination et ainsi mieux contrôler et optimiser le processus de nettoyage par mousse. Les résultats montrent que, par rapport au nettoyage en place conventionnel, le flux de mousse a éliminé efficacement les spores *B. subtilis* ainsi que les biofilms Bc-98/4, Ec-SS2 et Pf1. De plus, la combinaison d'une contrainte de cisaillement élevée au niveau de la paroi et de bulles de petite taille (<0,2 mm) s'est avérée prometteuse pour améliorer l'efficacité du nettoyage des spores. D'autre part, une nette amélioration de l'élimination des biofilms a été observée en augmentant la contrainte de cisaillement moyenne sur la paroi. La caractérisation de la mousse et des phénomènes d'interface (à l'aide de méthodes de polarographie, de conductimétrie et d'analyse de la taille des bulles) a indiqué que des mécanismes tels que la fluctuation des contraintes de cisaillement locales de la paroi, ou de l'épaisseur du film liquide entre les bulles et la paroi en acier induite par le passage des bulles, l'imbibition de la mousse et le balayage de la contamination dans le film liquide, pourraient participer largement aux mécanismes d'élimination. Enfin, l'étude d'analyse du cycle de vie a démontré que le nettoyage à la mousse peut être une technique appropriée pour réduire la consommation d'eau et d'énergie (7 et 8 fois moins, respectivement) présentant moins d'impacts environnementaux que les procédés CIP, avec environ 70%. Enfin, le nettoyage à la mousse peut être une méthode alternative, qui peut améliorer l'efficacité et réduire l'impact environnemental. D'autres activités menées au cours de la période de doctorat liées à la conception hygiénique sont présentées en soulignant le rôle des contaminants (spores et biofilms), du matériau (autre que l'acier inoxydable) et de la géométrie (conduits ou conception plus complexe) dans le contrôle de l'hygiène.